

DISSERTATION

SHEAR BEHAVIOR OF GEOSYNTHETIC CLAY LINERS AND TEXTURED
GEOMEMBRANES IN MINING APPLICATIONS

Submitted by

Shahin Ghazi Zadeh

Department of Civil and Environmental Engineering

In partial fulfillment of the requirements

For the Degree of Doctor of Philosophy

Colorado State University

Fort Collins, Colorado

Summer 2019

Doctoral Committee:

Advisor: Christopher A. Bareither

Charles D. Shackelford
Joseph Scalia
Travis Bailey

Copyright by Shahin Ghazi Zadeh 2019

All Rights Reserved

ABSTRACT

SHEAR BEHAVIOR OF GEOSYNTHETIC CLAY LINERS AND TEXTURED GEOMEMBRANES IN MINING APPLICATIONS

The objective of this study was to evaluate the shear behavior of a composite system consisting of geosynthetic clay liner (GCL) and textured geomembrane (GMX) in mining applications. In current practice, design of liner and cover systems for waste containment is based on results of displacement-controlled internal and interface shear tests, which commonly include GCL and GMX specimens hydrated in de-ionized or tap water and tested at room temperature (e.g., 20 °C). However, the use of GCL/GMX composite systems in liner and/or cover systems for mine waste containment (e.g., heap leach pads, tailings impoundments, waste rock piles) may be exposed to physical and environmental stresses that are not conventionally replicated in laboratory testing, such as high shear and normal stresses, elevated temperature, and/or non-standard solutions. Laboratory testing conducted under conventional experimental conditions may not represent appropriate stresses anticipated in field conditions.

To address the aforementioned concerns and aid the design of liner and cover systems for mining applications, four main objectives were defined: (i) assess variability of internal reinforcement fibers and shear strength in GCLs; (ii) evaluate the effect of GCL and GMX characteristics on shear behavior of GCL/GMX composite systems; (iii) evaluate temperature effects on the shear behavior of GCL/GMX composite systems; and (iv) evaluation the effects of non-standard solutions on GCL internal and GCL/GMX interface shear strength. These objectives were addressed via laboratory experiments, which included approximately 400 direct shear tests, 150 peel strength tests, and 50 swell index tests.

Comparable internal shear behavior was observed between 300 mm x 300 mm GCL specimens and 150 mm x 150 mm GCL specimens. Similar variability in peak internal shear strength was also observed in both size GCL specimens. Variation was also observed in GCL peel strength among specimens obtained from the same production roll. Variability in internal shear strength and peel strength were attributed to the spatial variability of reinforcement fiber characteristics within a given GCL roll.

The failure mode of a GCL/GMX composite system in an interface direct shear test was a function of shearing normal stress and characteristics of the GCLs and GMXs. An increase in spike density of a GMX increased the critical strength of GCL/GMX composites at all normal stress. However, an increase in GCL peel strength most effectively increased critical strength of a GCL/GMX composite at high normal stresses when GCL internal failure occurred.

Internal and interface direct shear testing at an elevated temperature to 80 °C resulted in reductions of both GCL internal and GCL/GMX interface shear strength. The reduction in GCL internal shear strength was due to a reduction in tensile strength of reinforcement fibers and reduction in the strength of the connection between reinforcement fibers and geotextile of the GCL. The reduction in GCL/GMX interface shear strength was attributed to a reduction in the interlocking strength between GMX spikes and fibers of the geotextile of the GCL, as well as a reduction in geotextile-GMX interface friction.

Hydration of GCL and GMX specimens up to 10 months in synthetic acidic and alkaline mining process solutions did not produce noteworthy change in GCL internal shear strength, GCL-GMX interface shear strength, or GCL peel strength. However, stiffer shear behavior was observed in internal and interface shear tests on GCL and GMX specimens hydrated with the synthetic acidic mine process solution. Hydration with the synthetic acidic mine process solution reduced swell behavior of sodium bentonite, whereas no conclusions were made regarding the effect of hydration with alkaline mine process solution on bentonite swell behavior.

ACKNOWLEDGEMENTS

I would like to thank everybody who contributed in the completion of this work. A special thanks to my advisor Dr. Christopher A. Bareither for all his academic and non-academic supports.

TABLE OF CONTENTS

ABSTRACT.....	ii
ACKNOWLEDGEMENTS	iv
LIST OF TABLES.....	viii
LIST OF FIGURES	ix
CHAPTER 1: EXECUTIVE SUMMARY.....	1
1.1 Introduction.....	1
1.2 Problem Statement.....	2
1.3 Major Findings.....	4
CHAPTER 2: VARIABILITY OF REINFORCEMENT AND INTERNAL SHEAR STRENGTH IN GEOSYNTHETIC CLAY LINER ROLLS.....	9
2.1 Introduction.....	9
2.2 Background	11
2.3 Materials and Characteristics.....	13
2.4 Experimental Procedure	15
2.4.1 Internal Direct Shear Tests.....	15
2.4.2 Peel Strength Tests.....	16
2.5 Results	17
2.5.1 Variability in Reinforcement Fiber Characteristics	17
2.5.2 Variability in Peel Strength	19
2.5.3 Variability in Internal Shear Strength	20
2.6 Discussion	22
2.7 Summary	26
CHAPTER 3: SHEAR MECHANISM OF TEXTURED GEOMEMBRANE – GEOSYNTHETIC CLAY LINER COMPOSITE SYSTEMS.....	44
3.1 Introduction.....	44
3.2 Shear Mechanism of GMX/GCL Composite System.....	46
3.3 Materials.....	48
3.3.1 Geosynthetic Clay Liners Specimens.....	48
3.3.2 Textured Geomembrane Specimens.....	48
3.3.3 GMX/GCL Composite Systems.....	48
3.4 Experimental Procedure	49
3.5 Results	51
3.5.1 GCL Internal Shear Tests.....	52
3.5.2 GMX/GCL Interface Shear Tests.....	54
3.6 Analysis.....	55
3.6.1 Internal Shear Behavior of Needle-Punched GCLs	56
3.6.2 Effect of Geotextile Mass per Area on GMX/GCL Shear Behavior	57
3.6.3 Effect of Geotextile Type on GMX/GCL Shear Behavior	59
3.6.4 Effect of GMX Spike Density on GMX/GCL Shear Behavior.....	61

3.6.4.1 Case 1: GMX1/GCL1 and GMX2/GCL1.....	61
3.6.4.2 Case 2: GMX1/GCL2 and GMX2/GCL2.....	63
3.6.5 Effect of GCL Peel Strength on GMX/GCL Shear Behavior.....	64
3.6.5.1 Case 1: GMX2/GCL1, GMX2/GCL2, and GMX2/GCL3.....	65
3.6.5.2 Case 2: GMX1/GCL1, GMX1/GCL2, and GMX1/GCL3.....	66
3.7 Design Consideration	68
3.8 Summary	70
CHAPTER 4: EFFECT OF TEMPERATURE ON CRITICAL STRENGTH OF GEOSYNTHETIC CLAY LINER / TEXTURED GEOMEMBRANE COMPOSITE SYSTEMS.....	100
4.1 Introduction.....	100
4.2 Background	102
4.2.1 Shear Behavior of GCL/GMX Composite Systems.....	102
4.2.2 Effect of Temperature on Geosynthetics and Polymers.....	104
4.3 MATERIALS	106
4.4 Direct Shear Testing.....	106
4.4.1 Experimental Procedure.....	106
4.4.2 Data Compilation and Analysis.....	109
4.5 Results	111
4.5.1 Internal shear tests.....	111
4.5.2 Interface shear tests.....	112
4.6 Analysis.....	114
4.6.1 Peak Critical Strength	114
4.6.2 Large-Displacement Critical Strength	118
4.7 Summary	121
CHAPTER 5: INTERNAL AND INTERFACE SHEAR STRENGTH OG GEOSYNTHETIC CLAY LINERS FOLLOWING HYDRATION IN SYNTHETIC MINE PROCESS SOLUIONS	142
5.1 Introduction.....	142
5.2 Materials.....	144
5.2.1 Material Description	144
5.2.2 Hydration Solutions	144
5.3 Experimental procedure.....	145
5.3.1 Specimen Preparation and Hydration in Non-Standard Solutions.....	145
5.3.2 Direct Shear Tests	146
5.3.3 Peel Strength Tests.....	149
5.4 Results	149
5.4.1 Displacement-Controlled Direct Shear Tests.....	149
5.4.1.1 Internal Direct Shear Tests	149
5.4.1.2 Interface Direct Shear Tests	153
5.4.2 Peel Strength	157
5.4.3 Swell Index.....	158
5.5 Summary	161

CHAPTER 6: FUTURE RESEARCH.....	184
6.1 Variability in texturing properties of textured geomembranes.....	184
6.2 Effect of geomembrane texturing on shear behavior of GMX/GCL composite systems	185
6.3 Evaluation of internal and interface shear behavior of enhanced bentonite GCLs..	187
6.4 Shear behavior of GCLs in MSW leachates with high surfactant concentrations....	187
REFERENCES	189

LIST OF TABLES

Table 2.1. Summary of the material characteristics for geosynthetic clay liners (GCLs) used in this study.	28
Table 2.2. Summary of reinforcement fibers characteristics for the six needle-punched geosynthetic clay liners (GCLs).	29
Table 2.3. Summary of peel strength for GCL-D specimens.....	30
Table 2.4. Summary of internal direct shear tests on 150-mm and 300-mm specimens cut from the 1 m x 3 m area of GCL-D.	31
Table 2.5. Summary of internal direct shear tests on 150-mm and 300-mm specimens cut from the 1 m x 3 m area of GCL-D.	32
Table 3.1. Characteristics and properties of geosynthetic clay liners.....	73
Table 3.2. Characteristics and properties of GMX.	74
Table 3.3. Components and schematics of GMX/GCL composite systems.	75
Table 3.4. A summary of displacement-controlled internal direct shear tests.	76
Table 3.5. A summary of displacement-controlled interface shear tests.	77
Table 4.1. Characteristics and properties of geosynthetic clay liners used in this study.	124
Table 4.2. A summary of displacement-controlled internal direct shear tests.	125
Table 4.3. A summary of displacement-controlled internal direct shear tests.	126
Table 5.1. Summary of material characteristics and properties for geosynthetic clay liners (GCLs) used in this study.	163
Table 5.2. Properties of synthetic solutions prepared to a represent a Copper mine process solution (Cu-PS) and bauxite mine process solution (B-PS).	164
Table 5.3. Properties of synthetic solutions prepared to a represent a Copper mine process solution (Cu-PS) and bauxite mine process solution (B-PS).	165
Table 5.4. Summary of displacement-controlled interface direct shear tests.	166
Table 5.5. Peel strength test results for non-hydrated geosynthetic clay liner (GCL) specimens and GCL specimens hydrated with B-PS and Cu-PS for hydration durations of 1, 6, and 10 months.....	167
Table 5.6. Summary of swell index tests performed on non-pre-hydrated bentonite and bentonite hydrated with non-standard solutions	168

LIST OF FIGURES

Fig. 2.1.	Digital images of a (a) fiber bundle and (b) individual monofilament fiber captured with a stereoscope microscope to facilitate measurement of number of fibers per bundle and fiber diameter. Fiber bundle is from GCL-E.....	33
Fig. 2.2.	Dot plots of the number of fiber bundles per centimeter in (a) machine direction (MD), and (b) cross-machine direction (CMD). Note: PS = GCL peel strength.....	34
Fig. 2.3.	Dot plots of the number of monofilament fibers per fiber bundles for 20 measurements on GCL-A, GCL-B, GCL-C, GCL-D, GCL-E, and GCL-F specimens. The mass of the cover geotextile of the GCL is provided for comparison.....	35
Fig. 2.4.	Dot plots of monofilament fiber diameter for 20 measurements on GCL-A, GCL-B, GCL-C, GCL-D, GCL-E, and GCL-F specimens.	36
Fig. 2.5.	Schematic of the 1 m x 3 m area of GCL-D that includes locations of 150-mm direct shear test specimens, 300-mm direct shear test specimens, and peel strength test specimens.....	37
Fig. 2.6.	Dot plot of peel strength test results for GCL-D.	38
Fig. 2.7.	Distribution of the peel strength within the 1 m x 3 m area sampled in GCL-D.....	39
Fig. 2.8.	Relationships between the shear stress (τ) and horizontal displacement (δ_h) from internal direct shear tests conducted under a shearing normal stress (σ_{n-s}) of 500 kPa on (a) 150-mm and (b) 300-mm GCL-D specimens.	40
Fig. 2.9.	Dot plots of (a) secant friction angle at peak shear strength (ϕ_{s-p}) and (b) secant friction angle at large-displacement shear strength (ϕ_{s-ld}) for direct shear tests conducted on 150-mm and 300-mm GCL-D specimens	41
Fig. 2.10.	Distribution of the secant friction angle at peak shear strength (ϕ_{s-p}) for the 150-mm and 300-mm direct shear test specimens from GCL-D.....	42
Fig. 2.11.	Relationships between peak shear strength (τ_p) measured at a normal stress of (σ_{n-s}) of 500 kPa and peel strength (PS) based on the following: (a) manufacturer reported peel strength for GCL-A, GCL-B, GCL-C, GCL-D (150 mm & 300 mm tests), and GCLF; (b) machine direction peel strength for GCL-D; and (c) cross-machine direction peel strength for GCL-D. Non-linear τ_p -PS relationship is from Athanassoupolous and Yuan (2011) based on τ_p measured under $\sigma_{n-s} = 479$ kPa.	43
Fig. 3.1.	Schematic shear and normal stresses within a composite system composed of a textured geomembrane (GMX) and needle-punched geosynthetic clay liner (GCL).....	78

Fig. 3.2. Relationships between shear stress (τ) and horizontal displacement (δ_h) for direct shear tests on the internal shear strength of GCLs: (a) GCL1, (b) GCL2, and (c) GCL3.....	79
Fig. 3.3. Photographs of post internal GCL-shear specimens of GCL-3 from direct shear tests conducted under normal stresses of (a) 160 kPa and (b) 1000 kPa.	80
Fig. 3.4. Relationships between shear stress (τ) and horizontal displacement (δ_h) for direct shear interface tests on (a) cover GT of GCL1 and GMX1, (b) carrier GT of GCL1 and GMX1, and (c) cover GT of GCL1 and GMX2	81
Fig. 3.5. Relationships between shear stress (τ) and horizontal displacement (δ_h) for direct shear interface tests on (a) carrier GT of GCL2 and GMX1, (b) cover GT of GCL2 and GMX1, and (c) cover GT of GCL2 and GMX2.....	82
Fig. 3.6. Relationships between shear stress (τ) and horizontal displacement (δ_h) for direct shear interface tests on (a) carrier GT of GCL3 and GMX1, and (b) cover GT of GCL3 and GMX2.....	83
Fig. 3.7. Photographs of post-shear GCL specimens from direct shear interface tests that show examples of (a) complete interface failure for experiments on Cover GT of GCL-1 and GMX-1 at $\sigma_{n-s} = 100$ kPa , (b) complete internal failure for experiments on Carrier GT of GCL-1 and GMX-1 at $\sigma_{n-s} = 2000$ kPa, and (c) partial interface/internal failure for experiments on Cover GT of GCL-3 and GMX-2 at $\sigma_{n-s} = 500$ kPa.....	84
Fig. 3.8. Shear strength and shear behavior relationships for GCL-internal direct shear tests on GCL1, GCL2, and GCL3: (a) peak shear strength (τ_p) versus shearing normal stress (σ_{n-s}), (b) horizontal displacement at peak shear stress (δ_{h-p}) versus σ_{n-s} , (c) area-corrected large-displacement shear stress at $\delta_h = 70$ mm (AC τ_{70}) versus area-corrected large-displacement normal stress at $\delta_h = 70$ mm (AC σ_{70}), and (d) stress reduction ratio ($R\tau$) versus σ_{n-s}	85
Fig. 3.9. Shear strength and shear behavior relationships for GCL-internal direct shear tests on GCL1 and GMX/GCL interface direct shear tests on GCL1-CAGT/GMX1 and GCL1-COGT/GMX1: (a) peak shear strength (τ_p) versus shearing normal stress (σ_{n-s}), (b) horizontal displacement at peak shear stress (δ_{h-p}) versus σ_{n-s} , (c) large displacement shear stress (τ_{ld}) versus large-displacement normal stress (σ_{ld}), and (d) post-peak strength reduction ratio ($R\tau$) versus σ_{n-s}	86
Fig. 3.10. Post shear pictures of GCL1 specimen in DC-IF tests on (a) GCL1-COGT/GMX1 at $\sigma_{n-s} = 300$ kPa, (b) GCL1-COGT/GMX1 at $\sigma_{n-s} = 1000$ kPa, (c) GCL1-COGT/GMX1 at $\sigma_{n-s} = 2000$ kPa, (d) GCL1-CAGT/GMX1 at $\sigma_{n-s} = 300$ kPa, (e) GCL1-CAGT/GMX1 at $\sigma_{n-s} = 1000$ kPa, and (f) GCL1-CAGT/GMX1 at $\sigma_{n-s} = 2000$ kPa.....	87
Fig. 3.11. Shear strength and shear behavior relationships for GCL-internal direct shear tests on GCL2 and GMX/GCL interface direct shear tests on GCL2-	

CAGT/GMX1 and GCL2-COGT/GMX1: (a) peak shear strength (τ_p) versus shearing normal stress (σ_{n-s}), (b) horizontal displacement at peak shear stress (δ_{h-p}) versus σ_{n-s} , (c)) large displacement shear stress (τ_{ld}) versus large-displacement normal stress (σ_{ld}), and (d) post-peak strength reduction ratio (R_τ) versus σ_{n-s}	88
Fig. 3.12. Post shear pictures of GCL1 specimen in DC-IF tests on (a) GCL2-COGT/GMX1 at $\sigma_{n-s} = 100$ kPa, (b) GCL2-COGT/GMX1 at $\sigma_{n-s} = 2000$ kPa, (c) GCL2-CAGT/GMX1 at $\sigma_{n-s} = 100$ kPa, and (d) GCL2-CAGT/GMX1 at $\sigma_{n-s} = 2000$ kPa.	89
Fig. 3.13. Shear strength and shear behavior relationships for GCL-internal direct shear tests on GCL1 and GMX/GCL interface direct shear tests on GCL1-COGT/GMX1 and GCL1-COGT/GMX2: (a) peak shear strength (τ_p) versus shearing normal stress (σ_{n-s}), (b) horizontal displacement at peak shear stress (δ_{h-p}) versus σ_{n-s} , (c) large displacement shear stress (τ_{ld}) versus large-displacement normal stress (σ_{ld}), and (d) Post-peak strength reduction ratio (R_τ) versus σ_{n-s}	90
Fig. 3.14. Post shear pictures of GCL1 specimen in DC-IF tests on (a) GCL1-COGT/GMX1 at $\sigma_{n-s} = 100$ kPa, (b) GCL1-COGT/GMX1 at $\sigma_{n-s} = 300$ kPa, (c) GCL1-COGT/GMX1 at $\sigma_{n-s} = 2000$ kPa, (d) GCL1-COGT/GMX2 at $\sigma_{n-s} = 100$ kPa, (e) GCL1-COGT/GMX2 at $\sigma_{n-s} = 300$ kPa, and (f) GCL1-COGT/GMX2 at $\sigma_{n-s} = 2000$ kPa	91
Fig. 3.15. Shear strength and shear behavior relationships for GCL-internal direct shear tests on GCL2 and GMX/GCL interface direct shear tests on GCL2-COGT/GMX1 and GCL2-COGT/GMX2: (a) peak shear strength (τ_p) versus shearing normal stress (σ_{n-s}), (b) horizontal displacement at peak shear stress (δ_{h-p}) versus σ_{n-s} , (c) large displacement shear stress (τ_{ld}) versus large-displacement normal stress (σ_{ld}), and (d) Post-peak strength reduction ratio (R_τ) versus σ_{n-s}	92
Fig. 3.16. Post shear pictures of (a) GCL2-COGT/GMX1 at $\sigma_{n-s} = 100$ kPa, (b) GCL2-COGT/GMX1 at $\sigma_{n-s} = 500$ kPa, (c) GCL2-COGT/GMX1 at $\sigma_{n-s} = 2000$ kPa, (d) GCL2-COGT/GMX2 at $\sigma_{n-s} = 100$ kPa, (e) GCL2-COGT/GMX2 at $\sigma_{n-s} = 500$ kPa, and (f) GCL2-COGT/GMX2 at $\sigma_{n-s} = 2000$ kPa.....	93
Fig. 3.17. Shear strength relationships for GMX/GCL interface direct shear tests on GCL1-CAGT/GMX1, GCL2-CAGT/GMX1, and GCL3-CAGT/GMX1: (a) peak critical strength (τ_{p-cr}) versus shearing normal stress (σ_{n-s}), and (b) large-displacement critical strength at $\delta_h = 70$ mm (τ_{70-cr}) versus σ_{n-s}	94
Fig. 3.18. Post shear pictures of (a) GCL1-COGT/GMX2 at $\sigma_{n-s} = 100$ kPa, (b) GCL1-COGT/GMX2 at $\sigma_{n-s} = 500$ kPa, (c) GCL1-COGT/GMX2 at $\sigma_{n-s} = 2000$ kPa, (d) GCL2-COGT/GMX2 at $\sigma_{n-s} = 100$ kPa, (e) GCL2-COGT/GMX2 at $\sigma_{n-s} = 500$ kPa, (f) GCL2-COGT/GMX2 at $\sigma_{n-s} = 2000$ kPa, (g) GCL3-COGT/GMX2 at $\sigma_{n-s} = 100$ kPa, and (h) GCL3-COGT/GMX2 at $\sigma_{n-s} = 500$ kPa.	95

Fig. 3.19. Shear strength relationships for GMX/GCL interface direct shear tests on GCL1-CAGT/GMX1, GCL2-CAGT/GMX1, and GCL3-CAGT/GMX1: (a) peak critical strength (τ_{p-cr}) versus shearing normal stress (σ_{n-s}), and (b) large-displacement critical strength at $\delta_h = 70$ mm (τ_{70-cr}) versus σ_{n-s} .	96
Fig. 3.20. Post shear pictures of (a) GCL1-CAGT/GMX1 at $\sigma_{n-s} = 100$ kPa, (b) GCL1-CAGT/GMX1 at $\sigma_{n-s} = 500$ kPa, (c) GCL1-CAGT/GMX1 at $\sigma_{n-s} = 2000$ kPa, (d) GCL2-CAGT/GMX1 at $\sigma_{n-s} = 100$ kPa, (e) GCL2-CAGT/GMX1 at $\sigma_{n-s} = 500$ kPa, (f) GCL2-CAGT/GMX1 at $\sigma_{n-s} = 2000$ kPa, (g) GCL3-CAGT/GMX1 at $\sigma_{n-s} = 100$ kPa, (h) GCL3-CAGT/GMX1 at $\sigma_{n-s} = 500$ kPa, (i) GCL3-CAGT/GMX1 at $\sigma_{n-s} = 200$.	98
Fig. 3.21. Comparison between peak critical strength (τ_{p-cr}) and normal stress (σ_{n-s}) relationships for eight GMX/GCL composite systems in this study.	99
Fig. 4.1. A schematic of the GCL-GMX composite system subjected to shear and normal stresses (τ and σ_n) in a containment application.	127
Fig. 4.2. A schematic of the non-woven geotextile of a GCL in contact with a textured geomembrane at low and high normal stresses (σ_n).	128
Fig. 4.3. Relationships between shear stress (τ) and horizontal displacement (δ_h) for internal shear tests on (a) GCLA at room temperature, (b) GCLA at 80 °C, (c) GCLB at room temperature, and (d) GCLB at 80 °C.	129
Fig. 4.4. Relationships between shear stress (τ) and horizontal displacement (δ_h) in interface shear tests on (a) GCLA (Non-woven GT)-GMX at T = 20 °C, (b) GCLA (Non-woven GT)-GMX at T = 80 °C, (c) GCLB (Woven GT)-GMX at T = 20 °C, (d) GCLB (Woven GT)-GMX at T = 80 °C, (e) GCLC (Non-woven GT)-GMX at T = 20 °C, and (f) GCLC (Non-woven GT)-GMX at T = 80 °C.	130
Fig. 4.5. Post-shear photograph of GCLs in DC-IF tests showing examples of (a) complete interface failure mode, (b) complete internal failure mode, and (c) partial interface/internal failure mode.	131
Fig. 4.6. Relationships between peak shear strength (τ_p) versus shearing normal stress (σ_{n-s}) for internal and interface shear tests on (a) GCLA, (b) GCLB, and (c) GCLC. Solid lines show strength envelope for peak critical strength at 20 °C whereas dash lines show strength envelope for peak critical strength at 80 °C.	132
Fig. 4.7. A schematic of the 175 mm x 300 mm GMX specimens with the initial and final positions of the 150 mm x 150 mm GCL specimens. Digital images are also shown from areas in the center and the back of the GMX from GCLC/GMX tested at $\sigma_{n-s} = 2000$ kPa and T = 80 °C.	133
Fig. 4.8. Photographs of GMX spikes in the center of (a) untested specimen, (b) specimen from GCL-C/GMX composite tested at $\sigma_{n-s} = 2000$ kPa and T = 20 °C, and (c) specimen from GCL-C/GMX composite tested at $\sigma_{n-s} = 2000$	

kPa and $T = 80\text{ }^{\circ}\text{C}$. Additional photographs are at higher magnification from area surrounding a single spike and the core of the GMX.....	136
Fig. 4.9. Relationships between percent change in peak shear strength ($\Delta\tau_p$) and shearing normal stress (σ_{n-s}) for (a) internal shear on GCLA and GCLB from this study and internal shear tests on GCLD and GCLE from, and (b) Interface shear tests on GCLA/GMX, GCLB/GMX, and GCLC/GMX composite systems.	137
Fig. 4.10. Relationships between area-corrected large displacement shear strength (AC τ_{ld}) versus area-corrected large displacement normal stress (AC σ_{ld}) in internal shear tests on GCLA and GCLB at room temperature and $T = 80\text{ }^{\circ}\text{C}$. Dashed lines are contours for the large-displacement secant friction angles (ϕ_{ld})	138
Fig. 4.11. Relationships between percent change in area-corrected large-displacement shear strength ($\Delta AC \tau_{ld}$) and area-corrected large-displacement normal stress (AC σ_{ld}) for internal shear tests on GCLA and GCLB. Results of internal shear tests at $\sigma_{n-s} = 80, 160, 250,$ and 500 kPa on GCLD and GCLE from Bareither et al. (2018) is also included in this figure	139
Fig. 4.12. Relationships between the large-displacement shear strength (τ_{ld}) versus shearing normal stress (σ_{n-s}) in interface shear tests on (a) GCLA/GMX, (b) GCLB/GMX, and (c) GCLC/GMX. Dashed and solid lines are strength envelopes for critical large-displacement critical strength at room temperature and $T = 80\text{ }^{\circ}\text{C}$ respectively.....	140
Fig. 4.13. Relationships between percent change in large-displacement shear strength ($\Delta\tau_{ld}$) and shearing normal stress (σ_{n-s}) for interface shear tests on GCLA/GMX, GCLB/GMX, and GCLC/GMX.	141
Fig. 5.1. Schematic of a hydration bin used for the prolonged hydration of geosynthetic clay liner specimens.	169
Fig. 5.2. Relationships of shear stress (τ) versus horizontal displacement (δ_h) in internal shear tests on geosynthetic clay liner (GCL) specimens hydrated with de-ionized water (DIW) for a hydration time (t_H) of 6 months.....	170
Fig. 5.3. Relationships of shear stress (τ) versus horizontal displacement (δ_h) in internal shear tests on GCL specimens hydrated with (a) B-PS for $t_H = 1\text{ m}$, (b) Cu-PS for $t_H = 1\text{ m}$, (c) B-PS for $t_H = 6\text{ m}$, (d) Cu-PS for $t_H = 6\text{ m}$, (e) B-PS for $t_H = 10\text{ m}$, and (f) Cu-PS for $t_H = 10\text{ m}$. Open and closed symbols represent the duplicate tests conducted on for each hydration and normal stress condition.	171
Fig. 5.4. Peak shear strength (τ_p) versus shearing normal stress (σ_{n-s}) from internal direct shear tests on GCL specimens hydrated with B-PS (a) and Cu-PS (b). Results of the experiments with DIW included for comparison.....	172
Fig. 5.5. Horizontal displacement at peak shear stress (δ_{h-p}) versus shearing normal stress (σ_{n-s}) from internal direct shear tests on GCL specimens hydrated with	

B-PS (a) and Cu-PS (b). Results of the experiments with DIW included for comparison.....	173
Fig. 5.6. Area-corrected large-displacement shear strength ($AC \tau_{ld}$) versus area-corrected shearing normal stress ($AC \sigma_{n-s}$) from internal direct shear tests on GCL specimens hydrated with B-PS (a) and Cu-PS (b). Results of the experiments with DIW included for comparison. Dash lines are contours of large-displacement friction angle (ϕ_{ld}).	174
Fig. 5.7. Relationship between shear stress (τ) versus horizontal displacement (δ_h) for interface shear tests between GCL and GMX specimens hydrated with de-ionized water (DIW) for hydration time (t_H) = 6 mo.	175
Fig. 5.8. Post-shear photographs of GCL specimens from interface direct shear tests showing examples of (a) complete interface failure mode, (b) complete internal failure mode, and (c) partial interface/internal failure mode.	176
Fig. 5.9. Relationships of shear stress (τ) versus horizontal displacement (δ_h) from interface direct shear tests on GCL and GMX specimens hydrated with (a) B-PS for a hydration time (t_H) = 1 m, (b) Cu-PS for t_H = 1m, (c) B-PS for t_H = 6 m, (d) Cu -PS for t_H = 6 m, (e) B-PS for t_H = 10 m, and (f) for t_H = 10.	177
Fig. 5.10. Relationships between peak shear strength (τ_p) versus shearing normal stress (σ_{n-s}) from interface direct shear tests on GCL specimens hydrated with (a) B-PS and (b) Cu-PS. Results of the experiments with DIW included for comparison.....	178
Fig. 5.11. Relationships between horizontal displacement at peak shear stress (δ_{h-p}) versus shearing normal stress (σ_{n-s}) from interface direct shear tests on GCL and GMX specimens hydrated with (a) B-PS and (b) Cu-PS. Results of the experiments with DIW included for comparison.	179
Fig. 5.12. Relationship between large-displacement shear strength (τ_{ld}) versus shearing normal stress (σ_{n-s}) from interface direct shear tests on GCL and GMX specimens hydrated with (a) B-PS and (b) Cu-PS. Results of the experiments with DIW included for comparison.....	180
Fig. 5.13. Dot plots of peel strength for geosynthetic clay liner specimens that were tested prior to any hydration (i.e., non-hydrated) as well as specimens hydrated with B-PS or Cu-PS for hydration times (t_H) = 1, 6, or 10 m.....	181
Fig. 5.14. Photograph of swell index tests conducted with non-hydrated bentonite (i.e., exhumed dry from as-received GCL) in de-ionized water (DIW), B-PS, and Cu-PS.....	182
Fig. 5.15. Bar charts of average swell index measured on bentonite that was non-hydrated and bentonite exhumed from GCLs hydrated in (a) B-PS and (b) Cu-PS.....	183

CHAPTER 1: EXECUTIVE SUMMARY

1.1 Introduction

Geosynthetic clay liners (GCLs) are hydraulic barriers that consist of a layer of bentonite clay encapsulated between two geotextiles or adhered to a geomembrane (ASTM D 4439). Geosynthetic clay liners commonly are used in combination with a textured geomembrane (GMX) in liner and cover systems of for waste containment applications. Liner and cover systems generally are designed and constructed without the intent to remove or replace system components in the future. The use of GCL/GMX composite systems in applications containing slopes can subject these materials to normal and shear stresses that must be resisted internally within the GCL and at the interfaces between the GCL and adjacent geosynthetic or soil layers.

The internal shear strength of GCLs is particularly important considering that the internal friction angle of sodium bentonite can be $\leq 4^\circ$ (Seed et al. 1964; Mesri and Olson 1970). The internal shear strength of GCLs is increased via stitch-bonding or needle-punching to provide reinforcement across the bentonite layer. In the needle-punching process, fibers from the non-woven cover geotextile of a GCL are punched through the bentonite layer via needles and entangled within the woven or non-woven carrier geotextile of the GCL. Therefore, the internal shear resistance of needle-punched reinforced GCLs (NP GCLs) depends on the tensile strength of reinforcement fibers and the strength of the connection between reinforcement fibers and carrier geotextile of the GCL.

Internal shear strength of a GCL and interface shear strength between a GCL and GMX commonly are defined based on the peak (τ_p) and large-displacement (τ_{ld}) shear strength from displacement-controlled direct shear tests. In previous studies on the internal shear strength of GCLs, researchers have evaluated the effects of hydration and consolidation procedures, shearing normal stress, displacement rate, GCL reinforcement type (i.e., needle-punching

versus stitched bonding), heat-treatment method, specimen size, specimen peel strength (for NP GCLs), dynamic loading, elevated temperature, hydration with non-standard solutions, and creep (e.g., Gilbert et al. 1996; Siebken et al. 1997; Trauger et al. 1997; Fox et al. 1998; Eid et al. 1999; Koerner et al. 2001; Zornberg et al. 2005; Fox et al. 2006; Muller et al. 2008; Fox et al. 2010; Fox and Ross 2011; Ghazizadeh and Bareither 2018 a,b; Bareither et al. 2018). In previous studies on the interface shear strength between a GMX and GCL, researchers have evaluated the effects of geotextile characteristics, GMX characteristics, surface roughness, monotonic loading, bentonite extrusion, polymer type, displacement rate, and out of plane deformation (Gilbert et al. 1996; Hewitt et al. 1997; Hillman and Stark 2001; Olsta and Swan 2001; Triplett and Fox 2001; Chiu and Fox 2004; Li and Gilbert 2006; Fox and Kim 2008; Vukelic´ et al. 2008; McCarthney et al. 2009; Zornberg and McCartney 2009; Chen et al. 2010; Bacas et al. 2011; Eid 2011; Fox and Ross 2011; Bacas et al. 2015; Hanson et al. 2015; Ross et al. 2015; Stark et al. 2015; Thielmann et al. 2016; Khilnani et al. 2017). This compilation of research was reviewed to support the research objectives for this study.

1.2 Problem Statement

Although previous studies provide a wealth of valuable information for understanding of the interface and internal shear behavior of GCL/GMX composites, there are still areas that have received little attention. For instance, design procedures for liner and cover systems containing GCL/GMX composites are based on results of laboratory internal and interface shear tests on sample products provided to laboratories by manufacturers. A limited number of laboratory direct shear tests can be conducted for a given GCL project, and moreover, shear testing is conducted on specimens with limited dimensions cut from sample rolls. In this case, a fundamental question is whether results of laboratory direct shear tests are representative of shear behavior of GCL rolls deployed in the field. If specimens cut from GCL sample rolls are all identical and shear behavior measured on the test specimens is representative of GCL rolls

deployed in the field, designers can confidently use laboratory results to design liner and cover systems. However, in the case that spatial variability exists in specimen characteristics across a GCL sample roll that is delivered to a given laboratory, design of liner or cover systems based on laboratory results can lead to unconservative or overly conservative designs.

Although extensive research has been done on the internal and interface shear behavior of GCLs, the shear behavior of GMX/GCL composite systems has not been holistically evaluated via coupled internal and interface shear tests to assess shear failure mechanisms and critical shear strength of GMX/GCL composite systems. In previous studies focused on the internal shear strength of GCLs, failure was forced to occur internally within the GCL. However, internal failure of a GCL in a GMX/GCL composite system may not occur if the internal shear resistance of the GCL is higher than the mobilized shear resistance at the GMX/GCL interface (e.g., Stark et al. 2015). In contrast, studies focused on interface shear strength between a GMX and GCL may not have observed internal shear deformation and potential internal failure of GCLs. The shear behavior of GMX/GCL composite systems via conducting GCL internal and GCL interface shear strength has only been evaluated in select studies (e.g., Fox and Ross 2011). There is a need for additional research related to GCL internal and GMX/GCL interface shear strength to understand shear behavior and failure of GMX/GCL composite systems.

Another topic related to GCL/GMX composites that has received limited attention is how environmental factors, such as elevated temperature and non-standard solutions, influence shear behavior and shear strength. Temperatures in heap leach pads can be as high as 45-50 °C in copper leaching and 75 °C in nickel leaching (Brierly 2008; Smith 2008) due to exothermic chemical and biological processes. Geosynthetic clay liners used in cover systems can also experience elevated temperatures up to 50 °C depending on geographical location and climatic conditions (Yeşiller et al 2005; Koerner and Koerner 2006; Hanson et al 2010). Previous studies have documented a decrease in the mechanical properties of geosynthetics and polymeric fibers, such as tensile strength and tensile modulus, with an increase in temperature as well as

an increase in the magnitude and rate of creep deformation (Andrawes et al. 1984; Ariyama et al. 1997; Kongkitkul et al. 2012; Karademir and Frost 2014; Stepien and Szymanski 2015). These previous studies raise concerns regarding the shear behavior of GCLs at elevated temperature considering a NP GCL develops a considerable amount of internal shear strength from the polymeric reinforcement fibers.

Finally, GCL/GMX composite used in waste containment systems such as heap leach facilities and municipal solid waste systems can be exposed to a broad range of non-standard solutions (Ruhl and Daniel 1997; Benson et al. 2008, 2010; Bouazza 2010; Lange et al. 2010; Shackelford et al. 2010). Exposure to solutions with high ionic strength or extreme pH can affect swell properties of bentonite and reduce hydraulic performance of the liner system (Shackelford et al. 2000, 2010; Kolstad et al. 2004; Jeon et al. 2005; Katsumi et al. 2008; Hornsey et al. 2010; Scalia and Benson 2010). Exposure to non-standard solutions can cause antioxidant depletion and induce oxidation and hydrolytic degradation of polymers (e.g. polypropylene, high density polyethylene, and polyester) commonly used in geosynthetics (Halse et al 1987 a,b; Mathur et al. 1994; Hsuan et al. 1993; Hsuan 2000; Jo et al. 2001, 2005; Row and Sangam 2002; Gulec et al. 2004, 2005; Jeon et al. 2005; Rowe et al. 2009; Hornsey et al. 2010). Despite these concerns, previous internal and interface shear experiments on GCLs and GMXs have been conducted using either de-ionized water (DIW) or tap water, and therefore, the effect of exposure to non-standard solutions on GCL/GMX shear strength is unknown.

1.3 Major Findings

The purpose of this study was to address the aforementioned concerns and enhance the understanding of the shear behavior of GCL/GMX composite systems. The research in this study can be divided in two parts. The first part was preliminary research that was completed to develop the experimental methods and support the objective of this dissertation. The second Part is the main body of the dissertation.

The first part of the research study included the following objectives: (i) develop synthetic mining solutions for laboratory testing of GCLs; (ii) develop a displacement-controlled direct shear apparatus capable of testing GCLs at elevated temperature and non-standard solutions; (iii) develop a stress-controlled direct shear apparatus capable of testing GCLs at elevated temperature and non-standard solutions; and (iv) micro-scale evaluation of temperature effects on internal shear strength of NP GCLs. These four objectives lead to five journal papers; four journal papers have been published and the fifth journal paper is under review. These five journal papers are attached electronically as Appendix I to Appendix V.

The second part of this research included the following objectives: (i) assess variability of internal reinforcement fibers and shear strength in GCLs; (ii) evaluate the effect of GCL and GMX characteristics on shear behavior of GCL/GMX composite systems; (iii) evaluate temperature effects on the shear behavior of GCL/GMX composite systems; and (iv) evaluation the effects of non-standard solutions on GCL internal and GCL/GMX interface shear strength. Each of the aforementioned objectives is discussed in detail in Chapter 2 to Chapter 5 of this dissertation. Each chapter has been prepared as a journal paper for subsequent submission.

Chapter 2 is titled *Variability of Fiber Reinforcement and Internal Shear Strength in Geosynthetic Clay Liner Rolls*. The objectives of this chapter were to (1) assess variability in reinforcement fiber properties in GCL samples, (2) assess variability in peel strength and internal shear strength of specimens from the same GCL sample roll, and (3) evaluate relationships between reinforcement fiber properties, peel strength, and internal shear strength of a NP GCL. The variability in reinforcement fiber properties was investigated via characterization of the number of fiber bundles per specimen length, number of monofilament fibers per fiber bundle, and monofilament fiber diameter. Characterization of reinforcement fiber properties was completed for six different NP GCLs via analyzing micro-scale digital images captured with a stereoscopic microscope. Peel strength and displacement-controlled direct shear tests were performed on specimens with two different dimensions (i.e. 300 mm x 300 mm

and 150 mm x 150 mm) cut from a single GCL roll to evaluate variability and investigate potential correlations between reinforcement fibers and strength properties.

Reinforcement fiber variability was observed in all six NP GCLs, which lead to spatial variability in peel strength and internal shear strength (τ_p) of specimens obtained from the same GCL roll. No pattern was observed for the spatial variability of peel strength along the machine or cross-machine directions. Despite the τ_p variation, comparable shear behavior was observed between 150 mm x 150 mm and 300 mm x 300 mm specimens. An increase in manufacturer reported peel strength from 790 N/m to 2170 N/m among different GCLs resulted in a higher range of measured τ_p . The range of τ_p for a given manufacturer peel strength was explained via localized peel strength measurements in machine direction.

Chapter 3 is titled *Shear Mechanisms of Textured Geomembrane – Geosynthetic Clay Liner Composite Systems*. The objective of this chapter was to evaluate shear behavior and failure mechanisms for composite systems consisting of textured geomembranes and geosynthetic clay liners. Different GMX/GCL composite systems were evaluated to assess the effects of (i) GCL peel strength, (ii) geotextile (of the GCL) type, (iii) geotextile (of the GCL) mass per area, and (iv) GMX spike density on shear failure. Displacement-controlled internal and interface direct shear tests were performed at normal stresses from 100 kPa to 2000 kPa on eight GMX/GCL composite systems consisting of different GCLs and GMXs.

Three failure modes were observed for GMX/GCL composite systems that are complete interface failure, complete internal failure, and partial interface/internal failure. Increased normal stress can transition the failure mode of a GMX/GCL composite system from complete interface failure to complete internal failure. The critical strength of GMX/GCL composite systems (i.e., minimum shear strength between GCL internal and GMX/GCL interface) increased with an increase in GMX spike density. However, the effect of geotextile type and mass per area influenced critical strength at normal stress > 500 kPa, whereby an increase in geotextile mass

per area resulted in an increased critical strength. Finally, GCL peel strength influenced the GMX/GCL critical strength only when the failure mode was complete internal failure.

Chapter 4 is titled *Effect of Temperature on Critical Shear Strength of Geosynthetic Clay Liners / Textured Geomembrane Composite Systems*. The objective of this chapter was to evaluate the effect of temperature on the shear behavior and critical strength of GCL/GMX composite systems. For this purpose a series of displacement-controlled GCL internal and GCL/GMX interface direct shear tests were performed at both room temperature (≈ 20 °C) and elevated temperature = 80 °C. For consistency, all specimens were hydrated with de-ionized water and sheared under the same shearing normal stresses from 100 kPa to 2000 kPa.

Increase in the temperature to 80 °C resulted in peak shear strength reduction up to 45% in GCL internal shear tests and up to 46% in GCL/GMX interface shear tests. Large-displacement shear strength at the elevated temperature also reduced by up to 32% in GCL internal shear tests and up to 48% in GCL/GMX interface shear tests. Considering the extent of strength reduction at elevated temperature, the use of conventional factor of safeties (e.g., 1.5 for peak shear strength and 1.1 for large-displacement shear strength) are not conservative for the design of GCL/GMX composite systems subjected to elevated temperatures.

Chapter 5 is titled *Internal and Interface Shear Strength of Geosynthetic Clay Liners Following Hydration in Synthetic Mine Process Solutions*. The objective of this chapter was to evaluate the effect of non-standard solutions on the internal and interface shear behavior of geosynthetic clay liners and textured geomembranes. Displacement-controlled internal and interface shear tests were performed on GCL and GMX specimens that were hydrated in an acidic and alkaline solution for 1, 6, and 10 months. Peel strength tests on GCLs and well index tests on bentonite extracted from GCLs were also conducted following hydration in both solutions for all three hydration durations.

Hydration in the acidic or alkaline solution did not have a noticeable effect on the internal or interface shear strength of GCLs in direct shear or on the peel strength. However, stiffer

shear behavior was observed in internal and interface shear tests on specimens hydrated in the acidic solution, whereas shear behavior of specimens hydrated in the alkaline solution was comparable to specimens hydrated in de-ionized water. Exposure to the acidic solution significantly reduced the swell behavior of bentonite, whereas exposure to alkaline solution did not have a significant effect on the swell behavior of the bentonite.

CHAPTER 2: VARIABILITY OF REINFORCEMENT AND INTERNAL SHEAR STRENGTH IN GEOSYNTHETIC CLAY LINER ROLLS

2.1 Introduction

Geosynthetic clay liners (GCLs) are hydraulic barriers consisting of a layer of bentonite clay encapsulated between two geotextile layers, or adhered to a geomembrane (ASTM D 4439). The use of GCLs in containment applications can subject GCLs to normal stresses as high as 4000 kPa (Lupo 2010). In applications containing slopes, high normal stresses can subject GCLs to high shear stresses that must be resisted internally, within the GCL, and at the interface between the GCL and adjacent materials.

Considering the low friction angle of hydrated sodium bentonite (Mesri and Olson 1970), internal shear resistance of GCLs is enhanced via needle punching or stitched bonding (Fox and Stark 2015). In needle-punched reinforced GCLs (NP GCLs), polymeric fibers from the top (i.e., cover) non-woven geotextile are punched through the bentonite layer and entangled into the lower (i.e., carrier) woven or non-woven geotextile of the GCL. Internal shear strength of NP GCLs is increased via the additional shear resistance from the tensile strength of needle-punched fibers as well as the strength of the connection between the needle-punched fibers and the carrier geotextile (Ghazizadeh and Bareither 2018b)

Internal shear strength of GCLs is conventionally evaluated using displacement-controlled (or stress-controlled) internal direct shear tests (Fox and Stark 2015). Direct shear tests in laboratories are performed on specimens cut from samples that represent the GCL rolls deployed in the field (ASTM D4439). The recommended specimen dimensions for GCL internal shear tests are 300 mm x 300 mm according to ASTM D6243. However, specimens with smaller dimensions are permitted provided that specimen size does not affect results of the shear tests (e.g., peak shear strength). Following criteria in ASTM D6243, specimens smaller than 300 mm x 300 mm have been used to evaluate internal GCL shear strength and interface

shear strength between GCLs and geomembranes Gilbert et al., 1997; Koerner et al. 1998; Olsta and Swan 2001; Vukelic et al. 2008; Zanzinger and Saathof 2012; Zanzinger 2016; Bareither et al. 2018; Ghazizadeh and Bareither 2018a,b).

There are some concerns regarding the use of laboratory results to design liner and cover systems for waste containment. For example, a limited number of laboratory direct shear tests can be conducted for a given project, and moreover, shear testing is conducted on specimens with limited dimensions cut from sample rolls. In this case, a fundamental question is whether results of laboratory direct shear tests are representative of shear behavior of GCL rolls deployed in the field. If specimens cut from GCL sample rolls are all identical and shear behavior measured on the test specimens is representative of GCL rolls deployed in the field, designers can confidently use laboratory results to design liner and cover systems. However, in the case that spatial variability exists in specimen characteristics across a GCL sample roll that is delivered to a given laboratory, design of liner or cover systems based on laboratory results can lead to unconservative or overly conservative designs.

Spatial variability in mass per area and fiber density of the cover geotextile, combined with gradual dulling of needle plates used for needle-punching, can result in spatial variability in the density of needle-punched fiber bundles (e.g., number of fibers per bundle) during the manufacture of a GCL roll. Considering that internal shear strength of NP GCLs is predominantly due to the strength of reinforcement fibers, specimens obtained from different locations in a sample GCL roll may contain different amounts of reinforcement fibers and have different internal shear strength.

To address the aforementioned concerns, three objectives were defined for this study: (1) assess variability in reinforcement fiber properties in GCL samples; (2) assess variability in peel strength and internal shear strength of specimens from the same GCL sample roll; and (3) evaluate relationships between reinforcement fiber properties, peel strength, and internal shear strength of a NP GCL. The variability in reinforcement fiber properties was investigated via

characterization of the number of fiber bundles per specimen length, number of monofilament fibers per fiber bundle, and monofilament fiber diameter. Characterization of reinforcement fiber properties was completed for six different NP GCLs via analyzing micro-scale digital images captured with a stereoscopic microscope. Peel strength and displacement-controlled direct shear tests were performed on specimens cut from a single GCL roll to evaluate variability and evaluate potential correlations between reinforcement fibers and strength properties.

2.2 Background

Variability in internal shear strength of GCLs has been reported in select studies (e.g. Gilbert et al. 1997; McCartney et al. 2004; Zornberg et al. 2005; Fox 2010; Fox and Stark 2015). McCartney et al. (2004) and Zornberg et al. (2005) evaluated a large data base of internal and interface shear tests on GCLs and identified two primary sources of variability in GCL internal shear strength: (i) material variability and (ii) variability in the direct shear testing procedure.

Material variability in GCL specimens can be categorized as variability between specimens from the same GCL lot (i.e., collection of rolls manufactured with a specified process and same source materials) and variability among specimens obtained from different GCL lots. Previous studies indicated good repeatability of internal shear testing on specimens from the same GCL lot, which was hypothesized to be due to minimal variability within the GCL lot (e.g., McCartney et al. 2004; Zornberg et al. 2005; Eid 2011; Fox and Stark 2015). In contrast, these studies also reported significant internal shear strength variability on specimens obtained from different GCL lots. Specimen variability has been attributed to differences in reinforcement fiber density and bentonite properties (Gilbert et al. 1996; Zornberg et al. 2005; McCartney et al. 2009; Fox 2010; Bacas et al. 2013). Differences in direct shear test procedures can include specimen hydration and consolidation, shear rate, equipment, and operators (Gilbert et al. 1997; McCartney et al. 2004; Zornberg et al. 2005; Dixon et al. 2006). Considering potential material and test procedure variability on GCL internal shear strength, previous researchers claimed that

designing based on a conventional factor of safety of 1.5 applied to peak shear strength may result in an available shear strength in the field that is lower than the required shear strength for the stability (Sabatini et al. 2002; McCartney et al. 2004; Dixon et al. 2006).

Index parameters such as peel strength and tensile shear strength have been proposed as predictive measures of the internal shear strength of NP GCLs (von Maubeuge and Ehrenberg 2000 & 2013; Bacas et al. 2015; Fox and Stark 2015). Peel strength is defined as the average tensile force per specimen width required to peel apart the carrier and cover geotextiles of a reinforced GCL (ASTM D6496/6496M). Contradicting relationships have been reported in the literature regarding the correlation between peel strength and GCL internal shear strength. Although numerous researchers identified positive correlations between peel strength and internal shear strength of NP GCLs in direct shear tests (Heerten et al. 1995; Richardson 1997; Athanassopolous and Yuan 2011; Von Maubeuge and Ehrenberg 2000,2013), Zornberg et al. (2005) argued that the mobilization of reinforcement fibers is different in peel strength and internal direct shear tests. Therefore, Zornberg et al. (2005) recommended that peel strength is not a good indicator of the contribution of needle-punched fibers to internal shear strength of NP GCLs. Regardless of whether a correlation between peel strength and internal shear strength of NP GCLs exists, variability in peel strength suggest variability in the structural reinforcement of polymeric fibers exists among NP GCL specimens cut from the same roll or from different GCL rolls that constitute a given lot.

Peel strength can be reported based on either the average value or minimum average roll value (MARV) for at least five peel strength tests (ASTM D6496/6496M). The MARV is defined according to Eq. 2.1:

$$\text{MARV} = \mu - 2 \sigma \quad (2.1)$$

where μ is the arithmetic average peel strength and σ is the standard deviation for the peel strength measurements. Peel strength is an index parameter reported by the manufacturer

currently used for the quality control and also used by engineers to select an appropriate GCL product for design. If peel strength is reported based on MARV, designers will ensure that the manufacturer reported peel strength is higher than the peel strength of any specimen randomly chosen from the roll with the probability of 97% assuming a normal distribution of peel strength across a GCL roll. However, most manufacturers report an average peel strength because variability among GCL peel strength measurements can result in low MARV values.

Previous studies have provided invaluable information regarding sources and statistical significance of GCL internal shear strength variability (e.g. McCartney et al. 2004; Zornberg et al. 2005). However, there remains uncertainty regarding (i) material variability among GCL specimens from the same lot and (ii) characterization of potential variability within reinforcement fibers of NP GCLs. Assuming material variability among a GCL lot is minimal (as is often claimed), minimal variation should exist in reinforcement fiber characteristics within a GCL roll. This premise contradicts the anticipated spatial variation in mass per area of geotextiles and gradual dulling of needles during the needle-punching process that will contribute to material variability. Furthermore, variation of internal fiber reinforcement among GCL specimens has been hypothesized to contribute to strength variability among GCL specimens (i.e. Zornberg et al. 2005; McCartney et al. 2009; Fox 2010; Bacas et al. 2013), but few attempts has been made to characterize the reinforcement fiber properties of GCLs (Ghazizadeh and Bareither 2019 and Rowe et al. 2017).

2.3 Materials and Characteristics

Characteristics of six different NP GCLs used in this study are tabulated in Table 2.1. The materials were all commercially available needle-punched reinforced GCLs, and were provided from the manufacturers as sample rolls cut across machine direction from full production rolls. Each sample roll was approximately 1-m long in machine direction. The GCLs were different in terms of peel strength, geotextile type (i.e., woven versus non-woven),

geotextile mass per area, heat treatment technique (heat-treated versus non-heat treated), and bentonite characteristics (i.e., bentonite type and bentonite mass per area). Characterization of reinforcement fibers was completed on all six GCLs to assess variability. However, peel strength and direct shear tests were only performed on GCL-D.

Material specific characterization was performed on ten, 75 mm x 75 mm specimens that were randomly cut from each GCL sample roll. Sides of the specimens were positioned in the machine direction (MD) and cross machine direction (CMD). Each GCL specimen was evaluated to characterize carrier and cover geotextile mass per area (ASTM D5261), bentonite mass per area (ASTM D5993), and characteristics of the reinforcement fibers. Reinforcement fibers characteristics included the number of fiber bundles per length, number of mono-filament fibers per fiber bundle, and fiber diameter. The number of fiber bundles per length were determined via counting the number of fiber bundles on the sides of each specimen parallel to MD and CMD directions; thus, 20 measurements were made in the MD and CMD on each GCL.

The number of monofilament fibers per bundle were determined from 20 measurements on each GCL using micro-scale digital images captured with a stereoscopic microscope. A digital image of a monofilament fiber bundle from GCL-E is shown in Fig. **2.1a**. Monofilament fibers constituting a given fiber bundle were separated using the tip of needle such that individual fibers could be identified. The number of monofilament fibers in a given bundle were counted by two people and the average of the two counts was taken as the number of fibers in a given fiber bundle. If the difference between counts from the two people differed by more than three, the process of separating, imaging, and counting the individual fibers was repeated until the difference between counts was less than three.

Monofilament fiber diameter was also determined from 20 measurements on each GCL using micro-scale digital images captured with a stereoscopic microscope. A digital image of an individual monofilament fiber is shown in Fig. **2.1b**. Fiber diameter was measured via a

calibrated digital scale in the stereoscopic microscope with measurement accuracy to 0.002 mm.

2.4 Experimental Procedure

2.4.1 Internal Direct Shear Tests

Internal direct shear tests were performed with a displacement-controlled direct shear apparatus capable of performing experiments on 150 mm x 150 mm GCL specimens and 300 mm x 300 mm GCL specimens. Design details and verification of the apparatus are in Bareither et al. (2018). Direct shear tests in this study were performed on 150-mm and 300-mm specimens to assess the effect of specimen size on internal shear strength variability. To limit variability to the GCL, all internal shear tests were performed by the same operator, with the same equipment, and at the same temperature (≈ 20 °C) and normal stress (500 kPa).

Specimens from GCL-D were cut with initial dimensions of 150 mm x 200 mm for 150-mm shear tests and 300 mm x 360 mm for 300-mm shear tests. In both cases, longer dimensions were cut in the machine direction to accommodate additional length needed to clamp the geotextiles to the pyramid-tooth gripping plates (Bareither et al. 2018). Bentonite was removed from both ends of the longer dimension via cutting reinforcement fibers such that a 150-mm-square or 300-mm-square GCL specimens remained with intact reinforcement fibers.

The same 2-stage hydration and consolidation procedure was used for 150-mm and 300-mm GCL specimens to remove any potential variability due to specimen conditioning prior to shear testing. In Stage I (i.e., hydration stage), specimens were placed in a plastic pan filled with de-ionized water and subjected to normal stress (σ_n) of 20 kPa for 48 hr. After completion of Stage I, specimens were sandwiched between two pyramid-tooth gripping plates, transferred to the hydration box of the direct shear apparatus, and subjected to an initial $\sigma_n = 20$ kPa. Stage II (i.e., consolidation stage) was conducted via doubling the normal stress every 4-6 hr until the

target normal stress for shearing (σ_{n-s}) was achieved. The same $\sigma_{n-s} = 500$ kPa was used for all direct shear tests in this study, and after reaching the σ_{n-s} , specimens remained under that normal stress for at least 24 h before the start of shearing.

After completion of the 2-stage hydration and consolidation procedure, shearing initiated with a constant displacement rate of 0.1 mm/min (ASTM D6243). The 150-mm specimens were sheared to a horizontal displacement (δ_h) of 70 mm and the 300-mm specimens were sheared to $\delta_h = 100$ mm. These maximum δ_h may not have been sufficient to capture true residual shear strength of a GCL (Fox and Stark 2015). However, the maximum δ_h were sufficient to capture large-displacement shear strength of NP GCLs, which represents shear strength when the reinforcement fibers no longer contribute to internal shear resistance (Bareither et al. 2018).

Horizontal displacement in the direct shear tests resulted in offset between the upper and lower shear platens, which decreased the shear plane area during the test. The reduced shear plane area was accounted for in the analysis of large-displacement shear strength via computing area corrected shear and normal stress. However, peak shear strength of internally reinforced GCLs engages reinforcement fibers that exist between the cover and carrier geotextiles and remain intact throughout the shear plane area. Thus, nominal shear and normal stresses (i.e., no area correction) were used in the assessment of peak shear strength.

2.4.2 Peel Strength Tests

Peel strength tests were performed with a fully-automated tensile testing machine capable of inducing a constant rate of axial extension. Specimens with dimensions of 100 mm x 150 mm, as specified by ASTM D6496/6496M, were tested with the longer dimension cut parallel to machine direction. Initial specimen dimensions of 100 mm x 200 mm were cut from the GCL roll and bentonite was removed from a 50-mm length at one end via cutting reinforcement fibers such that the carrier and cover geotextiles (of the GCL) could be secured

via a clamping system. The carrier and cover geotextiles were marked at the connection with the clamping system to monitor if slippage occurred between the clamps and geotextiles during the test.

Each peel strength test was conducted at a constant rate of axial displacement of 300 mm/min until reaching a final displacement of 250 mm between the clamps. Tensile force required for peeling a GCL specimen apart was measured using a load cell and displacement was monitored via an internal positioning system of the tensile test machine. Data were recorded at a rate of 25 measurements per second. Test specimens were visually inspected after peel strength testing, and in cases of geotextile slippage at clamp jaws, geotextile tearing, or geotextile elongation, test results were rejected and the tests were repeated. Peel strength was calculated as the average tensile force per specimen width.

2.5 Results

2.5.1 Variability in Reinforcement Fiber Characteristics

A summary of the reinforcement fiber characteristics is in Table 2.2, which includes the average, range, and coefficient of variation (COV) for (i) number of fiber bundles per length in the MD and CMD, (ii) number of fibers per bundle, and (iii) fiber diameter. Dot plots of the number of fiber bundles per length in MD and CMD are shown in Fig. 2.2. Comparable averages, ranges, and COVs were observed for the number of fiber bundles in both machine and cross-machine directions for a specific GCL (Table 2.2 and Fig. 2.2). Geosynthetic clay liners labeled as B, C, D, E, and F were all non-heat treated NP GCLs from the same manufacturer, and peel strength increased chronologically (i.e., GCL-B PS = 790 N/m and GCL-F PS = 3850 N/m). The increase in peel strength corresponded to an increase in the average number of fiber bundles per length in both MD and CMD (Fig. 2.2).

The GCLs labeled as GCL-D and GCL-E had comparable peel strength (PS \approx 2170 to 2180 N/m) and were products from the same manufacturer (Table 2.1). This similarity

corresponded to comparable average, range, and COV for the number of fiber bundles per length in both MD and CMD (Table 2.2 and Fig. 2.2). In contrast, GCL-A and GCL-B also had similar peel strength but were products from different manufacturers, which was contributed to differences in the average, range, and COV of the number of fiber bundles per length between the two GCLs. Therefore, differences in the amount of fiber bundles per length may be encountered for GCLs with comparable peel strength, but originating from different manufacturers, whereas products from the same manufacturer appear to exhibit consistency between the number of fibers bundles per length and peel strength.

The COV for the number of fiber bundles per specimen length reduced with an increase in GCL peel strength for GCL-B through GCL-F, which was products from the same manufacturer. This relationship was attributed to the higher number of fiber bundles per length with an increase in peel strength, which permitted a higher number of fiber bundles to be counted along the sides of a given test specimen (75 mm x 75 mm). In contrast, the smallest COV was obtained for GCL-A, which was from a different manufacturer and constructed with a different needle punching process. Regardless of the manufacturer or peel strength, the COV appears to decrease with an increase in the number of fiber bundles per length, which may suggest that larger specimens are needed to more effectively capture lower concentrations of fiber bundles per length of a GCL.

Dot plots of the number of monofilament fibers per fiber bundle are shown in Fig. 2.3 for the six GCLs. A relatively comparable average and range was observed for number of fibers per fiber bundle in GCL-C, GCL-D, GCL-E, and GCL-F. Considering that the cover geotextile mass per areas were comparable between these four GCLs, a comparable number of fibers in each fiber bundle was punched through the bentonite and entangled in the carrier geotextile during the needle-punching process. In contrast, the lower mass per area of the cover geotextile of GCL-B resulted in a lower number of fibers punched through the bentonite and entangled in the carrier geotextile for a given fiber bundle. Although GCL-A had the highest cover geotextile

mass per area among the GCLs in this study, the average number of monofilament fibers per fiber bundle was less than that observed in GCLs C through F (Fig. **2.3**). Different manufacturing equipment (e.g., needle plates) in the needle-punching process was likely used by the manufacturer of GCL-A that contributed to the differences observed between cover geotextile mass per area and number of fibers per bundle.

Higher COV was observed for the number of fibers per fiber bundle compared to the COV for the number of fiber bundles per specimen length. The COV for the number of fiber per fiber bundles decreased considerably with an increase in peel strength. Additional research is required to explain this observation.

Dot plots of monofilament fiber diameter for the six GCLs are shown in Fig. **2.4**. Comparable average, range, and COV were observed for monofilament fiber diameter in all six GCLs evaluated in this study. The polymeric monofilament fibers constituting the non-woven cover geotextiles were similar among the six GCLs that included different manufacturer, geotextile mass per area, and GCL peel strength.

Variability in reinforcement fiber characteristics was observed in the number of fiber bundles per length, number of monofilament fibers per fiber bundle, and fiber diameter for a given NP GCL and among the six GCLs. The presence of variability in reinforcement fiber characteristics suggests that variability also exists within the peel strength and internal shear strength because these GCL mechanical parameters are a function of the needle-punching process. Important uncertainties addressed in this study were (i) the amount of variability that can exist in peel strength and internal shear strength for a given NP GCL and (ii) whether similar variability exists in different sized specimens used for internal shear strength.

2.5.2 Variability in Peel Strength

The effect of reinforcement fiber variability on GCL peel strength was evaluated in a series of peel strength tests performed on 65 GCL-D specimens. Among the peel strength tests,

39 were performed on specimens obtained within a 1-m x 3-m area of a single roll of GCL-D as shown in Fig. **2.5**. The 1-m x 3-m area was comparable to the size of GCL sample rolls commonly delivered to commercial and research laboratories for testing (e.g., shear strength).

A summary of the peel strength test results on GCL-D are in Table 2.3. The summary includes the average, minimum, maximum, standard deviation, COV, and MARV (ASTM D4439) for the 39 specimens from the 1-m x 3-m area (Fig. **2.5**) and the combined 65 peel strength tests. Dot plots of GCL-D peel strength are shown in Fig. **2.6**. Peel strength varied between 1832 N/m and 3208 N/m, and the results demonstrate considerable variability within the 1-m x 3-m area and among all 65 test specimens. The average and standard deviation peel strength for the 39 test specimens from the 1-m x 3-m were 2389 ± 371 N/m and the average and standard deviation for the compilation of all 65 tests was 2471 ± 358 N/m. In general, summary peel strength statistics for the select 39 test specimens or composite 65 test specimens were similar.

A schematic of peel strength spatial variability within the 1-m x 3-m area of GCL-D is shown in Fig. **2.7**. The numeric quantities superimposed over locations of peel strength specimens are the individual peel strengths measured on each specimen. Peel strength variability across the GCL roll in machine direction or cross-machine direction did not appear to follow any particular pattern. The magnitude of variability and the lack of any pattern in variability in the GCL roll raise a concern regarding the ASTM D6496 suggested minimum of five peel strength tests to determine the peel strength of a given GCL roll. Performing peel strength tests on five random specimens may result in a considerably different range, average, and coefficient of variation.

2.5.3 Variability in Internal Shear Strength

Variability of internal shear strength within a GCL roll was evaluated via direct shear tests on five 150-mm and five 300-mm specimens from the 1-m x 3-m area of GCL-D (Fig. **2.5**).

A summary of the GCL direct shear tests is in Table **2.4** and includes the following: specimen size, test identification number, σ_{n-s} , τ_p , area-corrected large-displacement normal stress (AC σ_{ld}), area-corrected large-displacement shear strength (AC τ_{ld}), secant friction angle at peak shear strength (ϕ_{s-p}), secant friction angle at large-displacement shear strength (ϕ_{s-ld}), and COV for τ_p and AC τ_{ld} . Relationships between shear stress (τ) and horizontal displacement (δ_h) in the 150-mm and 300-mm shear tests are shown in Fig. **2.8**. All specimens exhibited a well-defined peak shear stress followed by displacement-softening behavior until reaching low value of shear stress at large displacements. However, the τ - δ_h behavior within the set of five test specimens appeared more similar for the 300-mm test specimens in comparison to the 150-mm shear tests specimens. Regardless of the modest variability in τ - δ_h behavior for a given test specimen size or between the two different sized shear test specimens, shear behavior was typical of needle-punched GCLs (e.g., Fox et al. 1998; Fox and Stark 2015; Bareither et al. 2018).

Variation was observed in the magnitudes of τ_p and AC τ_{ld} for both 150-mm and 300-mm direct shear tests (Table **2.4**, Fig. **2.8**). The average τ_p and standard deviation for the five 150-mm shear tests was 341.5 ± 25.2 kPa and for the 300-mm shear tests was 354.2 ± 22.8 kPa. The average AC τ_{ld} and standard deviation for the five 150-mm shear tests was 93.6 ± 7.5 kPa and for the 300-mm shear tests was 61.0 ± 3.7 kPa. Although similar averages and standard deviations were observed in τ_p for the two different GCL shear test specimen sizes, the 300-mm shear tests yielded lower AC τ_{ld} . The lower AC τ_{ld} for the 300-mm test specimens was attributed to a larger amount of horizontal displacement that further reduced the influence of reinforcement fibers on the measure of large-displacement shear strength.

Dot plots of ϕ_{s-p} and ϕ_{s-ld} for the 150-mm and 300-mm shear tests are shown in Fig. **2.9**. Similarity in peak shear strength was observed in the average (34° to 35°) and range ($\pm 2^\circ$) for ϕ_{s-p} computed for the 150-mm and 300-mm test specimens. Minor variability in the measurements of peak internal shear strength were attributed to variability in reinforcement

fibers among test specimens because internal shear strength of NP GCLs is predominantly due to the strength of internal reinforcement fibers. In contrast, the average ϕ_{s-ld} for the 300-mm shear tests was 4.6° , whereas the average ϕ_{s-ld} for the 150-mm shear tests was 5.8° . The lower average ϕ_{s-ld} in 300-mm shear tests was attributed to the lower large-displacement shear strength evaluated at $\delta_h = 100$ mm, whereas large-displacement shear strength in the 150-mm shear tests was evaluated at $\delta_h = 70$ mm. The larger δ_h in the 300-mm shear tests allow further reduction of shear stress with continued horizontal displacement. The standard deviation in ϕ_{s-ld} for both 150-mm and 300-mm shear tests was $< 0.5^\circ$.

A schematic of spatial variability in ϕ_{s-p} within the 1-m x 3-m area of GCL-D is shown in Fig. **2.10**. Similar to the spatial variability evaluated for peel strength, there was no definitive pattern identified in ϕ_{s-p} determined for the 150-mm and 300-mm shear test specimens. A general consensus of internal shear testing of NP GCLs has suggested that less variability exists along machine direction compared to cross-machine direction due to similar needle-punching that develops from a given zone of the needle-plate during manufacturing. The values of ϕ_{s-p} shown in Fig. **2.10** indicate that this was generally true for three of the five pairs of 150-mm and 300-mm test specimens. However, the adjacent test specimens cut in machine direction from the middle-region of the roll yielded $\phi_{s-p} = 31.7^\circ$ for a 150-mm specimen and $\phi_{s-p} = 36.5^\circ$ for a 300-mm specimen. Thus, the general consensus of less variability in machine direction compared to cross-machine direction was not universally true for the tests conducted in this study.

2.6 Discussion

Spatial variability of internal shear strength (Fig. **2.11**) and peel strength (Fig. **2.8**) were observed within a sample GCL roll (1 m x 3 m) that was representative of the size sent to commercial laboratories for testing. Variability in shear strength and peel strength were

attributed to the variability observed in the reinforcement fiber characteristics (Table 2.2). However, an important question for practicing engineers is whether there exists a relationship between peel strength and internal shear strength. Such a relationship would aid in preliminary design of barrier systems based on anticipated peel strength of the design GCL and provide an ability to check laboratory results to determine if the measured shear strength agrees with the reported (or measured) peel strength.

The relationship between peak shear strength at $\sigma_{n-s} = 500$ kPa and manufacturer reported peel strength (Table 2.1) is shown in Fig. 2.11a for the ten internal shear tests on GCL-D (Table 2.4), five internal shear tests on GCL-B, two internal shear tests on GCL-E, and a single shear test on GCL-A and GCL-C. No data was included for GCL-F as the internal shearing of this high-peel strength NP GCL was not successful. Data for GCL-A, GCL-B, GCL-C, and GCL-E are for 150-mm specimens tested following the same procedure outlined herein for GCL-D (i.e., same temperature, hydration solution, hydration / consolidation procedure, operator, and equipment). A non-linear model for predicting τ_p as a function of peel strength at $\sigma_{n-s} = 479$ kPa is included from Athanassopolous and Yuan (2011). The model developed by Athanassopolous and Yuan (2011) included GCLs from the same manufacturer as GCL-B and GCL-E in this study. Their work included 18 different GCL rolls, from which a single direct shear experiment was conducted to determine τ_p for each roll that was then connected to an average peel strength based on ASTM D6496/6496M.

The range of τ_p for GCL-D and GCL-E plot above the range of τ_p for GCL-B, which agrees with the higher manufacturer reported peel strength of 2170 and 2180 N/m for GCL-D and GCL-E relative to 790 kN/m reported for GCL-B (Table 2.1). The τ_p – peel strength relationship proposed by Athanassopolous and Yuan (2011) passes through the ranges of τ_p for GCL-B, GCL-D, and GCL-E which indicates there is general agreement between the two studies and that peak shear strength can be expected to increase with peel strength. However,

the model proposed by Athanassopolous and Yuan (2011) did not address variability, whereby ranges based on standard deviation could be added to the model to capture the anticipated variability in τ_p as a function peel strength. Furthermore, although the range of variability in τ_p is captured in the data sets for GCL-D, GCL-E, and GCL-B, plotting these shear strengths against manufacturer reported peel strength does not address the spatial variability in peel strength that was shown to exist within a sample roll (Fig. 2.7).

Variability in peel strength (Fig. 2.7) and internal shear strength (Fig. 2.10) were connected via computing an average peel strength in machine direction and an average peel strength in cross-machine direction. The average peel strength in CMD for the 150-mm direct shear specimens was computed as the arithmetic average of the two adjacent peel strength specimens to the right and left side of the direct shear specimen. For example, the average peel strength of the No. 3 150-mm shear specimen (Fig. 2.6) was computed as the average of peel strength specimens labeled No. 17 and No. 20 (Fig. 2.6), which was equal to 2087 N/m. The average peel strength in CMD for the 300-mm specimens was computed as the arithmetic average of four adjacent peel strength specimens, two on the right side and two on the left side of the shear specimen. Thus, the average peel strength of the No. 3 300-mm shear specimen was the arithmetic average of peel strength specimens labeled as No. 23, 34, 30, and 31 (Fig. 2.6), which was equal to 2617 N/m. The average peel strength in MD for both 150-mm and 300-mm shear specimens was defined as the arithmetic average of three peel strength specimens in a narrow strip constrained to the width of the 300-mm specimen. For example, the average peel strength in MD for the No. 2 300-mm specimen was the arithmetic average of peel strength specimens labeled as No. 12, 13, and 14 (Fig. 6), which was equal to 1958 N/m. The sample average peel strength in MD for the 300-mm specimen No. 2 was also taken as the average peel strength for the 150-mm specimen No. 2.

Relationships between peak shear strength for $\sigma_{n-s} = 500$ kPa and peel strength in MD and CMD for GCL-D are shown in Fig. **2.11b** and Fig. **2.11c**, respectively. The τ_p – peel strength equation from Athanassopolous and Yuan (2011) is reproduced in Fig. **2.11b** and Fig. **2.11c** for comparison. Peak shear strength for the 300-mm shear specimens plotted as a function of peel strength in machine direction exhibit a well-defined increasing relationship that aligns with the τ_p – peel strength equation from Athanassopolous and Yuan (2011). Peak shear strength for the 150-mm shear specimens plotted as a function of peel strength in machine direction also exhibit a similar increasing relationship, albeit with more scatter than the 300-mm shear test data set. In contrast to relating peak shear strength to peel strength in machine direction, the relationships of peak strength for both the 150-mm and 300-mm shear specimens plotted versus peel strength in cross-machine direction exhibit additional scatter and do not necessarily correspond to the non-linear relationship proposed by Athanassopolous and Yuan (2011).

Overall, variability in reinforcement fiber properties resulted in peel strength variability and internal shear strength variability among specimens obtained from a GCL roll that was representative the sample size (1 m x 3 m) sent to laboratories for testing. Similar shear behavior and shear strength measured for the 150-mm and 300-mm direct shear specimens indicates that smaller sized specimens can be used for evaluation of GCL internal shear strength. A considerable amount of variability was observed in peel strength, which may or may not correlate to the measured internal shear strength depending on how peel strength specimens are sampled relative to direct shear specimens. The overall variability observed in peel strength and internal shear strength for a GCL sample roll raises a concern about current practice of determining peel strength and internal direct shear tests from a low number of specimens (i.e., 5 peel strength tests according to ASTM D6496/6496M and 3 direct shear tests according to ASTM D6243/6243M).

2.7 Summary

The objectives of this study were to assess variability in reinforcement fiber characteristics within sample rolls of needle-punched geosynthetic clay liners (NP GCL), and investigate the effect of reinforcement fiber variability on peel strength and internal shear strength. The following conclusions have been drawn based on the results of this study.

- Variability in reinforcement fiber characteristics within NP GCLs were observed in the number of fiber bundles per length, number of monofilament fibers per fiber bundles, and fibers diameters.
- In GCL specimens from the same manufacturer, the average number of fiber bundles per specimen length increased with an increase in average peel strength. The number of monofilament fibers per fiber bundle correlated with mass per area of the cover geotextile of the GCL. A comparable average and range were observed for monofilament fiber diameter regardless of peel strength, mass per area of the cover geotextile, or GCL manufacturer.
- Significant spatial variability in peel strength was observed within specimens from the same GCL roll. No pattern was observed in the spatial variability of peel strength along the machine or cross-machine directions. The variability in GCL peel strength was attributed to the reinforcement fiber variability that existed throughout a given GCL roll.
- Comparable shear behavior and internal shear strength were observed in internal direct shear tests on 150 mm x 150 mm and 300 mm x 300 mm specimens. Comparable averages, ranges, and standard deviations were determined for peak shear strength and large-displacement shear strength for both 150-mm and 300-mm direct shear specimens.
- An increase in manufacturer reported peel strength from 790 N/m to 2170 N/m between different GCLs resulted in a higher range of measured τ_p . The range of τ_p for a given

manufacturer peel strength was explained via localized peel strength measurements in machine direction. The correlation between τ_p and peel strength in machine direction correlated with a τ_p – peel strength relationship for similar normal stress proposed by Athanassopolous and Yuan (2011).

Table 2.1. Summary of the material characteristics for geosynthetic clay liners (GCLs) used in this study.

Properties	GCL-A	GCL-B	GCL-C	GCL-D	GCL-E	GCL-F
Manufacturer	B	A	A	A	A	A
Peel strength (N/m) ^a	740	790	980	2170	2180	3850
Heat Treatment Method	HT	NHT	NHT	NHT	NHT	NHT
Carrier geotextile type	W	W	NW	NW	W	NW
Cover geotextile type	NW	NW	NW	NW	NW	NW
Carrier geotextile mass/area (g/m ²) ^b	180	110	260	280	130	360
Cover geotextile mass/area (g/m ²) ^b	410	130	230	240	230	280
Bentonite Type	Powder	Granular	Granular	Granular	Granular	Granular
Bentonite mass per area (g/m ²) ^c	3410	5220	4220	5610	4910	5570

Note: HT = Heat treated; NHT = Non-heat treated; W = woven; NW = non-woven

^a Values reported by manufacturers based on ASTM D6496/6496M

^b Average value based on 10 measurements (ASTM D5261)

^c Average value based on 10 measurements (ASTM D5993)

Table 2.2. Summary of reinforcement fibers characteristics for the six needle-punched geosynthetic clay liners (GCLs).

GCL	No. fiber bundles per centimeter (MD)		No. fiber bundles per centimeter (CMD)		No. fibers per bundles		Fiber diameter (mm)	
	Average (Range)	COV (%)	Average (Range)	COV (%)	Average (Range)	COV (%)	Average (Range)	COV (%)
GCL-A	2.84 (2.62-3.15)	6.2	3.02 (2.76-3.28)	4.5	33.4 (20-52)	22.2	0.051 (0.046-0.056)	5.3
GCL-B	1.33 (0.92-1.7)	15.1	1.65 (1.18-2.10)	21.3	18.6 (8-35)	38.2	0.050 (0.045-0.059)	6.8
GCL-C	2.31 (1.71-2.89)	12.9	2.22 (1.57-2.88)	16.4	38.8 (19-56)	27.3	0.051 (0.045-0.058)	6.7
GCL-D	2.90 (2.23-3.54)	11.3	2.78 (2.23-3.54)	11.2	42.1 (27-59)	22.3	0.050 (0.046-0.057)	5.2
GCL-E	3.03 (2.49-3.80)	13.2	3.01 (2.49-3.54)	11.1	41.9 (26-56)	21.9	0.051 (0.045-0.057)	7.1
GCL-F	3.83 (2.89-4.72)	10.6	3.86 (2.90-4.33)	9.9	41.9 (27-54)	15.2	0.051 (0.046-0.056)	5.7

Note: MD = Machine direction; CMD = cross-machine direction; COV = coefficient of variation (%)

Table 2.3. Summary of peel strength for GCL-D specimens.

Parameter	All peel strength specimens (65 tests)	Specimens from 1 m x 3 m area (39 tests)
Average PS (N/m)	2471	2389
Minimum PS (N/m)	1832	1832
Maximum PS (N/m)	3208	3147
Standard Deviation (N/m)	357.7	370.9
COV (%)	19.52	20.2
Reported Average PS (N/m)	2170	2170
Calculated Average PS (N/m)	2471	2389
MARV (N/m)	1756	1647

Notes: PS = peel strength; MARV = minimum average roll value (ASTM D4439); COV = coefficient of variation. All peel strength specimens were obtained from a single GCL-D roll.

Table 2.4. Summary of internal direct shear tests on 150-mm and 300-mm specimens cut from the 1 m x 3 m area of GCL-D.

Specimen dimensions	Specimen No. # ^a	σ_{n-s} (kPa)	τ_p (kPa)	AC σ_{ld} (kPa) ^b	AC τ_{ld} (kPa) _b	ϕ_{s-p} (°)	ϕ_{s-ld} (°)	C.O.V τ_p (%)	C.O.V AC τ_{ld} (%)
150-mm-squared	1	500	337	915.7	99	34.0	6.2	7.4	7.9
	2	500	329	915.7	94	33.4	5.9		
	3	500	373	915.7	87	36.7	5.4		
	4	500	309	915.7	85	31.7	5.3		
	5	500	359	915.7	103	35.7	6.4		
300-mm-squared	1	500	343	743.9	61	34.5	4.6	6.4	6.0
	2	500	325	743.9	56	33.0	4.3		
	3	500	349	743.9	59	34.9	4.5		
	4	500	369	743.9	65	36.5	4.9		
	5	500	384	743.9	65	37.5	4.9		

Notes: σ_{n-s} = shearing nominal normal stress; τ_p = nominal shear stress at peak; AC σ_{ld} = area-corrected large-displacement normal stress; AC τ_{ld} = area-corrected large-displacement shear strength; ϕ_{s-p} = secant peak friction angle; ϕ_{s-ld} = secant large-displacement friction angle; C.O.V τ_p = coefficient of variation for peak shear strength; C.O.V AC τ_{ld} = coefficient of friction for area-corrected large-displacement shear strength.

^a Location of specimens within GCLD-Sample 2 are represented in Fig. 2.6.

^b Area-corrected shear and normal stresses were calculated at $\delta_h = 70$ mm in 150-mm shear tests and at $\delta_h = 100$ mm in 300-mm shear tests.

Table 2.5. Summary of internal direct shear tests on 150-mm and 300-mm specimens cut from the 1 m x 3 m area of GCL-D.

Specimen dimensions	Specimen No. ^a	Average peel strength in CMD (N/m)	Average peel strength in MD (N/m)	τ_p (kPa)
150-mm-squared	1	2420	2104	337
	2	1990	1956	329
	3	2087	2153	373
	4	2692	2461	309
	5	2481	2669	359
300-mm-squared	1	2328	2104	343
	2	2275	1956	325
	3	2617	2153	349
	4	2643	2461	369
	5	2617	2669	384

Notes: τ_p = nominal shear stress at peak

^a Location of specimens in the sample are shown in Fig. 2.6.

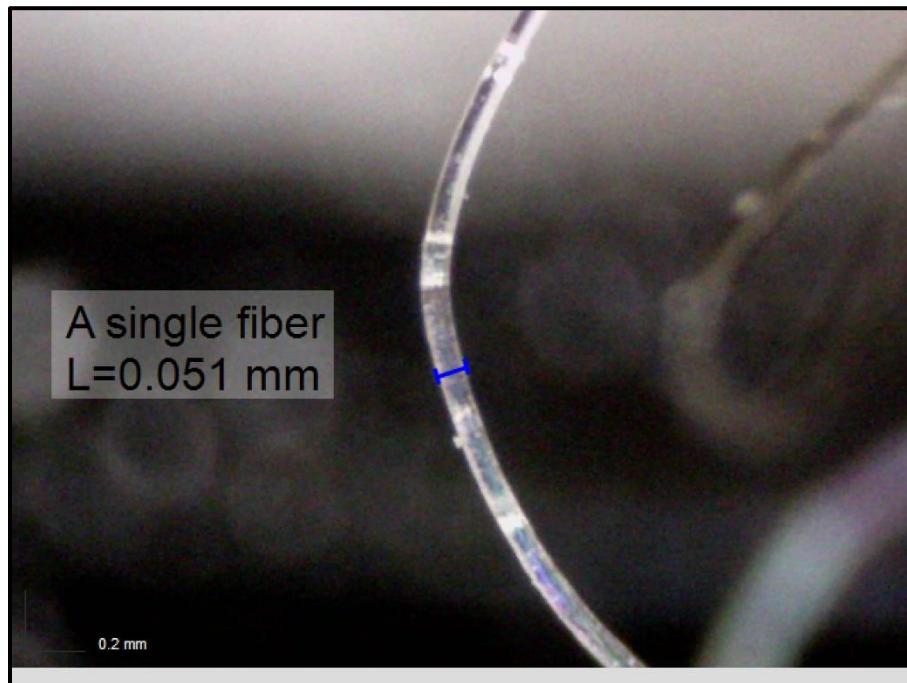


Fig. 2.1. Digital images of a (a) fiber bundle and (b) individual monofilament fiber captured with a stereoscope microscope to facilitate measurement of number of fibers per bundle and fiber diameter. Fiber bundle is from GCL-E.

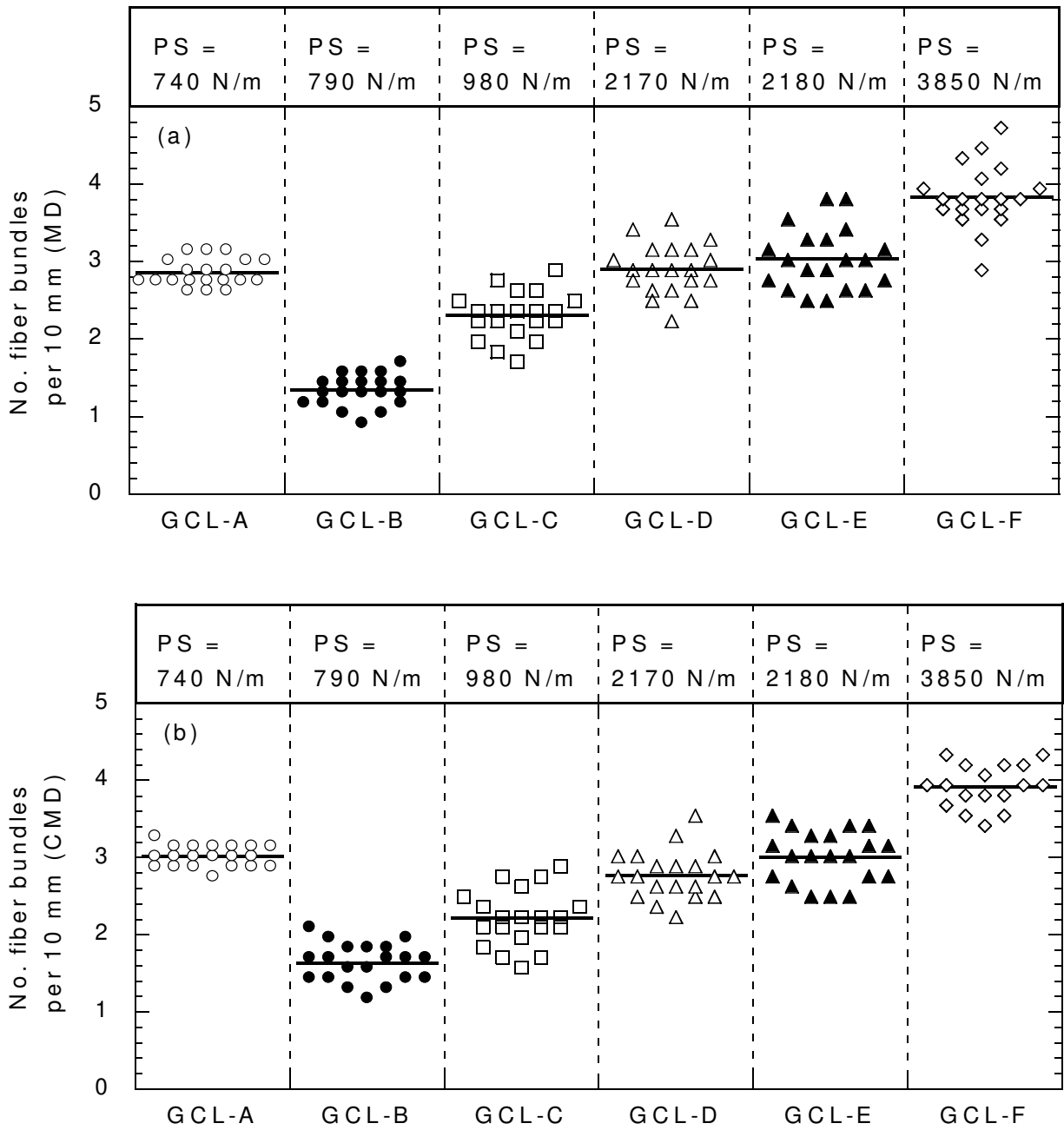


Fig. 2.2. Dot plots of the number of fiber bundles per centimeter in (a) machine direction (MD), and (b) cross-machine direction (CMD). Note: PS = GCL peel strength.

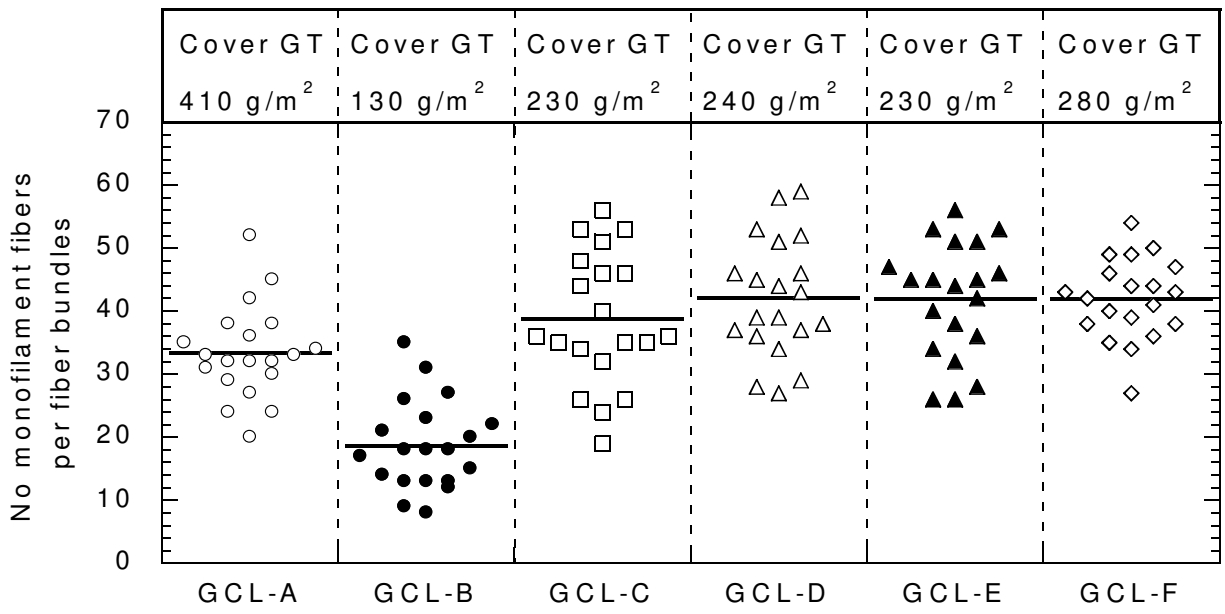


Fig. 2.3. Dot plots of the number of monofilament fibers per fiber bundles for 20 measurements on GCL-A, GCL-B, GCL-C, GCL-D, GCL-E, and GCL-F specimens. The mass of the cover geotextile of the GCL is provided for comparison.

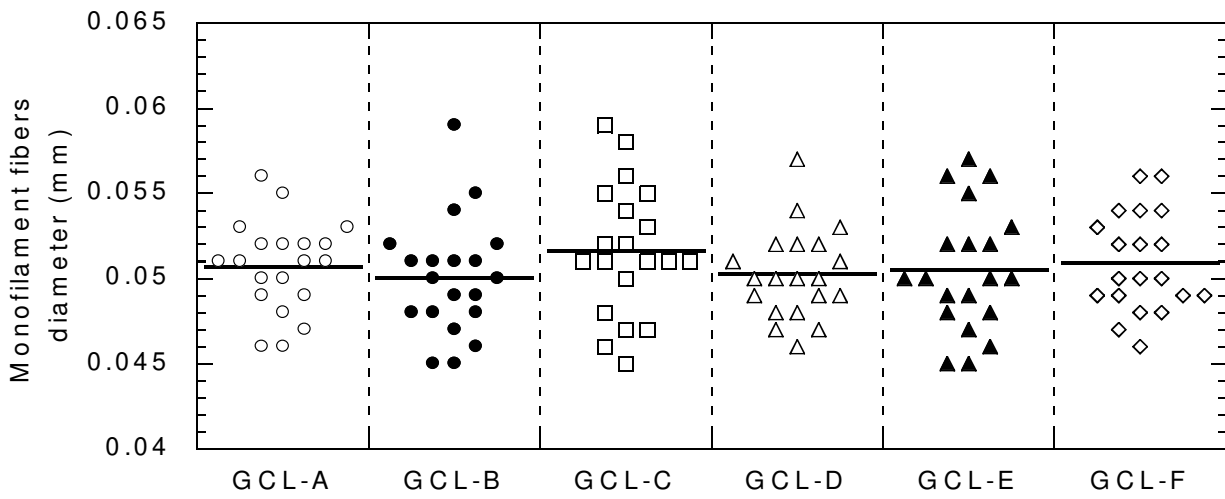


Fig. 2.4. Dot plots of monofilament fiber diameter for 20 measurements on GCL-A, GCL-B, GCL-C, GCL-D, GCL-E, and GCL-F specimens.

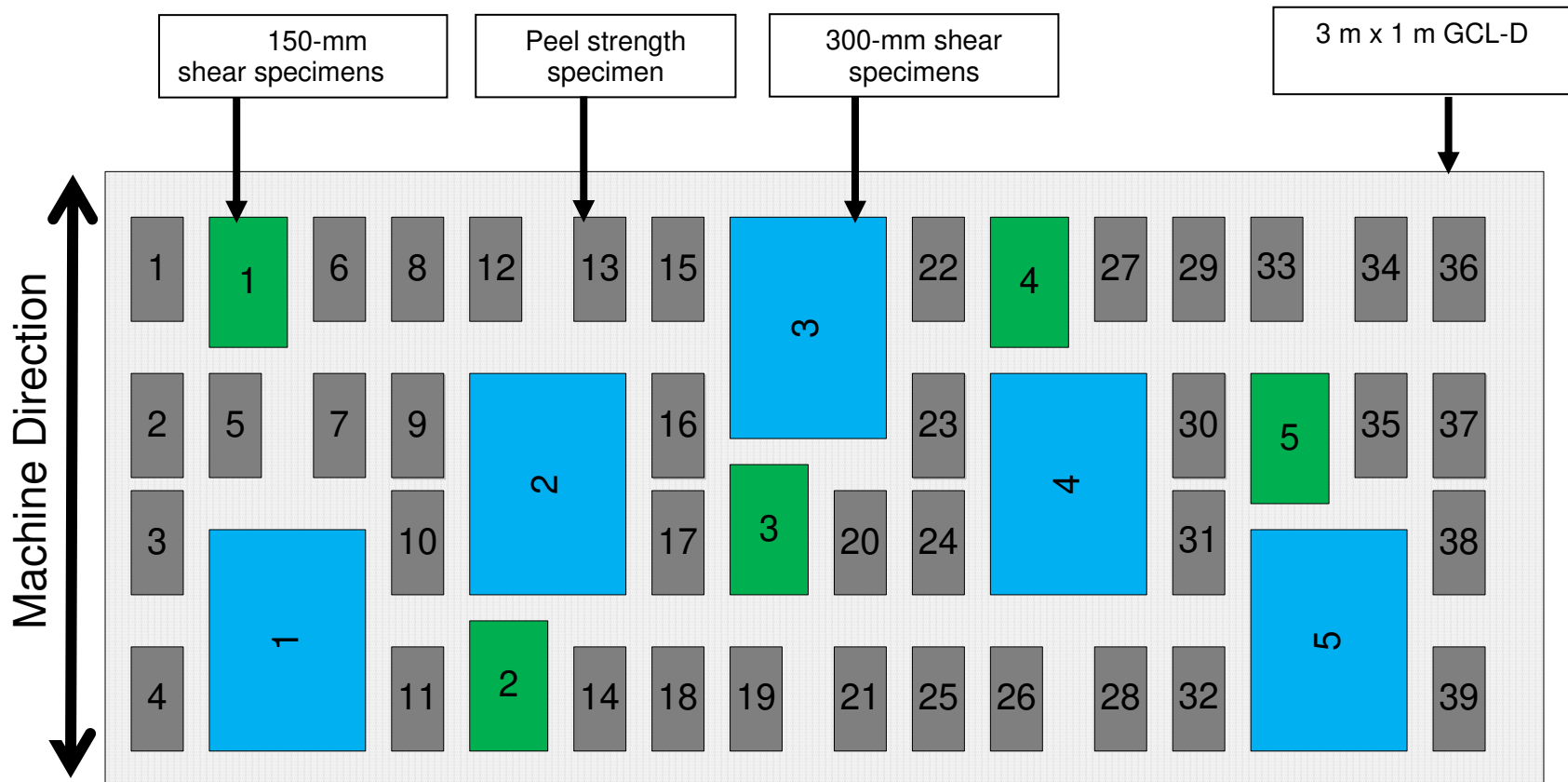


Fig. 2.5. Schematic of the 1 m x 3 m area of GCL-D that includes locations of 150-mm direct shear test specimens, 300-mm direct shear test specimens, and peel strength test specimens.

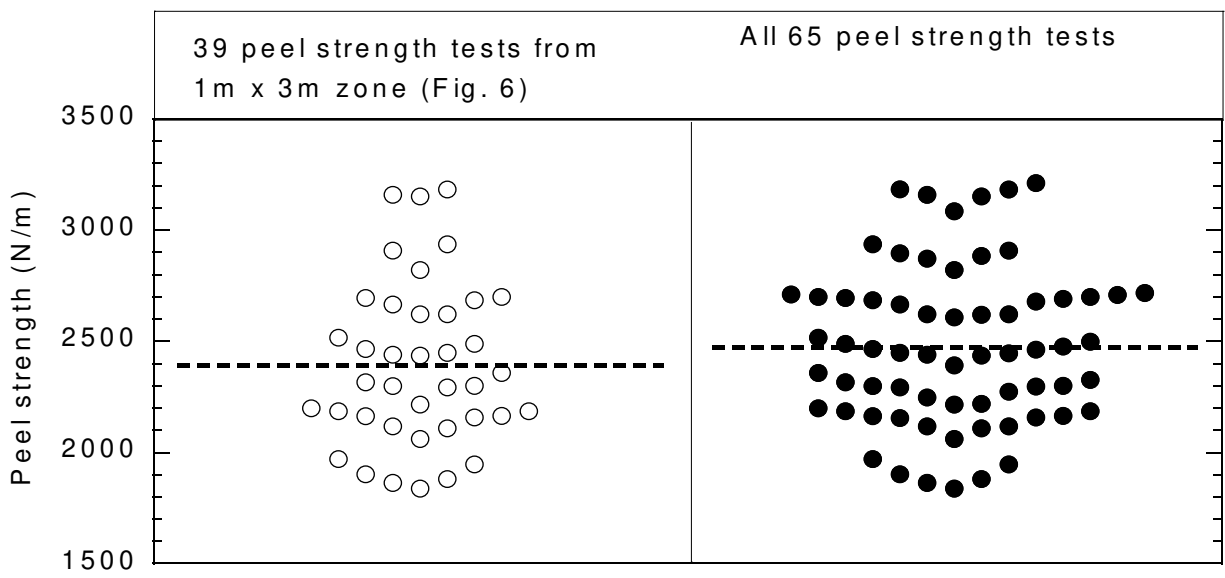


Fig. 2.6. Dot plot of peel strength test results for GCL-D.

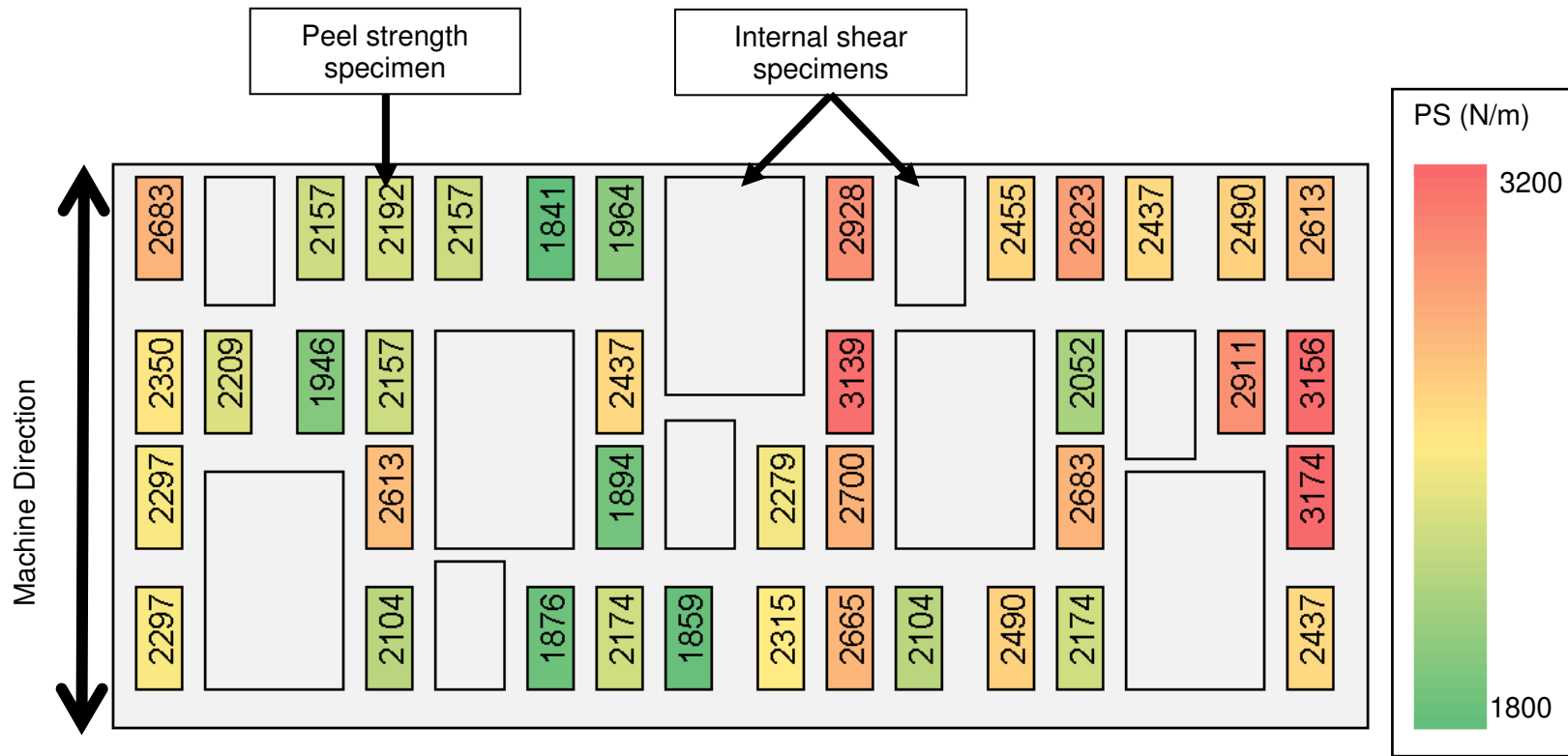


Fig. 2.7. Distribution of the peel strength within the 1 m x 3 m area sampled in GCL-D.

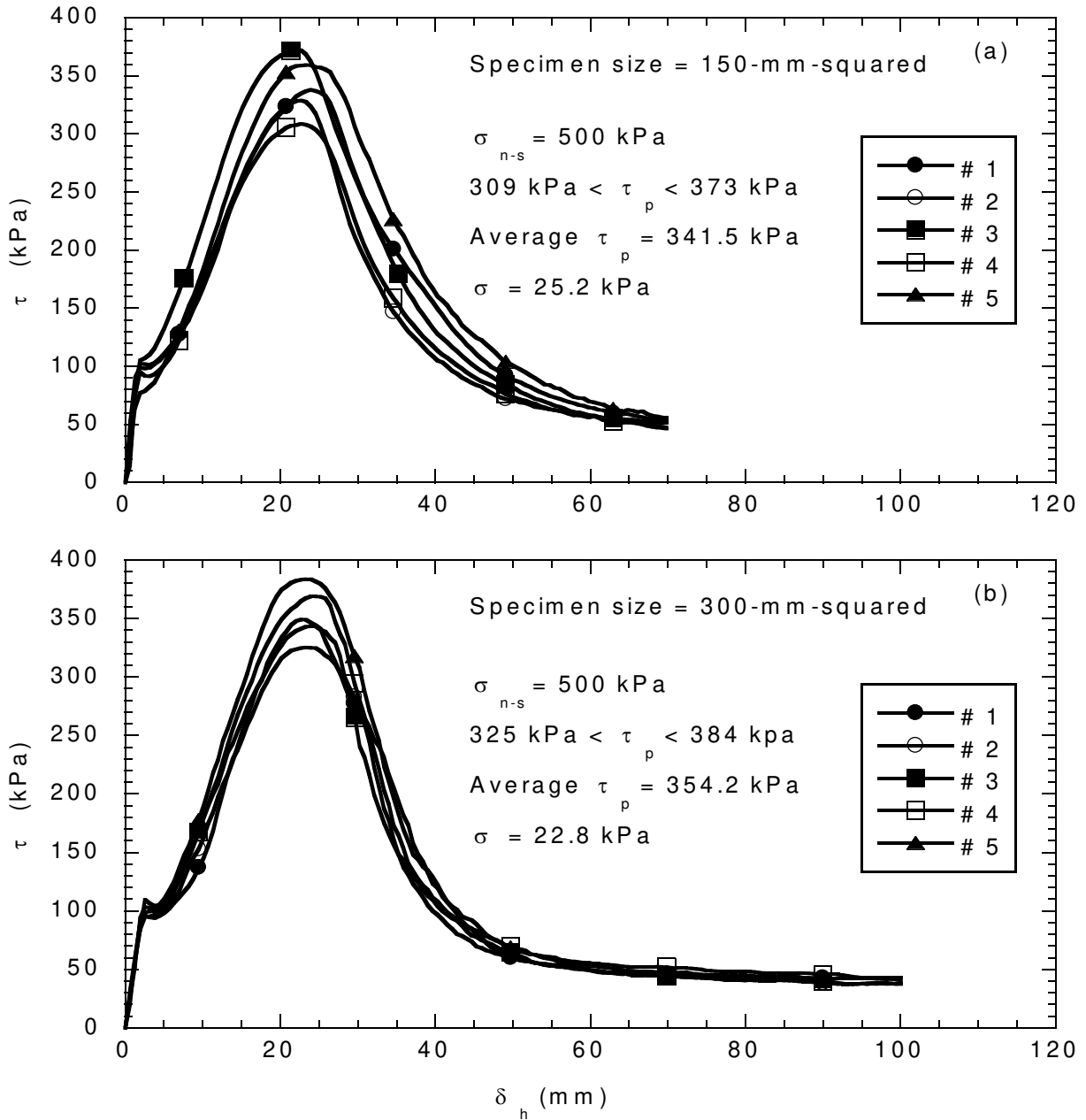


Fig. 2.8. Relationships between the shear stress (τ) and horizontal displacement (δ_h) from internal direct shear tests conducted under a shearing normal stress (σ_{n-s}) of 500 kPa on (a) 150-mm and (b) 300-mm GCL-D specimens.

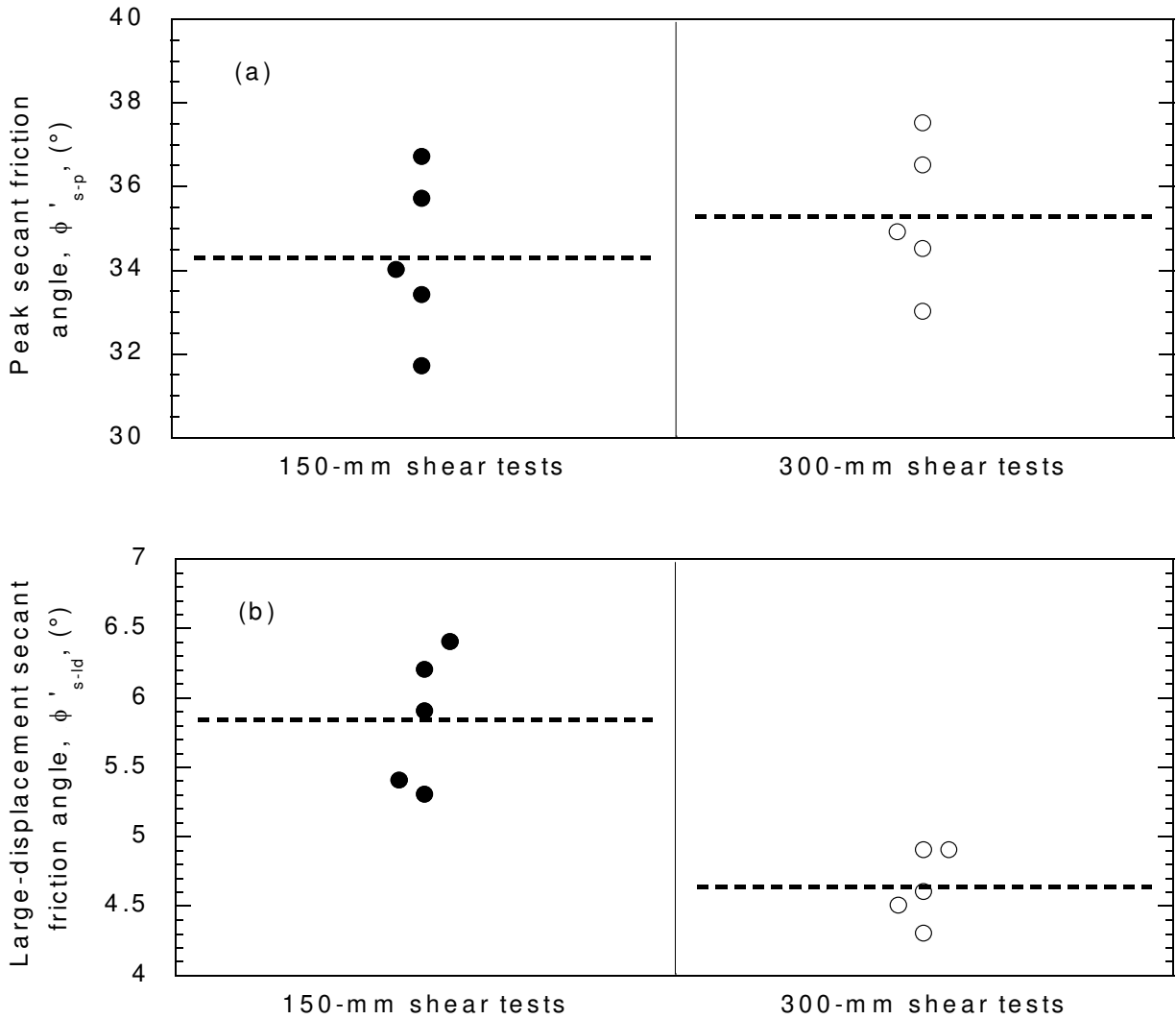


Fig. 2.9. Dot plots of (a) secant friction angle at peak shear strength (ϕ_{s-p}) and (b) secant friction angle at large-displacement shear strength (ϕ_{s-id}) for direct shear tests conducted on 150-mm and 300-mm GCL-D specimens

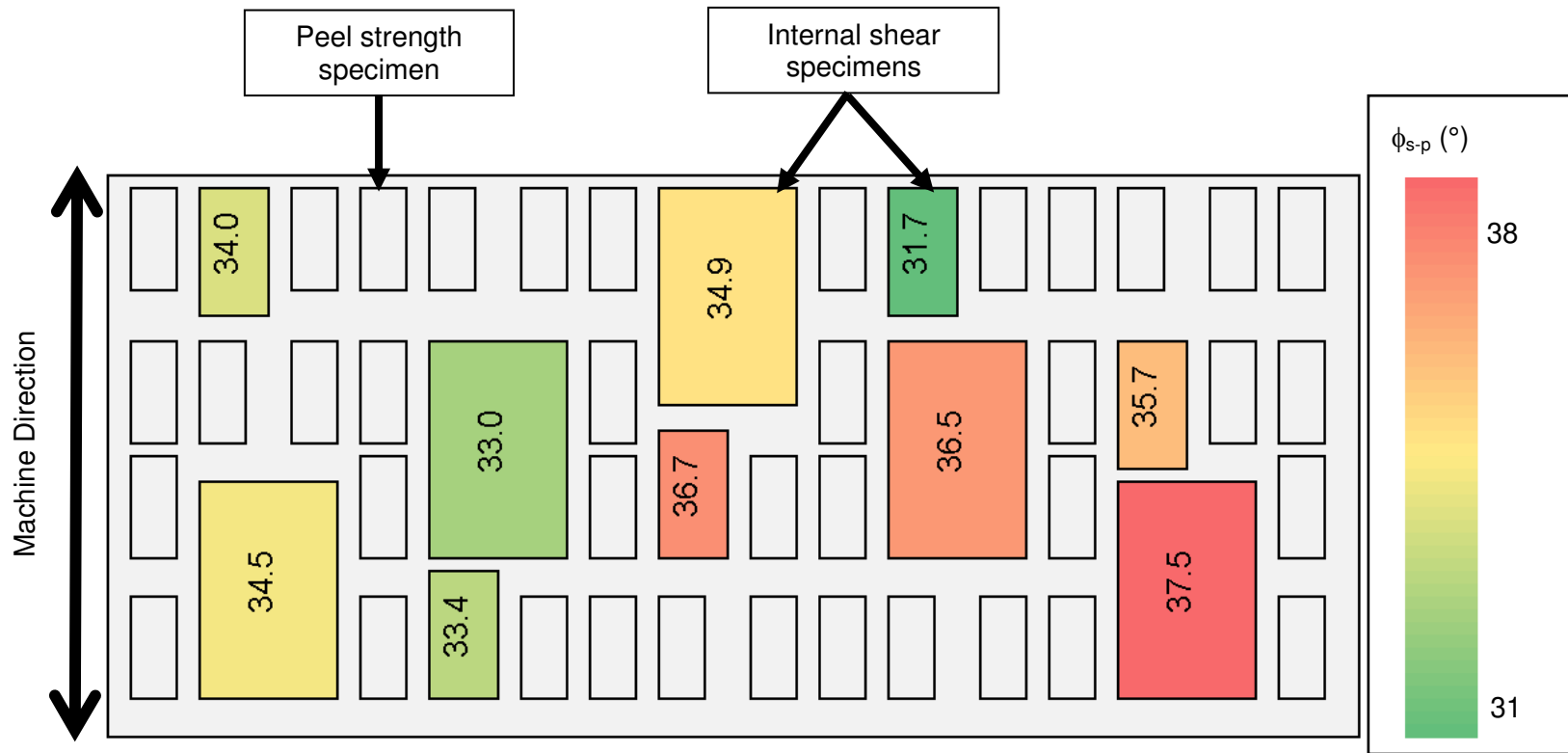


Fig. 2.10. Distribution of the secant friction angle at peak shear strength (ϕ_{s-p}) for the 150-mm and 300-mm direct shear test specimens from GCL-D.

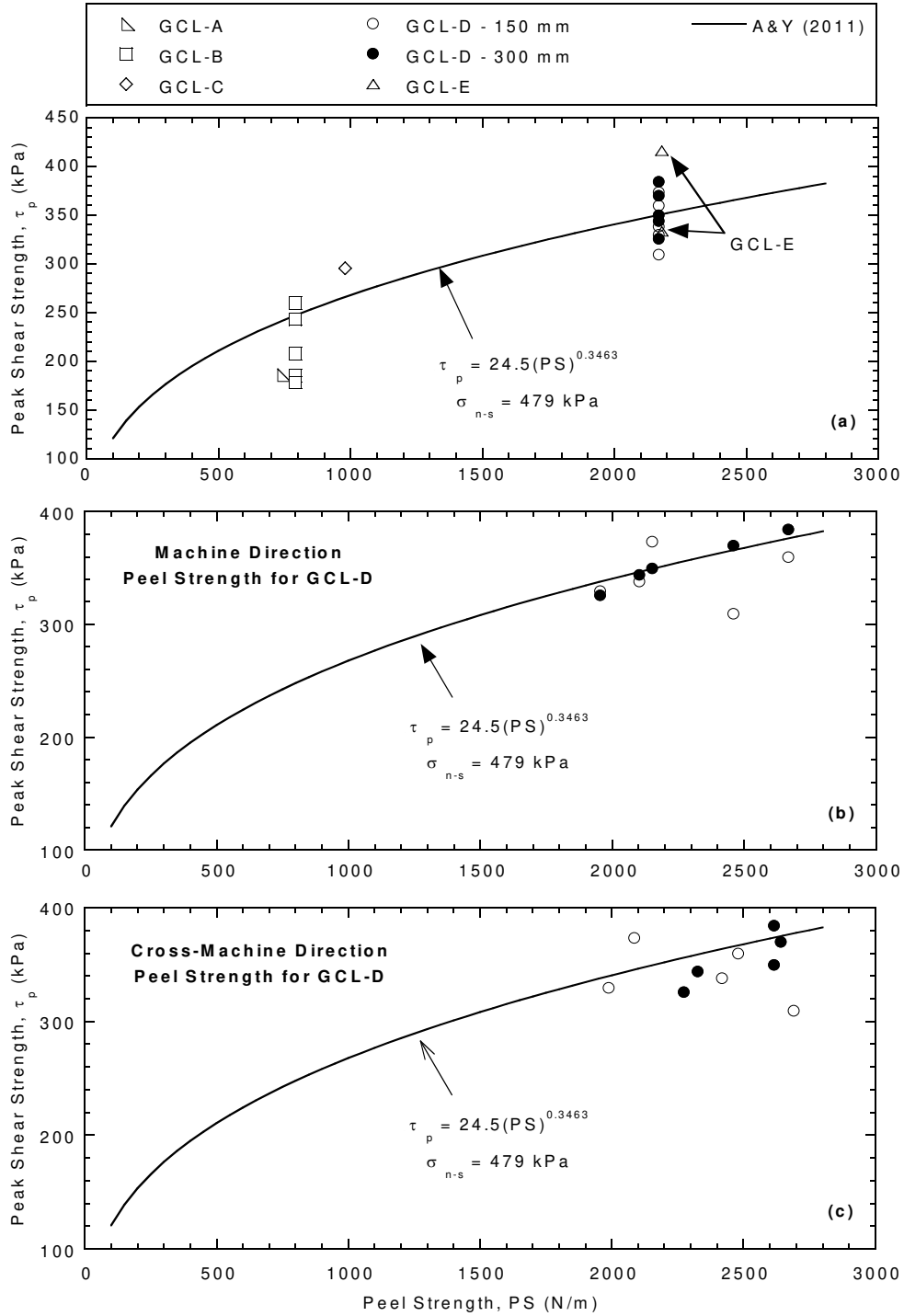


Fig. 2.11. Relationships between peak shear strength (τ_p) measured at a normal stress of (σ_{n-s}) of 500 kPa and peel strength (PS) based on the following: (a) manufacturer reported peel strength for GCL-A, GCL-B, GCL-C, GCL-D (150 mm & 300 mm tests), and GCL-F; (b) machine direction peel strength for GCL-D; and (c) cross-machine direction peel strength for GCL-D. Non-linear τ_p -PS relationship is from Athanassoupolous and Yuan (2011) based on τ_p measured under $\sigma_{n-s} = 479$ kPa.

CHAPTER 3: SHEAR MECHANISM OF TEXTURED GEOMEMBRANE – GEOSYNTHETIC CLAY LINER COMPOSITE SYSTEMS

3.1 Introduction

Geosynthetic clay liners (GCLs) are used in waste containment barrier systems due to their hydraulic performance, economic advantages, ease of installation, and self-healing properties (Guyonnet et al. 2009; Fox and Stark 2015). In side-slope and base liner systems of containment applications, GCLs are often combined with textured geomembranes (GMX). A GMX/GCL composite system is exposed to shear and normal stresses (Lupo 2010) that must be resisted internally within the GCL and along the GCL and GMX interface to prevent failure of the barrier system. Determining the critical shear strength (τ_{cr}) of the GMX/GCL composite system, which is defined herein as the minimum of the GCL internal shear strength and GMX/GCL interface shear strength, is important for the design and integrity of barrier systems.

The internal shear strength of GCLs often is enhanced via needle-punching, whereby fibers from a non-woven cover geotextile are punched through the bentonite layer and entangled into the carrier geotextile of the GCL. Internal shear strength of needle-punched reinforced GCLs (NP GCLs) increases due to contributions from tensile strength of the reinforcement fibers and connection strength between the fibers and carrier geotextile. The entangled fibers can be thermally fused to the carrier geotextile to create a heat-treated NP GCL (HT NP GCL) or if the fibers are not thermally-fused the GCL is a non-heat-treated NP GCL (NHT NP GCL).

Internal and interface shear strength of GCLs are commonly evaluated via direct shear and torsional ring shear tests. In previous studies on the internal shear strength of GCLs, researchers have evaluated the effects of hydration and consolidation procedures, shearing normal stress, displacement rate, GCL reinforcement type (i.e., needle-punching versus stitched bonding), heat-treatment method, specimen size, specimen peel strength (for NP GCLs),

dynamic loading, elevated temperature, hydration with non-standard solutions, and creep (e.g., Gilbert et al. 1996; Siebken et al. 1997; Trauger et al. 1997; Fox et al. 1998; Eid et al. 1999; Koerner et al. 2001; Zornberg et al. 2005; Fox et al. 2006; Muller et al. 2008; Fox et al. 2010; Fox and Ross 2011; Ghazizadeh and Bareither 2018 a,b; Bareither et al. 2018). In previous studies on the interface shear strength between a GMX and GCL, researchers have evaluated the effects of geotextile characteristics, GMX characteristics, surface roughness, monotonic loading, bentonite extrusion, polymer type, displacement rate, and out of plane deformation (Gilbert et al. 1996; Hewitt et al. 1997; Hillman and Stark 2001; Olsta and Swan 2001; Triplett and Fox 2001; Chiu and Fox 2004; Li and Gilbert 2006; Fox and Kim 2008; Vukelic´ et al. 2008; McCarthney et al. 2009; Zornberg and McCartney 2009; Chen et al. 2010; Bacas et al. 2011; Eid 2011; Fox and Ross 2011; Bacas et al. 2015; Hanson et al. 2015; Ross et al. 2015; Stark et al. 2015; Thielmann et al. 2016; Khilnani et al. 2017). Although these studies provide a wealth of valuable information, their focus typically has been either GCL internal shear strength or GMX/GCL interface shear strength. The shear behavior of GMX/GCL composite systems has not been holistically evaluated via coupled internal and interface shear tests to assess shear failure mechanisms and critical shear strength of GMX/GCL composite systems.

In studies focused on the internal shear strength of GCLs, failure is forced to occur internally within the GCL. However, internal failure of a GCL in a GMX/GCL composite system may never occur if the internal shear resistance of the GCL is higher than the mobilized shear resistance at the GMX/GCL interface (e.g., Stark et al. 2015). In contrast, studies focused on interface shear strength between GMX and GCL may not have observed internal shear deformation and potential internal failure of GCLs. Currently, shear behavior of GMX/GCL composite systems via evaluation of both GCL internal and GCL interface shear strength have only been the focus of select studies (e.g., Fox and Ross 2011). Therefore, there is a need to build on past research related to GCL internal and GMX/GCL interface shear strength to fully understand shear behavior and failure of GMX/GCL composite systems.

The objective of this study was to systematically evaluate GCL internal shear strength and GMX/GCL interface shear strength for different composite systems and a range of normal stress to define potential failure mechanisms. Direct shear tests on GMX/GCL composite systems were conducted to assess the following variables: (i) geotextile mass per area; (ii) geotextile type (i.e., woven versus non-woven); (iii) GCL peel strength; and (iv) GMX spike density. A total of 17 GCL-internal direct shear tests and 38 GMX/GCL interface direct shear tests were performed on three NHT NP GCLs with different peel strength and geotextile characteristics and two GMXs with different spike densities.

3.2 Shear Mechanism of GMX/GCL Composite System

A schematic of a GMX/GCL composite system subjected to shear stress (τ) and normal stress (σ_n) is shown in Fig. 3.1. Stresses applied to the GMX lead to a developed normal stress (σ_D) and shear stress (τ_D) along the GMX/GCL interface. Shear resistance of the GMX/GCL interface develops from (i) frictional resistance between the GMX and geotextile of the GCL and (ii) interlocking (i.e., hook and loop) between the geomembrane asperities (e.g., spikes) and geotextile fibers (Frost et al. 2001; Hebelier et al. 2005; Bacas et al. 2011, 2015). Shear resistance mechanisms controlling the interface shear strength and magnitude of τ_D are dependent on σ_n . At low σ_n , interlocking occurs superficially between GMX spikes and fibers of the geotextile, and τ_D is primarily attributed to frictional resistance. As σ_n increases, the geotextile of the GCL achieves more intimate contact with the GMX (i.e., interbedding) and interlocking of the GMX occurs within the geotextile structure. Interbedding of the geotextile with the GMX can also increase frictional resistance due to increased contact area. The improved interlocking and increased frictional resistance increases τ_D at high σ_n (Bacas et al. 2015).

Under a certain σ_n , τ and τ_D increase to a point at which three scenarios may occur that correspond to three distinct failure modes in a GMX/GCL composite system. In Scenario 1, τ_D

reaches a maximum mobilized shear stress (τ_{DMAX}) at the interface between the geotextile of a GCL and GMX, and slippage initiates between the GMX and GCL to create interface failure. Assuming that the internal peak shear strength of the GCL ($\tau_{\text{P-IN}}$) is considerably greater than τ_{DMAX} , negligible deformation of reinforcement fibers will develop such that internal GCL deformation is limited. Thus, for Scenario 1, the failure mode of the GMX/GCL composite system complete interface failure.

In Scenario 2, τ_{DMAX} is mobilized in a similar manner to Scenario 1 such that slippage occurs between the GMX and the GCL. However, in Scenario 2 τ_{DMAX} is sufficient to yield some internal deformation within the GCL and potentially led to failure of some reinforcement fibers. Despite this internal GCL deformation, τ_{DMAX} is still lower than $\tau_{\text{P-IN}}$, and complete GCL internal failure does not occur. The failure mode in Scenario 2 is defined as partial interface/internal failure.

In Scenario 3, τ_{D} increases to become comparable to $\tau_{\text{P-IN}}$ of the GCL. In this case, internal GCL failure occurs before full mobilization of τ_{DMAX} along the GMX/GCL interface and negligible slippage occurs between the GCL and GMX. The failure mode in Scenario 3 is defined as the complete internal failure.

The shear behavior and failure mode of a GMX/GCL composite system depends on factors affecting GCL internal shear strength and GMX/GCL interface shear strength, such as σ_n , geotextile and GMX characteristics, and GCL peel strength. Past research has shown a transition from complete interface, to partial interface/internal, to complete internal failure of GMX/GCL composite systems with increasing σ_n (e.g. Gilbert et al. 1996; Fox and Ross 2011; Theilmann et al. 2016; Khilanin et al. 2017). Furthermore, GCL peel strength and geotextile and geomembrane properties have been shown to affect the interface shear strength between a geotextile and GMX. For example, Gilbert et al. (1996) reported complete internal failure in GMX/GCL interface shear tests at σ_n as low as 13.8 kPa. In contrast, internal GCL failure was

not reported until σ_n exceeded 300 kPa in Eid (2011), 1300 kPa in Fox and Ross (2011), and never developed in Stark et al. (2015) for $\sigma_n = 2070$ kPa. These differences in failure modes are attributed to the differences in geotextile and GMX properties as well as GCL peel strength.

3.3 Materials

3.3.1 Geosynthetic Clay Liners Specimens

The characteristics and properties of the three non-heat treated, needle-punched GCLs used in this study are in Table **3.1**. These GCLs were commercially available, included polypropylene geotextiles, and had the same granular bentonite. However, the GCLs had unique peel strength (PS) and geotextile characteristics. Peel strength was provided by the manufacturer and ranged from 980 N/m (GCL1) to 3850 N/m (GCL3). The carrier and cover geotextiles were all non-woven geotextiles with different mass per area, except for the carrier geotextile of the GCL2, which was woven (Table **3.1**). Characterization of the GCLs conducted on twenty 100 mm x 100 mm specimens cut from each GCL roll evaluated the carrier and cover geotextiles mass per area and bentonite mass per area. GCL3 had the highest geotextile mass per area and GCL2 had the lowest mass per area. Bentonite mass per area ranged from 4220 g/m² to 5570 g/m² among the three GCLs (Table **3.1**).

3.3.2 Textured Geomembrane Specimens

Characteristics of GMX1 and GMX2 are tabulated in Table **3.2**. Both GMXs included a spike-structured texturing and were made of linear low density polyethylene. They had the same average core thickness (1.5 mm) and average asperity height (0.5 mm), but had different spike spacing in the machine direction and cross-machine direction that contributed to different spike densities. Spike density was computed for a 10-cm x 10-cm area, and GMX1 had a spike density ≈ 340 spikes/100-cm² and GMX2 had a spike density ≈ 840 spikes/100-cm².

3.3.3 GMX/GCL Composite Systems

A summary of the eight GMX/GCL composite systems evaluated in this study is in Table 3.3. These composite systems consisted of GMX1 or GMX2 placed on top of either the carrier or cover geotextile of GCL1, GCL2, or GCL3. The following nomenclature was adopted herein to distinguish the composite systems: GCL#-COGT/GMX# and GCL#-CAGT/GMX#. In this nomenclature, GCL# refers to the GCL used in the composite system (i.e., GCL1, GCL2, or GCL3). The COGT and CAGT refer to the cover (CO) and carrier (CA) geotextile (GT), respectively, of the GCL that was in contact with the GMX during shearing. The GMX# refers to the GMX used in the composite system (i.e., GMX1 or GMX2). For example, the composite systems GCL1-COGT/GMX1, indicates that shear testing was conducted on the GMX1.

3.4 Experimental Procedure

Experiments were performed with a displacement-controlled direct shear apparatus. All internal and interface shear tests were performed on 150 mm by 150 mm GCL specimens instead of conventional 300 mm specimens. A comprehensive discussion on the direct shear apparatus and verification that the 150 mm test specimens yield similar shear behavior to larger specimens is in Bareither et al. (2018).

The GMX and GCL specimens were cut along machine direction following recommendations in ASTM D6072. The GCL specimens were cut to initial dimensions of 150-mm wide by approximately 200-mm long in machine direction to facilitate gripping the GCL in the direct of shear. The GMX specimens were cut to dimensions of 175 mm by 300 mm, with the longer dimension in the direction of shear. The longer GMX specimens ensured that the GCL remained in contact with the GMX during the entire duration of shear displacement.

Specimen hydration and consolidation were performed according to a 2-stage procedure (e.g., Fox et al. 1998; Bareither et al. 2018). In the hydration stage (i.e., first stage), GCL specimens were sandwiched between two perforated PVC plates and hydrated in a plastic bin

with de-ionized water (DIW) for 48 hr under $\sigma_n = 20$ kPa. The hydration stage was similar for all GCL specimens tested in the GCL-internal and GMX/GCL interface shear tests.

At the end of the hydration, specimens were transferred to the direct shear box to start consolidation (i.e., second stage). Specimens prepared for the internal shear tests were sandwiched between two 150-mm by 150-mm pyramid-tooth plates for consolidation and subsequent shearing. The extra 50 mm of geotextile along the shear direction were clamped to both ends of the pyramid-tooth plates in the direction of shear. The GCL specimens prepared for interface shear tests were secured to a single pyramid tooth plate and placed in contact with a GMX. The GMX was sandwiched between the GCL (COGT or CAGT based on desired shearing surface) and a 300-mm by 300-mm pyramid-tooth plate. Thus, pyramid teeth gripped into and secured the GMX in place during shear. Consolidation initiated inside the direct shear apparatus via reapplying $\sigma_n = 20$ kPa, and subsequently doubling σ_n every 4-6 hr to obtain the target normal stress for shearing (σ_{n-s}). Once σ_{n-s} was obtained, test specimens were equilibrated in the shear box under σ_{n-s} for at least 24 hr.

All internal and interface shear tests were conducted at a horizontal displacement rate of 0.1 mm/min to a horizontal displacement (δ_h) ≈ 70 mm. This magnitude of horizontal displacement was sufficient to capture peak shear behavior in all internal and interface shear tests, but may underestimate residual shear strength of NP GCLs in the internal shear tests (Fox and Stark 2015). Therefore, the large-displacement shear stress at $\delta_h = 70$ mm (τ_{ld}) is used herein for the analysis of the internal and interface shear behavior of GCLs.

The shear area of the GCL specimens during the internal shear tests decreased with horizontal displacement due to offset between the upper and lower shear platens. Prior to reaching peak shear strength, needle-punched fibers remain in contact with the geotextiles and an area correction was not required to analyze peak internal shear strength. However, once peak shear strength was reached, failure of reinforcement fibers initiated and increased with

increasing horizontal displacement. Therefore, an area corrected normal stress and area-corrected large-displacement shear stress were computed for the stress state at large displacement (Bareither et al. 2018). Nominal stresses (i.e., non-area-corrected) were used for peak and large displacement shear strength for all interface shear tests since the full shear plane area of the GCL remained in contact with the GMX.

At the end of the internal shear tests, GCL specimens were visually inspected to ensure successful internal shear failure. Any signs of stress localization, geotextile tearing, geotextile elongation, or slippage at the gripping surface indicated unsuccessful internal shear of the GCLs. Visual inspection of specimens was also performed after interface shear tests on both GMX and GCL to help identify the failure mode of the GMX/GCL composite systems.

3.5 Results

A summary of the GCL internal direct shear tests is in Table 3.4 and includes σ_{n-s} , τ_p , secant friction angle at peak shear strength (ϕ_{s-p}), horizontal displacement at peak shear strength (δ_{h-p}), area-corrected normal stress at $\delta_h = 70$ mm (AC σ_{70}), area-corrected large-displacement shear strength at $\delta_h = 70$ mm (AC τ_{70}), and post-peak strength reduction ratio ($R\tau$). The $R\tau$ was computed based on Eq. 3.1. for the internal shear tests.

$$R\tau = \frac{AC \tau_{70} / AC \sigma_{70}}{\tau_p / \sigma_{n-s}} \quad (3.1)$$

The ϕ_{s-p} , δ_{h-p} , AC σ_{70} , AC τ_{70} , and $R\tau$ were not defined in Table 3.4 for GCL3 due to unsuccessful internal shearing (described subsequently).

Summaries of the GMX/GCL interface direct shear tests are in Table 3.5, and include σ_{n-s} , τ_p , ϕ_{s-p} , δ_{h-p} , large-displacement shear strength at $\delta_h = 70$ mm (τ_{70}), $R\tau$, and observed failure mode. The $R\tau$ was computed based on Eq. 3.2. for the interface shear tests.

$$R\tau = \frac{\tau_{70}}{\tau_p} \quad (3.2)$$

Different definitions of $R\tau$ for the internal and interface shear tests were due to the use of nominal versus area-corrected shear and normal stresses in the analysis of the large-displacement shear stress.

3.5.1 GCL Internal Shear Tests

Relationships of shear stress versus horizontal displacement for internal shear tests on GCL1, GCL2, and GCL3 are shown in Fig. 3.2. The internal shear tests were conducted on each GCL for σ_{n-s} in the range of 80 kPa to 2000 kPa. Shear stress measured for GCL1 and GCL2 increased to a well-defined peak that coincides with maximum internal shear resistance of the GCL, and then decreased with increasing displacement, which is typical shear behavior for reinforced GCLs (e.g., Gilbert et al. 1996; Fox et al. 1998; Zornberg et al. 2005; Fox and Ross 2011; Fox and Stark 2015; Bareither et al. 2018). The post-peak strength reduction was attributed to decreasing internal shear resistance of NP GCLs as fiber bundles disentangle from the carrier geotextile and/or experience tensile rupture. In post shear inspection of GCL1 and GCL2 specimens, fiber disentanglement, fiber rupture, or a combination of both were observed without any sign of stress-localization, geotextile tearing, geotextile elongation, or slippage at the gripping surface. The τ - δ_h relationships (Fig. 3.2a and Fig. 3.2b) and post-shear specimen inspection support successful internal shearing of GCL1 and GCL2.

Contrary to the shear behavior of GCL1 and GCL2, irregularities were observed in τ - δ_h relationships of the high peel strength GCL3 (Fig. 3.2c). For example, peak strength and post-peak strength reduction were not observed for $\sigma_{n-s} \leq 500$ kPa. Although peak strength and post-peak strength reduction were observed for $\sigma_{n-s} \geq 1000$ kPa, τ - δ_h relationships at higher σ_{n-s} exhibited abnormal undulations not observed in GCLs undergoing complete internal failure (e.g.,

Fig. 3.2a or Fig. 3.2b). Irregularities in the τ - δ_h relationships of GCL3 were indications of unsuccessful internal shearing, as suggested by Fox and Kim (2008) and Fox and Stark (2015).

Post shear pictures of GCL3 specimens from the internal shear tests are shown in Fig. 3.3a for $\sigma_{n-s} = 160$ kPa and in Fig. 3.3b for $\sigma_{n-s} = 1000$ kPa. For $\sigma_{n-s} \leq 500$ kPa, there were no signs of internal shear behavior (e.g., fiber disentanglement, tensile rupture), but instead a combination of geotextile elongation and geotextile tearing along the surface in contact with the gripping system. For $\sigma_{n-s} \geq 1000$ kPa, varying amounts of fiber bundle disentanglement were observed that indicated some internal deformation occurred. However, there were also indications of geotextile elongation, specimen necking, and geotextile separation (near the clamping area), which implied that complete internal failure was not successful.

The failure surface is forced to occur internally within a GCL when conducted an internal shear test. However, successful internal shearing only occurs if the applied shear force can be completely transferred to the internal region of the GCL to mobilize the maximum internal shear resistance. Unsuccessful internal shear failure of GCL-3 was not due to inefficiency of the gripping system (i.e., pyramid tooth plates), as this system surpassed requirements of ASTM D6243. The inability of transferring shear force to the internal region of GCL3 was attributed to low tensile strength of the carrier and cover geotextiles relative to the high internal shear strength. The PS of GCL3 (3850 N/m) was nearly double that of GCL2 (2180 N/m), and can be used as an indicator for a NP GCL that may be difficult to shear internally without excessively strong carrier and cover geotextiles. Unsuccessful internal failure of high peel strength NP GCLs has also been reported in ASTM D 6243, Fox et al. (1998), Fox and Ross (2011), Fox and Stark (2015), and Bareither et al. (2018).

The unsuccessful internal shearing of the high peel strength GCL3 is noteworthy. Considering that geosynthetic or earthen materials in contact with GCLs in waste containment systems are unlikely to provide a better gripping with the GCLs relative to the pyramid tooth

plates used in the internal shear tests, internal failure of GCL3 is unlikely to occur in field applications.

3.5.2 GMX/GCL Interface Shear Tests

Relationships of shear stress versus horizontal displacement for interface shear tests on GCL1, GCL2, and GCL3 are shown in Fig. 3.4, Fig. 3.5, and Fig. 3.6, respectively. All DC-IF tests were performed at $\sigma_{n-s} = 100, 300, 500, 1000, \text{ and } 2000$ kPa except for GCL3-COGT/GMX2 (Fig. 3.6b), which was only tested at $\sigma_{n-s} = 100, 300, 500$ kPa due to limited resources. Each τ - δ_h data set for an interface shear test exhibited peak shear strength and post-peak strength reduction, which is common behavior of GMX/GCL interfaces (e.g. Triplett and Fox 2001; McCartney et al. 2009; Fox and Stark 2015; Thielmann et al. 2016). However, τ - δ_h data were unique for different GMX/GCL composite systems and for different σ_{n-s} , which were attributed to whether the GMX/GCL composite was undergoing complete interface failure, partial interface/internal failure, or complete internal failure.

Failure modes of the GMX/GCL composite systems were determined via post-shear specimen inspection. An example of (i) complete interface failure, (ii) complete internal failure, and (iii) partial interface/internal failure are shown in Fig. 3.7. The photograph in Fig. 3.7a is for GCL1-COGT/GMX1 sheared at $\sigma_{n-s} = 500$ kPa (τ - δ_h data in Fig. 3.4a) that documents complete interface failure. The parallel lines across the specimen in the direction of shear developed from the GMX spikes as slippage occurred between the GCL and GMX. Furthermore, there was no indication of internal shear deformation. Shear behavior characteristic of complete interface failure was development of a relatively low horizontal deformation at peak shear strength (δ_{h-p}), low post-peak shear stress reduction, and large-displacement shear strength greater than a corresponding larger-displacement shear strength for an internal shear test. The GMX/GCL composites that experienced complete interface failure are defined in Table 3.5.

The photograph in Fig. 3.7b is for GCL1-CAGT/GMX1 at 2000 kPa that shows complete internal failure. In post-shear GMX/GCL specimens where complete internal failure was identified, the carrier geotextile of the GCL completely separated from the GCL as reinforcement fibers were either ruptured or disentangled. Furthermore, there were no signs of slippage or relative displacement between the GMX and GCL. The shear behavior characteristic of complete internal failure was similar to that described for the internal GCL shear tests, whereby shear stress increased to a peak and then decreased with continuous horizontal deformation that represented the post-peak strength reduction. The GMX/GCL composites that experienced complete interface failure are defined in Table 3.5.

The photograph in Fig. 3.7c is for GCL1-COGT/GMX2 at 300 kPa that shows partial interface/internal failure. The parallel lines across the geotextile indicate slippage between the GCL and GMX, similar to the observation in Fig. 3.7a. However, indications of reinforcement fiber failure and internal deformation were also observed, which rendered the failure mode partial interface/internal. The shear behavior characteristic of partial interface/internal was not consistent since the amount of interface relative to internal failure changed the observed shear behavior. Thus, successful identification of the partial interface/internal failure mode relied on post-shear specimen inspection. The GMX/GCL composites that experienced partial interface/internal failure are defined in Table 3.5.

3.6 Analysis

Differences between the failure modes of GMX/GCL composite systems were attributed to variation in GCL peel strength, geotextile type, geotextile mass per area, and GMX spike density. Effects of the aforementioned parameters on the failure mode of a GMX/GCL composite system was evaluated via grouping different GMX/GCL interface shear tests to isolate specific variables and comparing to GCL internal shear behavior. The subsequent analysis of GMX/GCL composite system shear behavior includes the following relationships: (i)

peak shear strength – τ_p versus σ_{n-s} ; (ii) large-displacement shear strength – τ_{70} versus σ_{n-s} or AC τ_{70} versus AC σ_{n-s} ; (iii) shear displacement at peak strength – δ_{h-p} versus σ_{n-s} ; and (iv) post-peak shear reduction – $R\tau$ versus σ_{n-s} .

3.6.1 Internal Shear Behavior of Needle-Punched GCLs

Relationships of τ_p versus σ_{n-s} , δ_{h-p} versus σ_{n-s} , AC τ_{70} versus AC σ_{70} , and $R\tau$ versus σ_{n-s} from the internal shear tests on GCL1, GCL2, and GCL 3 are shown in Fig. 3.8. Data from GCL3 are only included for the τ_p versus σ_{n-s} relationship (Fig. 3.8a) due to the unsuccessful internal failure. In addition, τ_p plotted in Fig. 3.8a for GCL3 represent the maximum shear stress during the internal shear test and not necessarily the actual internal peak shear strength.

Bi-linear shear strength envelopes for τ_p were defined for GCL1 and GCL2 based on $\sigma_{n-s} \leq 500$ kPa and $\sigma_{n-s} \geq 500$ kPa (Fig. 3.8a). The corresponding friction angles (ϕ_p) and cohesion intercepts (c_p) for the strength envelopes are shown in Fig. 3.8a. An increase in peel strength from GCL1 (PS = 980 N/m) to GCL2 (PS = 2180 N/m) increased peak shear strength for a given normal stress. Furthermore, even though internal failure of GCL3 was unsuccessful, the maximum shear stress measured for GCL3 was higher than the peak shear strength of both GCLs. The increase in shear strength with increasing peel strength agrees with previous research (e.g., Athanassopoulos and Yuan 2011; Fox and Stark 2015; Bareither et al. 2018).

The δ_{h-p} versus σ_{n-s} relationships shown in Fig. 3.8b depict a change in behavior at $\sigma_{n-s} \approx 500$ kPa, whereby δ_{h-p} decreases for $\sigma_{n-s} \leq 500$ kPa and then remains approximately constant with continued increase in σ_{n-s} . This bi-linear behavior coincided with the change in slope of the strength envelopes identified in Fig. 3.8a and was attributed to a change in internal shear mechanism of NP GCLs from disentanglement of reinforcement fiber bundles from the carrier geotextile at low σ_{n-s} to internal rupture of fibers at high σ_{n-s} (Gilbert et al. 1996; Bacas et al. 2013; Thielmann et al. 2016; Bareither et al. 2018). Despite the similarity in the δ_{h-p} trends as a

function of σ_{n-s} , δ_{h-p} of GCL1 was always higher than GCL2. The higher δ_{h-p} was hypothesized to be due to the woven carrier geotextile of GCL1 relative to the non-woven carrier geotextile of GCL2. The non-woven carrier geotextile hypothetically had reduced entanglement potential with the reinforcement fibers relative to the woven carrier geotextile, which resulted in a lower δ_{h-p} .

The AC τ_{70} versus AC σ_{70} data for GCL1 and GCL2 in Fig. 3.8c reveals that the area correction applied to compute AC σ_{70} yielded a substantial increase in normal stress relative to σ_{n-s} . Dash lines in Fig. 3.8c correspond to different values of ϕ_{ld} . The ϕ_{ld} of GCL1 and GCL2 plot within a range of 2° to 6°, which is comparable to the previously reported ϕ_{ld} (e.g., Fox and Ross 2011; Fox et al. 2015; Bareither et al. 2018).

The relationship between R_τ and σ_{n-s} is shown in in Fig. 3.8d for internal shear tests on GCL1 and GCL2. Based on the definition, R_τ represents the amount of post-peak strength reduction in NP GCLs. The higher R_τ of the GCL1 was attributed to the comparable AC τ_{70} of both GCLs and lower τ_p of GCL1 compared to GCL2. Thus, the higher value of R_τ for GCL1 indicates lower overall post-peak strength reduction relative to GCL2.

3.6.2 Effect of Geotextile Mass per Area on GMX/GCL Shear Behavior

The effect of geotextile mass per area on the shear behavior of GMX/GCL composite systems was evaluated via interface shear tests that incorporated GCL1 and GMX1. The non-woven carrier geotextile (CAGT) of GCL1 had mass per area = 260 g/m², whereas the non-woven cover geotextile (COGT) of GCL1 had mass per area = 230 g/m². Interface shear tests conducted with GCL1 and GMX1 were such that the CAGT was in contact with GMX1 for one series of tests (GCL1-CAGT/GMX1) and the COGT was in contact with GMX1 for another series of tests (GCL1-COGT/GMX1). These GMX/GCL composite systems isolated the variable of mass per area of a non-woven geotextile such that any differences in shear behavior between the two composite systems could be attributed to the geotextiles in contact with GMX1.

Relationships of τ_p versus σ_{n-s} , δ_{h-p} versus σ_{n-s} , τ_{ld} versus σ_{ld} , and $R\tau$ versus σ_{n-s} for interface shear tests on GCL1-COGT/GMX1 and GCL1-CAGT/GMX1 are shown in Fig. 3.9 along with data from the internal shear tests on GCL1 for comparison. Post shear pictures of GCL1 specimens in each of the interface shear tests are included in Fig. 3.10. Assessment of post-shear specimens helped to identify the failure mode of each interface shear test (Table 3.5).

Peak shear strength plotted in Fig. 3.9a indicates that internal τ_p of GCL1 was higher than τ_p from the interface shear tests on GCL1 with the cover or carrier geotextile in contact with GMX1. This observation indicates that critical strength of the GMX1/GCL1 composite system was always dependent on the GMX1/GCL1 interface. Post-shear specimen inspection suggested either complete interface or partial interface/internal occurred for all test specimens (Table 3.5). The one exception was the interface shear test with the CAGT in contact with GMX1 at $\sigma_{n-s} = 2000$ kPa where internal failure was observed (Table 3.5). Although τ_p measured in the interface shear test with CAGT in contact with GMX was lower than τ_p of GCL1 at $\sigma_{n-s} \leq 2000$ kPa, internal failure was identified and the small difference in τ_p (Fig. 3.9a) was attributed to the lower stiffness of the GMX1 spikes compared to the metal teeth of the pyramid tooth plates.

Shear behavior of the GMX1/GCL1 composite systems with either the carrier or cover geotextile in contact with GMX1 was similar for $\sigma_{n-s} \leq 500$ kPa (Fig. 3.9a to Fig. 3.9d), and failure mode was identified as complete interface failure (Table 3.5). However, shear behavior of these two composite systems were completely different relative to the internal shear behavior of GCL1. For example, lower τ_p and δ_{h-p} as well as higher τ_{ld} and $R\tau$ were observed for composite systems relative to internal shear of GCL1. The lower δ_{h-p} was due to quick mobilization of the maximum developed shear stress at the GMX/GCL interface that allowed interface slippage relative to the available internal peak strength of GCL1. The higher τ_{ld} of the composite systems

relative to τ_{ld} of GCL1 was due to large-displacement shearing at the interface of the geotextile and GMX1 versus shearing between hydrated bentonite and geotextile. The higher τ_{ld} and lower τ_p of the composite systems resulted in higher $R\tau$ relative to internal shear behavior of GCL1.

The influence of geotextile mass per area on the shear behavior of GMX1/GCL1 composite systems was most observed for interface shear tests at $\sigma_{n-s} = 1000$ kPa and 2000 kPa. At $\sigma_{n-s} = 1000$ kPa, complete interface failure was identified for the lower mass per area cover geotextile in contact with GMX1 as opposed to partial interface/internal failure for the higher mass per area carrier geotextile in contact with GMX1. Due to the transition in failure mode, the large-displacement strength envelope for the carrier geotextile of GCL1 in contact with GMX1 approaches the large-displacement strength envelope of GCL1 at $\sigma_{n-s} \geq 1000$ kPa (Fig. 3.9c)

At low normal stress, interlocking between the non-woven geotextile and spikes of a GMX developed superficially, such that frictional resistance between the GMX and geotextile was the dominant mechanism for shear resistance. Therefore, differences in mass per area of the non-woven geotextiles in contact with the GMX did not result in considerably different shear behavior. As normal stress increased, interlocking between the non-woven geotextile and spikes of a GMX was more effective and an increase in mass per area of a non-woven geotextile enhanced interlocking. This enhanced interlocking due to an increase in mass per area of a non-woven geotextile contributed to higher shear resistance that transitioned the failure mode of the GMX/GCL composite system to complete internal failure of the GCL.

3.6.3 Effect of Geotextile Type on GMX/GCL Shear Behavior

The effect of geotextile type on shear behavior of GMX/GCL composite systems was evaluated using GCL2 and GMX1. The cover geotextile of GCL2 was non-woven, whereas the carrier geotextile of GCL2 was woven. Thus, interface shear tests of the GMX1/GCL2

composite system were conducted with the cover geotextile in contact with GMX1 (GCL2-COGT/GMX1) and with the carrier geotextile in contact with GMX1 (GCL2-CAGT/GMX1). These two composite systems included the same GCL and GMX such that differences in shear behavior could be linked to the different geotextiles in contact with the GMX. Relationships of τ_p versus σ_{n-s} , δ_{h-p} versus σ_{n-s} , τ_{ld} versus σ_{ld} , and $R\tau$ versus σ_{n-s} for interface shear tests on GCL2-COGT/GMX1 and GCL2-CAGT/GMX1 are shown in Fig. 3.11 along with shear data obtained from the internal shear tests on GCL2. Post-shear pictures of GCL2 specimens from interface shear tests are included in Fig. 3.12. The failure mode for the interface shear tests on GMX1 and GCL2 was complete interface failure for both the cover geotextile and carrier geotextile sheared in contact with GMX1 and at all normal stress (Table 3.5). Therefore, critical strength for both composite systems was controlled by the interface shear strength between the carrier or cover geotextile of GCL2 and GMX1.

The interface shear tests on GMX1/GCL2 with the cover and carrier geotextiles in contact with GMX1 yielded nearly identical τ_p , τ_{ld} , δ_{h-p} , and $R\tau$ for $\sigma_{n-s} \leq 500$ kPa (Fig. 3.11). The negligible difference in shear behavior at low normal stress with respect to the non-woven cover or woven carrier geotextiles was due to superficial interlocking (i.e., hook and loop mechanism) between the GMX and geotextiles such that the dominant shear resistance mechanism was friction. However, for normal stress ≥ 1000 kPa, τ_p and τ_{ld} were larger for the interface between the non-woven cover geotextile and GMX1 as compared to the woven carrier geotextile and GMX1, regardless of failure occurring via complete interface failure in all shear tests. The increase in shear strength was attributed to enhanced interlocking between the non-woven cover geotextile and GMX1 as normal stress increased, whereas the woven carrier geotextile provided negligible interlocking potential for the full range of normal stress evaluated in this study.

Shear resistance for the interface between GMX1 and the woven carrier geotextile of GCL2 was frictional for the entire range of normal stress. The predominant frictional resistance was observed as essentially linear relationships of τ_p and τ_{ld} as a function of σ_{n-s} , as well as the essentially constant values of δ_{h-p} and $R\tau$ as a function of σ_{n-s} . Thus, for a given normal stress the mobilized shear strength was directly proportional to frictional resistance at the interface, required the same amount of deformation to mobilized peak strength, and yielded the same post-peak strength reduction. In contrast, a change in the interface shear mechanism from frictional resistance at low normal stress to interlocking resistance at high normal stress for the non-woven cover geotextile in contact with GMX1 can be observed as changes in slopes of τ_p and τ_{ld} as σ_{n-s} increased from 1000 to 2000 kPa. Assuming complete interface failure for a given GMX/GCL composite system, as normal stress increases, a non-woven geotextile in contact with the GMX will lead to higher critical strength relative to a woven geotextile due to a transition in the dominant interface shear resistance mechanism from friction to interlocking.

3.6.4 Effect of GMX Spike Density on GMX/GCL Shear Behavior

The effect of GMX spike density (i.e., texturing) on the shear behavior of GMX/GCL composite systems was evaluated via two cases: Case 1 – cover geotextile of GCL1 sheared in contact with GMX1 and GMX2; and Case 2 – cover geotextile of GCL2 sheared in contact with GMX1 and GMX2. In each case the isolated variable was GMX spike density as both GMX1 and GMX had the same spike height, but GMX1 had a spike density of 339 spikes/100-cm² (less textured) and GMX2 had a spike density of 841 spikes/100-cm² (more textured).

3.6.4.1 Case 1: GMX1/GCL1 and GMX2/GCL1

Relationships of τ_p versus σ_{n-s} , δ_{h-p} versus σ_{n-s} , τ_{ld} versus σ_{ld} , and $R\tau$ versus σ_{n-s} for interface shear tests on GCL1-COGT/GMX1 and GCL1-COGT/GMX2 are shown in Fig. **3.13**

along with shear data from internal shear tests on GCL1. Post shear pictures of the GCL1 specimens from each of the internal shear tests are included in Fig. 3.14. Peak shear strength of the GMX2/GCL1 composite system yielded comparable τ_p to the internal shear strength of GCL1 (Fig. 3.13a). Post-shear specimen analysis revealed that failure of the composite system of GCL1 in contact with GMX2 was partial interface/internal failure for $\sigma_{n-s} \leq 500$ kPa and complete internal failure for $\sigma_{n-s} \geq 1000$ kPa (Table 3.5). In contrast, τ_p for GMX1/GCL1 consistently plotted below peak internal shear strength of GCL1 (Fig. 3.13a). Post-shear specimen analysis indicated that failure of the composite system with GCL1 in contact with GMX1 was complete interface failure for $\sigma_{n-s} \leq 1000$ kPa and a transition to partial interface/internal failure at $\sigma_{n-s} = 2000$ kPa.

In Fig. 3.13, the linear relationships between peak and large-displacement shear strength as a function of normal stress, as well as the nearly constant values of δ_{h-p} and R_τ as a function of normal stress, indicate that the failure mode of GMX1/GCL1 remained the same with an increase in normal stress. Although interlocking between the GMX1 spikes and non-woven geotextile of GCL1 was enhanced at higher σ_{n-s} , the combined shear resistance from friction and interlocking was insufficient to transition the failure mode from complete interface failure to complete internal failure. Interlocking between the cover geotextile of GCL1 and GMX1 enhanced at $\sigma_{n-s} = 2000$ kPa based on the observed partial interface/internal failure in the post-shear specimen and slight increase in δ_{h-p} , which suggests some resistance to frictional slippage and onset of engagement of the reinforcement fibers of GCL1 in the shear resistance.

An increase in spike density yielded higher peak shear strength of GMX2/GCL1 compared to GMX1/GCL1 due to an enhanced friction and interlocking between the cover geotextile of GCL1 and GMX2. The higher interface friction and interlocking in the GMX2/GCL1 composite system resulted in a comparable shear behavior measured in the interface shear tests at $\sigma_{n-s} \geq 1000$ kPa as was measured in the internal shear tests on GCL1.

3.6.4.2 Case 2: GMX1/GCL2 and GMX2/GCL2

Relationships of τ_p versus σ_{n-s} , δ_{h-p} versus σ_{n-s} , τ_{ld} versus σ_{ld} , and $R\tau$ versus σ_{n-s} for interface shear tests on GCL1-COGT/GMX1 and GCL1-COGT/GMX2 are shown in Fig. **3.15** along with data from internal shear tests on GCL2. Post shear pictures of the GCL2 specimens from interface shear tests are included in Fig. **3.16**. The peak shear strength of the GMX2/GCL1 composite system was consistently lower than peak shear strength of GMX1/GCL2 and GCL2 (Fig. **3.15a**). Post-shear specimen analysis revealed that failure of the composite system of GCL2 in contact with GMX1 was always complete interface failure regardless of the normal stress. In contrast, GMX2/GCL2 yielded comparable peak shear strength to the internal shear strength of GCL2 at $\sigma_{n-s} \geq 1000$ kPa. Post-shear specimen analysis revealed that failure of the composite system of GCL2 in contact with GMX2 transitioned from complete interface failure at $\sigma_{n-s} = 100$ kPa to partial interface/internal failure for $300 \text{ kPa} \leq \sigma_{n-s} \leq 1000$ kPa, and to complete internal failure for $\sigma_{n-s} = 2000$ kPa.

The linear relationships of peak and large-displacement shear strength as a function of normal stress, as well as the nearly constant values of δ_{h-p} and $R\tau$ as a function of normal stress, for GMX1/GCL2 indicate that the failure mode of the composite systems remained the same at all normal stress. Considering that complete interface failure was identified for both GMX1/GCL1 and GMX2/GCL1 at $\sigma_{n-s} = 100$ kPa, comparable values of τ_p , τ_{ld} , δ_{h-p} , and $R\tau$ were observed. However, with the transition of failure mode from complete interface failure to partial interface/internal failure in GMX2/GCL2 at $300 \text{ kPa} \leq \sigma_{n-s} \leq 1000$ kPa, τ_p , δ_{h-p} and $R\tau$ of GMX2/GCL2 approached τ_p , δ_{h-p} , and $R\tau$ of GCL2 as measured in the internal shear tests. Eventually, complete internal failure in GMX2/GCL2 at $\sigma_{n-s} = 2000$ kPa resulted in comparable shear behavior between GMX2/GCL2 evaluated in the interface shear tests and GCL2 evaluated in the internal shear tests.

In conclusion, incorporating the high spike density GMX2 in composite systems with GCL1 (Fig. 3.13) and GCL2 (Fig. 3.15) resulted in a higher peak shear strength measured in the interface shear tests regardless of the normal stress. This observation was due to the enhanced friction and interlocking between the GMX and non-woven geotextiles of the GCLs. Despite the higher developed shear resistance in composite systems with GMX2, failure mode of the composite systems depended on the internal shear strength of the GCL.

3.6.5 Effect of GCL Peel Strength on GMX/GCL Shear Behavior

To evaluate the effect of GCL peel strength on the shear behavior of GMX/GCL composite systems, comparisons were made for two cases: Case 1 – non-woven cover geotextiles of GCL1, GCL2, and GCL3 sheared in contact with GMX2; and Case 2 – non-woven carrier geotextiles of GCL1 and GCL3 and non-woven cover geotextile of GCL2 sheared in contact with GMX1. In Case 1, interface shear tests on GMX2/GCL3 were performed only at $\sigma_{n-s} = 100, 300, \text{ and } 500 \text{ kPa}$ due to limited resources.

Contrary to the evaluation of the effects of geotextile mass per area, geotextile type, and GMX spike density where a single parameter was isolated, limiting the variables to only peel strength in Case1 and Case 2 was not possible. The reason is that the geotextile characteristics of the GCLs were not necessarily the same. To minimize the effect of geotextile properties, comparison has been made in Case 1 and Case 2 between composite systems with the same geotextile type (i.e., non-woven geotextile) in contact with a GMX. In Case 1, non-woven cover geotextiles of GCL1 and GCL2 were the same and the mass per area of the geotextile of these two GCLs was comparable to the mass per area of the non-woven cover geotextile of GCL3 (230 g/m² in GCL1 and GCL2 versus 260 g/m² in GCL3). Therefore, the effect of GCL peel strength on shear behavior of composite systems is expected to be significantly greater than the effect of geotextile mass per area. In Case 2, comparison has been made between the shear behavior of composite systems with GMX1 sheared against the non-woven geotextile of GCL1,

GCL2, and GCL3 with the highest mass per area. The mass per area of non-woven geotextiles ranges from 230 g/m² in GCL2 up to 360 g/m² in GCL3. In this case, the effect of geotextile mass per area is expected to be significant. Therefore, the evaluation will be on the effect of “GCL”, and not just the peel strength, on the shear behavior of GMX/GCL composite systems.

3.6.5.1 Case 1: GMX2/GCL1, GMX2/GCL2, and GMX2/GCL3

Relationships of peak shear strength and large-displacement shear strength versus normal stress for interface shear tests on GCL1-COGT/GMX2, GCL2-COGT/GMX2, and GCL3-COGT/GMX2 are shown in Fig. 3.17. Post shear pictures of GCL1, GCL2, and GCL3 specimens are included in Fig. 3.18. The failure mode of the GCL1-COGT/GMX2 was partial interface/internal failure for $\sigma_{n-s} \leq 500$ kPa and complete internal failure at $\sigma_{n-s} \geq 1000$ kPa. The failure mode of GCL2-COGT/GMX2 was complete interface failure at $\sigma_{n-s} = 100$ and 300 kPa, partial interface/internal failure at $\sigma_{n-s} = 500$ and 1000 kPa, and complete internal failure at $\sigma_{n-s} = 2000$ kPa. Finally, failure mode of GCL3-COGT/GMX2 was complete interface failure for $\sigma_{n-s} = 100$ kPa and partial interface/internal failure for $\sigma_{n-s} = 300$ and 500 kPa (Table 3.5).

Relatively linear τ_p and τ_{ld} relationships as a function of normal stress were observed at $\sigma_{n-s} \leq 500$ kPa for all composite systems, and values of τ_p and τ_{ld} were comparable. This observation is attributed to the complete interface failure or partial interface/internal failure modes where the internal shear resistance of the GCLs were not fully mobilized. Therefore at $\sigma_{n-s} \leq 500$ kPa, increase in the GCL peel strength did not contribute to peak shear strength of the composite systems.

In contrast, the different peel strength between GCL1 and GCL2 resulted in considerably different peak shear strength between the GMX2/GCL1 and GMX2/GCL2 composite systems at $\sigma_{n-s} \geq 1000$ kPa. For example, the relatively low internal shear resistance of GCL1 (PS = 980 N/m) resulted in complete internal failure at $\sigma_{n-s} = 1000$ kPa, whereas the higher internal shear

resistance of GCL2 (PS = 2180 N/m) led to partial interface/internal failure at $\sigma_{n-s} = 1000$ kPa and development of a higher peak shear strength. The higher large-displacement shear strength of GMX2/GCL2 compared to GMX2/GCL1 at $\sigma_{n-s} = 1000$ kPa was also attributed to the different shear mechanism at large displacement. The decrease in large-displacement shear strength for the GMX2/GCL1 system as σ_{n-s} increased from 500 kPa to 1000 kPa supports the transition to complete internal failure, whereas the higher large-displacement shear strength of GMX2/GCL2 suggests that complete internal failure was not yet achieved at $\sigma_{n-s} = 1000$ kPa. Full mobilization of GCL internal shear resistance for both GMX2/GCL1 and GMX2/GCL2 was observed at $\sigma_{n-s} = 2000$ kPa, which corresponded to complete internal failure for both GCLs. The higher peak shear strength of GMX2/GCL2 was attributed again to the higher peel strength of GCL2. Finally, the large-displacement shear strength of both composite systems was comparable at $\sigma_{n-s} = 2000$ kPa, which supports complete internal failure and comparable shear strength along the bentonite-geotextile interface within the GCL.

3.6.5.2 Case 2: GMX1/GCL1, GMX1/GCL2, and GMX1/GCL3.

Relationships of peak shear strength and large-displacement shear strength versus normal stress for interface shear tests on GCL1-CAGT/GMX1, GCL2-COGT/GMX1, and GCL3-CAGT/GMX1 are shown in Fig. 3.19. Post-shear pictures of GCL1, GCL2, and GCL3 specimens are included in Fig. 3.20. The failure mode of the GCL1-CAGT/GMX2 was complete interface failure for $\sigma_{n-s} \leq 500$ kPa, partial interface/internal failure at $\sigma_{n-s} = 1000$ kPa, and complete internal failure at $\sigma_{n-s} = 2000$ kPa. The failure mode of GCL2-COGT/GMX2, was complete interface for all σ_{n-s} . The failure mode of GCL3-CAGT/GMX2 was complete interface failure for $\sigma_{n-s} \leq 500$ kPa and partial interface/internal failure for $\sigma_{n-s} \geq 1000$ kPa (Table 3.5).

The peak shear strength envelopes of all composite systems were comparable at $\sigma_{n-s} \leq 1000$ kPa, and the peak shear strength envelopes of GMX1/GCL1 and GMX1/GCL2 were

comparable at all normal stress (Fig. 3.19a). At $\sigma_{n-s} \leq 500$ kPa, the comparable τ_p indicates a comparable developed shear stress between the low spike density GMX1 and different geotextiles of GCL1, GCL2, and GCL3. This observation suggests that the GMX-geotextile interlocking mechanism was not significant and shear resistance was predominantly frictional. The linear τ_p - σ_{n-s} and τ_{id} - σ_{n-s} relationship at $\sigma_{n-s} \leq 500$ kPa for all composite systems further supports this behavior. Therefore, incorporating GCLs with different peel strength did not result in different shear strength in composite systems with GMX1 at $\sigma_{n-s} \leq 500$ kPa.

At $\sigma_{n-s} = 1000$ kPa, peak shear strength of the composite systems remained the same despite the difference in observed failure modes (Table 3.5). This observation suggests that interlocking between GMX1 and geotextiles of the GCLs was still limited at $\sigma_{n-s} = 1000$ kPa. An increase in σ_{n-s} to 2000 kPa resulted in a considerably different τ_p and τ_{id} for GMX1/GCL3 compared to GMX1/GCL1 and GMX1/GCL2. Considering the larger mass per area of the non-woven carrier geotextile of GCL3 in contact with GMX1, the higher observed shear strength of the GMX1/GCL3 composite system (Fig. 3.19) suggests that GMX1-geotextile interlocking became the predominant mechanism of interface shear resistance at $\sigma_{n-s} = 2000$ kPa. The similar peak shear strength of GMX1/GCL1 and GMX1/GCL2 at $\sigma_{n-s} = 2000$ kPa indicates that the developed shear resistance between the geotextile of GCL2 and GMX1 (complete interface failure) was comparable to the internal shear resistance of GCL1 in the GMX1/GCL1 composite system (complete internal failure). However, the authors believe that this observation was a coincidence, and the complete internal failure of GMX1/GCL1 composite system could have limited τ_p of this composite system had the internal shear resistance of GCL1 been lower than the developed interface shear stress between the GMX1 and geotextile of GCL2. Regardless of the same τ_p , the τ_{id} of these two composite systems were different because of their different failure modes.

In conclusion, the GCL peel strength can only affect the τ_p and τ_{ld} of a composite system if internal shear resistance of the GCL is fully mobilized, and composite system experience complete internal failure or partial interface/internal failure with high internal deformation within the GCL. Considering that the fully mobilization of the GCL internal shear resistance requires relatively high developed interface shear stress between the GMX and geotextile (of the GCL), increase in the peel strength may not affect the τ_p and τ_{ld} of a composite system when low developed interface shear stress resulted in complete interface failure mode. Therefore, the effect of peel strength on shear behavior and shear strength of a composite system is directly related to the characteristics of GMX and geotextile of the GCL.

3.7 Design Consideration

Relationships between peak shear strength and normal stress for all eight GMX/GCL composite systems evaluated in this study are shown in Fig. **3.21**. Differences in GCL peel strength, GMX spike density, and geotextile characteristics (of GCL in contact with GMX) among the eight composite systems resulted in a broad range of peak shear strength. In particular, the overall lowest and highest peak shear strength envelopes were observed for composite systems with GCL2, whereby the lowest strength envelope corresponded to the woven carrier geotextile of GCL2 sheared in contact with GMX1 and the highest strength envelope corresponded to the non-woven cover geotextile of GCL2 sheared in contact with GMX2. This observation supports the importance of the geotextile and GMX characteristics on the shear strength of GMX/GCL composite systems.

Peak shear strength envelopes for composite systems that included the high spike density GMX2 were always higher than composite systems that included the low spike density GMX1. In the range of $\sigma_{n-s} \leq 500$ kPa, an increase in specimen peel strength or increase in the geotextile mass per area did not result in a considerable increase in τ_p for composite systems

with a same GMX. This observation is supported by frictional interface resistance as the dominant shear mechanism of composite systems at $\sigma_{n-s} \leq 500$ kPa. Considering complete interface failure or partial interface/internal failure, an increase in GCL peel strength cannot substantially increase the peak shear strength as internal shear resistance of a GCL is not fully mobilized. In addition, since interface shear resistance between the geotextile and GMX is predominantly frictional, an increase in the non-woven geotextile mass per area cannot substantially increase peak shear strength along the interface as the GMX spikes-geotextile interlocking is minimal. However, an increase in GMX spike density increases the contact area between asperities of the geotextile fibers and GMX spikes such that an increase is observed in the frictional resistance and peak interface shear strength. Therefore, use of a high spike density GMX is necessary to obtain a high peak interface shear strength in GMX/GCL composite systems at low normal stress (i.e., $\sigma_{n-s} \leq 500$ kPa in this study).

The effects of geotextile characteristics (i.e., geotextile type and mass per area of non-woven geotextiles) on peak shear strength of composite systems were only pronounced in situations where interlocking between the GMX and GCL was the predominant interface shear resistance mechanism. Under high normal stress where interlocking became a dominant shear resistance mechanism (i.e., $\sigma_{n-s} \geq 1000$ kPa in this study), GCLs with thick non-woven geotextiles yielded higher peak shear strength. For instance the highest peak shear strength from the interface shear tests in this study was observed for GCL3-CAGT/GMX1 at $\sigma_{n-s} = 2000$ kPa. However, GCLs with woven geotextiles should be avoided in applications with high shear stresses as low interface shear resistance between the woven geotextile and GMX may yield low peak shear strength of the composite system regardless of the GCL internal shear strength.

The effect of GCL peel strength on peak shear strength of GMX/GCL composite systems depends on GMX and geotextile characteristics. Incorporating a GCL with high peel strength in a composite system does not necessarily guarantee a high peak shear strength. An

example of this scenario was the low observed peak shear strength for woven carrier geotextile of GCL2 sheared in contact with GMX1. However, in order to insure a high peak shear strength in applications with high normal stresses, GCL peel strength must be high enough to allow an increase in the developed interface shear stress between the geotextile and GMX without reaching internal GCL failure. For instance, the low peel strength (and therefore low internal shear strength) of GCL1 limited the peak shear strength of the composite systems despite the use of a high spike density GMX and non-woven geotextile in this composite system. Therefore, low peel strength GCLs should not be used in high normal stress applications in the case that high peak shear strength is desired for the GMX/GCL composite system.

3.8 Summary

The objective of this study was to evaluate the effect of geotextile type, geotextile mass per area, GMX spike density, and GCL peel strength on the shear behavior of GMX/GCL composite systems. For this aim, a shear mechanism was proposed and the effect of the aforementioned parameters were evaluated on the proposed mechanism via a series of DC-IN and DC-IF experiments on 8 GMX/GCL composite systems with different GCLs, GMX, and geotextiles (in contact with the GMX). The following conclusions have been obtained from the results of the experiments:

- The internal τ_p of NP GCLs in DC-IN tests increased with an increase in the GCL peel strength. However, comparable τ_{id} were observed.
- Three different failure modes were observed for GMX/GCL composite systems: (i) complete interface failure, (ii) partial interface/internal failure, and (iii) complete internal failure. The failure mode of the GMX/GCL composite systems is controlled by the value of the developed shear stress at the interface between the GMX and GCL. The failure

mode of a specific composite system can transition from complete interface failure to complete internal failure with an increase in σ_{n-s} .

- In composite systems with high peel strength GCLs, the failure mode may never be complete internal failure if the low tensile properties of the carrier and cover geotextile limits the transfer of the shear stress applied to the GMX/GCL composite system into internal region of the GCL.
- At a certain σ_{n-s} , the failure mode of the GMX/GCL composite system depends on characteristics of the GMX, geotextile (of the GCL) in contact with GMX, and the GCL peel strength.
- Increase in the GMX spike density can increase the τ_p of GMX/GCL composite systems at all σ_{n-s} range. The reason is increased GMX spike density enhances both friction and interlocking mechanisms and increases the developed interface shear stress between the GMX and GCL.
- Increase in the mass per area of the non-woven geotextile (of the GCL) in contact with the GMX can increase the τ_p of a GMX/GCL composite system if the GMX-geotextile interlocking is the predominant mechanism in developed interface shear stress. As the result, the effect of geotextile mass per area on the τ_p of a GMX/GCL composite system is noteworthy only at high σ_{n-s} .
- Incorporating a GCL with a woven geotextile can result in a low τ_p in a GMX/GCL composite system. The reason is the minimal interlocking between the GMX and woven geotextile limited the developed interface shear stress between the GCL and GMX. Therefore, GCLs with woven geotextile should not be used in liner and cover systems of containment applications with high shear stress.
- The GCL peel strength can affect to the τ_p of a GMX/GCL composite system only if the failure mode of the composite system is complete internal failure. Considering that the

complete internal failure usually occurs at high σ_{n-s} (e.g. $\sigma_{n-s} \geq 1000$ kPa), increase in the GCL peel strength can increase the τ_p of a GMX/GCL composite system at these σ_{n-s} .

Table 3.1. Characteristics and properties of geosynthetic clay liners.

Category	Properties	GCL1	GCL2	GCL3
General properties	Peel strength (N/m) ^a	980	2180	3850
	Heat treatment method	NHT	NHT	NHT
Geotextile Properties	Polymer type	PP	PP	PP
	Carrier geotextile type	NW	W	NW
	Cover geotextile type	NW	NW	NW
	Carrier geotextile mass/area (g/m ²) ^b	260	130	360
	Cover geotextile mass/area (g/m ²) ^b	230	230	280
Bentonite properties	Bentonite type	Granular	Granular	Granular
	Bentonite mass per area (g/m ²) ^c	4220	4910	5570

NOTE: NHT = Non-heat treated; PP = Polypropylene; W = woven; NW = non-woven

^a Reported by manufacturers, ASTM D6496/6496M

^b Based on 20 measurements, ASTM D5261

^c Based on 20 measurements, ASTM D5993

Table 3.2. Characteristics and properties of GMX.

Properties	Standard	GMX1	GMX2
Manufacturing Process	-	Structured	Structured
Polymer Type ^a	-	LLDPE	LLDPE
Average Core Thickness (mm) ^a	ASTM D5994	1.5	1.5
Average Asperity Height (mm) ^a	ASTM D7466	0.5	0.5
Spikes Density (No. Spikes/100 cm ²)	-	340	840

^a Reported by manufacturers.

Table 3.3. Components and schematics of GMX/GCL composite systems.

Composite System	GCL	GMX	GT	Schematics
GCL1-CAGT/GMX1	GCL1	GMX1	CAGT	
GCL1-COGT/GMX1	GCL1	GMX1	COGT	
GCL1-COGT/GMX2	GCL1	GMX2	COGT	
GCL2-CAGT/GMX1	GCL2	GMX1	CAGT	
GCL2-COGT/GMX1	GCL2	GMX1	COGT	
GCL2-COGT/GMX2	GCL2	GMX2	COGT	
GCL3-COGT/GMX2	GCL3	GMX2	COGT	
GCL3-CAGT/GMX1	GCL3	GMX1	CAGT	

Note: GT = Geotextile of the GCL that is in contact with the GMX; CAGT = Carrier geotextile of the GCL; COGT = Cover geotextile of the GCL; GCL (i)-CA (or CO) GT/GMX (j) = a composite system consisting of GMX(j) in contact with the carrier (or cover) geotextile of GCL(i).

Table 3.4. A summary of displacement-controlled internal direct shear tests.

GCL	σ_{n-s} (kPa)	τ_p (kPa)	ϕ_{s-p} (kPa)	δ_{h-p} (mm)	AC σ_{70} (kPa)	AC τ_{70} (kPa)	$R\tau$	Test Status
GCL1	100	141.0	54.7	25.2	183.1	23.4	0.09	Successful Internal shear failure
	300	233.7	37.9	23.9	549.4	39.7	0.09	
	500	295.5	30.6	21.9	915.7	78.6	0.15	
	1000	413.7	22.5	21.4	1831.4	130.9	0.17	
	2000	570.5	15.9	17.1	3662.7	199.1	0.19	
GCL2	100	164.2	58.7	20.7	183.1	16.8	0.06	Successful Internal shear Failure
	300	293.3	44.4	15.8	549.4	51.3	0.10	
	500	416.2	39.8	16.7	915.7	84.6	0.11	
	1000	541.2	28.4	17.0	1831.4	122.2	0.12	
	2000	700.6	19.3	15.6	3662.7	145.6	0.11	
GCL3 ^a	80	199.7	-	-	-	-	-	Unsuccessful Internal shear Failure
	160	279.5	-	-	-	-	-	
	250	294.2	-	-	-	-	-	
	500	462	-	-	-	-	-	
	1000	626.5	-	-	-	-	-	
	1500	690.4	-	-	-	-	-	
	2000	934.3	-	-	-	-	-	

NOTE: DC-IN = Displacement-controlled internal direct shear test. σ_{n-s} = shearing normal stress; τ_p = peak internal shear strength; ϕ_{s-p} = secant friction angle for peak shear strength; δ_{h-p} = horizontal displacement at peak shear strength; AC σ_{70} = area-corrected shearing normal stress; AC τ_{70} = area-corrected shear strength at horizontal displacement (δ_h) = 70 mm; $R\tau$ = Post-peak strength reduction ratio = $\frac{AC \tau_{70} / AC \sigma_{70}}{\tau_p / \sigma_{n-s}}$.

^a Internal shear failure of GCL3 was not successful in DC-IN tests. Therefore, the values of τ_p for GCL3 represent the maximum shear stress during the test and not necessarily the peak shear strength. ϕ_{s-p} , δ_{h-p} , AC σ_{70} , AC τ_{70} , and $R\tau$ are not defined in experiments on GCL3 for the same reason.

Table 3.5. A summary of displacement-controlled interface shear tests.

GCL	GMX	GT	σ_{n-s} (kPa)	τ_p (kPa)	ϕ_{s-p} (kPa)	δ_{h-p} (mm)	τ_{70} (kPa)	R_τ	Failure mode
GCL1	GMX1	COGT	100	51.1	27.1	9.9	36.7	0.72	IF
			300	128	23.1	10	76.2	0.60	IF
			500	163	18.1	10.9	100.6	0.62	IF
			1000	255	14.3	10.8	167.1	0.66	IF
			2000	462.3	13	13.9	320.2	0.69	IF/IN
	CAGT	100	47.7	25.5	9.9	40.8	0.86	IF	
		300	116.1	21.2	10.5	77	0.66	IF	
		500	178.8	19.7	12.3	137	0.77	IF	
		1000	315.8	17.5	13.7	125.7	0.40	IF/IN	
		2000	516.3	14.5	15.5	190.2	0.37	IN	
	GMX2	COGT	100	115.8	49.2	16.7	43.9	0.38	IF/IN
			300	208.1	34.8	15.7	82.9	0.40	IF/IN
			500	284.1	29.6	17.8	116.6	0.41	IF/IN
			1000	391.7	21.4	16.5	72.05	0.18	IN
			2000	560.5	15.7	17.7	167.1	0.30	IN
GCL2	GMX1	CAGT	100	51.6	27.3	8.4	35.5	0.69	IF
			300	108.2	19.8	8.5	68.4	0.63	IF
			500	154.6	17.2	8.6	107	0.69	IF
			1000	249.3	14	9.3	152	0.61	IF
			2000	423.9	12	11.2	283	0.67	IF
	GMX1	COGT	100	55.9	29.2	8.3	40.1	0.72	IF
			300	126.3	22.8	9.2	76.7	0.61	IF
			500	183	20.1	8.8	114.9	0.63	IF
			1000	297.2	16.6	8.6	179.3	0.60	IF
			2000	500.2	14.0	13.5	297.7	0.60	IF
	GMX2	COGT	100	93.4	43.1	9.8	55.4	0.59	IF
			300	249.1	39.7	13.6	104.3	0.42	IF/IN
			500	328.5	33.3	14.6	134.4	0.42	IF/IN
			1000	549.2	28.8	14.9	195.4	0.36	IF/IN
			2000	679.7	18.8	16.4	183.1	0.27	IN
GCL3	GMX1	CAGT	100	60.8	31.3	9.4	48.3	0.79	IF
			300	159.4	28	12.3	119.3	0.75	IF
			500	196.8	21.5	11.2	145.3	0.74	IF
			1000	329.9	18.3	12.2	216.6	0.66	IF/IN
			2000	712.3	19.6	16.2	566.4	0.79	IF/IN
	GMX2	COGT	100	119.8	50.1	14.3	65.4	0.54	IF
			300	277.6	42.8	16.7	115.7	0.42	IF
			500	337.3	34	18.6	133.5	0.39	IF/IN

NOTE: DC-IF = Displacement-controlled interface direct shear tests; GT = geotextile of the GCL in contact with GMX in DC-IF tests; CAGT = carrier geotextile (of the GCL); COGT = cover geotextile (of the GCL); σ_{n-s} = shearing normal stress; τ_p = peak internal shear strength; ϕ_{s-p} = secant friction angle at peak shear strength; δ_{h-p} = horizontal displacement at peak shear strength; τ_{70} = area-corrected shear strength at horizontal displacement (δ_h) = 70 mm; R_τ = Post-peak strength reduction ratio = τ_{70}/τ_p ; IF = complete interface failure; IF/IN = partial interface/internal failure; IN = complete internal failure.

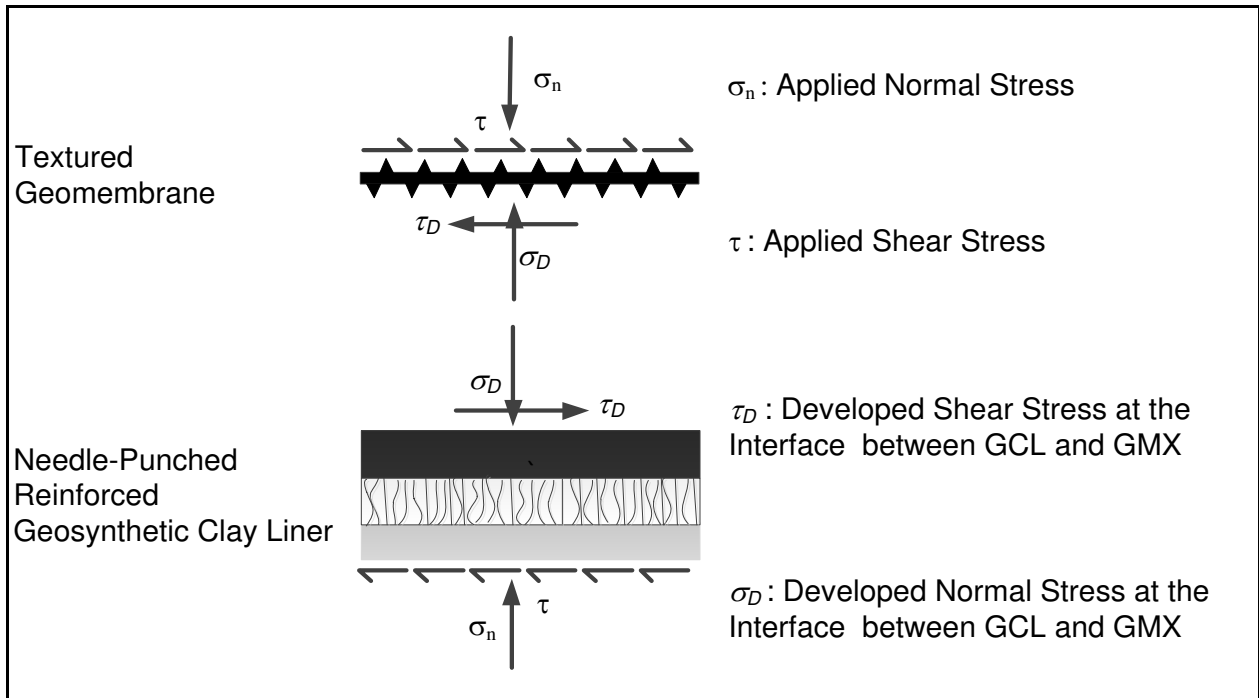


Fig. 3.1. Schematic shear and normal stresses within a composite system composed of a textured geomembrane (GMX) and needle-punched geosynthetic clay liner (GCL).

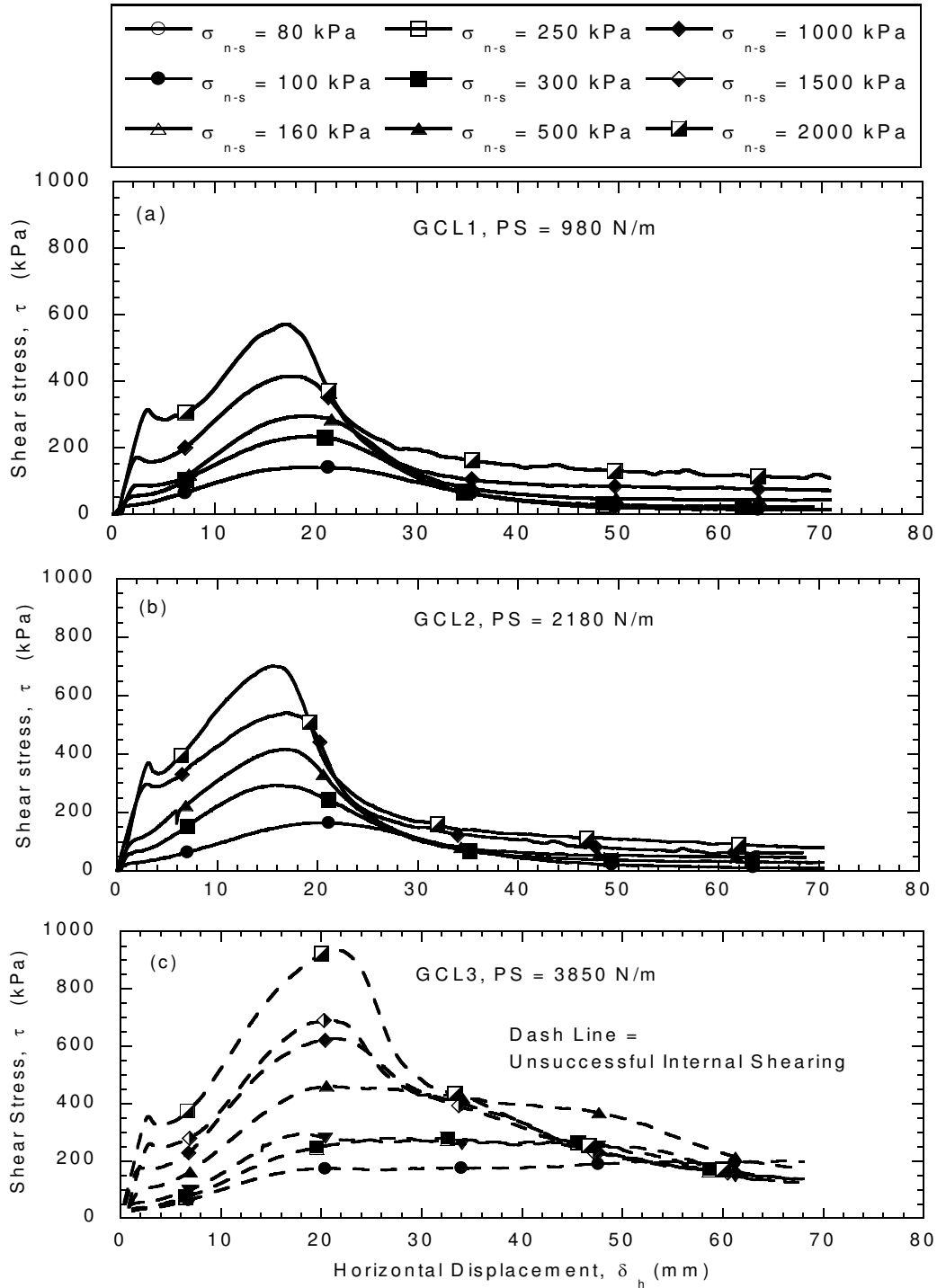


Fig. 3.2. Relationships between shear stress (τ) and horizontal displacement (δ_h) for direct shear tests on the internal shear strength of GCLs: (a) GCL1, (b) GCL2, and (c) GCL3.

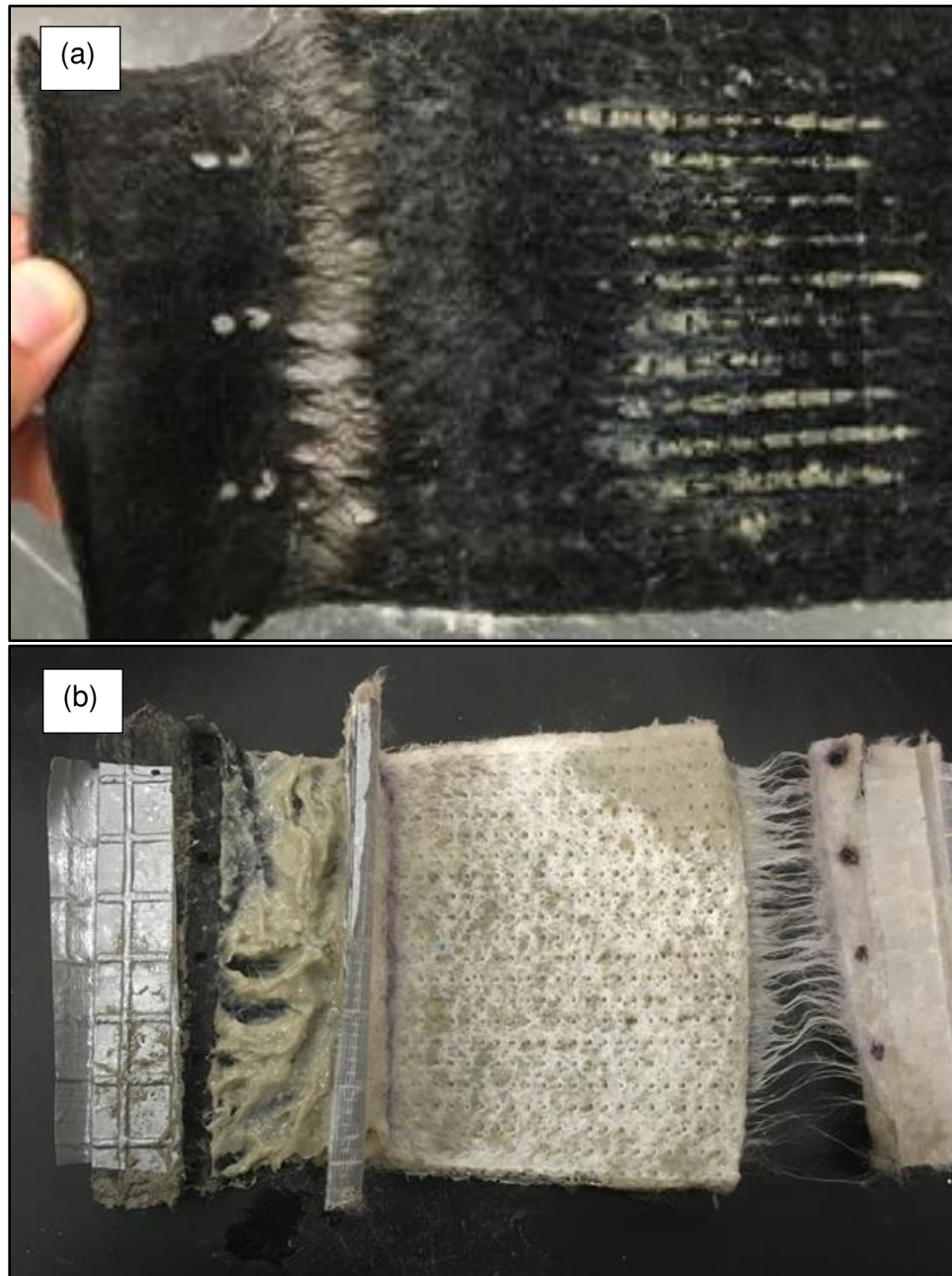


Fig. 3.3. Photographs of post internal GCL-shear specimens of GCL-3 from direct shear tests conducted under normal stresses of (a) 160 kPa and (b) 1000 kPa.

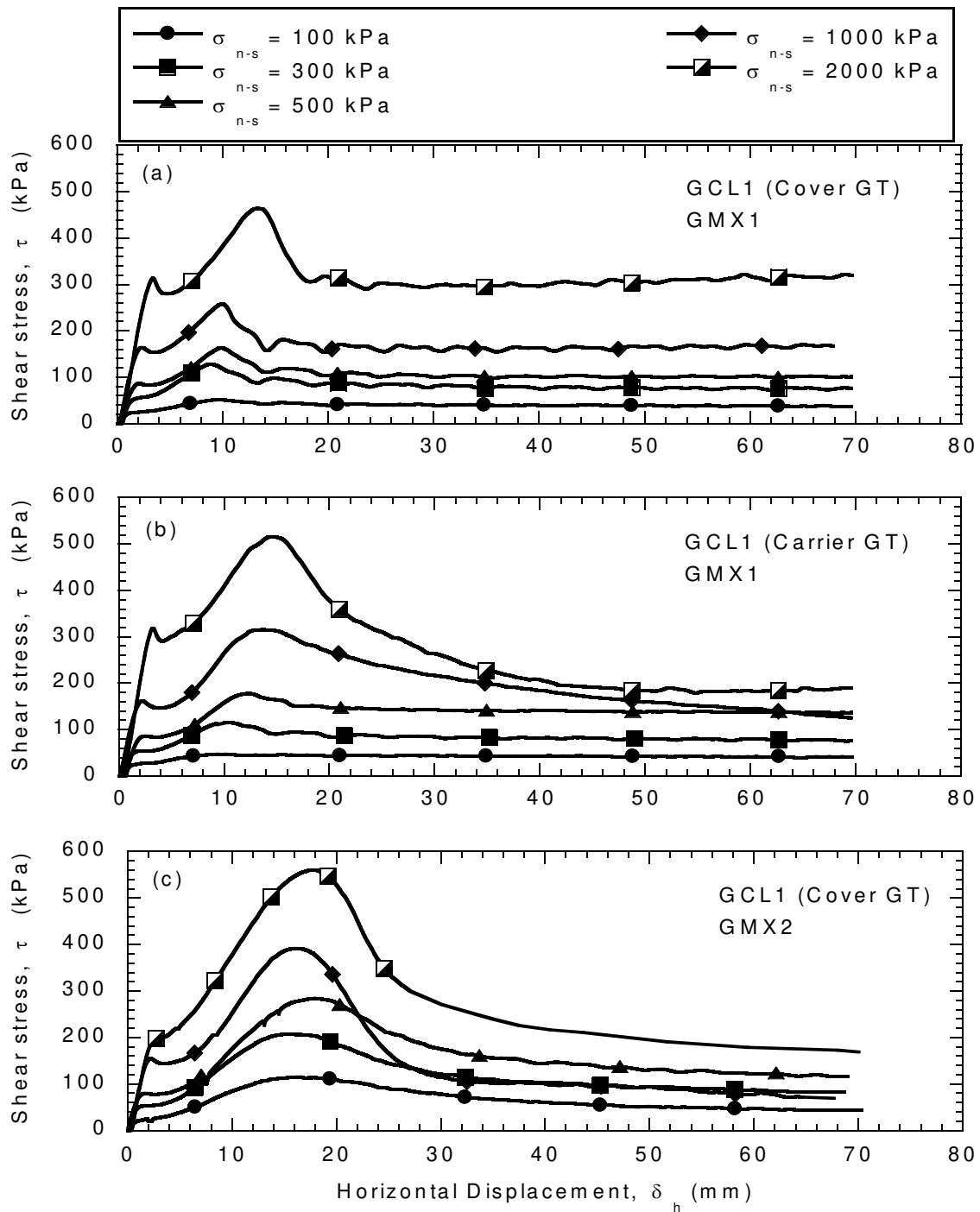


Fig. 3.4. Relationships between shear stress (τ) and horizontal displacement (δ_h) for direct shear interface tests on (a) cover GT of GCL1 and GMX1, (b) carrier GT of GCL1 and GMX1, and (c) cover GT of GCL1 and GMX2

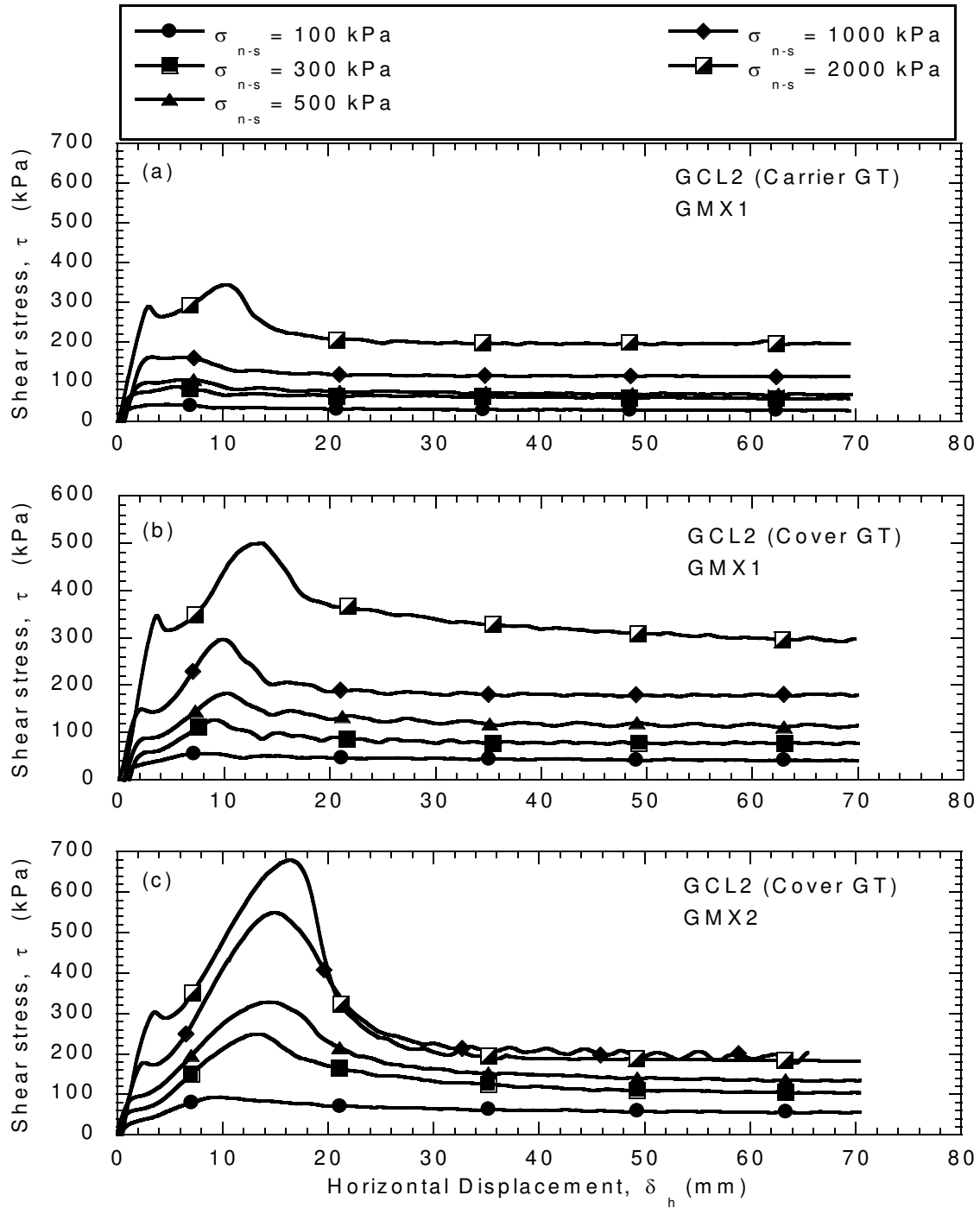


Fig. 3.5. Relationships between shear stress (τ) and horizontal displacement (δ_h) for direct shear interface tests on (a) carrier GT of GCL2 and GMX1, (b) cover GT of GCL2 and GMX1, and (c) cover GT of GCL2 and GMX2.

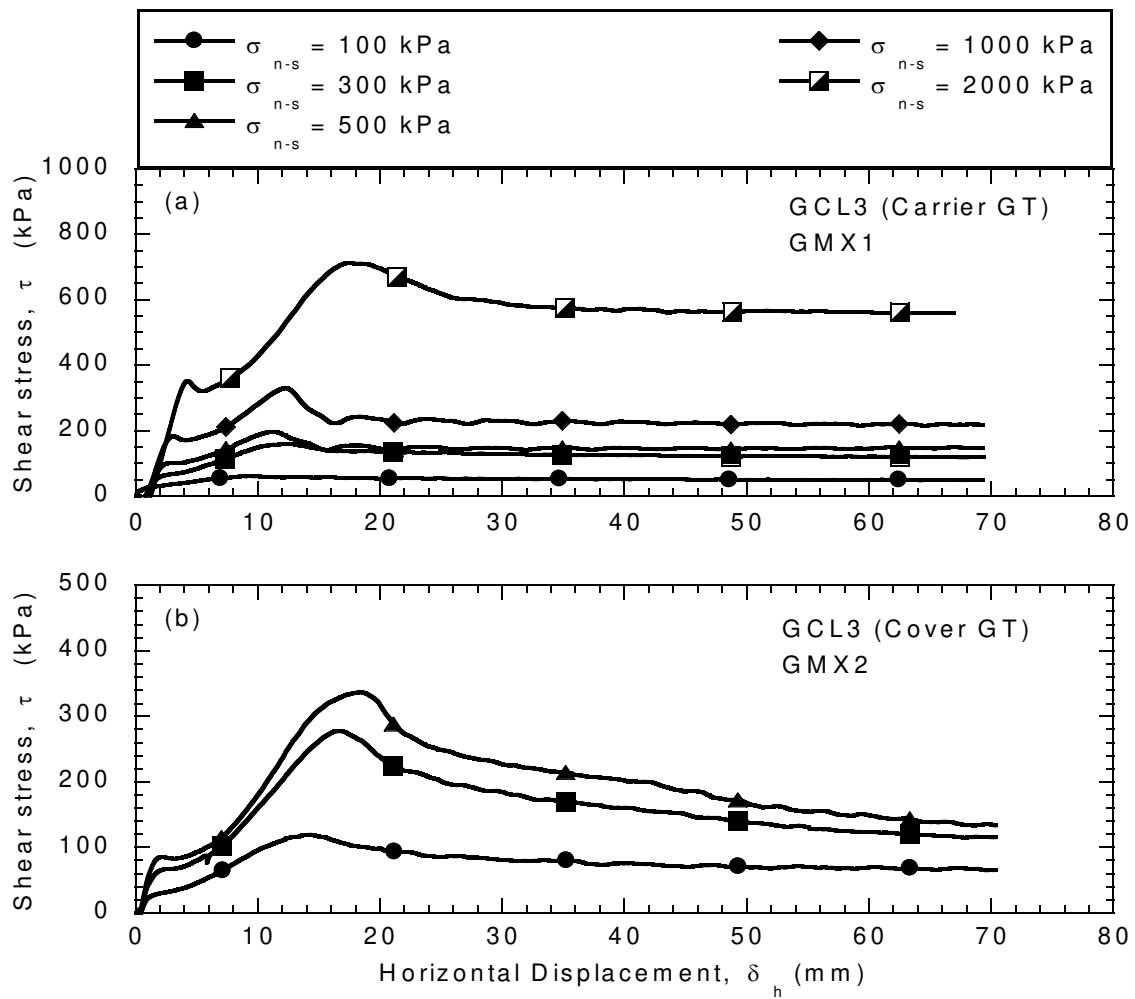


Fig. 3.6. Relationships between shear stress (τ) and horizontal displacement (δ_h) for direct shear interface tests on (a) carrier GT of GCL3 and GMX1, and (b) cover GT of GCL3 and GMX2.

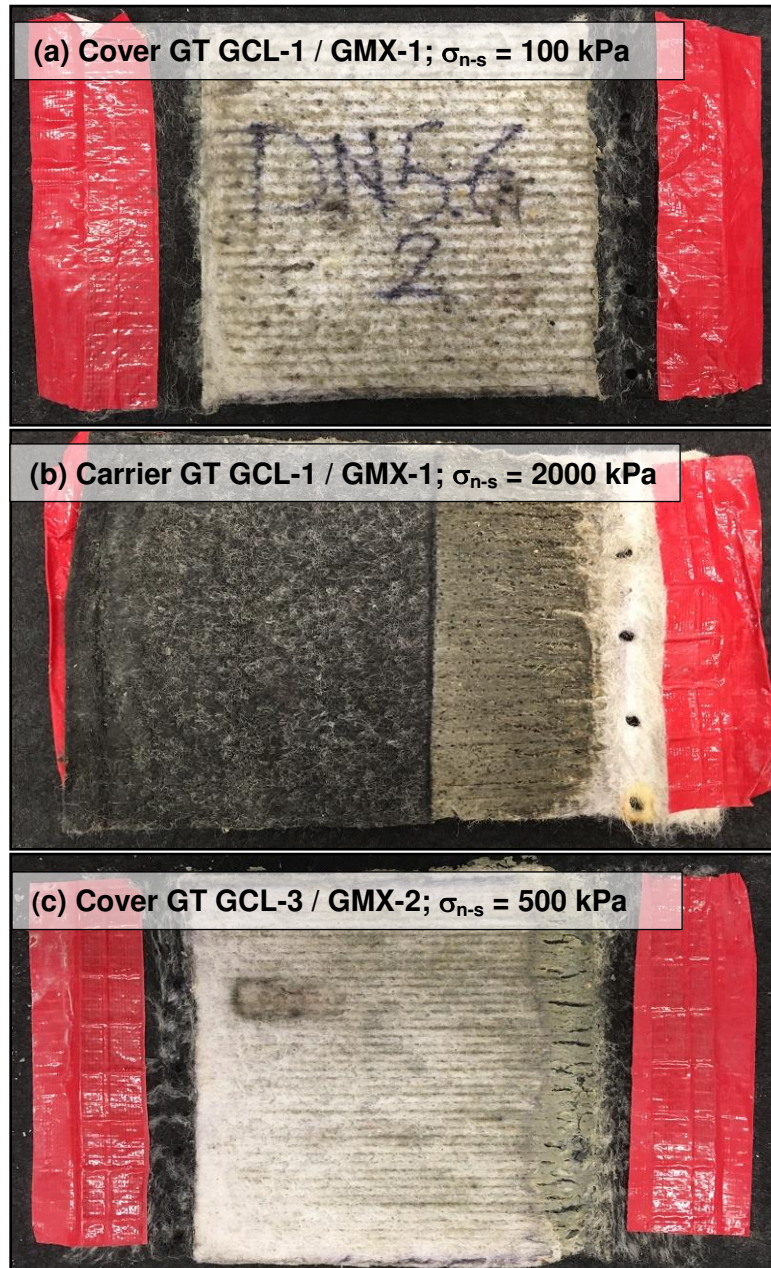


Fig. 3.7. Photographs of post-shear GCL specimens from direct shear interface tests that show examples of (a) complete interface failure for experiments on Cover GT of GCL-1 and GMX-1 at $\sigma_{n-s} = 100$ kPa, (b) complete internal failure for experiments on Carrier GT of GCL-1 and GMX-1 at $\sigma_{n-s} = 2000$ kPa, and (c) partial interface/internal failure for experiments on Cover GT of GCL-3 and GMX-2 at $\sigma_{n-s} = 500$ kPa.

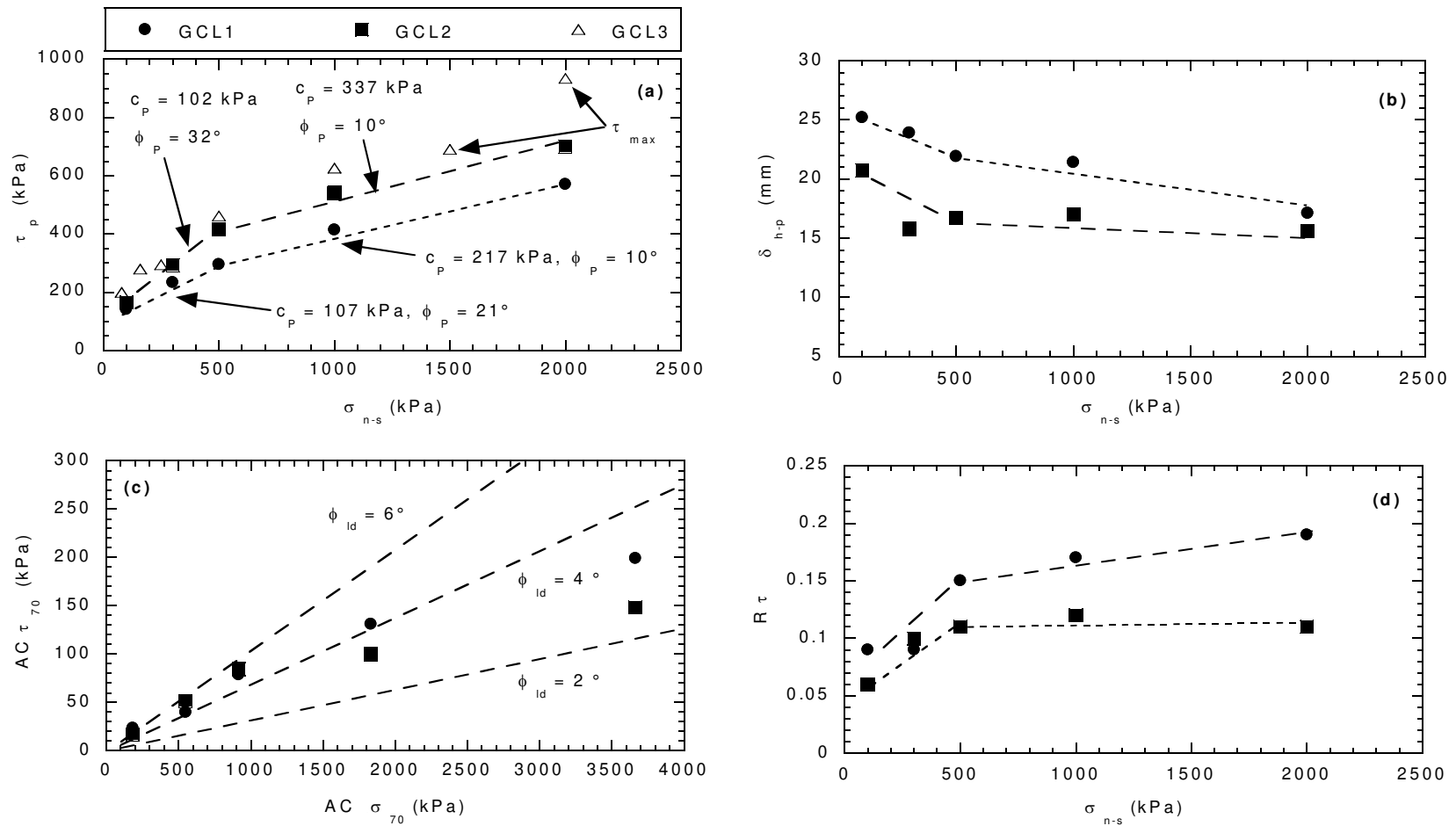


Fig. 3.8. Shear strength and shear behavior relationships for GCL-internal direct shear tests on GCL1, GCL2, and GCL3: (a) peak shear strength (τ_p) versus shearing normal stress (σ_{n-s}), (b) horizontal displacement at peak shear stress (δ_{h-p}) versus σ_{n-s} , (c) area-corrected large-displacement shear stress at $\delta_h = 70$ mm ($AC \tau_{70}$) versus area-corrected large-displacement normal stress at $\delta_h = 70$ mm ($AC \sigma_{70}$), and (d) stress reduction ratio ($R\tau$) versus σ_{n-s} .

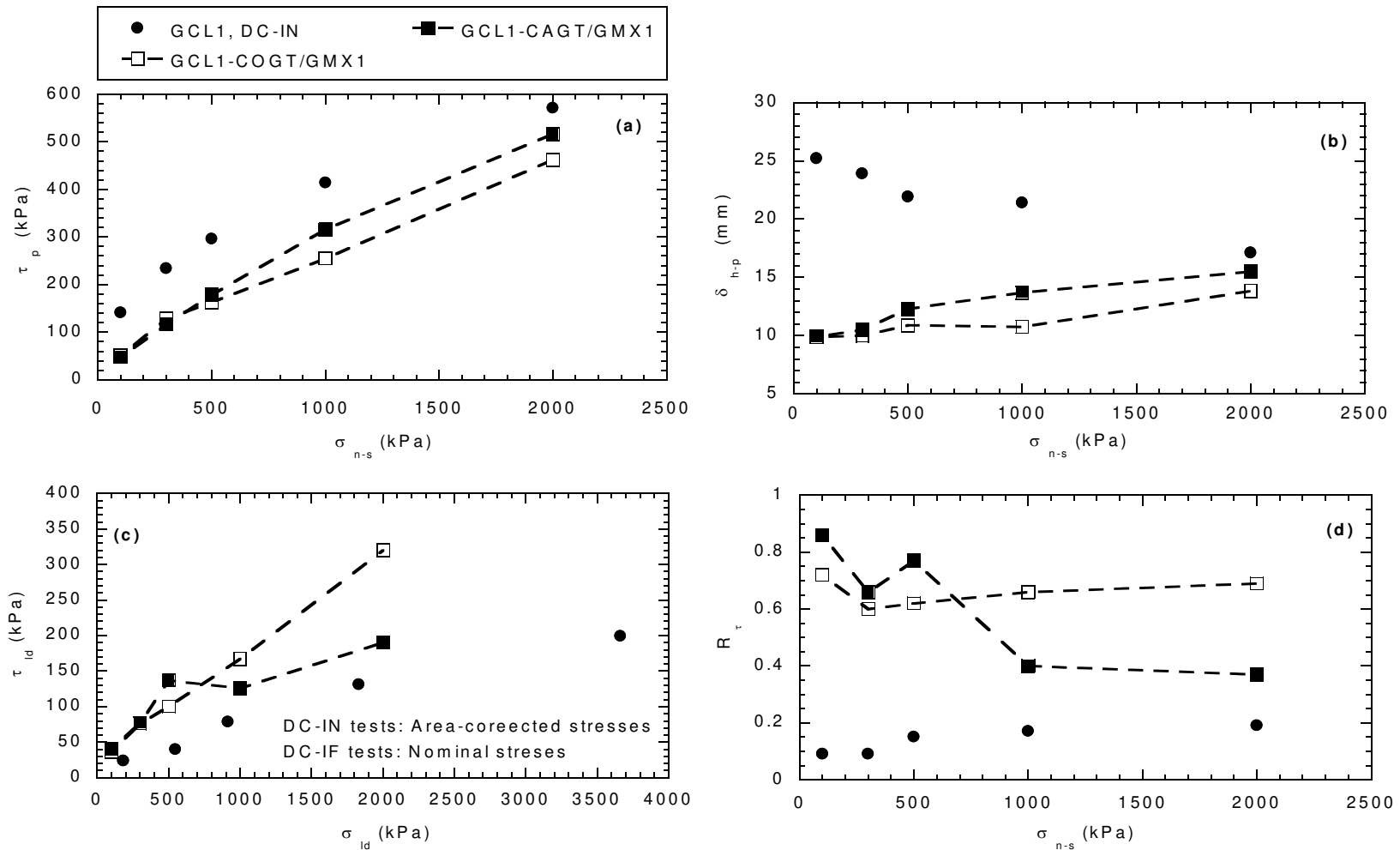


Fig. 3.9. Shear strength and shear behavior relationships for GCL-internal direct shear tests on GCL1 and GMX/GCL interface direct shear tests on GCL1-CAGT/GMX1 and GCL1-COGT/GMX1: (a) peak shear strength (τ_p) versus shearing normal stress (σ_{n-s}), (b) horizontal displacement at peak shear stress (δ_{h-p}) versus σ_{n-s} , (c) large displacement shear stress (τ_{ld}) versus large-displacement normal stress (σ_{ld}), and (d) post-peak strength reduction ratio (R_τ) versus σ_{n-s} .



Fig. 3.10. Post shear pictures of GCL1 specimen in DC-IF tests on (a) GCL1-COGT/GMX1 at $\sigma_{n-s} = 300$ kPa, (b) GCL1-COGT/GMX1 at $\sigma_{n-s} = 1000$ kPa, (c) GCL1-COGT/GMX1 at $\sigma_{n-s} = 2000$ kPa, (d) GCL1-CAGT/GMX1 at $\sigma_{n-s} = 300$ kPa, (e) GCL1-CAGT/GMX1 at $\sigma_{n-s} = 1000$ kPa, and (f) GCL1-CAGT/GMX1 at $\sigma_{n-s} = 2000$ kPa.

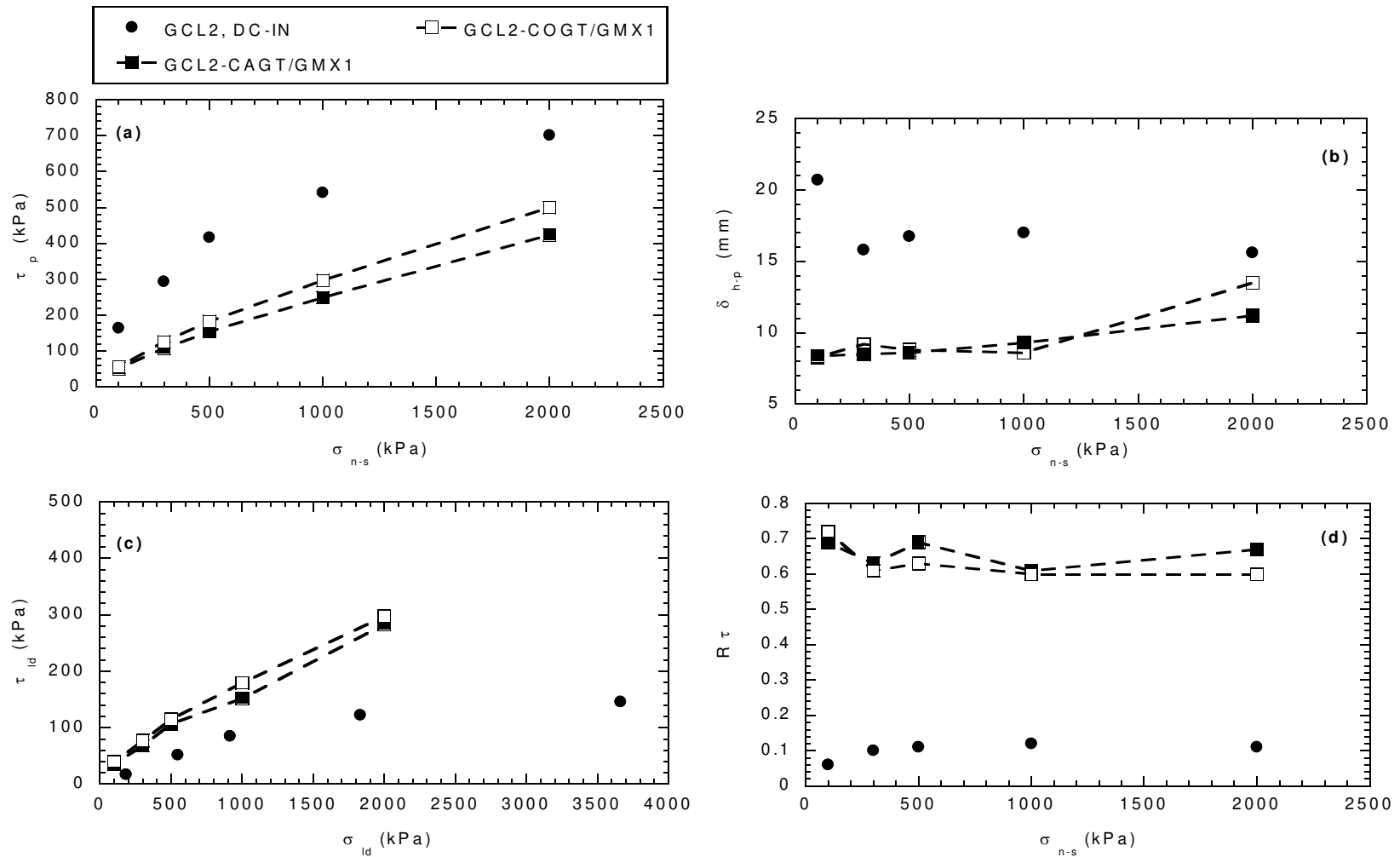


Fig. 3.11. Shear strength and shear behavior relationships for GCL-internal direct shear tests on GCL2 and GMX/GCL interface direct shear tests on GCL2-CAGT/GMX1 and GCL2-COGT/GMX1: (a) peak shear strength (τ_p) versus shearing normal stress (σ_{n-s}), (b) horizontal displacement at peak shear stress (δ_{h-p}) versus σ_{n-s} , (c) large displacement shear stress (τ_{ld}) versus large-displacement normal stress (σ_{ld}), and (d) post-peak strength reduction ratio (R_τ) versus σ_{n-s} .

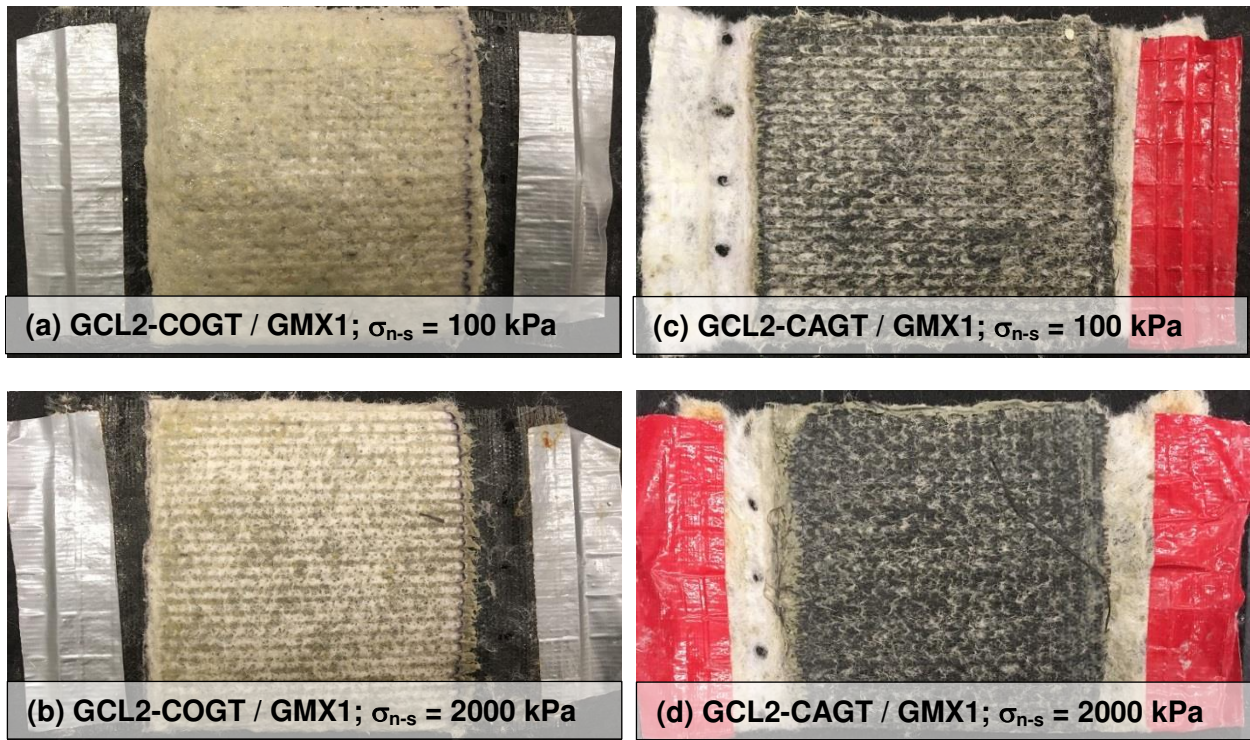


Fig. 3.12. Post shear pictures of GCL1 specimen in DC-IF tests on (a) GCL2-COGT/GMX1 at $\sigma_{n-s} = 100$ kPa, (b) GCL2-COGT/GMX1 at $\sigma_{n-s} = 2000$ kPa, (c) GCL2-CAGT/GMX1 at $\sigma_{n-s} = 100$ kPa, and (d) GCL2-CAGT/GMX1 at $\sigma_{n-s} = 2000$ kPa.

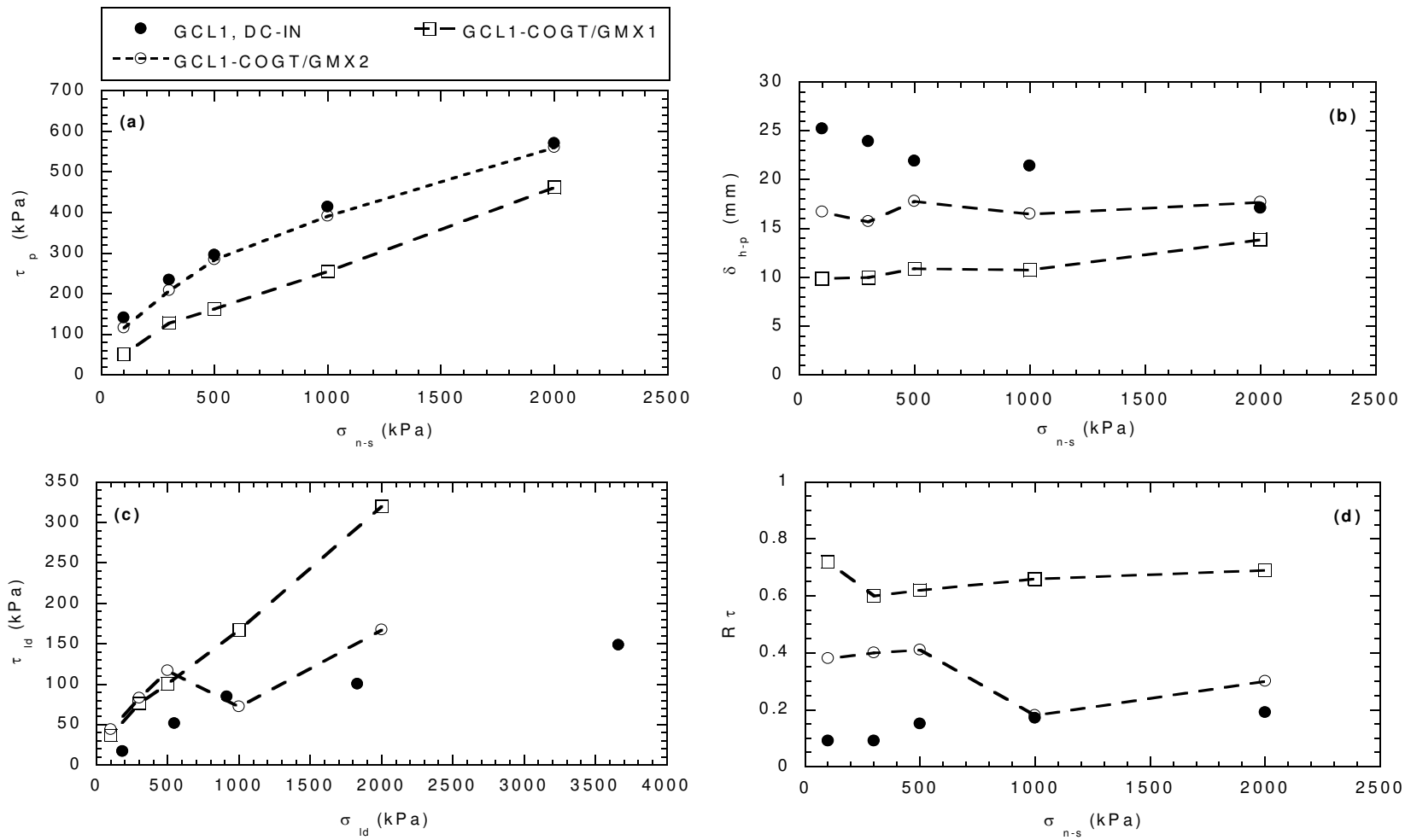


Fig. 3.13. Shear strength and shear behavior relationships for GCL1 and GMX/GCL interface direct shear tests on GCL1-COGT/GMX1 and GCL1-COGT/GMX2: (a) peak shear strength (τ_p) versus shearing normal stress (σ_{n-s}), (b) horizontal displacement at peak shear stress (δ_{h-p}) versus σ_{n-s} , (c) large displacement shear stress (τ_{ld}) versus large-displacement normal stress (σ_{ld}), and (d) Post-peak strength reduction ratio ($R\tau$) versus σ_{n-s} .



Fig. 3.14. Post shear pictures of GCL1 specimen in DC-IF tests on (a) GCL1-COGT/GMX1 at $\sigma_{n-s} = 100$ kPa, (b) GCL1-COGT/GMX1 at $\sigma_{n-s} = 300$ kPa, (c) GCL1-COGT/GMX1 at $\sigma_{n-s} = 2000$ kPa, (d) GCL1-COGT/GMX2 at $\sigma_{n-s} = 100$ kPa, (e) GCL1-COGT/GMX2 at $\sigma_{n-s} = 300$ kPa, and (f) GCL1-COGT/GMX2 at $\sigma_{n-s} = 2000$ kPa

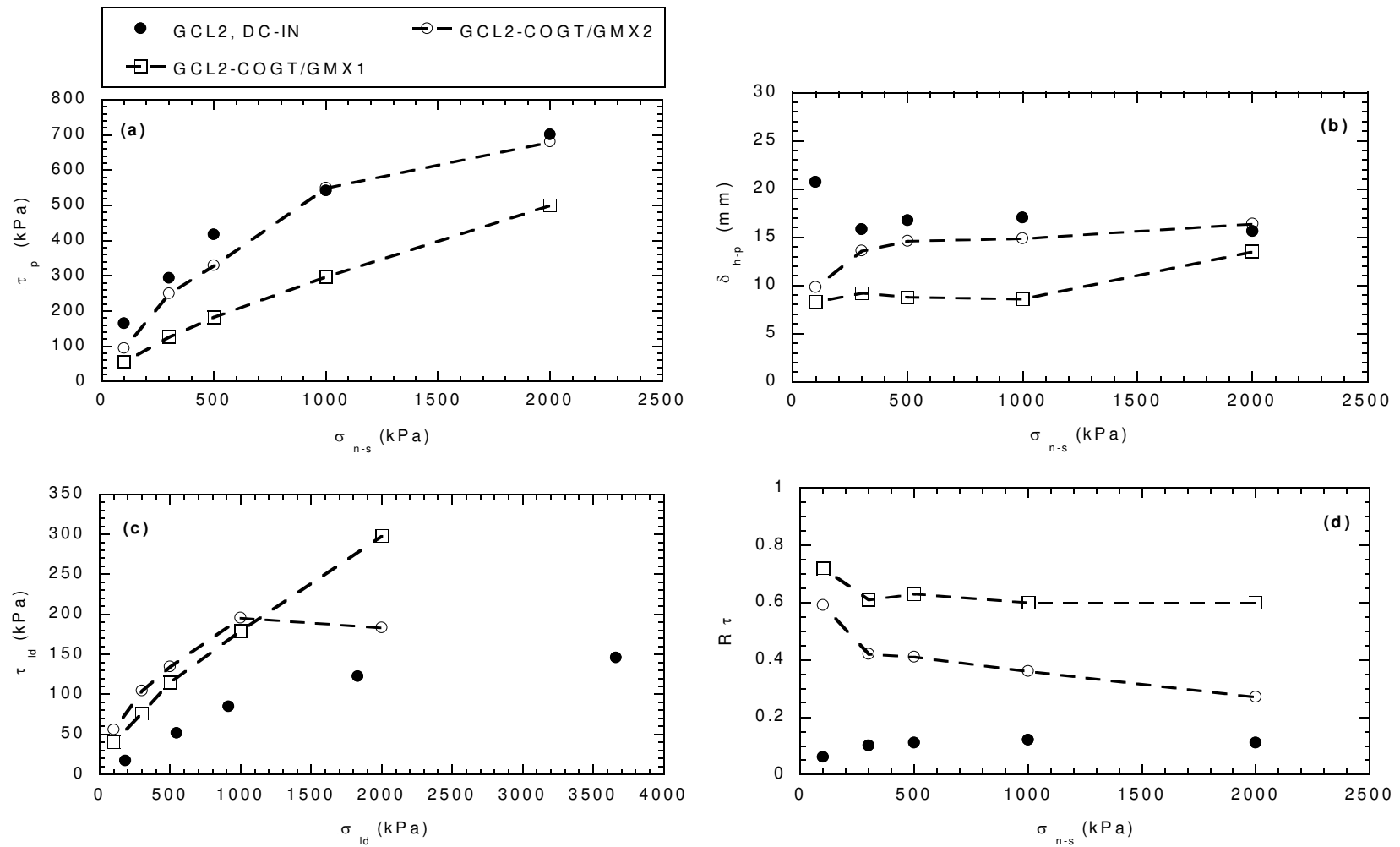


Fig. 3.15. Shear strength and shear behavior relationships for GCL-internal direct shear tests on GCL2 and GMX/GCL interface direct shear tests on GCL2-COGT/GMX1 and GCL2-COGT/GMX2: (a) peak shear strength (τ_p) versus shearing normal stress (σ_{n-s}), (b) horizontal displacement at peak shear stress (δ_{h-p}) versus σ_{n-s} , (c) large displacement shear stress (τ_{ld}) versus large-displacement normal stress (σ_{ld}), and (d) Post-peak strength reduction ratio ($R\tau$) versus σ_{n-s} .



Fig. 3.16. Post shear pictures of (a) GCL2-COGT/GMX1 at $\sigma_{n-s} = 100$ kPa, (b) GCL2-COGT/GMX1 at $\sigma_{n-s} = 500$ kPa, (c) GCL2-COGT/GMX1 at $\sigma_{n-s} = 2000$ kPa, (d) GCL2-COGT/GMX2 at $\sigma_{n-s} = 100$ kPa, (e) GCL2-COGT/GMX2 at $\sigma_{n-s} = 500$ kPa, and (f) GCL2-COGT/GMX2 at $\sigma_{n-s} = 2000$ kPa.

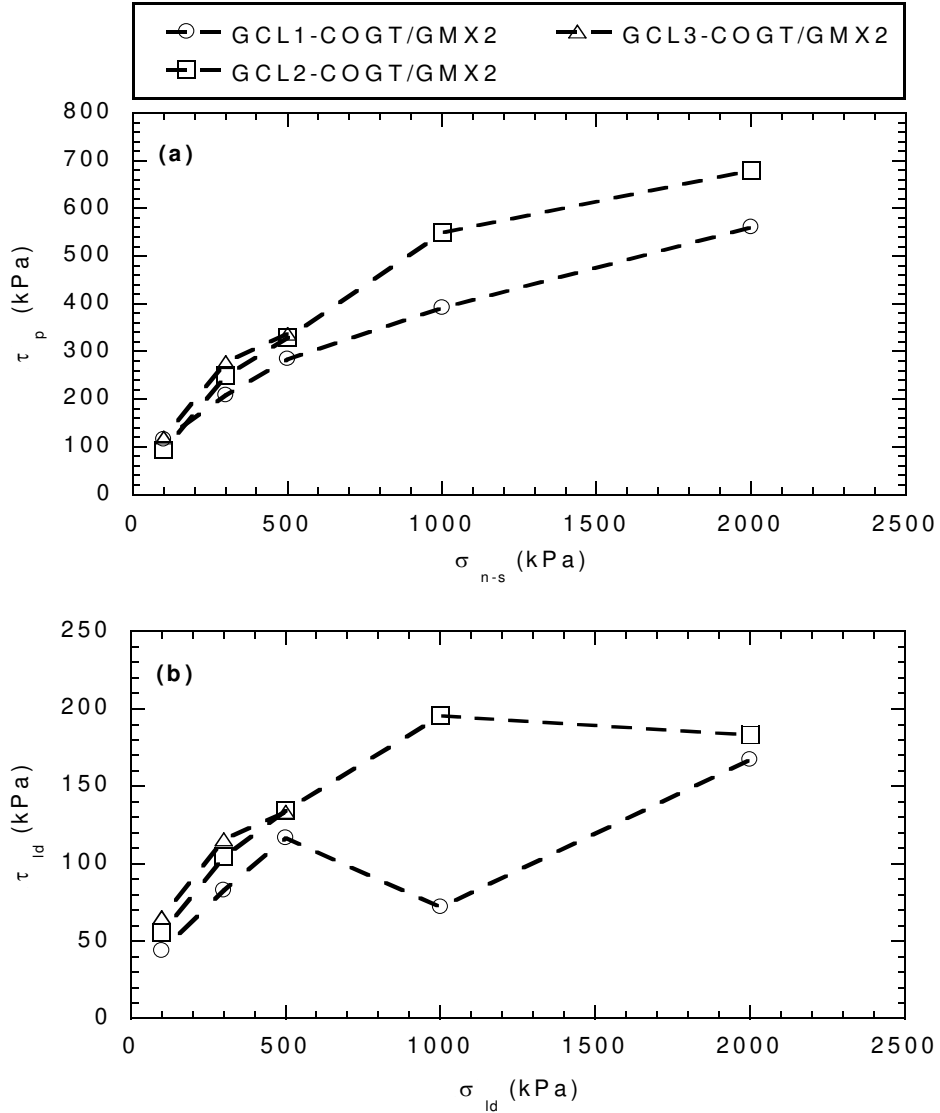


Fig. 3.17. Shear strength relationships for GMX/GCL interface direct shear tests on GCL1-CAGT/GMX1, GCL2-CAGT/GMX1, and GCL3-CAGT/GMX1: (a) peak critical strength (τ_{p-cr}) versus shearing normal stress (σ_{n-s}), and (b) large-displacement critical strength at $\delta_h = 70$ mm (τ_{70-cr}) versus σ_{n-s} .

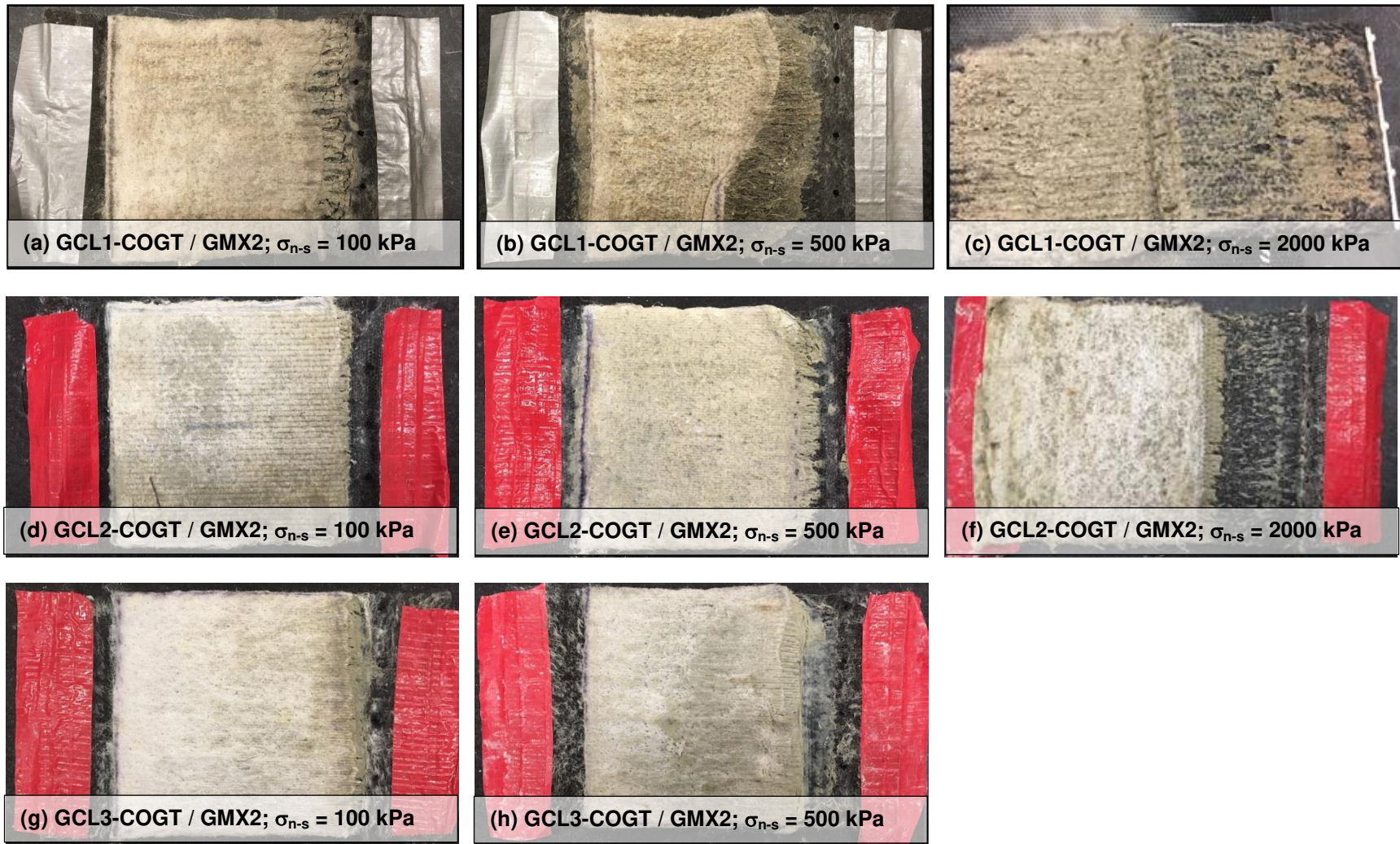


Fig. 3.18. Post shear pictures of (a) GCL1-COGT/GMX2 at $\sigma_{n-s} = 100$ kPa, (b) GCL1-COGT/GMX2 at $\sigma_{n-s} = 500$ kPa, (c) GCL1-COGT/GMX2 at $\sigma_{n-s} = 2000$ kPa, (d) GCL2-COGT/GMX2 at $\sigma_{n-s} = 100$ kPa, (e) GCL2-COGT/GMX2 at $\sigma_{n-s} = 500$ kPa, (f) GCL2-COGT/GMX2 at $\sigma_{n-s} = 2000$ kPa, (g) GCL3-COGT/GMX2 at $\sigma_{n-s} = 100$ kPa, and (h) GCL3-COGT/GMX2 at $\sigma_{n-s} = 500$ kPa.

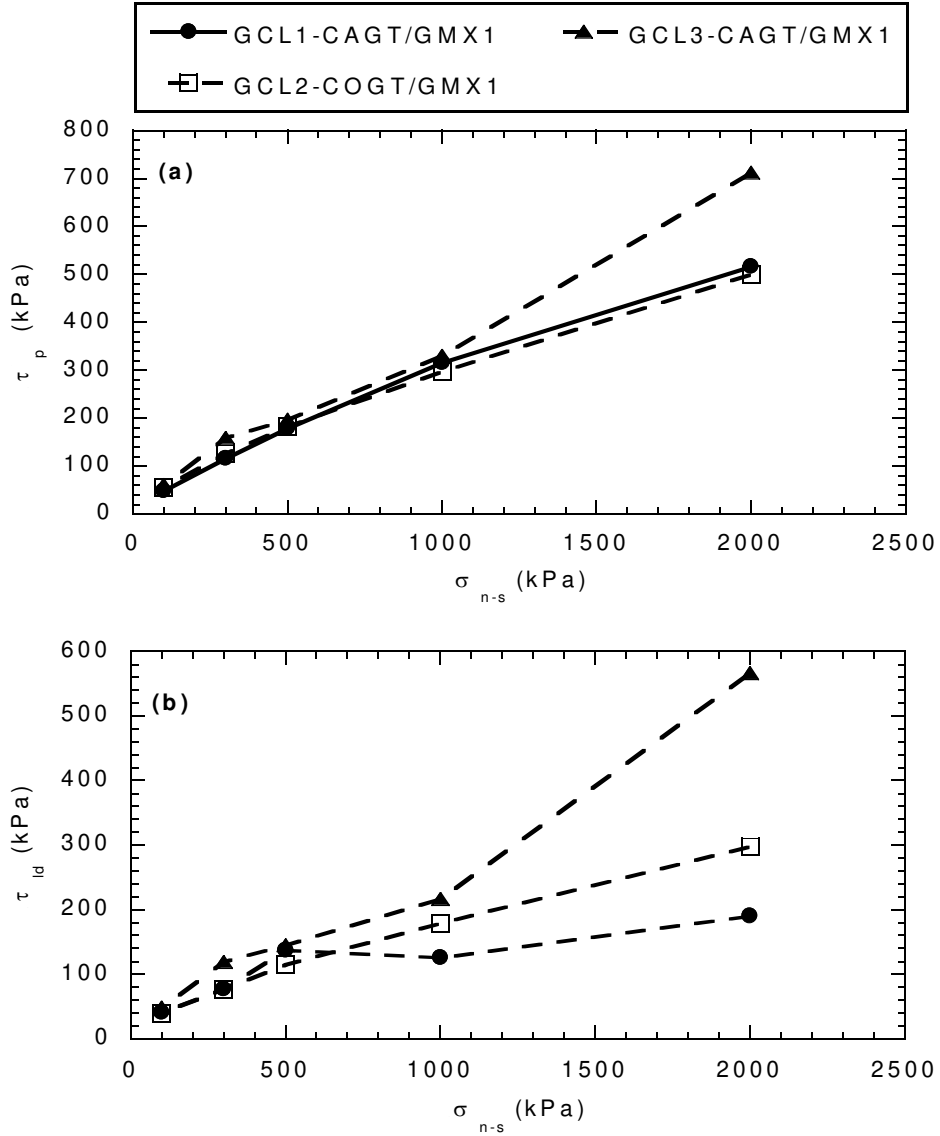


Fig. 3.19. Shear strength relationships for GMX/GCL interface direct shear tests on GCL1-CAGT/GMX1, GCL2-CAGT/GMX1, and GCL3-CAGT/GMX1: (a) peak critical strength (τ_{p-cr}) versus shearing normal stress (σ_{n-s}), and (b) large-displacement critical strength at $\delta_h = 70$ mm (τ_{70-cr}) versus σ_{n-s} .

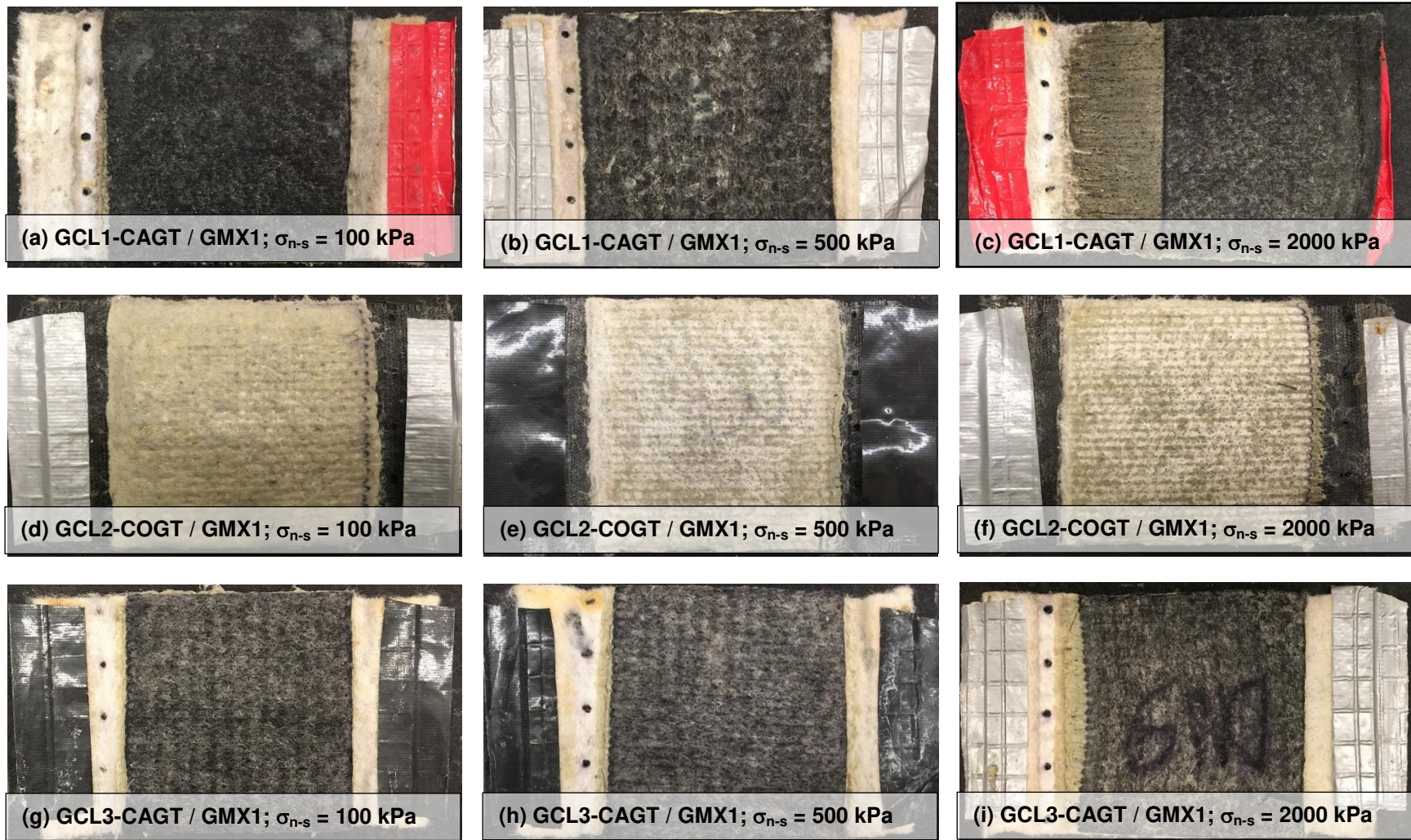


Fig. 3.20. Post shear pictures of (a) GCL1-CAGT/GMX1 at $\sigma_{n-s} = 100$ kPa, (b) GCL1-CAGT/GMX1 at $\sigma_{n-s} = 500$ kPa, (c) GCL1-CAGT/GMX1 at $\sigma_{n-s} = 2000$ kPa, (d) GCL2-CAGT/GMX1 at $\sigma_{n-s} = 100$ kPa, (e) GCL2-CAGT/GMX1 at $\sigma_{n-s} = 500$ kPa, (f) GCL2-CAGT/GMX1 at $\sigma_{n-s} = 2000$ kPa, (g) GCL3-CAGT/GMX1 at $\sigma_{n-s} = 100$ kPa, (h) GCL3-CAGT/GMX1 at $\sigma_{n-s} = 500$ kPa, (i) GCL3-CAGT/GMX1 at $\sigma_{n-s} = 200$.

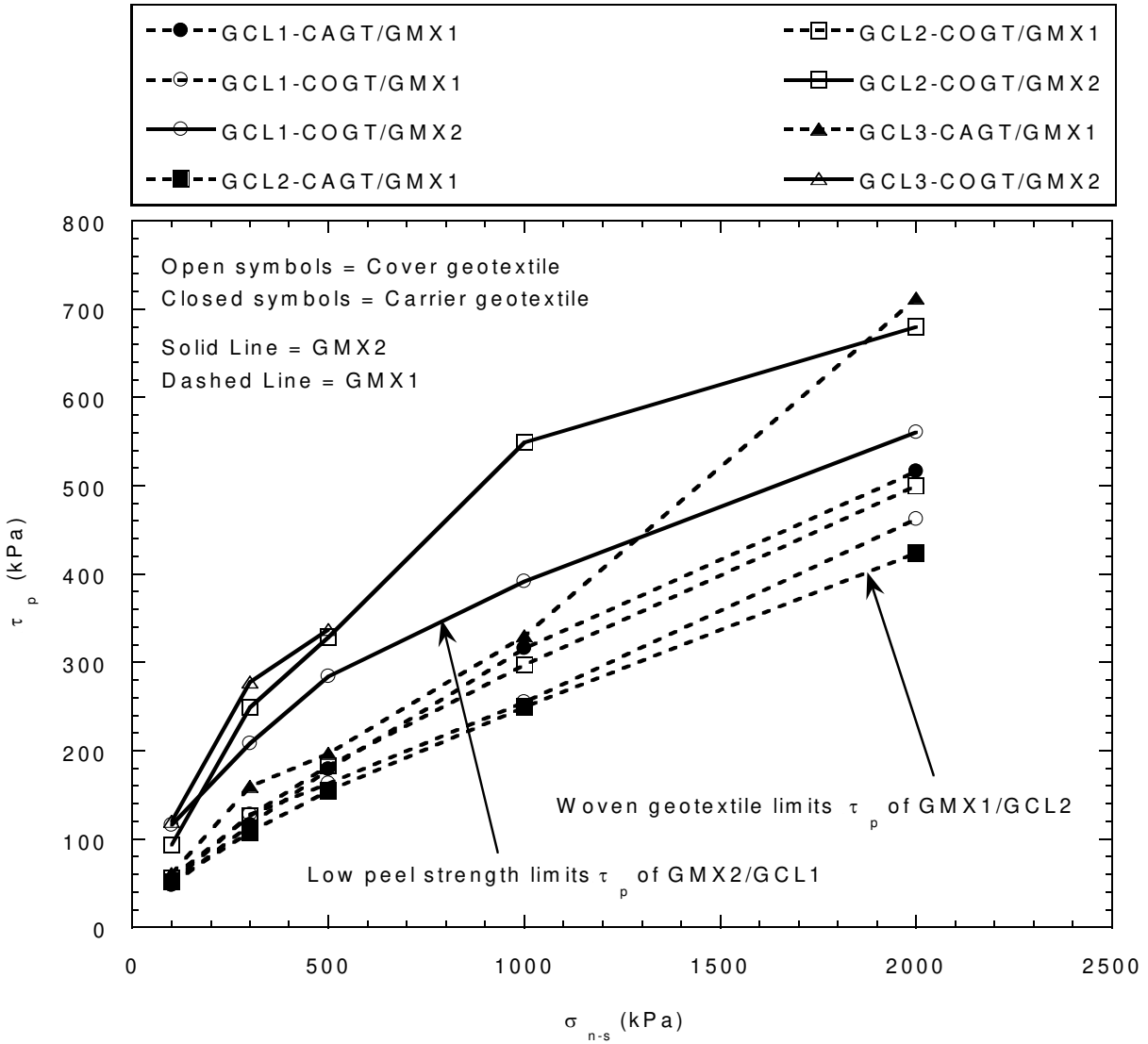


Fig. 3.21. Comparison between peak critical strength (τ_{p-cr}) and normal stress (σ_{n-s}) relationships for eight GMX/GCL composite systems in this study.

CHAPTER 4: EFFECT OF TEMPERATURE ON CRITICAL STRENGTH OF GEOSYNTHETIC CLAY LINER / TEXTURED GEOMEMBRANE COMPOSITE SYSTEMS

4.1 Introduction

Geosynthetic clay liners (GCLs) often are used in combination with a textured geomembrane (GMX) in liner and cover systems for waste containment. The normal stress at the bottom of a liner system in containment applications such as heap leach pads can be as high as 4 MPa (Lupo 2010). High normal stresses in GCL/GMX composite systems can also coincide with high shear stresses in applications containing slopes. The integrity of barrier system must be maintained via resisting the applied shear stress internally within the GCL and at the interface between the GCL and adjacent geosynthetic and/or earthen material.

The design of liner and cover systems requires the critical strength of a GCL/GMX composite system. Critical strength (τ_{cr}) is the shear strength at failure in a GCL/GMX composite system, which can be defined at shear deformation corresponding to peak or large-displacement. The critical strength depends on the failure mode of a composite system, and can be controlled by internal shear strength of a GCL or by interface shear strength between a GCL and GMX. Current practice is to use a factor of safety = 1.5 for peak shear strength and 1.1 for large-displacement shear strength of a GCL/GMX composite.

Considering the low shear strength of the hydrated bentonite (Mesri and Olson 1977; Mitchel and Soga 2005), GCLs are internally reinforced via needle-punching or stitched bonding (Fox and Stark 2015). In needle-punched reinforced GCLs (NP GCLs), a series of fibers from the cover geotextile of the GCL are punched through the bentonite and entangled within the carrier geotextile of the GCL. Therefore, internal shear resistance in NP GCLs is attributed to the tensile strength of the reinforcement fibers and entanglement strength of fiber connection

with the carrier geotextile of the GCL (Gilbert et al. 1996; Fox et al. 1998; Athanassopoulos and Yuan 2010; Fox and Stark 2015; Ghazizadeh and Bareither 2018 b,c).

Interface shear strength between a GCL and GMX is enhanced relative to the interface shear strength between a GCL and smooth geomembranes. The higher interface shear resistance of a GCL and GMX developed from two mechanisms: (i) the presence of macro-scale asperities on a GMX that interlock with fibers of the non-woven geotextile of the GCL (also known as Velcro effect); and (ii) higher surface friction between the GMX and geotextile of the GCL due to increased surface area contact (Jones and Dixon 1998; Chiu and Fox 2004; Hebel et al. 2005; Bacas et al. 2011 & 2015; Eid 2011; Ghazizadeh and Bareither 2018a)

Barrier systems in containment applications can be exposed to elevated temperatures (e.g., ≥ 50 °C) as a result of biological activity (e.g., anaerobic biodegradation in municipal solid waste), exothermic reactions (e.g., chemical reactions in heap leach pads), and climate conditions (e.g., sunlight exposure to cover systems) (Thiel and Smith 2004; Rowe 2005; Yeşiller et al. 2005; Touze-Foltz et al. 2008; Steemson and Smith 2009; Bouazza et al. 2011; Stark et al. 2011; Jafari et al. 2013; Apiwantragoon et al. 2014; Yeşiller et al. 2015; Jafari and Stark 2017). Elevated temperatures ≥ 50 °C have been shown to adversely affect the mechanical properties of polymeric materials (Andrawes et al. 1984; Ariyama et al. 1997; Kongkitkul et al. 2012; Karademir and Frost 2014; Stepien and Szymanski 2015). Considering that current design of GCL/GMX composite systems is based on results of internal and interface direct shear tests at room temperature, there are concerns regarding the shear behavior of GCL/GMX composite systems at elevated temperatures.

The objectives of this study were to (i) assess the effect of temperature on shear behavior and critical strength of GCL/GMX composite systems and (ii) provide design considerations for containment applications subjected to elevated temperatures. Internal shear tests on GCLs and interface shear tests on GCL/GMX composite systems were performed at room temperature (≈ 20 °C) and an elevated temperature of 80 °C. Identical specimen

conditioning and test procedures were followed in all internal and interface shear tests to ascertain the effects of test temperature and material variability. The failure mode of GCL/GMX composite systems was determined and changes in peak and large-displacement critical strength were quantified.

4.2 Background

4.2.1 Shear Behavior of GCL/GMX Composite Systems

A schematic of a GCL/GMX composite system used in a liner for waste containment is shown in Fig. 4.1. The composite system is subjected to normal stress (σ_n) and shear stress (τ). Holistically, critical strength of the liner system can be controlled by interface strength between the GMX and adjacent material, interface strength along the GCL/GMX interface, internal strength of the GCL, or interface strength between the GCL and adjacent material. In this study, critical strength of a GCL/GMX composite system was constrained to focus on the internal shear strength of a GCL and interface shear strength between a GCL and GMX.

Internal and interface shear behavior of GCLs have been evaluated in numerous studies via direct shear, torsional ring shear, and inclined plane shear tests (e.g. Gilbert et al. 1996; Siebken et al. 1997; Trauger et al. 1997; Fox et al. 1998; Eid et al. 1999; Koerner et al. 2001; Olsa and Swan 2001; Triplett and Fox 2001; Chiu and Fox 2004; Zornberg et al. 2005; Nye and Fox 2007; Fox and Kim 2008; Muller et al. 2008; McCarthney et al. 2009; Chen et al. 2010; Fox et al. 2010; Bacas et al. 2011; Eid 2011; Fox and Ross 2011; Bacas et al. 2015; Hanson et al. 2015; Stark et al. 2015; Thielmann et al. 2016; Khilnani et al. 2017; Bareither et al. 2018; and Ghazizadeh and Bareither 2019b). These previous experiments has generated an abundance on knowledge, and in particular, identified three different failure modes in GCL/GMX composite systems: (i) complete interface failure, (ii) partial interface/internal failure, and (iii) complete internal failure mode. In complete interface failure, shear displacement develops along the interface between the GCL and GMX while no failure occurs within the GCL reinforcement

fibers. In partial interface/internal failure, although slippage and shear deformation occurs along the GCL/GMX interface, the GCL also experiences internal deformation due to failure of some reinforcement fibers (i.e., via fiber bundle disentanglement and/or tensile fiber rupture). In complete internal failure, failure develops internally within the GCL due to failure of reinforcement fibers and no slippage occurs between the GCL and GMX.

Failure modes of GCL/GMX composite systems develop due to different magnitudes of developed shear resistance at the interface between the GCL and GMX. For example, if the developed shear resistance is considerably less than the internal shear strength of the GCL, failure occurs via slippage between the GCL and GMX and complete interface failure will occur. In contrast, if the developed shear resistance surpasses the internal shear strength of the GCL, the failure mode of the composite system will be complete internal failure (Ghazizadeh and Bareither 2019b).

In previous GCL/GMX interface shear tests, development of interface frictional resistance has been attributed to two factors: (i) interface friction between the geotextile of the GCL and GMX; and (ii) interlocking between the geotextile fibers and GMX asperities. The contribution of each mechanism to the developed shear resistance between the geotextile of the GCL and GMX depends on various factors, including polymer type, geotextile type, geotextile mass per area, GMX manufacturing method, GMX roughness, and extent of bentonite extrusion on the GMX (Jones and Dixon 1998; Hebelier 2005; Chen et al. 2010; Bacas et al. 2011, 2015). For various GCL/GMX composite systems, complete interface failure was mainly observed at lower σ_n , whereas complete internal failure were reported at high σ_n . (Fox and Ross 2011; Thielmann et al. 2016; Khilnani et al. 2017; Ghazizadeh and Bareither 2019b). Therefore, the contribution of interface friction and interlocking to the magnitude of developed shear resistance between a specific GCL and GMX changes as a function of σ_n .

A schematic of the interface between the geotextile of a GCL and GMX subjected to low and high σ_n is shown in Fig. 4.2. The schematic in Fig. 4.2 was drawn for an interface between a non-woven geotextile and GMX; however, woven geotextiles of GCLs can also be in contact with a GMX. At low σ_n , developed shear resistance between the geotextile and GMX primarily is due to friction as interlocking occurs only at a superficial level (Hebeler 2005; Bacas et al. 2011 and 2015). Considering that the developed frictional resistance is proportional to σ_n , relatively low interface shear stresses are mobilized between the geotextile and GMX interface at low σ_n . These low interface shear stresses are insufficient to cause failure of reinforcement fibers within NP GCLs, particularly NP GCLs with high internal shear strength. Thus, failure of the composite system will be complete interface failure.

As normal stress increases, the geotextile will compress and become interbedded between asperities of the GMX, which results in interlocking of the two geosynthetics at high σ_n (Hebeler 2005; Bacas et al. 2011). Interlocking between geosynthetic surfaces at high σ_n is the predominant shear resistance mechanism contributing to shear resistance between a non-woven geotextile and GMX. The increase in developed shear stress along the interface between the GCL and GMX can force failure to occur internally within a GCL such that complete internal failure develops. However, interlocking is negligible between a woven geotextile and GMX, such that friction remains the dominant interface shear resistance mechanism and interface and/or partial interface/internal failure develop even at high σ_n .

4.2.2 Effect of Temperature on Geosynthetics and Polymers

Reinforcement fibers in GCLs commonly are made of polypropylene and polyethylene, which are members of polyolefin family (Hsuan 2002). Geomembranes commonly are made of high density polyethylene, linear low density polyethylene, or polyvinyl chloride. The intermolecular forces in the polymer structure weaken with an increase in temperature, which also

increases the mobility of polymer chains (Daniels 1989; Lakes and Lakes 2009; Karademir 2011; Koerner 2012; McKeen 2014). Prior research involving tensile and shear testing of polymeric materials and geosynthetics has shown a decrease in tensile strength and Young's modulus, and increase in tensile elongation, creep deformation, and creep rate with an increase in temperature (Andrawes et al. 1984, Budiman 1994; Lord et al. 1995; Ariyama et al. 1997, Hsieh and Tseng 2008; Kongkitkul et al. 2012, Karademir and Frost 2014; Stepien and Szymanski 2015). Considering that GMXs and GCLs are polymeric materials, internal shear strength of GCLs and interface shear strength of a GCL/GMX composite system are influenced by elevated temperatures.

Bareither et al. (2018) performed displacement-controlled internal shear tests on NP GCLs and reported up to 40% reduction in peak shear strength (τ_p) with an increase in temperature from 20 °C to 80 °C. Ghazizadeh and Bareither (2019a,b) reported larger amounts of internal shear deformation and failure under lower shear stress for NP GCL specimens tested at elevated temperatures ($40\text{ °C} \leq T \leq 80\text{ °C}$) in stress-controlled shear tests. In constant-stress creep shear tests conducted by Muller et al. (2008), time until failure (i.e., time between application of shear stress and internal GCL failure) for a given applied shear stress and reinforced GCL reduced for specimens tested at elevated temperature. Based on results from Muller et al. (2008). Zanzinger and Saathof (2012) and Zanzinger (2016) performed elevated temperature creep experiments to facilitate internal shear failure of reinforced GCLs in a shorter elapsed time relative to creep tests at room temperature. Results of the aforementioned internal GCL shear tests indicate that the internal shear strength of reinforced GCLs reduced at elevated temperatures. The reduced internal shear strength in NP GCLs was attributed to a reduction in the tensile modulus of reinforcement fibers as well as a reduction in the entanglement strength of the fiber bundles-geotextile connection (Ghazizadeh and Bareither 2019a).

The effect of temperature on interface shear strength of GCLs has received limited attention. Hanson et al. (2015) investigated interface shear strength between a NP GCL and a

co-extruded GMX for temperatures ranging from 2 °C to 40 °C. Their results showed an increase in interface shear strength from 2 °C to 20 °C following by a decrease in interface shear strength from 20 °C to 40 °C. Results from Hanson et al. (2015) contradict elevated temperature interface shear tests between geomembranes and geotextile, which have shown a consistent increase in the geotextile-geomembrane interface shear strength with increasing temperature (Pasqualini et al.1993; Akpınar and Benson 2005; Karademir and Frost 2011). Although these previous studies provide valuable information, there are still uncertainties and undefined mechanisms regarding interface shear strength of GCLs and GMXs at elevated temperature.

4.3 MATERIALS

Characteristics and properties of GCLs used in this study are tabulated in Table **4.1**. All three GCLs were commercially available, non-heat-treated, NP GCLs containing polypropylene geotextiles and granular bentonite. However, the three GCLs had different geotextile type (i.e., woven versus non-woven), geotextile mass per area, and peel strength (PS).

Interface shear tests were conducted with all three NP GCLs sheared against the same GMX. The GMX was a spike-structured geomembrane with uniform spike pattern. The GMX was linear low density polyethylene (LLDPE) and had a nominal core thickness = 1.5 mm, spike height = 0.51 mm, and contained approximately 340 spikes in a 100-cm² surface area.

4.4 Direct Shear Testing

4.4.1 Experimental Procedure

Geosynthetic clay liner internal shear tests and GCL/GMX interface shear tests were performed with a displacement-controlled direct shear apparatus equipped with a feedback-controlled heating system capable of maintaining a constant temperature up to 80 ± 1 °C.

Design details and results of experiments to evaluate functionality and applicability of the direct shear apparatus are in Bareither et al. (2018).

In this study, internal and interface shear tests were performed on 150 mm x 150 mm GCL specimens. The 150 mm GCL specimens was used in lieu of conventional 300 mm x 300 mm specimens because the smaller specimens have been shown to yield similar shear behavior to larger specimens (Bareither et al. 2018). Geosynthetic clay liner specimens were cut with a razor knife (ASTM D6072) with initial dimensions of 150 mm by 200 mm, with the larger dimension in machine direction to facilitate clamping geotextiles of the GCL to the upper and lower gripping plates. Textured geomembrane specimens were cut with dimensions of 175 mm by 300 mm, with the larger dimension in machine direction. The larger size of the GMX specimens in comparison to GCL specimens was to ensure that the GCL remained in contact with GMX during the interface shear tests.

Hydration and consolidation of a GCL specimen was performed according to a two-stage procedure (Fox et al. 1998; Bareither et al. 2018). The GCL specimens were hydrated in de-ionized water at room temperature under a 20 kPa normal stress for 48 hr. This hydration procedure was the same for all GCL specimens used in internal and interface shear tests. At the end of hydration, GCLs for internal shear tests were sandwiched between two pyramid-tooth plates and transferred to the shear box for consolidation. Pyramid-tooth plates served as the gripping system in this study, and were designed based on Allen and Fox (2007). The GCL specimens used in interface shear tests were clamped to a single pyramid-tooth plate and placed in contact with a GMX such that the interface was between the carrier geotextile of the GCL and the GMX. The GMX was placed in contact with a pyramid-tooth plate with 1-mm tall teeth, which penetrated into the GMX and held the GMX in-place during shear.

Specimens for internal or interface shear tests were transferred to the shear box and a normal stress of 20 kPa was applied to represent conditions at the end of hydration. The normal stress was doubled every 4-6 h until the target shearing normal stress (σ_{n-s}) was achieved.

Specimens for internal or interface shear tests at room temperature were equilibrated in the shear box under the σ_{n-s} for an additional 24 h before shearing. Specimens for internal or interface shear tests at elevated temperature were subjected to a temperature ramp-up period to achieve 80 °C (i.e., approximately 4 hr) and subsequently equilibrated under the target σ_{n-s} and 80 °C for 24 h before shearing.

Shearing was conducted with a horizontal displacement rate of 0.1 mm/min in both internal and interface shear tests, and specimens were sheared until horizontal displacement (δ_h) was approximately equal to 70 mm (i.e., maximum displacement capacity of a 150 mm GCL specimen). This maximum δ_h was sufficient to capture peak shear strength in internal and interface shear tests; however, residual shear strength of reinforced GCLs typically requires larger δ_h (Fox and Stark 2015). Therefore, large-displacement shear strength was used instead of residual strength in this study and was defined as the shear stress at $\delta_h = 70$ mm.

The shear plane area decreased with horizontal displacement during GCL internal shear due to offset between the upper and lower shear platens. Nominal shear and normal stresses, computed based on the initial shear plane area of a GCL specimen, were used in the analysis of the peak shear strength. Despite an offset between the upper and lower shear platens, reinforcement fibers within the initial shear plane remain intact between the cover and carrier geotextiles to generate peak shear strength. However, reinforcement fibers fail post peak strength, and thus, area corrected normal and shear stresses were used in the analysis of the large-displacement shear strength. In contrast, the shear plane area between the GCL and GMX in the interface shear tests remained constant due to the larger dimensions of the GMX, and thus, nominal normal and shear stresses were used for analysis of peak and large-displacement shear strength.

The GCL specimens were visually inspected after a given internal shear test to identify successful internal shear. Any signs of stress localization, geotextile tearing, geotextile

elongation, or slippage between the GCL and gripping surfaces indicated an unsuccessful internal shear test. The GCL and GMX specimens were visually inspected after a given interface shear test to identify the failure mode of the GCL/GMX composite system.

4.4.2 Data Compilation and Analysis

A summary of the GCL internal direct shear tests is in Table 4.2. The summary in Table 4.2 includes test temperature (T), σ_{n-s} , τ_p , secant friction angle (ϕ_{s-p}), horizontal displacement at peak shear strength (δ_{h-p}), area-corrected normal stresses at $\delta_h = 70$ mm (AC σ_{ld}), area-corrected large-displacement shear strength at $\delta_h = 70$ mm (AC τ_{ld}), percent change in peak shear strength ($\Delta\tau_p$), and percent change in area-corrected large-displacement shear strength ($\Delta AC\tau_{ld}$). The $\Delta\tau_p$ and $\Delta AC\tau_{ld}$ were defined according to Eq. 4.1 and 4.2 to express the reduction in shear strength when increasing test temperature from 20°C to 80°C

$$\Delta \tau_p = 100 \frac{\tau_{p-20^\circ C} - \tau_{p-80^\circ C}}{\tau_{p-20^\circ C}} \quad (4.1)$$

$$\Delta AC \tau_{ld} = 100 \frac{AC \tau_{ld-20^\circ C} - AC \tau_{ld-80^\circ C}}{AC \tau_{ld-20^\circ C}} \quad (4.2)$$

where $\tau_{p-20^\circ C}$ is τ_p at 20 °C, $\tau_{p-80^\circ C}$ is the τ_p at 80 °C, $AC \tau_{ld-20^\circ C}$ is AC τ_{ld} at 20 °C, and $AC \tau_{ld-80^\circ C}$ is AC τ_{ld} at 80 °C.

Internal shear tests were performed on GCLA, GCLB, and GCLC at $\sigma_{n-s} = 100, 300, 500, 1000,$ and 2000 kPa at $T = 20^\circ C$ and $80^\circ C$. Post-shear inspection of GCLA and GCLB indicated successful internal shearing for all internal shear tests. In contrast, geotextile tearing and geotextile elongation were observed in post-shear specimens of GCLC at $T = 20^\circ C$ and $80^\circ C$, which indicated unsuccessful internal shearing of GCLC. Considering the unsuccessful internal shearing of GCLC, the summary in Table 4.2 only includes results from internal direct shear tests conducted on GCLA and GCLB.

Unsuccessful internal shearing of GCLC was attributed to low tensile strength of the carrier and cover geotextiles relative to the high peel strength of the GCL (Table 4.1). The high peel strength likely corresponded to high internal shear strength of GCLC (e.g., Athanassopoulos and Yuan 2011). Thus, the geotextiles of GCLC were unable to remain intact against the pyramid-tooth plates and fully transfer the developed shear stress to the internal region of the GCL. The pyramid tooth plates surpassed specifications of gripping systems outlined in ASTM D6243 (e.g., number of teeth per square centimeter and tooth height), which suggests that very high peel strength GCLs (e.g., comparable to GCLC) may be impractical to shear internally without high strength geotextiles used in the GCL construction.

A summary of the GCL/GMX interface direct shear tests is in Table 4.3. Interface shear tests were performed at $T = 20\text{ }^{\circ}\text{C}$ and $80\text{ }^{\circ}\text{C}$ on composite systems of GCLA/GMX, GCLB/GMX, and GCLC/GMX (Table 4.3). The summary in Table 4.3 include σ_{n-s} , ϕ_{s-p} , δ_{h-p} , nominal large-displacement shear strength at $\delta_h = 70\text{ mm}$ (τ_{ld}), $\Delta\tau_p$, percent change in nominal large-displacement shear strength ($\Delta\tau_{ld}$), and failure mode of the composite system. Failure modes of the GCL/GMX composite systems were determined via post-shear inspection of the GCL and GMX specimens. The $\Delta\tau_p$ in the interface shear tests was calculated according to Eq. 4.3. However, $\Delta\tau_{ld}$ in the interface shear tests was computed as

$$\Delta\tau_{ld} = 100 \frac{\tau_{ld-20^{\circ}\text{C}} - \tau_{ld-80^{\circ}\text{C}}}{\tau_{ld-20^{\circ}\text{C}}} \quad (4.3)$$

where $\tau_{ld-20^{\circ}\text{C}}$ is τ_{ld} at $20\text{ }^{\circ}\text{C}$, and $\tau_{ld-80^{\circ}\text{C}}$ is τ_{ld} at $80\text{ }^{\circ}\text{C}$. Nominal shear stresses were used to calculate $\Delta\tau_{ld}$ for interface shear tests since the shear plane area remained constant.

4.5 Results

4.5.1 Internal shear tests

Relationships between shear stress and horizontal displacement are shown in Fig. 4.3 for internal direct shear tests on GCLA and GCLB at 20 °C and 80 °C. The internal shear behavior exhibits an increase in shear stress with increasing displacement until reaching a peak when the maximum internal shear resistance is mobilized, identified as τ_p . Subsequently, shear stress reduced to exhibit displacement-softening behavior. The τ - δ_h relationships in Fig. 4.3 are typical of internal shear behavior for NP GCLs (e.g., Fox and Stark 2015; Bareither et al. 2018). The peak shear strength for a given GCL and temperature increased with increasing σ_{n-s} , and furthermore, higher peak shear strength was observed for GCLB relative to GCLA for a given temperature and σ_{n-s} . The GCLB had a higher peel strength than GCLA, and peak shear strength of internally reinforced GCLs has been reported to increase with increasing peel strength (e.g., Athanassopoulos and Yuan 2011; Fox and Stark 2015; Bareither et al. 2018).

The post-peak, displacement-softening behavior of internally reinforced GCLs is attributed to the gradual failure of reinforcement fibers via a combination of fiber bundle disentanglement from the carrier geotextile and tensile rupture of fibers (Fox and Stark 2015; Bareither et al. 2018). Displacement-softening continued until reaching a minimum shear stress corresponding to $\delta_h \geq 60$ mm, whereupon relatively small decreases in τ were observed with continued displacement. Upon achieving large displacements in NP GCLs, the predominant fraction of internal reinforcement fibers have failed, and internal shear resistance is controlled by the interface shear resistance between the hydrated bentonite and the geotextile of the GCL.

The internal shear behavior for both GCLs sheared at $T = 80$ °C was similar to the internal shear behavior at $T = 20$ °C with the key differences being reductions in the magnitude of peak shear strength and less pronounced displacement-softening behavior. The peak shear strength at $T = 80$ °C was always lower than the peak shear strength at $T = 20$ °C regardless of

σ_{n-s} and GCL. The reduction in peak shear strength of GCLA and GCLB with an increase in temperature from 20 °C to 80 °C is in agreement with previous studies that reported reduced peak internal shear resistance of NP GCLs at elevated temperature (e.g., Bareither et al. 2018; Ghazizadeh and Bareither 2019).

4.5.2 Interface shear tests

Relationships of shear stress versus horizontal displacement from interface shear tests on the three GCL/GMX composite systems are shown in Fig. 4.4. All interface shear tests exhibited a peak strength and post-peak strength reduction (Fig. 4.4); however, the magnitude of the post-peak reduction was less than that observed in the GCL internal shear tests and varied as a function of normal stress, GCL, and temperature. Furthermore, there was no noticeable trends of higher peak shear strength observed with increasing GCL peel strength (i.e., peel strength increased from GCLA to GCLB to GCLC). The majority of shear failure modes were identified as interface failure (Table 4.3); however, the identification of partial interface/internal failure and also internal failure in select specimens contributed to differences observed in the τ - δ_h relationships.

Photographs of post-shear GCL specimens from GCL/GMX composite systems are shown in Fig. 4.5 that exhibit complete interface failure, complete internal failure, and partial interface/internal failure. The photograph in **Error! Reference source not found.a** is from the CLB/GMX interface shear test at $\sigma_n = 100$ kPa and $T = 80$ °C, which exhibits complete interface failure. Complete interface failure was the predominant failure mode for the GCL/GMX composite systems in this study (Table 4.3). Shear behavior for complete interface failure was characterized by a relatively small horizontal displacement at peak shear strength (i.e., δ_{h-p} in Table 4.3) and low post-peak stress reduction.

Complete internal failure was only observed for the GCLA-GMX composite system at $\sigma_{n-s} = 2000$ kPa and $T = 20$ °C (Fig. 4.5b). Complete internal failure was characterized by a relatively large horizontal displacement to peak shear strength and large post-peak stress reduction. Therefore, interface shear behavior of a GCL/GMX composite system is comparable to the internal shear behavior of a GCL internal shear test when internal shear failure occurs during an interface shear test.

The photograph in Fig. 4.5c is an example of a composite system with partial interface/internal failure (i.e., GCLC/GMX at $\sigma_n = 100$ kPa and $T = 80$ °C). The shear behavior and corresponding τ - δ_h relationship in partial interface/internal failure depends on the extent of internal shear deformation within the GCL. In the event a GCL experiences relatively minor internal deformation (e.g., GCLB/GMX at $T = 20$ °C and $\sigma_{n-s} = 2000$ kPa), the τ - δ_h relationship is more reflective of a τ - δ_h relationship in which complete interface failure developed. In contrast, in the event a GCL experiences a pronounced amount of internal deformation (e.g., GCLA-GMX at $T = 20$ °C and $\sigma_{n-s} = 1000$ kPa), the τ - δ_h relationship will be more comparable to τ - δ_h relationships of composite systems with complete internal failure.

An increase in test temperature from 20 °C to 80 °C did not necessarily result in the same failure mode for composite systems. For instance, complete internal failure of GCLA/GMX was observed at $T = 20$ °C and $\sigma_{n-s} = 2000$ kPa, whereas failure of this composite system at $T = 80$ °C and $\sigma_{n-s} = 2000$ kPa was partial internal/interface failure. However, independent of failure mode of the GCL/GMX composites, GCL peel strength, and normal stress, peak shear strength at $T = 80$ °C was always less than $T = 20$ °C (Fig. 4.4 and Table 4.3). The decrease in peak shear strength for the GCL/GMX interface shear tests indicates that there was a consistent decrease in interface shear resistance between the geotextile of the GCL and GMX at $T = 80$ °C. This observation contradicts results of previous elevated temperature interface shear tests between textured geomembranes and GCLs or geotextiles (e.g., Hanson et al. 2015).

4.6 Analysis

4.6.1 Peak Critical Strength

Relationships between the τ_p and σ_{n-s} for internal and interface shear tests are shown in Fig. 4.6. Peak critical strength envelopes of the GCL/GMX composite systems were determined via comparing peak shear strength from GCL internal and GCL/GMX interface shear tests. The peak critical strength envelopes at $T = 20$ °C are shown as solid lines and at $T = 80$ °C as dash lines. Peak internal shear strength data for GCLC are not shown in

Fig. 4.6c since internal shear failure was not successful.

Internal peak shear strength of GCLA was larger than peak shear strength measured in the GCLA/GMX interface shear tests for $\sigma_{n-s} \leq 1000$ kPa at both temperatures. The lower value of peak shear strength measured in the GCLA/GMX interface shear tests at $\sigma_{n-s} \leq 1000$ kPa was attributed to complete interface failure or partial interface/internal failure that was more predominantly interface failure. However, comparable peak shear strengths were observed between GCLA internal and GCLA/GMX interface shear tests at $\sigma_{n-s} = 2000$ kPa. This was attributed to complete internal failure (at $T = 20$ °C) or partial internal/interface failure that was more predominantly internal failure (at $T = 80$ °C). Thus, as shear failure transitions from interface to internal failure, there is a larger contribution of internal shear resistance mobilized and critical strength is reflective of GCL internal shear strength.

The critical strength envelopes for GCLB/GMX were consistently lower than the internal peak strength of GCLB at both 20 °C and 80 °C (

Fig. 4.6b). The interface shear failure of the GCLB/GMX composite and lower critical peak strength relative to GCL internal shear strength was attributed to lower potential interface shear resistance between the woven carrier geotextile of GCLB and the GMX. The peak critical strength of GCLC/GMX composite system was also defined by the interface shear strength

between GCLC and GMX since internal shear failure was not possible in the GCL internal shear tests.

Reductions in the internal peak shear strength of GCLA and GCLB as well as interface peak shear strength of all GCL/GMX composites were observed with an increase in temperature from 20 °C to 80 °C. Thus, all critical strength envelopes defined via the GCL/GMX composite systems decreased with an increase in temperature from 20 °C to 80 °C. A decrease in internal shear strength of NP GCLs at elevated temperatures has been attributed to a decrease in entanglement strength between reinforcement fiber bundles and the carrier geotextile of a GCL as well as a decrease in tensile modulus of the reinforcement fibers (Bareither et al. 2018; Ghazizadeh and Bareither 2019a).

The mechanism of shear strength reduction in interface shear tests at elevated temperature depends on failure mode of the GCL/GMX composite system. Although complete internal failure in GCL/GMX interface shear tests at $T = 80$ °C was not observed in this study, the mechanism contributing to a reduction in peak strength of a composite system with complete internal failure would be analogous to the strength reduction mechanism in internal shear tests at elevated temperature. In GCL/GMX composite systems with complete interface failure or partial interface/internal failure with low GCL internal deformation, interface shear strength results predominantly from interlocking between the GMX asperities and geotextile fibers, and friction at the interface between the geotextile and GMX. The decrease in peak shear strength measured in the GCL/GMX interface shear tests at $T = 80$ °C suggests that one or both of the aforementioned strength mechanisms reduces at elevated temperatures.

Interlocking between GMX asperities and geotextile fibers depends on the tensile properties of geotextile fibers (e.g., tensile strength, tensile deformation behavior) and rheological behavior of the GMX (e.g., deformation behavior, compressive strength). Karademir and Frost (2014) reported a decrease in tensile properties of reinforcement fibers with

increasing temperature. The change in deformation behavior and rheology of GMX asperities at $T = 80\text{ }^{\circ}\text{C}$ was investigated via post-shear inspection of GMX specimens.

A schematic of a 175 mm x 300 mm GMX specimen is shown in Fig. 4.7 along with initial and post-shear positions of the 150 mm x 150 mm GCL specimen. Areas at the front and back of the GMX specimen in shear direction never came in contact with the GCL during the shear. In contrast, the area in the middle of the GMX was consistently in contact with the GCL during shear. Photographs of 19 mm x 14 mm areas from the back and central area of the GMX specimen in the GCLC/GMX composite tested under $\sigma_{n-s} = 2000\text{ kPa}$ and $T = 80\text{ }^{\circ}\text{C}$ are shown in Fig. 4.7. Photographs of the GMX were captured with a stereoscopic microscope (Dino-Lite V2). The GMX area at the back of the specimen was only in contact with the hydration solution (i.e., de-ionized water) and did not change during shear. In contrast, GMX spikes in the central area were bent in the direction of shear and there were notable signs of wear and tear on surface of the GMX. Damage to the GMX spikes and abrasion along the GMX surface are related to GMX rheology, whereby differences in deformation of the spikes abrasion of the GMX surface can indicate a change in rheology of the GMX as a function of temperature.

Digital images of GMXs captured with a stereoscopic microscope are shown in Fig. 4.8 for the following: (a) unsheared GMX; (b) GCLC/GMX composite tested at $\sigma_{n-s} = 2000\text{ kPa}$ and $T = 20\text{ }^{\circ}\text{C}$; and (c) GCLC/GMX composite tested at $\sigma_{n-s} = 2000\text{ kPa}$ and $T = 80\text{ }^{\circ}\text{C}$. High-resolution images are shown in Fig. 4.8 for individual GMX spikes and the surface of the GMX. The GMX spike on the unsheared GMX is conical, whereas GMX spikes from GMXs sheared at $20\text{ }^{\circ}\text{C}$ to $80\text{ }^{\circ}\text{C}$ exhibit deformation in direction of shear and abrasion on the spike surface. The GMX spike from the GCLC/GMX interface shear test at $T = 80\text{ }^{\circ}\text{C}$ appeared more deformed in the direction of shear and the surface of the GMX appeared to exhibit more abrasion relative to the GMX at $T = 20\text{ }^{\circ}\text{C}$. Considering the same normal stress ($\sigma_{n-s} = 2000\text{ kPa}$), the more pronounced deformation at $T = 80\text{ }^{\circ}\text{C}$ suggests lower interface frictional and lower GMX spike-geotextile

interlocking against the applied shear stress. The combination of a reduced friction and interlocking strength can support the hypothesis regarding the reduction of GCL-GMX interface shear strength at elevated temperatures.

Relationships between the percent change in peak shear strength versus normal stress are shown in Fig. 4.9 for internal shear tests and in Fig. 4.9b for interface shear tests. Additional data are shown in Fig. 4.9a from a heat-treated and a non-heat-treated NP GCL evaluated in internal direct shear tests at 20 °C to 80 °C by Bareither et al. (2018). The non-heat-treated NP GCL had a non-woven cover and woven carrier geotextile and average peel strength = 790 N/m, whereas the heat-treated NP GCL had a non-woven cover and woven carrier geotextile with average peel strength = 740 N/m. The solid lines in Fig. 4.9 indicate the maximum allowable strength reduction considering the factor of safety of 1.5 for design based on peak shear strength.

The reduction in peak internal GCL shear strength ranged between 19% and 45% for an increase in temperature from 20 °C to 80 °C. Data are scattered and no relationship was observed between $\Delta\tau_p$ and specimen peel strength, type of the GCL carrier geotextile, or σ_{n-s} . The reduction in peak critical strength from GCL/GMX interface shear tests ranged between 16% and 46%, which was comparable to the range of $\Delta\tau_p$ in internal shear tests. No relationship was observed between the $\Delta\tau_p$ in interface shear tests and GCL peel strength or type and mass per area of geotextiles in contact with the GMX. Considering that all experiments were performed with the shear equipment and same operator, variability in $\Delta\tau_p$ can be attributed to variability among GCL and GMX specimens.

Considering the extent of $\Delta\tau_p$ in Fig. 4.9a and Fig. 4.9b, designers should avoid using results of laboratory experiments at room temperature for the design of composite systems subjected to elevated temperatures without considering an appropriate strength reduction factor. Currently, the factor of safety = 1.5 is used for the design with peak critical strength. This factor

of safety corresponds to the maximum $\Delta\tau_p = 33\%$ which is lower than upper $\Delta\tau_p$ limits in both internal and interface shear tests.

4.6.2 Large-Displacement Critical Strength

Relationships between area-corrected large-displacement shear strength and normal stress for internal direct shear tests on GCLA and GCLB at 20 °C to 80 °C are shown in Fig. 4.10. Dashed lines in Fig. 4.10 correspond to contours of large-displacement friction angles (ϕ_{ld}). Non-linear area-corrected τ_{ld} - σ_{ld} relationships were observed for GCLA and GCLB 20 °C to 80 °C, whereby lower ϕ_{ld} were computed for higher normal stress and were attributed to a potential increase in pore water pressure during shear that lowered the ratio of shear-to-normal stress. Large-displacement friction angles for both GCLs at 20 °C to 80 °C were $\leq 6^\circ$, which were comparable to results of previous studies (e.g., Fox and Stark 2015; Bareither et al. 2018) and indicate that temperature had negligible influence on large-displacement shear strength measured in GCL internal shear tests.

Relationships of change in area-corrected large-displacement shear strength (i.e., from 20 °C to 80 °C) versus area-corrected normal stress for internal shear tests on GCLA and GCLB are shown in Fig. 4.11. Data from internal shear tests reported in Bareither et al. (2018) for a non-heat-treated and heat-treated NP GCL are also included in Fig. 4.11. Based on the definition of $\Delta AC \tau_{ld}$ in Eq. 4.2, negative values indicate a higher AC τ_{ld} at 80 °C compared to 20 °C. Thus, increasing the temperature from 20 °C to 80 °C did not produce a consistent effect on large-displacement shear strength, whereby the temperature increase resulted in large-displacement shear strengths approximately $\pm 40\%$ of the strength measured at 20 °C. No identifiable trends were observed to characterize $\Delta AC \tau_{ld}$ as a function of GCL type, geotextile characteristics, normal stress, or heat-treatment method. The solid line in Fig. 4.11 is the maximum allowable reduction in $\Delta AC \tau_{ld}$ assuming design based on FS = 1.1, which is the FS

commonly considered for design with large-displacement shear strength. Although a conclusive argument cannot be made based on the scatter in Fig. 4.11, designing a barrier system with a GCL/GMX composite based on $FS = 1.1$ could be conservative or unconservative if designs do not account for a potential increase in temperature.

Relationships of nominal large displacement shear strength versus normal stress for GCL/GMX interface shear tests are shown in Fig. 4.12. Large-displacement shear strength envelopes for the critical τ_{ld} at $T = 20\text{ }^{\circ}\text{C}$ are shown as solid lines and for $T = 80\text{ }^{\circ}\text{C}$ as dashed lines. Linear large-displacement shear strength envelopes was observed for GCLB/GMX and GCLC/GMX composite systems at $T = 20\text{ }^{\circ}\text{C}$ and $80\text{ }^{\circ}\text{C}$, whereas the strength envelope for GCLA/GMX exhibited multi-linear behavior at both test temperatures. The non-linear nature of the large-displacement strength envelopes for GCLA/GMX was due to different failure modes of the composite system as a function of normal stress (Table 4.3).

Linear large-displacement strength envelopes for GCL/GMX composite systems (i.e., GCLB/GMX, GCLC/GMX, and GCLA/GMX for $\sigma_{n-s} \leq 500\text{ kPa}$) corresponded to failure modes of complete interface failure or partial interface/internal failure with minor GCL internal deformation. In these cases, mechanisms of interface friction and interlocking between the geotextile of the GCL and GMX controlled interface shear strength for the entire range of normal stress. Large displacement friction angles (ϕ_{ld}) and cohesion intercepts (c_{ld}) are included in Fig. 4.12 for the linear strength envelopes. Comparable values of ϕ_{ld} and c_{ld} were observed between GCLC/GMX and GCLA/GMX at $\sigma_{n-s} \leq 500\text{ kPa}$ at $T = 20\text{ }^{\circ}\text{C}$ ($\phi_{ld} \approx 13\text{-}15^{\circ}$ and $c_{ld} \approx 13\text{-}14\text{ kPa}$) and $T = 80\text{ }^{\circ}\text{C}$ ($\phi_{ld} \approx 8\text{-}9^{\circ}$ and $c_{ld} \approx 9\text{-}14\text{ kPa}$). Similarity between the strength envelopes for these two composite systems was due to the same geotextile type (non-woven) with comparable mass per area (Table 4.1) sheared in contact with the GMX. These GCL/GMX interfaces produced higher interface shear resistance relative to the interface between the woven geotextile of GCLB and GMX. Thus, lower ϕ_{ld} were determined for the GCLB/GMX

composite system at $T = 20\text{ }^{\circ}\text{C}$ ($\phi_{ld} \approx 7^{\circ}$) or $80\text{ }^{\circ}\text{C}$ ($\phi_{ld} \approx 5^{\circ}$) relative to the composite systems with GCLA and GCLC.

The multi-linear large-displacement strength envelope of the GCLA-GMX composite system at $T = 20\text{ }^{\circ}\text{C}$ or $80\text{ }^{\circ}\text{C}$ was attributed to a transition from complete interface failure to complete or near complete internal failure with an increase in normal stress to 2000 kPa. Complete internal failure was identified for GCLA/GMX at $T = 20\text{ }^{\circ}\text{C}$ and $\sigma_{n-s} = 2000\text{ kPa}$ and partial interface/internal failure predominated by internal failure was identified for GCLA/GMX at $T = 80\text{ }^{\circ}\text{C}$ and $\sigma_{n-s} = 2000\text{ kPa}$. Secant friction angles at large-displacement of approximately $5\text{--}6^{\circ}$ were determined for these two failure conditions, which were comparable to large-displacement friction angles observed in the GCL internal shear tests (Fig. 4.10).

The increase in temperature to $80\text{ }^{\circ}\text{C}$ reduced the large-displacement shear strength in all composite systems that exhibited complete interface failure mode. For example, $\phi_{ld} = 14.8^{\circ}$ for GCLC/GMX at $T = 20\text{ }^{\circ}\text{C}$ and reduced to 8.8° at $T = 80\text{ }^{\circ}\text{C}$. Similarly, the ϕ_{ld} of GCLB-GMX reduced from 7° to 5° with the change in temperature from $20\text{ }^{\circ}\text{C}$ to $80\text{ }^{\circ}\text{C}$. Considering that the GMX spikes deformed during shear (e.g. Fig. 4.8b and Fig. 4.8c), the potential for interlocking can be assumed negligible after reaching peak shear strength in GCL/GMX composite systems with complete interface failure; thus, the mechanism controlling large-displacement shear strength is can only due to interface friction between the geotextile of the GCL and GMX. The reduction in ϕ_{ld} of a GCL/GMX composite system with complete interface failure indicates a reduction in interface friction between the sheared GMX and sheared geotextile at $T = 80\text{ }^{\circ}\text{C}$. This is also believed the reason for a decrease in large-displacement shear strength of composite systems with partial interface/internal failure mode at $T = 80\text{ }^{\circ}\text{C}$ (Table 4.3).

An increase in the large-displacement shear strength of GCLA/GMX was observed with an increase in temperature to $80\text{ }^{\circ}\text{C}$ at $\sigma_{n-s} = 2000\text{ kPa}$ (

Fig. 4.12a). This increase in strength was attributed to the different failure modes of GCLA/GMX at $T = 20\text{ }^{\circ}\text{C}$ and $80\text{ }^{\circ}\text{C}$. Considering complete internal failure at $T = 20\text{ }^{\circ}\text{C}$, the mechanism controlling large-displacement shear strength was interface friction between the hydrated bentonite and carrier geotextile of GCLA. In contrast, the partial interface/internal failure of GCLA/GMX at $T = 80\text{ }^{\circ}\text{C}$ suggests that there was a combination of interface friction between hydrated bentonite and geotextile and interface friction between the sheared geotextile and GMX.

Relationships of change in large-displacement shear strength (i.e., from $20\text{ }^{\circ}\text{C}$ to $80\text{ }^{\circ}\text{C}$) versus normal stress for interface shear tests are shown in Fig. 4.13. Positive values of $\Delta\tau_{ld}$ were observed for the majority of composite systems in this study, which indicates that τ_{ld} of GCL/GMX composite systems reduced with an increase in temperature from $20\text{ }^{\circ}\text{C}$ to $80\text{ }^{\circ}\text{C}$. The only negative value for $\Delta\tau_{ld}$ was for the GCLA/GMX composite system at $\sigma_{n-s} = 2000\text{ kPa}$, which was due to complete internal failure of the GCL in the composite system tested at $20\text{ }^{\circ}\text{C}$ relative to the partial interface/internal failure for the composite system tested at $80\text{ }^{\circ}\text{C}$. Thus, in all cases where the same failure mode was identified at $20\text{ }^{\circ}\text{C}$ and $80\text{ }^{\circ}\text{C}$ (e.g., complete interface failure), large-displacement shear strength reduced with an increase in temperature. The solid line in Fig. 4.13 identifies the maximum allowable $\Delta\tau_{ld}$ that would be acceptable assuming design based on $FS = 1.1$. Considering that essentially all data plot above the maximum allowable reduction of τ_{ld} , a potential reduction in large-displacement shear strength need to be accounted for in GCL/GMX composite systems that will experience elevated temperatures in field applications.

4.7 Summary

The purpose of this study was to evaluate the effect of temperature on the shear behavior and critical strength of GCL/GMX composite systems. For this aim a series of internal

and interface direct shear tests were performed at room temperature ($\approx 20\text{ }^{\circ}\text{C}$) as well as the elevated temperature = $80\text{ }^{\circ}\text{C}$. The following conclusions were obtained from the results of this study:

- The GCL/GMX composite can experience different failure modes that are: (i) complete interface failure, (ii) partial interface/internal failure, and (iii) complete internal failure. The failure mode of the GCL/GMX composite depends on the characteristics of GCL and GMX as well as the applied σ_{n-s} . For a specific GCL/GMX composite, increase in σ_{n-s} can result in the transition of the failure mode from complete interface failure to complete internal failure.
- For the experimental conditions of this study, the critical strength of the composite system with the highest peel strength GCL (PS = 3850 N/m) was always complete interface failure or partial interface/internal failure. The reason was the low tensile strength of the carrier and cover geotextile of this GCL prevented the transfer of applied shear stress to the GCL internal region, and internal shearing of the GCL.
- Increase in the temperature to $80\text{ }^{\circ}\text{C}$ resulted in up to 45 % reduction in the τ_p of NP GCLs regardless the geotextile (of the GCL) characteristics, GCL heat treatment method, or σ_{n-s} . The decrease in the τ_p of NP GCLs is attributed to the decrease in the entanglement strength of fiber bundles-geotextile connection as well as a decrease in the tensile modulus of reinforcement fibers.
- An increase in the temperature to $80\text{ }^{\circ}\text{C}$ resulted in a decrease in peak interface shear strength of GCL/GMX composite systems by up to 46 %. No relationship was observed between the values of $\Delta\tau_p$ and GCL type, σ_{n-s} , or failure mode of the composite system. The reduction in τ_p of GCL/GMX composite systems with complete interface failure mode and partial interface/internal failure mode are attributed to the reduced interlocking strength as well as the reduced friction between GMX spikes and the geotextile of GCLs.

- Considering the $\Delta\tau_p$ up to 45 % in internal shear tests and up to 46% in interface shear tests, the conventional factor of safety = 1.5 that is used for the design based on peak shear strength is not conservative.
- An increase in the temperature to 80 °C did not have a noticeable effect on the large-displacement shear strength of NP GCLs in internal shear tests as the large-displacement friction angle (ϕ'_{ld}) was $\leq 6^\circ$.
- The effect of temperature on τ_{ld} of GCL/GMX composite systems depends on the failure mode of the composite system. The τ_{ld} in composite systems with complete interface failure mode and partial interface/internal failure mode decreased up to 48% at $T = 80^\circ\text{C}$ due to the reduced friction between GMX and geotextile (of the GCL).
- Considering the extent of large-displacement shear strength decrease in internal and interface shear tests, the conventional factor of safety = 1.1 for the design based on large-displacement shear strength is not conservative.

Table 4.1. Characteristics and properties of geosynthetic clay liners used in this study.

Properties	Standard	GCLA	GCLB	GCLC
Peel strength (N/m) ^a	ASTM D6496	980	2180	3850
Heat treatment method	-	NHT	NHT	NHT
Polymer type ^a	-	PP	PP	PP
Carrier geotextile type	-	NW	W	NW
Cover geotextile type	-	NW	NW	NW
Carrier geotextile mass/area (g/m ²) ^b	ASTM D5261	260	130	360
Cover geotextile mass/area (g/m ²) ^b	ASTM D5261	230	230	280
Bentonite type	-	Granular	Granular	Granular
Bentonite mass per area (g/m ²) ^b	ASTM D5993	4220	4910	5570

Note: NHT = Non-heat-treated; PP = Polypropylene; NW = Non-woven; W = woven

^a Reported by the manufacturer

^b Measured in this study

Table 4.2. A summary of displacement-controlled internal direct shear tests.

GCL ^a	T	σ_{n-s} (kPa)	τ_p (kPa)	ϕ'_{s-p} (kPa)	AC σ_{ld} (kPa)	AC τ_{ld} (kPa)	$\Delta\tau_p$ (%)	Δ AC τ_{ld} (%)
GCLA	20 °C	100	141.0	54.7	183.1	23.4	-	-
		300	233.7	37.9	549.4	39.7	-	-
		500	295.5	30.6	915.7	78.6	-	-
		1000	413.7	22.5	1831.4	130.9	-	-
		2000	570.5	15.9	3662.7	199.1	-	-
	80 °C	100	85.2	40.4	183.1	17.6	39.6	24.8
		300	187.5	32	549.4	33.2	19.8	16.4
		500	204.8	22.3	915.7	53.1	30.7	32.4
		1000	311.4	17.3	1831.4	125.8	24.7	3.9
		2000	364.5	10.3	3662.7	152.6	36.1	23.3
GCLB	20 °C	100	164.2	58.7	183.1	16.8	-	-
		300	293.3	44.4	549.4	51.3	-	-
		500	416.2	39.8	915.7	84.6	-	-
		1000	541.2	28.4	1831.4	122.2	-	-
		2000	700.6	19.3	3662.7	145.6	-	-
	80 °C	100	132.2	52.9	183.1	24.2	19.5	-43.5
		300	232.6	37.8	549.4	52.2	20.7	-1.8
		500	312.9	32	915.7	59.5	24.8	29.7
		1000	390.4	21.3	1831.4	105.1	27.9	13.9
		2000	541.9	15.2	3662.7	115.2	22.7	20.9

NOTE: T = testing temperature; σ_{n-s} = shearing normal stress; τ_p = peak shear strength; ϕ'_{s-p} = secant friction angle at peak shear stress; AC σ_{ld} = area-corrected shearing normal stress at horizontal displacement (δ_h) = 70 mm; AC τ_{ld} = area-corrected large-displacement shear strength at δ_h = 70 mm; $\Delta\tau_p$ = percent change in peak shear strength (Eq. 4.1), and $\Delta\tau_{ld}$ = percent change in large-displacement shear strength (Eq. 4.2).

^a Internal shear failure of GCLC was not successful in internal shear tests. Therefore, no data was shown in Table 1 for GCLC.

Table 4.3. A summary of displacement-controlled internal direct shear tests.

Composite system	T	σ_{n-s} (kPa)	τ_p (kPa)	ϕ'_{s-p} (kPa)	δ_{h-p} (mm)	τ_{ld} (kPa)	$\Delta\tau_p$ (%)	$\Delta\tau_{ld}$ (%)	Failure mode
GCLA-GMX	20 °C	100	47.7	25.5	9.9	40.8	-	-	IF
		300	116.1	21.2	10.5	77	-	-	IF
		500	178.8	19.7	12.3	137	-	-	IF
		1000	315.8	17.5	13.7	125.7	-	-	IF/IN
		2000	516.3	14.5	15.5	190.2	-	-	IN
	80 °C	100	35.8	19.7	5.9	21.3	24.9	47.8	IF
		300	82.7	15.4	8.4	52.7	28.8	31.6	IF
		500	126.9	14.2	8.5	76.2	29	44.4	IF
		1000	188.9	10.7	15.2	86.1	40.2	31.5	IF/IN
		2000	323.4	9.2	12.3	219	37.4	-15.1	IF/IN
GCLB-GMX	20 °C	100	51.6	27.3	8.4	35.5	-	-	IF
		300	108.2	19.8	8.5	68.4	-	-	IF
		500	154.6	17.2	8.6	107	-	-	IF
		1000	249.3	14	9.3	152	-	-	IF
		2000	423.9	12	11.2	283	-	-	IF
	80 °C	100	43	23.3	4.8	27	16.6	23.9	IF
		300	86.4	16.1	5.8	57.4	20.1	16.1	IF
		500	105.4	11.9	6.4	67.6	31.8	36.8	IF
		1000	168	9.5	7	119.5	32.6	21.4	IF
		2000	344.1	9.7	10.4	195.8	18.8	30.8	IF
GCLC-GMX	20 °C	100	60.8	31.3	9.4	48.3	-	-	IF
		300	159.4	28	12.3	119.3	-	-	IF
		500	196.8	21.5	11.2	145.3	-	-	IF
		1000	329.9	18.3	12.2	216.6	-	-	IF
		2000	712.3	19.6	16.2	566.4	-	-	IF/IN
	80 °C	100	38.2	20.9	2.8	26.2	37.1	45.8	IF
		300	86	16	5.5	61.7	46.1	48.3	IF
		500	145.6	16.2	8	93.9	26	35.4	IF
		1000	255.9	14.4	11.5	169.4	22.4	21.8	IF
		2000	474.6	13.3	18.8	322.7	33.4	43	IF/IN

NOTE: T = testing temperature; σ_{n-s} = shearing normal stress; τ_p = peak internal shear strength; ϕ'_{s-p} = secant friction angle at peak shear strength; δ_{h-p} = horizontal displacement at peak shear strength; τ_{ld} = large-displacement shear strength; $\Delta\tau_p$ = percent change in peak shear strength (Eq. 4.1), $\Delta\tau_{ld}$ = percent change in large-displacement shear strength (Eq. 4.2). IF = complete interface failure mode; IF/IN = partial interface/internal failure mode; and IN= complete internal failure mode.

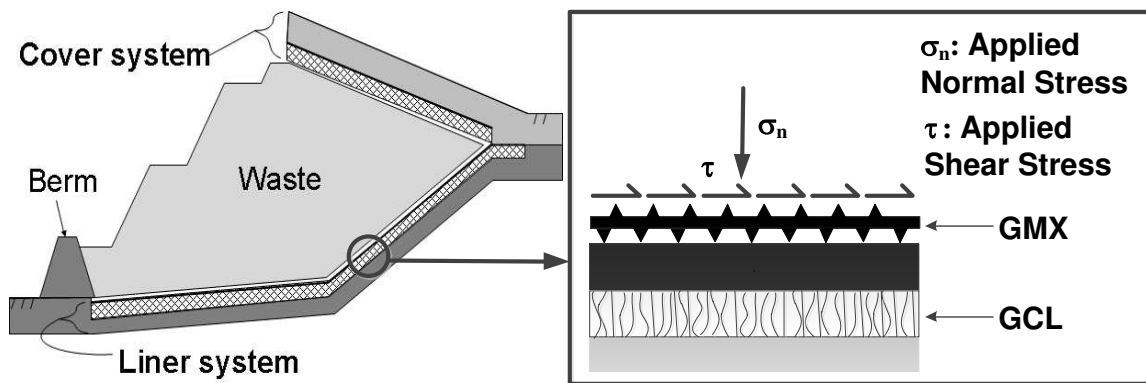


Fig. 4.1. A schematic of the GCL-GMX composite system subjected to shear and normal stresses (τ and σ_n) in a containment application.

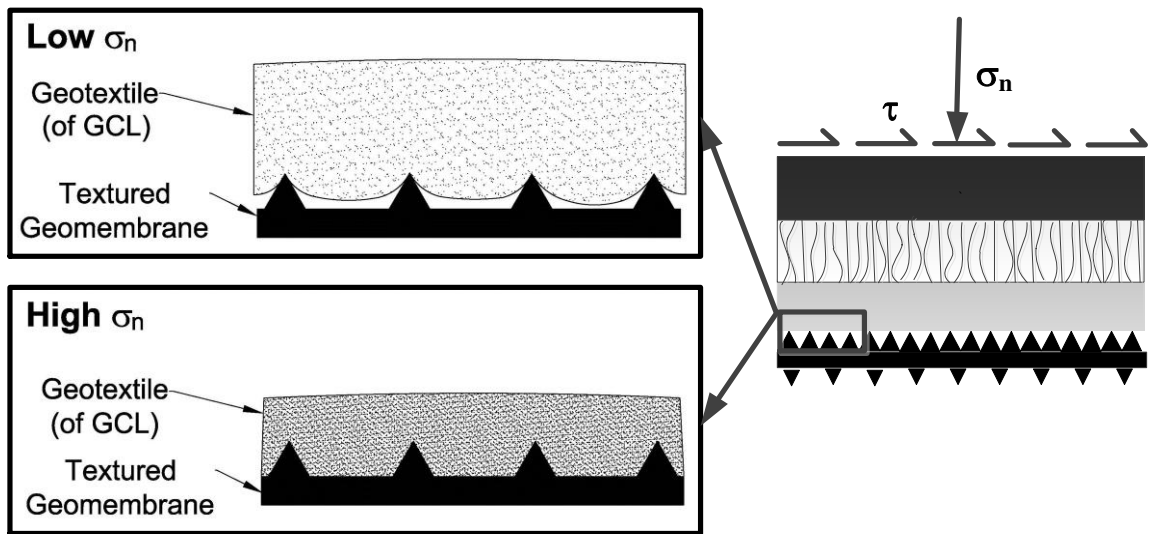


Fig. 4.2. A schematic of the non-woven geotextile of a GCL in contact with a textured geomembrane at low and high normal stresses (σ_n).

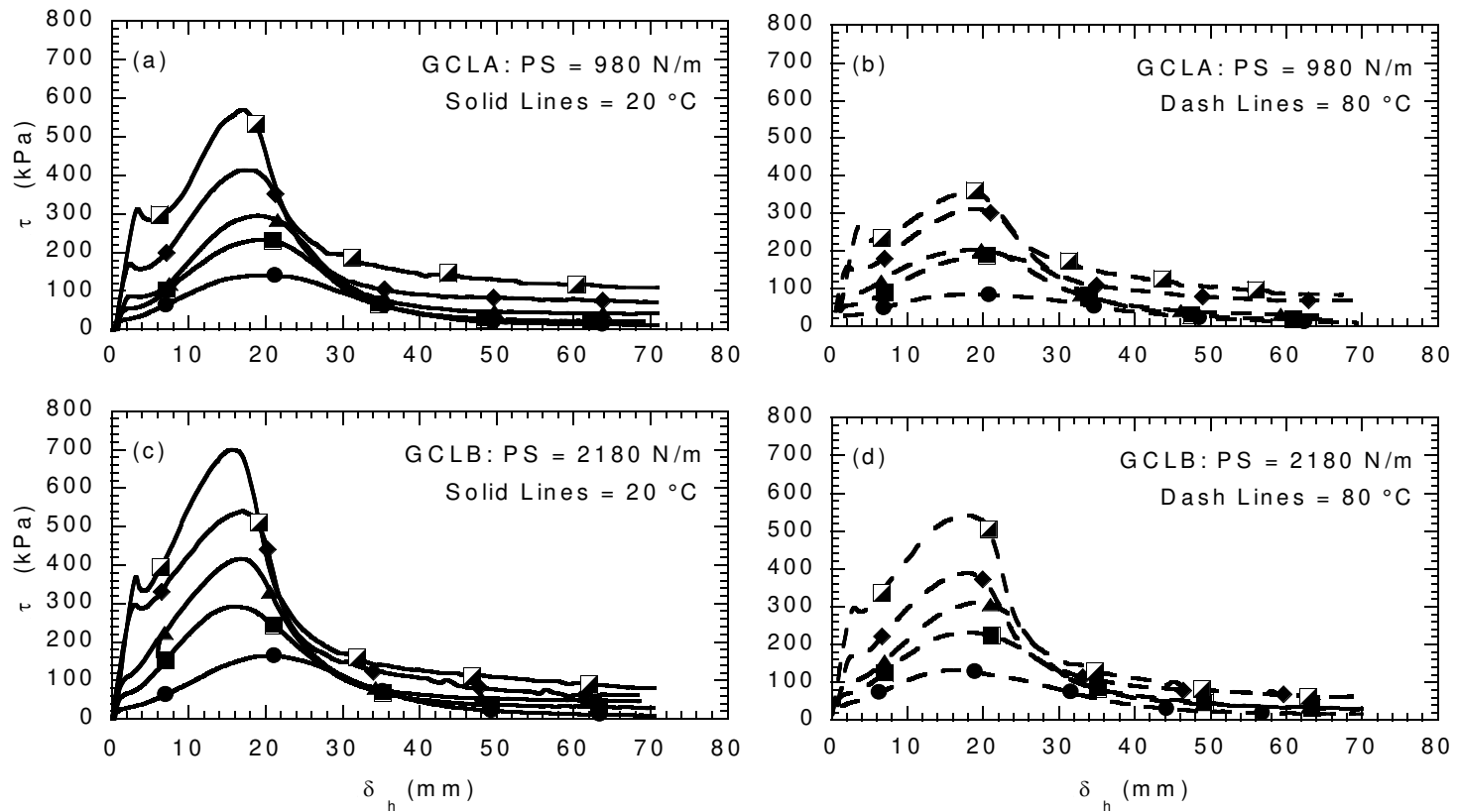
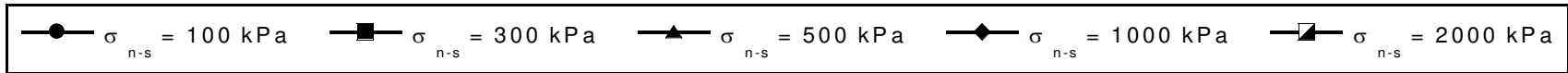


Fig. 4.3. Relationships between shear stress (τ) and horizontal displacement (δ_h) for internal shear tests on (a) GCLA at room temperature, (b) GCLA at 80 °C, (c) GCLB at room temperature, and (d) GCLB at 80 °C.

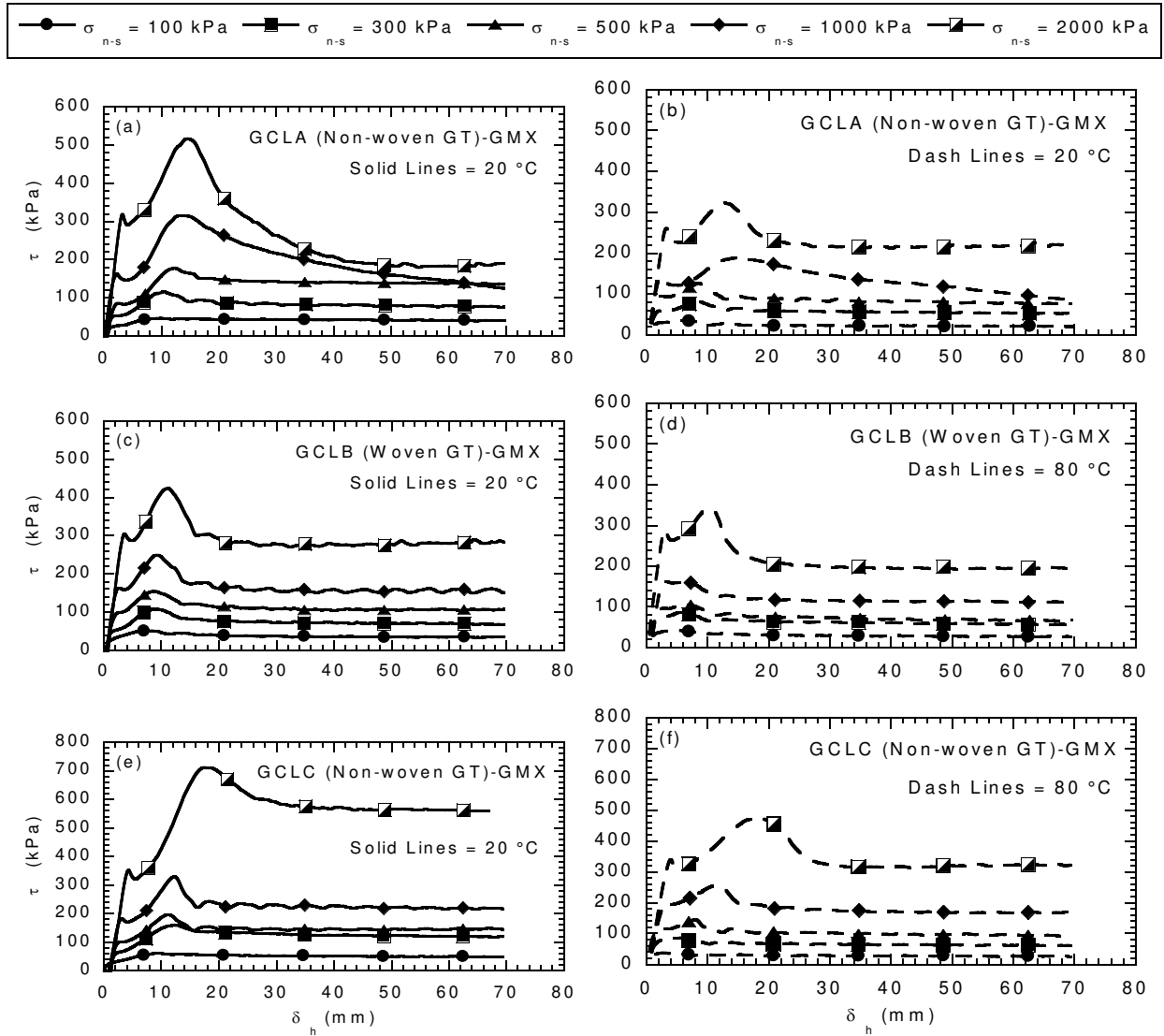


Fig. 4.4. Relationships between shear stress (τ) and horizontal displacement (δ_h) in interface shear tests on (a) GCLA (Non-woven GT)-GMX at $T = 20$ °C, (b) GCLA (Non-woven GT)-GMX at $T = 80$ °C, (c) GCLB (Woven GT)-GMX at $T = 20$ °C, (d) GCLB (Woven GT)-GMX at $T = 80$ °C, (e) GCLC (Non-woven GT)-GMX at $T = 20$ °C, and (f) GCLC (Non-woven GT)-GMX at $T = 80$ °C.

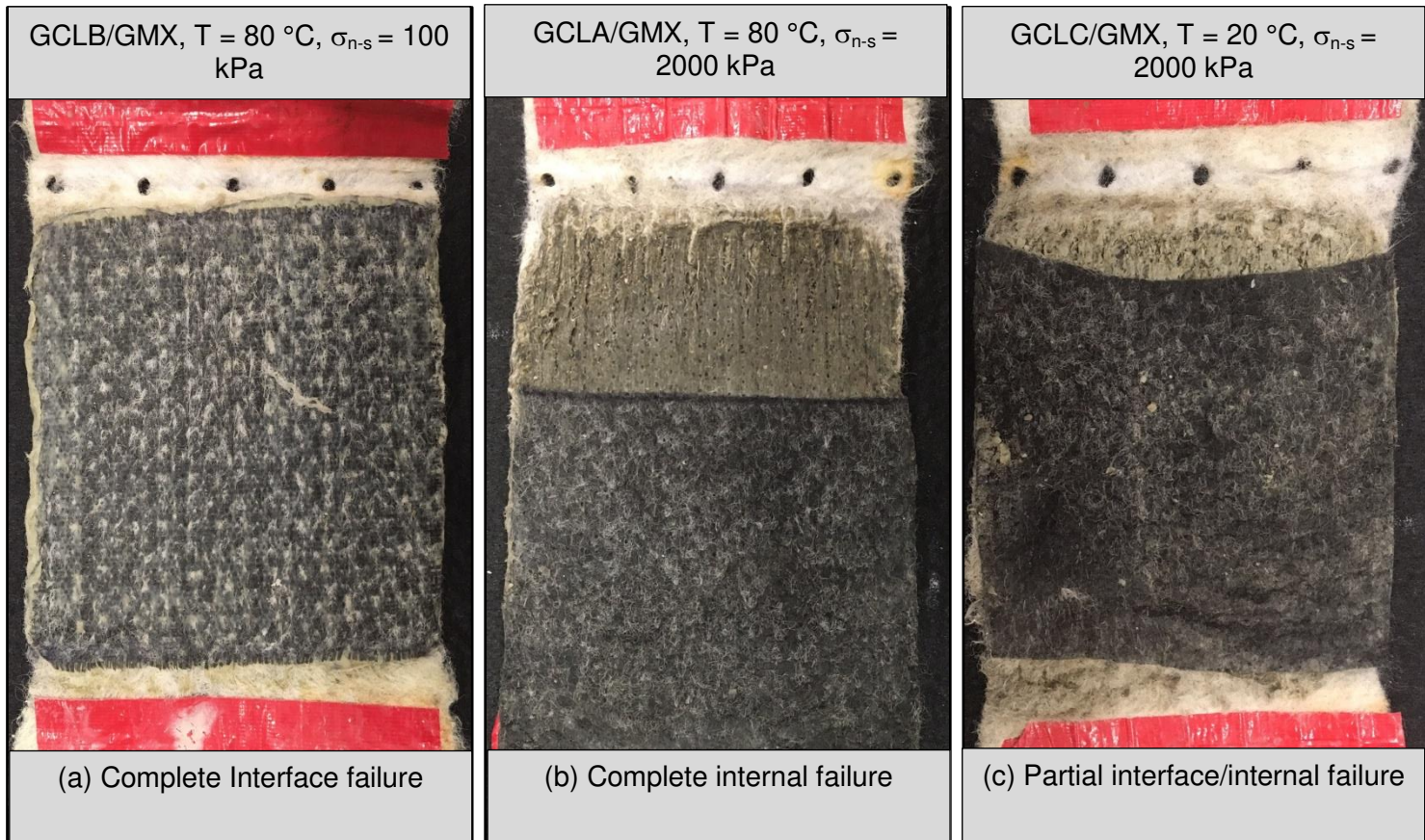


Fig. 4.5. Post-shear photograph of GCLs in DC-IF tests showing examples of (a) complete interface failure mode, (b) complete internal failure mode, and (c) partial interface/internal failure mode.

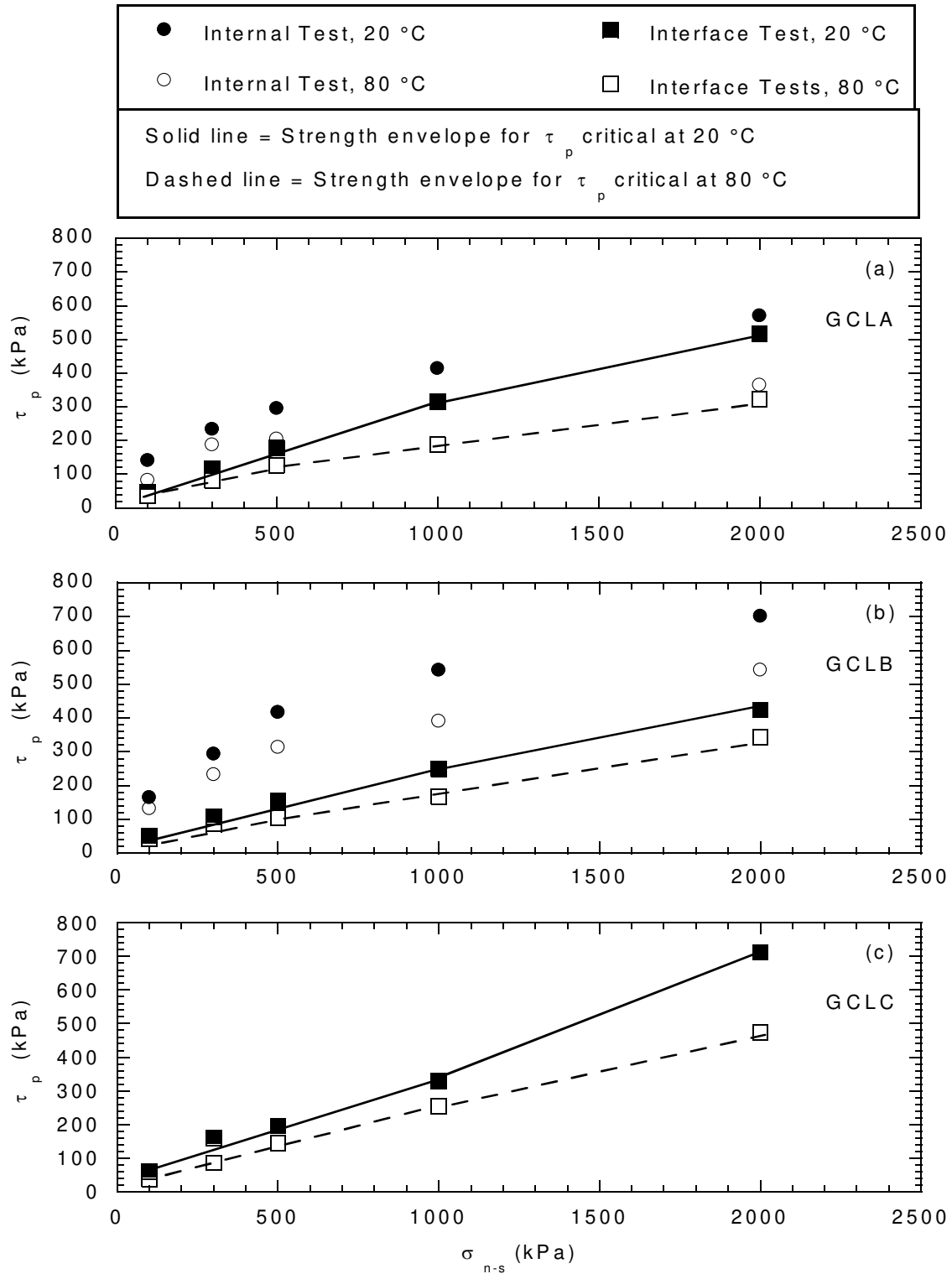


Fig. 4.6. Relationships between peak shear strength (τ_p) versus shearing normal stress (σ_{n-s}) for internal and interface shear tests on (a) GCLA, (b) GCLB, and (c) GCLC. Solid lines show strength envelope for peak critical strength at 20 °C whereas dash lines show strength envelope for peak critical strength at 80 °C.

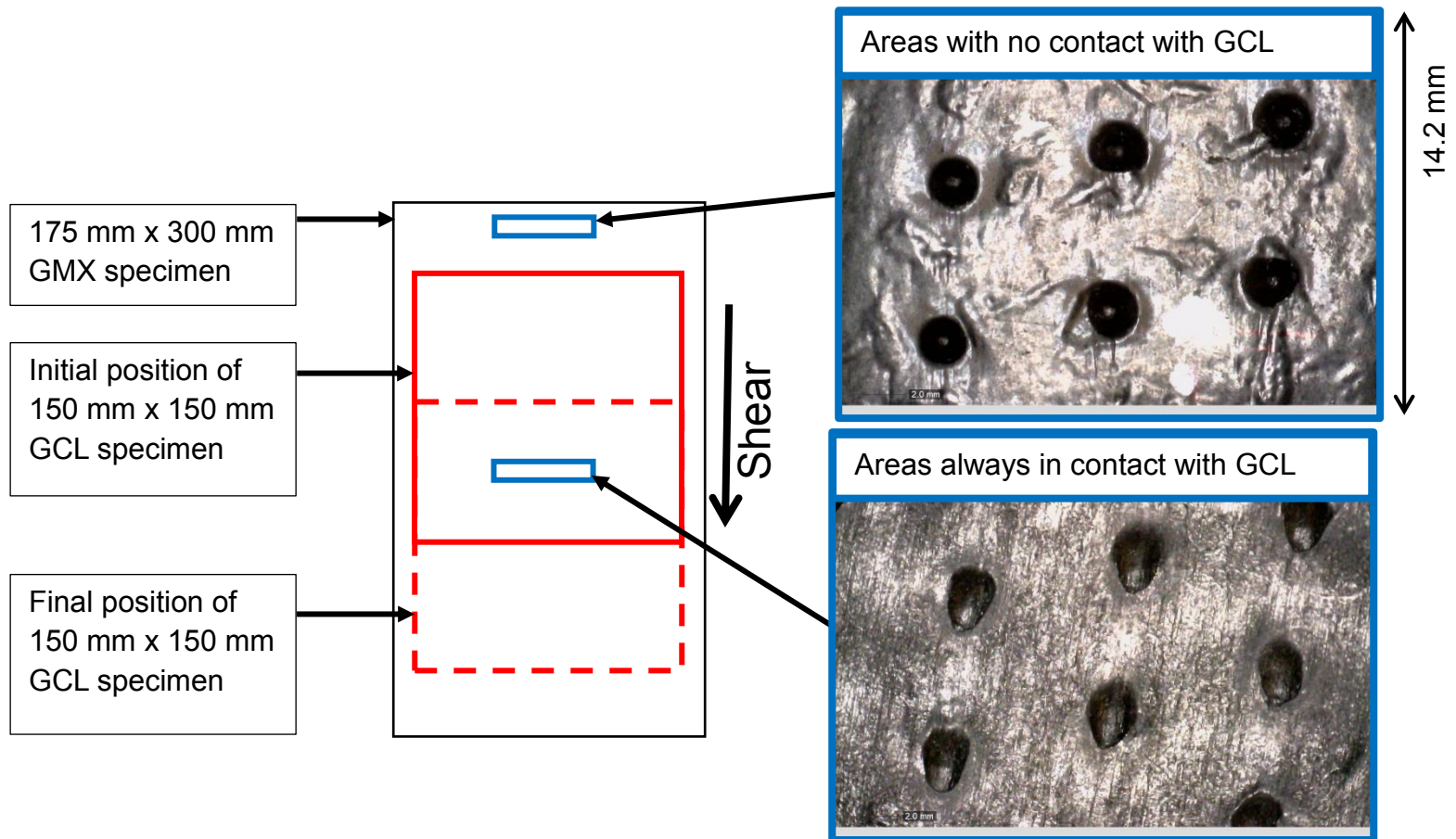
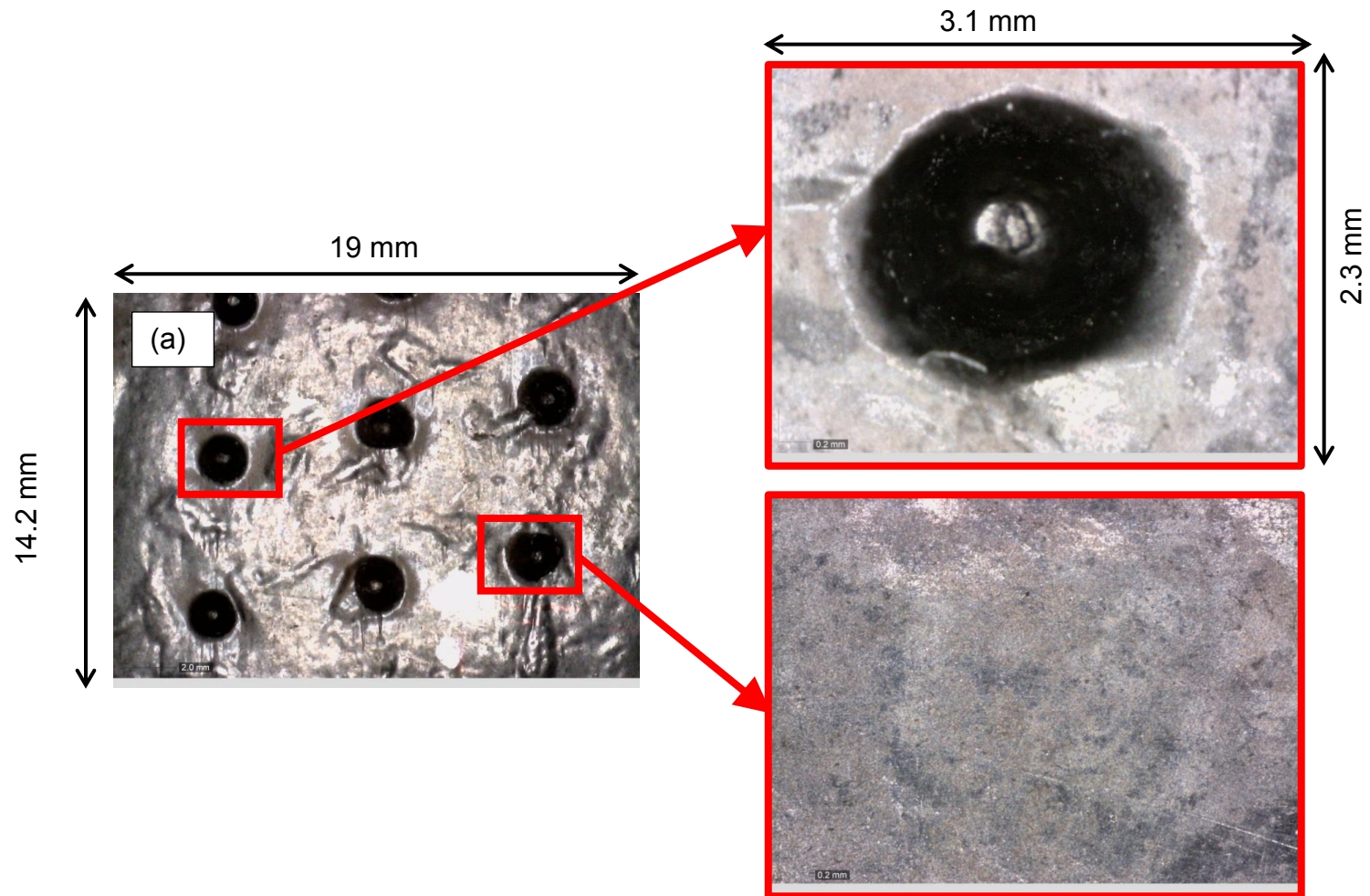
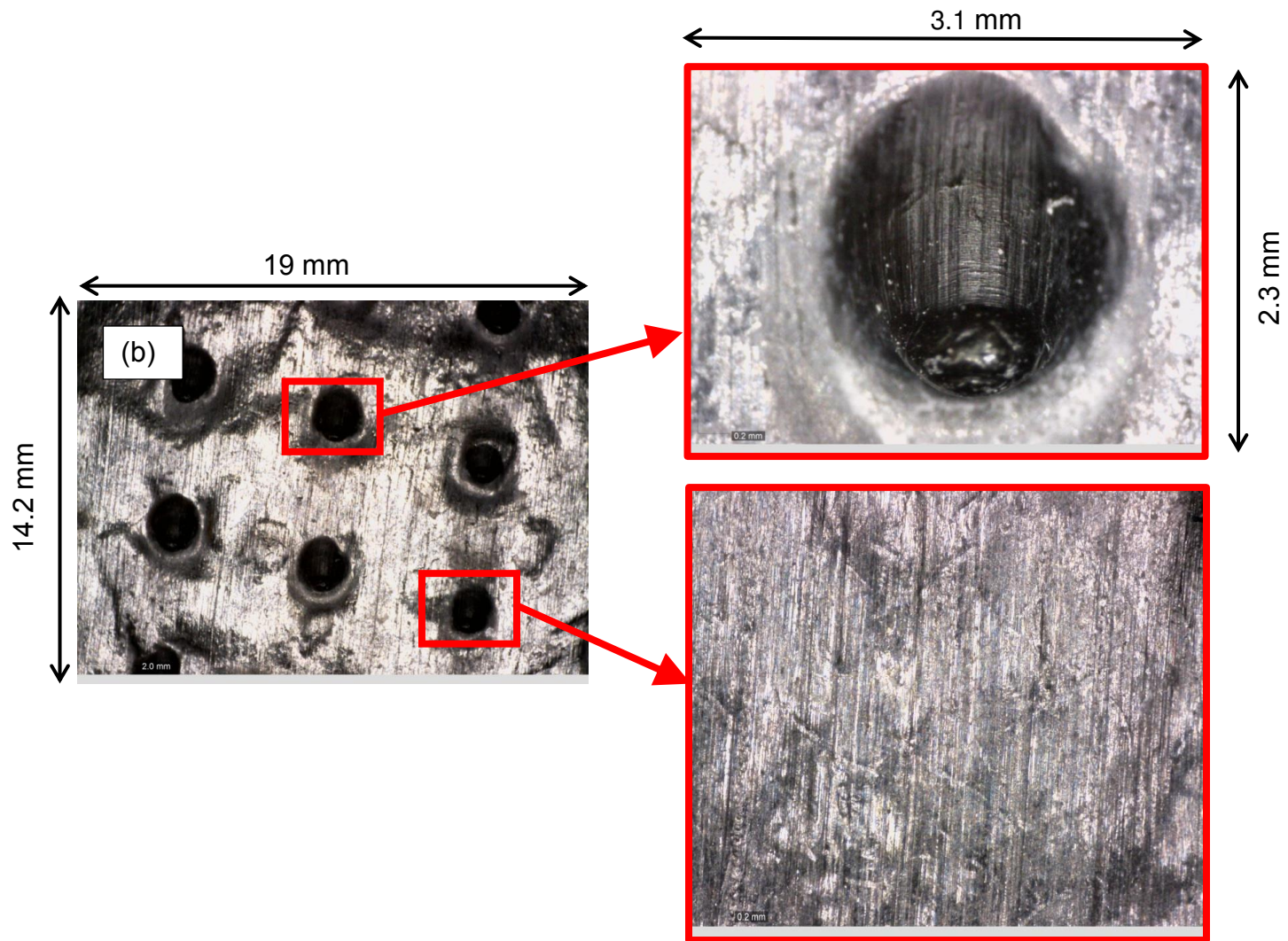


Fig. 4.7. A schematic of the 175 mm x 300 mm GMX specimens with the initial and final positions of the 150 mm x 150 mm GCL specimens. Digital images are also shown from areas in the center and the back of the GMX from GCLC/GMX tested at $\sigma_{n-s} = 2000$ kPa and $T = 80$ °C.





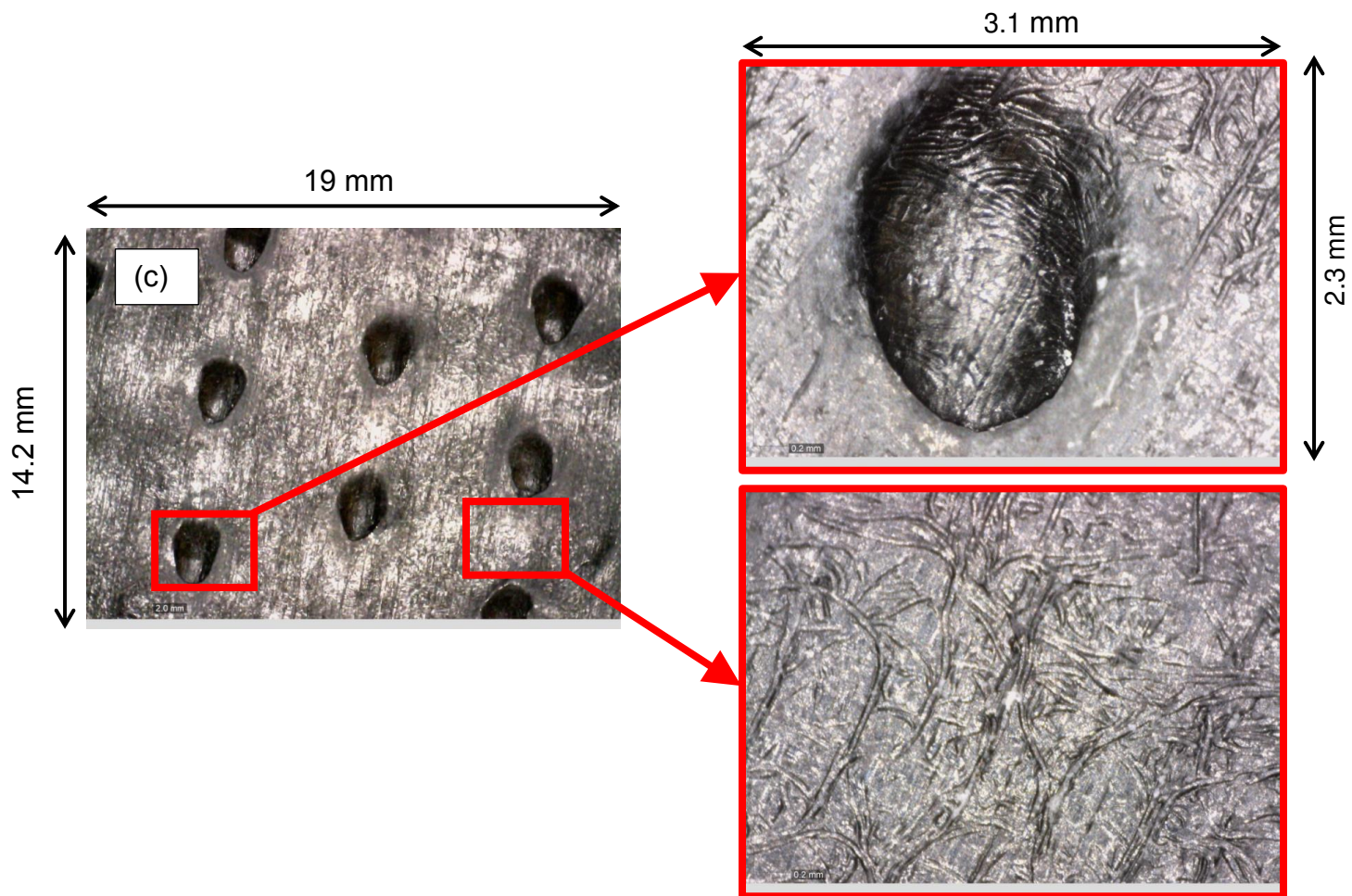


Fig. 4.8. Photographs of GMX spikes in the center of (a) untested specimen, (b) specimen from GCL-C/GMX composite tested at $\sigma_{n-s} = 2000$ kPa and $T = 20$ °C, and (c) specimen from GCL-C/GMX composite tested at $\sigma_{n-s} = 2000$ kPa and $T = 80$ °C. Additional photographs are at higher magnification from area surrounding a single spike and the core of the GMX.

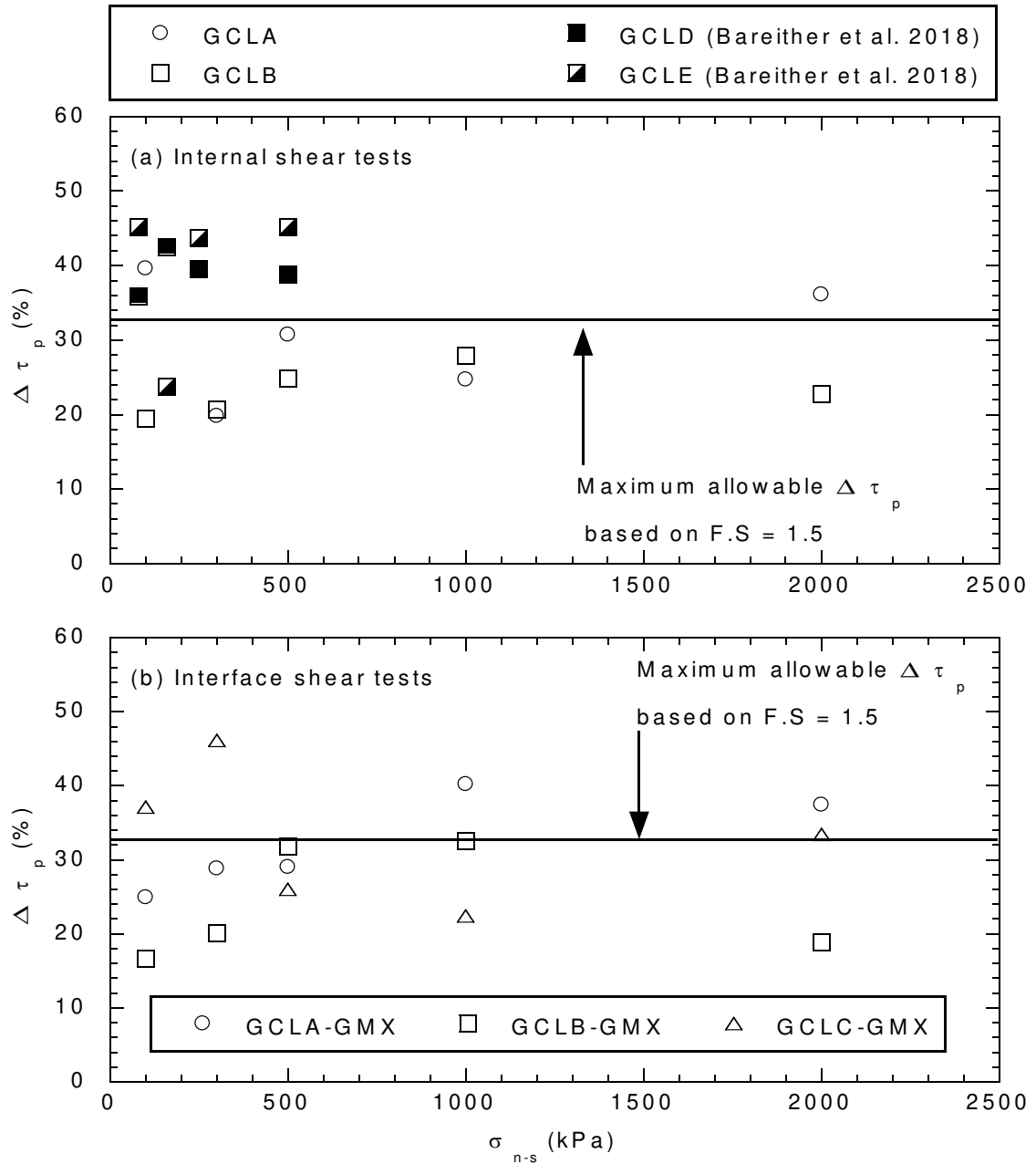


Fig. 4.9. Relationships between percent change in peak shear strength ($\Delta\tau_p$) and shearing normal stress (σ_{n-s}) for (a) internal shear on GCLA and GCLB from this study and internal shear tests on GCLD and GCLE from, and (b) Interface shear tests on GCLA/GMX, GCLB/GMX, and GCLC/GMX composite systems.

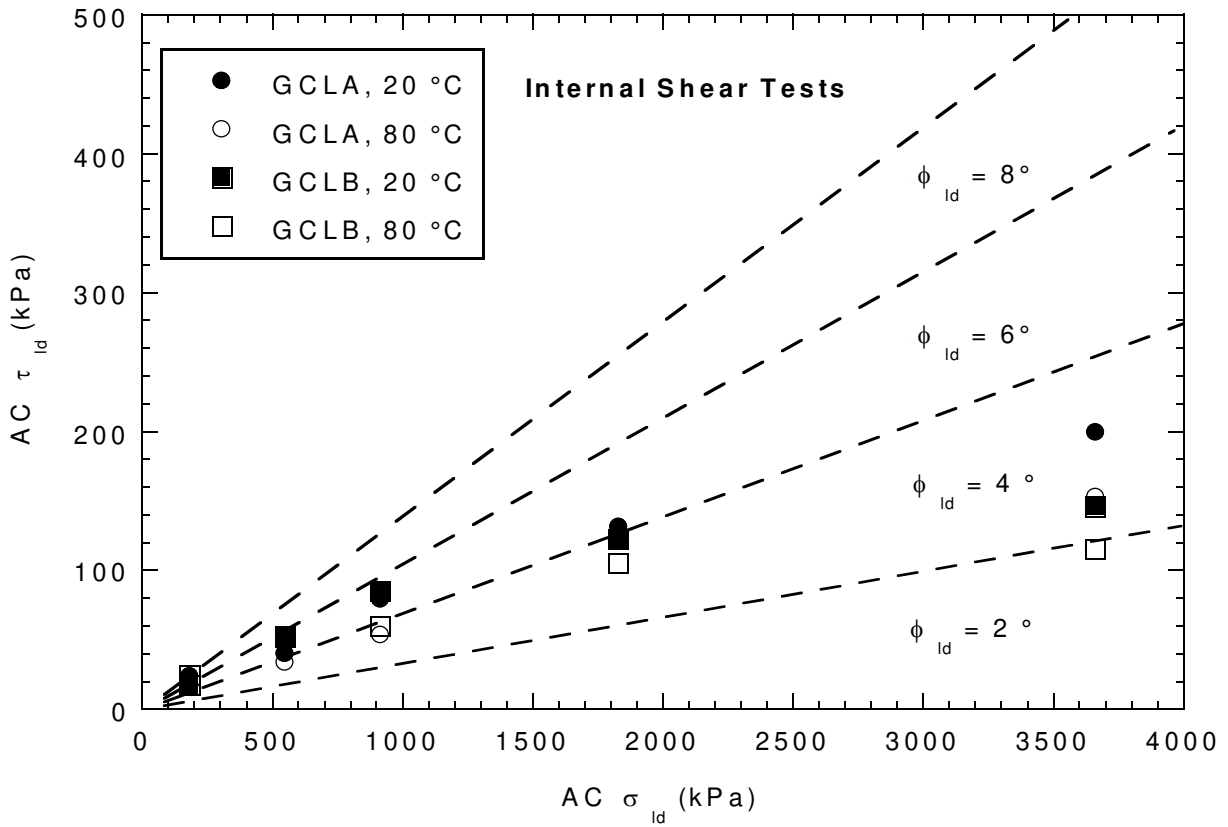


Fig. 4.10. Relationships between area-corrected large displacement shear strength ($AC \tau_{ld}$) versus area-corrected large displacement normal stress ($AC \sigma_{ld}$) in internal shear tests on GCLA and GCLB at room temperature and $T = 80^\circ\text{C}$. Dashed lines are contours for the large-displacement secant friction angles (ϕ_{ld})

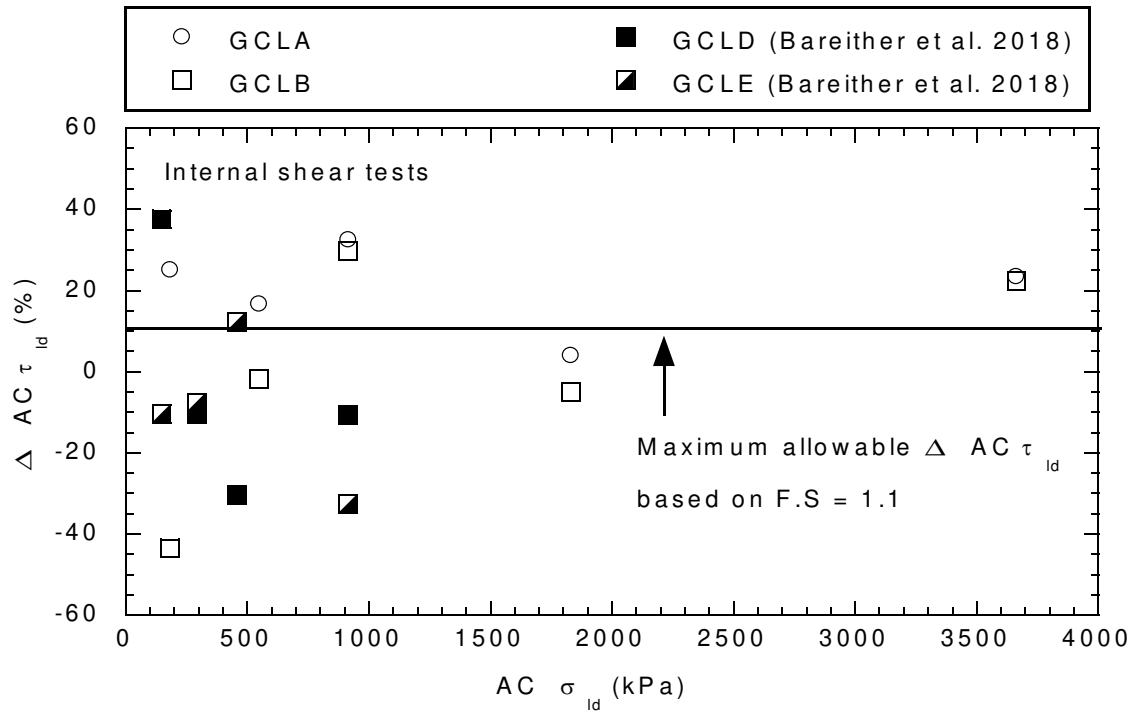


Fig. 4.11. Relationships between percent change in area-corrected large-displacement shear strength ($\Delta AC \tau_{id}$) and area-corrected large-displacement normal stress ($AC \sigma_{id}$) for internal shear tests on GCLA and GCLB. Results of internal shear tests at $\sigma_{n-s} = 80, 160, 250,$ and 500 kPa on GCLD and GCLE from Bareither et al. (2018) is also included in this figure

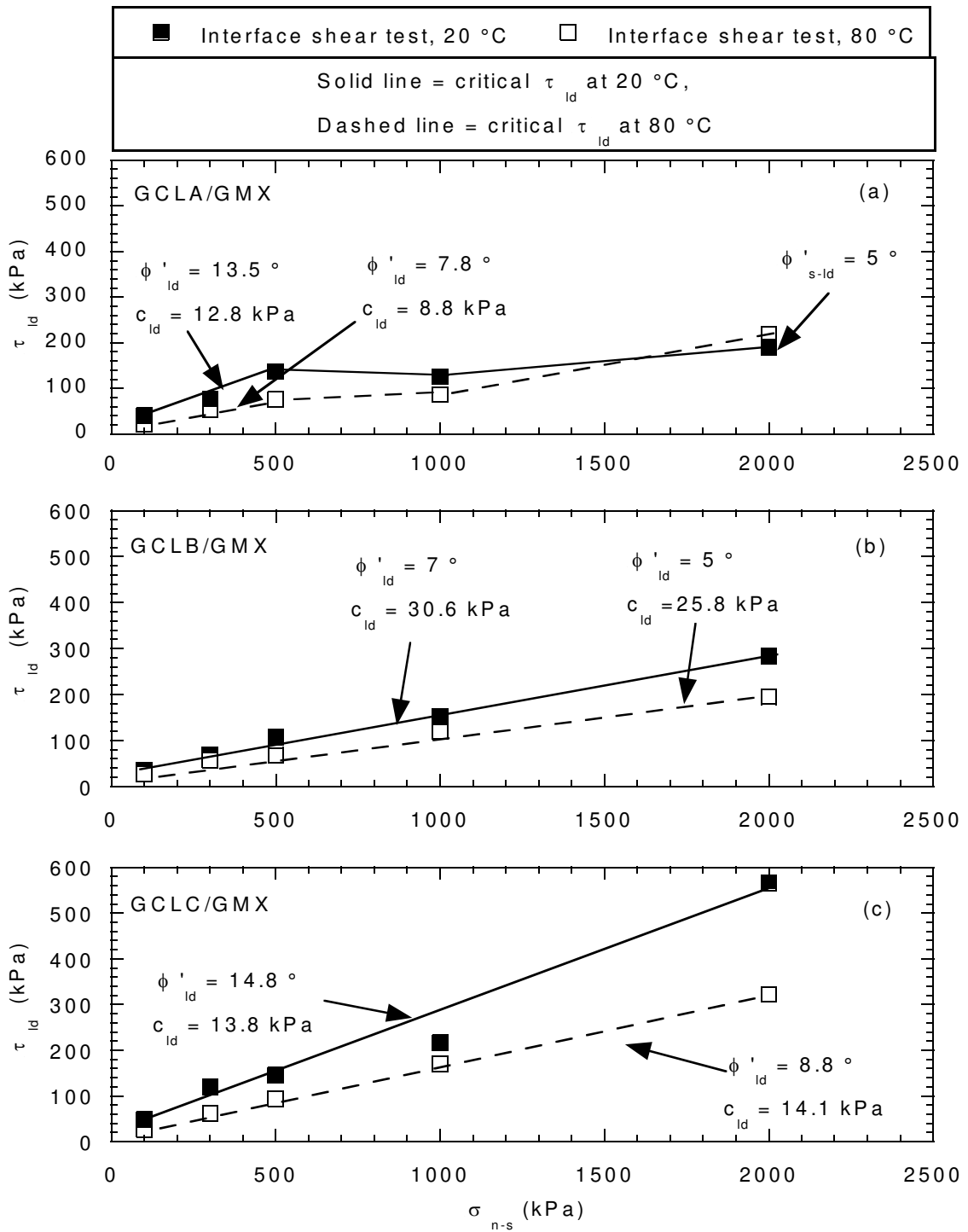


Fig. 4.12. Relationships between the large-displacement shear strength (τ_{ld}) versus shearing normal stress (σ_{n-s}) in interface shear tests on (a) GCLA/GMX, (b) GCLB/GMX, and (c) GCLC/GMX. Dashed and solid lines are strength envelopes for critical large-displacement critical strength at room temperature and $T = 80^\circ\text{C}$ respectively.

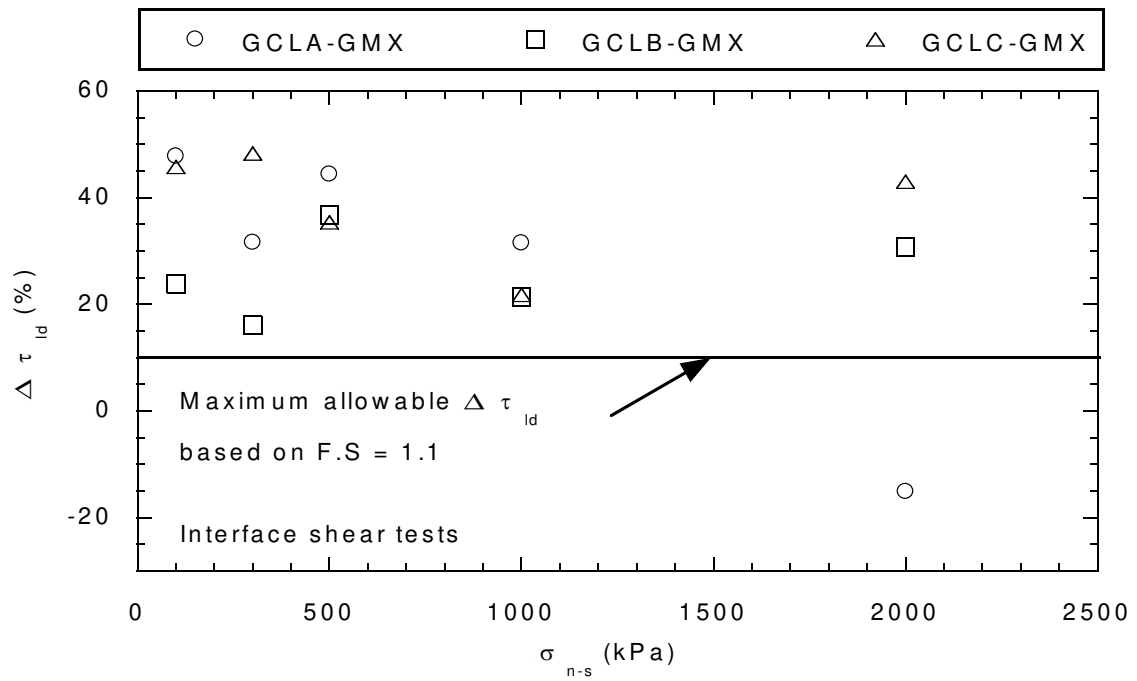


Fig. 4.13. Relationships between percent change in large-displacement shear strength ($\Delta\tau_{id}$) and shearing normal stress (σ_{n-s}) for interface shear tests on GCLA/GMX, GCLB/GMX, and GCLC/GMX.

CHAPTER 5: INTERNAL AND INTERFACE SHEAR STRENGTH OF GEOSYNTHETIC CLAY LINERS FOLLOWING HYDRATION IN SYNTHETIC MINE PROCESS SOLUTIONS

5.1 Introduction

Geosynthetic clay liners (GCLs) often are used in combination with a textured geomembrane (GMX) in liner and cover systems for waste containment. The normal stress at the bottom of a liner system in containment applications such as heap leach pads can be as high as 4 MPa (Lupo 2010). High normal stresses in GCL/GMX composite systems can also coincide with high shear stresses in applications containing slopes. The integrity of barrier system must be maintained via resisting the applied shear stress internally within the GCL and at the interface between the GCL and adjacent geosynthetic and/or earthen material.

Geosynthetic clay liners (GCLs) are used in waste containment barrier systems due to their hydraulic performance, economic advantages, ease of installation, and self-healing properties (Guyonnet et al. 2009; Fox and Stark 2015). In side-slopes and base liner systems, GCLs are often combined with textured geomembranes (GMX) to create a composite liner. A GMX/GCL composite system can be exposed to high shear and normal stresses (Lupo 2010) that must be resisted internally within the GCL and along the GCL and GMX interface to prevent failure. The shear strength of a GMX/GCL composite system is important for the design and long-term performance of barrier systems.

Considering that the internal friction angle of hydrated sodium bentonite can be $\leq 4^\circ$ (Mesri and Olson 1970), the internal shear strength of GCLs are reinforced via processes called stitched bonding and needle-punching. The manufacturing process to create a needle-punched reinforced GCL (NP GCL) involves punching fibers from the non-woven carrier geotextile of the GCL through the bentonite and leaving the fibers entangled within the carrier geotextile of the GCL (woven or non-woven). Higher internal shear strength is achieved due to the tensile

strength of reinforcement fibers and frictional resistance between the reinforcement fibers and carrier geotextile.

Geosynthetic clay liners used in waste containment systems, such as heap leach pads, coal combustion residuals, municipal solid waste, etc., can be exposed to a broad range of non-standard solutions (Ruhl and Daniel 1997; Benson et al. 2008, 2010; Bouazza 2010; Lange et al. 2010; Shackelford et al. 2010; Hornsey et al. 2010; Hosney and Rowe 2013; Bouazza and Gates 2014; Wang et al. 2019). Exposure of GCLs to non-standard solutions can affect swell properties of the bentonite and reduce hydraulic conductivity of the liner system (Shackelford et al. 2000, 2010; Kolstad et al. 2004; Jeon et al. 2006; Katsumi et al. 2007, 2008; Hornsey et al. 2010; Scalia and Benson 2010; Bouazza and Gates 2014). Moreover, long-term exposure of common polymeric geosynthetics (e.g., polypropylene, high density polyethylene, polyester) to non-standard solutions can cause antioxidant depletion that leads to oxidation and hydrolytic degradation of the polymers (Halse et al 1987; Mathur et al. 1994; Hsuan et al. 1993, 1998; Koerner et al. 1998, 2007; Jo et al. 2001, 2005; Row and Sangam 2002; Gulec et al. 2004, 2005; Jeon et al. 2005; Rowe et al. 2009; Hornsey et al. 2010).

Despite concerns about changes to hydraulic and mechanical performance of GCLs in applications containing non-standard solutions, GCL internal and interface shear strength commonly are evaluated via direct shear tests on specimens hydrated in either tap water or de-ionized water (DIW). In this study, displacement-controlled internal and interface direct shear tests were performed on GCL and GMX specimens hydrated in two synthetic mine process solutions and DIW for different hydration durations. The objective was to enhance our understanding about the effects of non-standard solution exposure on GCL internal shear strength and GCL/GMX interface shear strength. Potential changes in shear behavior of GCLs following exposure to non-standard solutions was investigated by conducted peel strength tests on GCLs and swell index tests on bentonite for the same hydration period the as shear tests.

5.2 Materials

5.2.1 Material Description

Characteristics of the NP GCL used in this study are in Table **5.1**. This GCL was a commercially available, non-heat-treated, NP GCL containing granular sodium bentonite encapsulated between non-woven geotextiles. Material specific characteristics of the GCL were conducted on ten, 100 mm x 100 mm specimens randomly cut from a sample roll. Reinforcement fibers were cut to separate the carrier and cover geotextiles, extract bentonite, and measure geotextile and bentonite mass per area (Table **5.1**). Water content and Atterberg limits were conducted on the bentonite. The natural bentonite water content was between 9.8% and 11.0%, and plasticity limits reflected typical sodium bentonite (Seed et al. 1964; Mesri and Olsen 1970). The average peel strength of the GCL was determined via 10 peel strength tests on specimens randomly cut from the sample roll in accordance with ASTM D6496/6496M.

The textured geomembrane (GMX) used in the interface shear tests was composed of linear low density polyethylene (LLDPE) and the texture was a uniform spike pattern. The GMX had a nominal core thickness of 1.5 mm, average spike height of 0.51 mm, and contained approximately 340 spikes in a surface area of 100-cm².

5.2.2 Hydration Solutions

Internal direct shear tests, interface direct shear tests, and peel strength tests were conducted on the GCL following hydration with type II DIW (ASTM D1193, 2011) and two synthetic mine process solutions. The synthetic solutions were developed to represent a bauxite mine process solution (B-PS) and copper mine process solution (Cu-PS), and characteristics of the two solutions are tabulated in Table **5.2**. The solutions were prepared following procedures outlined in Ghazizadeh et al. (2018). The B-PS was prepared with calcium sulfate (CaSO₄), magnesium sulfate (MgSO₄), sodium sulfate (Na₂SO₄), and sodium hydroxide (NaOH), which yielded an ionic strength = 0.067 M, ratio of monovalent to divalent cations = 1.2, and pH ≈ 12.

The Cu-PS was prepared with Aluminum Sulfate ($\text{Al}_2(\text{SO}_4)_3$), Calcium Chloride (CaCl_2), Copper (ii) Chloride (CuCl_2), Hydro Chloric Acid (HCl), Magnesium Chloride (MgCl_2), magnesium sulfate (MgSO_4), Manganese sulfate (MnSO_4), Potassium Chloride (KCl), Sodium Phosphate Tribasic (Na_3PO_4), sodium Chloride (NaCl), and sodium sulfate (Na_2SO_4). The Cu-PS had an ionic strength = 0.848 M, ratio of monovalent to divalent cations = 0.33, and $\text{pH} \approx 1$.

5.3 Experimental procedure

5.3.1 Specimen Preparation and Hydration in Non-Standard Solutions

Internal and interface direct shear tests were performed on 150 mm x 150 mm GCL specimens in lieu of 300 mm x 300 mm specimens recommended in ASTM D6432. Bareither et al. (2018) reported comparable GCL shear behavior between 150-mm and 300-mm GCLs, which supported the use of smaller GCL specimens for direct shear testing. The GCL specimens were cut with a razor knife to initial dimensions of 150 mm by 200 mm, with the larger dimension in machine direction to facilitate clamping geotextiles of the GCL to upper and lower gripping plates. Textured geomembrane specimens were cut with dimensions of 175 mm by 300 mm, with the larger dimension in machine direction. The larger size of the GMX specimens in comparison to GCL specimens was to ensure that the GCL remained in contact with a GMX during the interface shear tests.

Peel strength tests were conducted on specimens from locations in the vicinity of the direct shear specimens. Peel strength tests were performed on specimens with final dimensions of 100 mm x 150 mm (ASTM D6496/6496M). Specimens were cut with initial dimensions of 100 mm x 200 mm with the longer dimension parallel to GCL machine direction. The additional length was required to secure the carrier and cover geotextile of the GCL to the upper and lower jaws of the tensile testing apparatus.

Geosynthetic clay liner specimens used for direct shear and peel strength testing, as well as GMXs used for direct shear testing, were hydrated (or exposed in regards to the GMXs)

in DIW, B-PS, and Cu-PS for different hydration times (t_H) prior to testing. Hydration times of 1 mo, 6 mo, and 10 mo were used for the B-PS and Cu-PS, whereas only a hydration time of 6 mo was used for DIW. A schematic of a hydration bin used for GCL hydration is shown in **Error! Reference source not found.** Hydration bins were constructed via epoxying 13-mm-thick PVC sheet together to form boxes with outside dimensions of 0.91-m long, 0.46-m wide, and 0.41-m tall. The GCL test specimens were placed between non-woven geotextile and geocomposite layers facilitate specimen hydration and application of a uniform surface stress. Each GCL specimen was wrapped with Teflon tape along the cut edges to minimize bentonite loss during hydration. Specimens were then distributed evenly across a given layer in the hydration bin and the bins were then filled with the appropriate hydration solution (DIW, B-PS, or Cu-PS). A PVC load plate was placed on top of the uppermost geocomposite layer and a scissor-jack was used to apply a normal stress (σ_n) of 20 kPa. An S-type load cell and digital readout were used to monitor the applied load, and the load was adjusted as-needed to maintain the target 20 kPa normal stress. The DIW, B-PS, and Cu-PS solutions were replaced once a month to re-introduce fresh solution to the hydrating GCLs.

Textured geomembranes were also hydrated in DIW, B-PS, and Cu-PS to similar hydration times as the GCLs. However, GMX specimens for interface shear testing were hydrated in separated plastic bins filled with the appropriate hydration and under a normal stress of approximately 1 kPa. Solutions used for GMX hydration / exposure, were also replaced once a month. Geosynthetic clay liner specimens for peel strength testing were also included in the hydration bins used to hydrate GCL specimens for direct shear testing.

5.3.2 Direct Shear Tests

Internal and interface direct shear tests were performed with a displacement-controlled direct shear apparatus (Bareither et al. 2018). This apparatus was specifically designed for experiments with a broad range of non-standard solutions, including highly acidic and highly

alkaline solutions. In this study, internal and interface shear tests were performed on 150 mm x 150 mm GCL specimens. The 150 mm GCL specimens was used instead of conventional 300 mm x 300 mm specimens because Bareither et al. (2018) reported comparable shear behavior between the smaller and larger GCLs.

The GCL specimens were cut with a razor knife to initial dimensions of 150 mm by 200 mm, with the larger dimension along the machine direction to facilitate clamping geotextiles of the GCL to upper and lower gripping plates. A two-stage hydration and consolidation procedure was implemented for all GCL specimens used in the internal and interface shear tests. The hydration stage was conducted in the hydration bins (Fig. 5.1) under $\sigma_n = 20$ kPa to target hydration periods of 1, 6, and 10 months. Following hydration, GCL specimens were removed from the hydration bins, fixed between two pyramid-tooth gripping plates, and transferred to the direct shear box for consolidation. The pyramid-tooth gripping plates were designed based on Allen and Fox (2007) and had 1-mm-tall teeth. The GCL specimens used in for interface shear testing only were clamped to a single pyramid-tooth plate and placed in contact with a GMX such that the interface was between the carrier geotextile of the GCL and GMX. The GMX was removed from a hydration bin that corresponded to the same hydration time as the GCL and placed in contact with a pyramid-tooth plate. The 1-mm tall teeth penetrated into, but not through, the GMX to hold the GMX in-place during shear.

Specimens for internal or interface shear tests were transferred to the shear box and $\sigma_n = 20$ kPa was applied to represent conditions at the end of the hydration period. The shear box was then filled with the appropriate hydration solution (i.e., DIW, B-PS, or Cu-PS) and σ_n was doubled every 4-6 h until the target shearing normal stress (σ_{n-s}) was achieved. Specimens for internal and interface direct shear tests were equilibrated in the shear box under the σ_{n-s} for an additional 24 h before shearing. All shear tests were conducted at ambient room temperature, which was approximately 20 °C.

Shearing was conducted with a horizontal displacement rate of 0.1 mm/min for the internal and interface direct shear tests. Specimens were sheared to a horizontal displacement (δ_h) of approximately 70 mm, which was the maximum displacement capacity for a 150-mm GCL specimen. The $\delta_h = 70$ mm was sufficient to capture peak shear strength for the internal and interface shear tests; however, residual shear strength of reinforced GCLs typically requires larger δ_h (Fox and Stark 2015). Therefore, large-displacement shear strength was used instead of residual strength, and was defined as the shear stress at $\delta_h = 70$ mm.

The shear plane area of the GCL decreased with horizontal displacement internal shear testing due to offset between the upper and lower shear platens. Nominal shear and normal stresses, computed based on the initial shear plane area of a GCL specimen, were used in the analysis of peak shear strength. Despite an offset between the upper and lower shear platens, reinforcement fibers within the initial shear plane remain intact between the cover and carrier geotextiles to generate peak shear strength. However, reinforcement fibers fail post peak strength, and thus, area corrected normal and shear stresses were used to analyze large-displacement shear strength. In contrast, the shear plane area between a GCL and GMX in the interface shear tests remained constant due to the larger dimensions of the GMX. Thus, nominal normal and shear stresses were used to analyze peak and large-displacement shear strength for the interface shear tests.

All GCL specimens were visually inspected after internal shear tests to identify if internal shear was successful. Signs of stress localization, geotextile tearing, geotextile elongation, or slippage between the GCL and gripping surfaces indicated an unsuccessful internal shear test. An average bentonite water content was determined from water content measurements on three samples collected from spatially outward from the middle of the specimen. All GCL and GMX specimens were visually inspected following the interface shear tests to identify failure mode of the GCL/GMX composite system.

5.3.3 Peel Strength Tests

Peel strength tests were performed with a fully automated tensile testing machine on non-pre-hydrated GCL specimens and hydrated GCL specimens. Non-pre-hydrated GCL specimens were evaluated to determine the average peel strength of the GCL sample roll (Table 5.1). Peel strength tests on hydrated specimens were performed to evaluate if a change in peel strength occurred with respect to hydration solution and/or hydration solution. All peel strength tests were performed with a constant rate of axial extension (CRE) = 300 mm/min in accordance with ASTM D 6496/6496M.

Peel strength tests on non-pre-hydrated specimens were conducted immediately after cutting the GCL specimens from the sample roll. Peel strength tests on hydrated specimens were conducted on GCL specimens placed in the target hydration solutions (i.e., DIW, B-PS, and Cu-PS) for varying hydration periods (i.e., 1, 6, and 10 months). At the end of the hydration period for a given set of peel strength specimens (e.g., B-PS and $t_H = 1$ mo), specimens were removed from the hydration bins and placed under a ventilated hood to air-dry. Peel strength tests were performed on air-dried GCL specimens following hydration in a similar manner as tests on non-pre-hydrated specimens. All peel strength specimens were visually inspected after testing, and in the event of geotextile slippage at clamp jaws, geotextile tearing, or geotextile elongation, test results were rejected.

5.4 Results

5.4.1 Displacement-Controlled Direct Shear Tests

5.4.1.1 Internal Direct Shear Tests

A summary of the internal direct shear tests is in Table 5.3. The summary includes t_H , σ_{n_s} , peak shear strength (τ_p), secant friction angle for peak shear strength (ϕ_{s-p}), horizontal

displacement at peak shear strength (δ_{n-p}), area-corrected large-displacement normal stress (AC σ_{ld}), Area-corrected large-displacement shear strength at $\delta_h = 70$ mm (AC τ_{ld}), secant friction angle for large-displacement shear strength (ϕ_{s-ld}), and post-shear average bentonite water content (w). A total of 14 internal shear tests were performed under $\sigma_{n-s} = 500$ kPa and 14 under $\sigma_{n-s} = 2000$ kPa. Duplicate internal shear tests were conducted for a given hydration solution, t_H , and σ_{n-s} to assess help verify internal shear behavior and capture potential variability. The $\sigma_{n-s} = 500$ kPa and 2000 kPa were chosen to represent a reasonable range of normal stress anticipated in liner systems for mine waste. Internal shear tests conducted on GCLs hydrated in DIW were only tests for $t_H = 6$ mo; results from these tests were considered to represent baseline conditions to compare all internal shear tests conducted following hydration in B-PS and Cu-PS. The GCL specimens for B-PS and Cu-PS were hydrated for $t_H = 1, 6,$ and 10 months (Table 5.3).

Relationships of shear stress (τ) versus horizontal displacement (δ_h) for internal direct shear tests on GCL specimens hydrated in DIW for $t_H = 6$ mo are shown in Fig. 5.2. The τ - δ_h relationships in Fig. 5.2 represent typical internal shear behavior of reinforced GCLs (e.g., Gilbert et al. 1996; Fox et al. 1998; Zornberg et al. 2005; Fox and Ross 2011; Fox and Stark 2015; Bareither et al. 2018). An increase in δ_h resulted in a well-defined peak shear stress that followed by displacement-softening behavior. Peak shear stress, taken as τ_p , was attributed to development of maximum shear resistance within the fiber reinforcements of the GCL, which was following by a displacement-softening response due to tensile rupture and/or disentanglement of reinforcement fibers from the carrier geotextile. A smaller localized peak shear stress was observed at $2 \text{ mm} \leq \delta_h \leq 4 \text{ mm}$, which developed prior to τ_p . This observation has been attributed to the mobilization of the gripping system in internal shear tests on reinforced and non-reinforced GCLs (Fox et al. 1998).

Internal shear tests on the GCL specimens hydrated in DIW and tested under $\sigma_{n-s} = 500$ kPa exhibited similar τ - δ_h relationships and yielded comparable peak shear strength and nearly identical large-displacement shear strength. In contrast, considerable difference was observed in the τ - δ_h relationships and peak shear strength for the GCL specimens tested at $\sigma_{n-s} = 2000$ kPa (Fig. 5.3, Table 5.3). These differences were attributed to spatial variability in reinforcement fibers characteristics within a given GCL sample roll (Chapter 2; Zornberg et al. 2004, McCartney et al. 2005).

The τ - δ_h relationships for GCL specimens hydrated for in B-PS and Cu-PS for $t_H = 1, 6,$ and 10 months are shown in Fig. 5.3 The τ - δ_h relationships for all GCL internal direct shear tests shown in Fig. 5.3 exhibit similar behavior as observed for GCLs hydrated in DIW, whereby shear stress increased to a well-defined peak and subsequently reduced per the displacement-softening behavior. However, the general shape of the τ - δ_h relationships were different between specimens hydrated in B-PS and Cu-PS. For example, GCL specimens hydrated in B-PS and sheared under $\sigma_{n-s} = 2000$ kPa exhibited a localized peak shear stress ranging between 320 kPa and 400 kPa (Fig. 5.3). This range was comparable to the localized peak shear stress measured for GCL specimens hydrated in DIW and sheared under $\sigma_{n-s} = 2000$ kPa (Fig. 5.2). In contrast, a considerably larger localized peak shear stress ranging from 600 kPa to 660 kPa was measured on GCL specimens hydrated in Cu-PS and sheared under $\sigma_{n-s} = 2000$ kPa (Fig. 5.3). The higher localized peak shear stresses measured in the GCLs hydrated in Cu-PS was hypothesized to be due to an increase in the stiffness of the cover geotextile and reinforcement fibers of the GCL following the hydration with Cu-PS.

Relationships between τ_p and σ_{n-s} from the internal direct shear tests on GCLs hydrated in B-PS and Cu-PS are shown in Fig. 5.4. The τ_p measured on GCLs hydrated in DIW for 6 months are included in Fig. 5.4 for comparison. A broad range of τ_p was observed for GCLs hydrated in both B-PS and Cu-PS and at both normal stresses. No correlation was found

between τ_p and either the hydration solutions or hydration time. The range of τ_p measured on GCLs hydrated in B-PS and Cu-PS were comparable to the range of τ_p for GCLs hydrated in DIW. Therefore, the differences in peak shear strength could not be attributed to hydration solution or hydration time, but were instead attributed to inherent variability within a given GCL sample roll. Additional testing and analysis to support the inherent variability in a needle-punched, reinforced GCL is in Chapter 2.

Relationships between horizontal displacement at peak shear stress (δ_{h-p}) versus σ_{n-s} from the GCL specimen hydrated in B-PS and Cu-PS are shown in Fig. 5.5. The values of δ_{h-p} from internal shear tests in GCLs hydrated in DIW are included in Fig. 5.5 for comparison. Variation was observed in the values of δ_{h-p} for GCL specimens hydrated in all three hydration solutions. However, there was a general trend of decreasing δ_{h-p} with increasing σ_{n-s} for a given GCL hydration solution and hydration time. The range of δ_{h-p} observed for GCLs hydrated in B-PS was comparable to the range of δ_{h-p} observed for GCLs hydrated in DIW (Fig. 5.5a). In contrast, the δ_{h-p} observed for GCLs hydrated in Cu-PS were consistently lower compared to δ_{h-p} observed for GCLs hydrated in DIW. This observation further supports the hypothesis of an increase in geosynthetic reinforcement stiffness following hydration in Cu-PS, which would lead to more brittle behavior of the reinforcement fibers and failure at lower values of horizontal displacement.

Relationships between the AC τ_{ld} and AC σ_{n-s} from the internal direct shear tests on GCLs following hydration in B-PS and Cu-PS are shown in Fig. 5.6. Area-corrected τ_{ld} for GCL specimens hydrated in DIW are included for comparison. Dashed lines in Fig. 5.6 represent large-displacement friction angle (ϕ_{s-ld}). In general, the ϕ_{s-ld} for all GCL specimens range between 3.2° and 9.4°. The ϕ_{s-ld} determined for GCL shear tests conducted under AC $\sigma_{n-s} = 3700$ kPa were smaller than those determined for GCL shear tests conducted under AC $\sigma_{n-s} = 925$ kPa. This difference has been observed in previous studies and attributed to potential excess pore

pressure that develops from an increase in normal stress as the shear plane area decreases with horizontal displacement. Regardless, the ϕ_{s-ld} for GCLs hydrated in Cu-PS typically were larger than the ϕ_{s-ld} for GCLs hydrated in DIW or in B-PS for a similar hydration time. This increase in shear strength may also be attributed to the increased stiffness of the geosynthetics in the GCL, or perhaps due to cation exchange and an increase in the internal shear strength of the bentonite.

5.4.1.2 Interface Direct Shear Tests

A summary of the 35 interface direct shear tests is in Table **5.4**. The summary includes t_H , σ_{n-s} , τ_p , ϕ_{s-p} , δ_{h-p} , nominal large-displacement shear stress at $\delta_h = 70$ mm (τ_{ld}), ϕ_{s-ld} , and failure mode of the composite system. Interface shear tests were performed under five normal stresses on GCL and GMX specimens hydrated in DIW, B-PS, and Cu-PS. Similar to the internal direct shear tests, experiments conducted on GCLs and GCMs in DIW only were hydrated for $t_H = 6$ mo, whereas GCLs and GMXs were hydrated in B-PS and Cu-PS $t_H = 1, 6, \text{ and } 10$ mo.

Replicate interface shear tests was performed, but instead interface shear tests were conducted under five different normal stresses (100, 300, 500, 1000, and 2000 kPa). The GMX used in this study was a structured GMX with a uniform spike pattern, which renders specimen variability minor relative to what would be anticipated internally in a GCL. In addition, failure modes during the interface shear tests predominantly were complete interface failure or partial interface/internal failure. In these two failure modes, the maximum internal shear resistance of a GCL is not mobilized during interface shear and the effect of GCL reinforcement fiber variability on interface shear strength was not expected to be noteworthy. These reasons supported an interface shear testing program over a broader range of stress in-place of conducting replicated tests at a given normal stress.

Relationships of shear stress versus horizontal displacement from the interface direct shear tests conducted on GCLs and GMXs hydrated in DIW for 6 months are shown in Fig. 5.7. The failure mode that was visually identified for the GCL/GMX composite systems is also identified in Fig. 5.7. Interface shear tests in which failure occurred along the interface between the GCL and GMX exhibited a small peak strength followed by a modest post-peak strength reduction and nearly constant shear stress with continued horizontal displacement. An increase in normal stress to 1000 kPa and 2000 kPa shifted failure to partial interface/internal and complete internal, respectively. As shear failure shifted to engaged partial to full internal resistance within the GCL, a more well-defined peak shear strength and post-peak, displacement-softening behavior was observed. In general, the GCL/GMX interface shear behavior agreed with interface shear tests between GCLs and textured geomembranes (e.g. Triplett and Fox 2001; McCartney et al. 2009; Fox and Stark 2015; Thielmann et al. 2016; Ghazizadeh and Bareither 2019).

Failure modes for the interface direct shear tests were determined via post-shear inspection of GCL and GMX specimens. Photographs of GCLs showing examples of (i) complete interface failure, (ii) complete internal failure, and (iii) partial interface/internal failure are shown in Fig. 5.8. The GCL in Fig. 5.8a was hydrated in Cu-PS for 1 month and sheared under $\sigma_{n-s} = 100$ kPa. The failure mode was complete interface failure as no internal shear deformation was observed within the GCL. Parallel lines across the geotextile of the GCL in machine direction developed as slippage occurred between the GMX spikes and geotextile of the GCL. The GCL in Fig. 5.8b was hydrated in B-PS for 10 months and sheared under $\sigma_{n-s} = 2000$ kPa. The failure mode was complete internal failure as evidenced by complete failure of the internal reinforcement fibers. No signs of slippage were observed between the GMX and geotextile of the GCL. Finally, the GCL in Fig. 5.8c was hydrated in Cu-PS for 10 months and sheared under $\sigma_{n-s} = 1000$ kPa. The failure mode was partial interface/internal failure. Parallel

lines were observed on the geotextile of the GCL that indicated slippage occurred between the geotextile and GMX; however, internal deformation in the GCL also was observed that indicates failure of some reinforcement fibers.

The τ - δ_h relationships from GCL/GMX interface direct shear tests on specimens hydrated in B-PS and Cu-PS for 1, 6, and 10 months are shown in Fig. 5.9. Peak strength and post-peak, displacement-softening behavior were observed in all interface shear tests; however, the different τ - δ_h relationships were attributed to different failure modes (Table 5.4). Similar to the GCL/GMX interface shear tests in DIW, an increase in σ_{n-s} for the specimens hydrated in B-PS resulted in a transition of failure mode from complete interface failure at $\sigma_{n-s} \leq 500$ kPa to either complete internal failure or partial interface/internal failure at $\sigma_{n-s} = 2000$ kPa. In the GCL/GMX interface shear tests on specimens hydrated in Cu-PS a transition in failure modes from complete interface failure to complete internal failure only was observed for the 1-month hydration time (Table 5.4). Complete interface failure was observed in all GCL/GMX interface shear tests with Cu-PS at $t_H = 6$ and 10 m; the one exception was the test conducted under $\sigma_{n-s} = 1000$ kPa following 10 months of hydration, which experienced partial interface/internal failure. The different failure modes for the interface shear tests conducted on GCLs and GMXs hydrated in Cu-PS was also attributed to the increased stiffness of the geosynthetics following exposure to the Cu-PS.

Relationships of τ_p versus σ_{n-s} from the GCL/GMX interface shear tests on materials hydrated in B-PS and Cu-PS are shown in Fig. 5.10, along with data from the interface shear tests on materials hydrated in DIW. Negligible differences were observed among τ_p at $\sigma_{n-s} \leq 500$ kPa for specimens hydrated with different solutions and for different durations. However, differences in τ_p were more noticeable among the data sets in Fig. 5.10 for $\sigma_{n-s} \geq 1000$ kPa. The modest differences in τ_p for $\sigma_{n-s} \geq 1000$ kPa were attributed to different failure modes observed in the GCL/GMX interface shear tests (Table 5.4). Regardless of the modest differences, no

correlations were found between τ_p from the interface shear tests and hydration solution or duration.

Horizontal deformations at peak shear strength from the GCL/GMX interface shear tests are plotted as a function of σ_{n-s} in Fig. 5.11 for materials hydrated in B-PS and Cu-PS. Data from interface tests on materials hydrated in B-PS (Fig. 5.11a) and materials hydrated in DIW depict a general trend of increasing δ_{h-p} with increasing σ_{n-s} . The increase in δ_{h-p} was due to a progressive transition from interface shear failure to interface/internal failure and finally to internal shear failure as σ_{n-s} increased (Table 5.4). Thus, comparable δ_{h-p} in the range of 18 to 20 mm were observed in the internal and interface direct shear tests for materials hydrated in DIW and B-PS at $\sigma_{n-s} = 1000$ and 2000 kPa. The δ_{h-p} identified in the GCL/GMX interface shear tests on materials hydrated in Cu-PS were consistently lower than δ_{h-p} of specimens tested with DIW (Fig. 5.11b) and B-PS (Fig. 5.11a). The lower δ_{h-p} measured in the Cu-PS interface shear tests was attributed to an increased stiffness in the GMX and cover geotextile of the GCL following hydration with Cu-PS.

Relationships between τ_{ld} and σ_{n-s} from the GCL/GMX interface shear tests conducted with B-PS and Cu-PS are shown in Fig. 5.12. Comparable τ_{ld} were observed between specimens hydrated in B-PS, Cu-PS, and DIW for $\sigma_{n-s} \leq 1000$ kPa. These interface shear tests nearly all yielded complete interface failure or partial interface/interface failure, and minimal internal GCL deformation was observed in the latter failure mode. Thus, large-displacement shear strength predominantly was controlled by interface shear resistance between the GMX and geotextile of GCL, which yielded comparable shear strength regardless of hydration solution or duration. More pronounced differences in τ_{ld} were observed at $\sigma_{n-s} = 2000$ kPa, which reflects the different failure modes observed in the GCL/GMX interface shear tests (Table 5.4). The secant friction angle ranged between 6° to 7° for those interface shear tests that

experienced complete internal failure, which was comparable to secant friction angles observed for the internal GCL direct shear tests (Fig. 5.6).

5.4.2 Peel Strength

A summary of results from the peel strength tests conducted on non-hydrated and hydrated GCLs is in Table 5.5. Ten peel strength tests were conducted on non-hydrated GCL specimens (i.e., specimens cut from as-received sample roll) and ten peel strength tests were conducted on for GCLs hydrated to each of the three hydration durations (1, 6, and 10 mo) in the B-PS and Cu-PS. The summary in Table 5.5 includes the average, minimum, maximum, and standard deviation for each set of 10 peel strength tests.

Dot plots of the measured peel strengths are shown in Fig. 5.13 for tests conducted on the non-hydrated GCL and hydrated GCL in B-PS and Cu-PS. Considerable variability in peel strength was observed within any given set of 10 tests that represent a single hydration condition. Furthermore, a similar amount of variability in the magnitude of peel strength was observed in all seven sets of 10 peel strength tests (Fig. 5.13). The average peel strength for the seven sets of tests ranged between approximately 2600 and 2800 N/m, which suggests that despite the peel strength variability, similar ranges and average value were measured for GCL specimens that were not hydrated and those that were hydrated to varying durations in both the B-PS and Cu-PS.

As discussed previously in Chapter 2, variability in peel shear strength can be explained via the variability in peel strength. However, sufficient peel strength tests were not conducted to permit spatially locating individual peel strengths to individual peel shear strengths as was conducted in the study described in Chapter 2. Although variability in peak internal shear strength cannot be directly linked to variability in peel strength from the lack of sufficient testing and spatial correlation, the variability in peak shear strength would be anticipated based on the variability measured in peel strength. Additional testing is needed, similar to that completed in

Chapter 2, to evaluate whether (i) unique trends exist between τ_p and peel strength for a given hydration solution and duration, and (ii) select hydration conditions change τ_p and peel strength in an understandable manner.

5.4.3 Swell Index

Swell index tests were performed to evaluate (i) the effect of non-standard solutions on swell behavior of bentonite and (ii) if changes observed in shear behavior could be linked to changes in bentonite. A summary of the swell index test conducted on non-hydrated bentonite and bentonite extracted from GCLs hydrated for different durations in B-PS and Cu-PS is in Table 5.6. Swell index tests on non-hydrated bentonite were performed in DIW, B-PS, and Cu-PS, whereas swell index tests on bentonite exhumed from hydrated GCLs were performed in DIW and the solution in which the GCLs were hydrated. Duplicate swell index tests were performed for a given test condition (e.g., non-hydrated bentonite in DIW), and that average of each two swell index tests are tabulated in Table 5.6 that were rounded to the nearest 0.5 mL/2-g.

A photograph of swell index tests conducted with non-hydrated bentonite in DIW, B-PS, and Cu-PS is in Fig. 5.14. The largest swell index of 34 mL/2-g was measured on non-hydrated bentonite tested in DIW. This high swell index was anticipated due to high bentonite swell in a low ionic strength solution that did not contain multi-valent cations (McBride 1994). The swell index of the non-hydrated bentonite decreased to 24.5 mL/2-g in B-PS (Fig. 5.14, Table 5.6). Reduced swell index in B-PS was attributed to reduced thickness of the diffuse double layer (DDL) of bentonite due to higher ionic strength of the B-PS and the presence of Ca^{2+} . Diffuse double layer thickness is inversely related to the square root of ionic strength of a hydration solution and divalent cations can reduce DDL thickness due to cation exchange (Evans 1986; Hunter 1988; Shackelford 1994; Shackelford et al. 2000; Lyklema 2005).

The lowest swell index of 8 c was measured for non-hydrated bentonite in Cu-PS (Fig. 5.14, Table 5.6). The ionic strength of the Cu-PS was considerably higher than B-PS and the Cu-PS contained an abundance of divalent and trivalent cations (i.e. Ca^{2+} , Cu^{2+} , Mn^{2+} , Al^{3+} , and Mg^{2+}) that could contribute to cation exchange. Thus, bentonite swell could only be attributed to osmotic swell as crystalline swell most likely could not occur in Cu-PS (Norish 1954; Norish and Quirk 1954; Scalia et al. 2018). Another potential reason for the lack of bentonite swell in the Cu-PS could be dissolution of clay structure due to the low pH of Cu-PS (Kashir and Yanful 2001; Lange et al. 2007; Shackelford et al. 2010; Bouazza and Gates 2014). Potential dissolution of the bentonite could be evaluated in future work via x-ray diffraction analysis of the bentonite before and after exposure to Cu-PS.

Bar charts of swell index for non-hydrated bentonite and bentonite hydrated in B-PS and Cu-PS are shown in Fig. 5.15. The two bars included for each hydration condition represent the swell index when using DIW or the specific hydration solution in the swell test. There were two interesting observations from swell test involving B-PS: (i) swell index of bentonite hydrated in B-PS and then tested in B-PS was similar to the baseline condition of non-hydrated bentonite tested in DIW; and (ii) swell index of non-hydrated bentonite tested in B-PS and bentonite hydrated in B-PS and tested in DIW were similar. In regards to the second observation, cation exchange may have occurred rapidly to the extent possible during exposure to B-PS, such that extended duration of exposure (e.g., $t_H = 1, 6, \text{ and } 10 \text{ mo}$) did not considerably change the swell behavior of B-PS.

The swell index of bentonite hydrated in B-PS and then tested in B-PS during the swell test ranged between 31.0 and 34.5 mL/2-g (Fig. 5.15a), which were comparable to the swell index of 34.5 mL/2-g determined for non-hydrated bentonite in DIW. This observation was hypothesized to be due a pH-driven mechanism and a concentration-driven mechanism. The pH-driven mechanism can explain the higher swell index of B-PS hydrated bentonite relative to the non-hydrated bentonite tested in B-PS. An increase in pH of the hydration solution can

increase the net negative surface charge of clay particles due to surface protonation. Considering the time-dependency of this pH-driven mechanism (Bergaya et al. 2013), the net negative surface charge of clay particles is expected to be higher for samples hydrated and tested with B-PS compared to non-hydrated bentonite tested in B-PS. The higher net negative surface charge of the B-PS hydrated bentonite particles produced a larger DDL and higher swell index compared to non-hydrated bentonite tested in B-PS.

The concentration-driven mechanism can explain the higher swell index of B-PS hydrated bentonite in swell index tests in B-PS in comparison to swell index tests in DIW. The higher swell index of B-PS hydrated bentonite tested in B-PS in comparison to tests in DIW was hypothesized to be due to the formation of a flocculated clay structure. Higher ionic strength and higher ion concentrations in the B-PS could reduce the thickness of the water layer bonded to the clay particles and allow formation of flocculated structure due to facilitated interactions among clay platelets. The increase in swell index of bentonite following swell index tests with higher-concentration solutions has been reported in Scalia et al. (2018). Considering different observations from swell index tests in B-PS or on bentonite hydrated in B-PS, an understanding of the swell behavior of bentonite exposed to B-PS requires additional research.

The swell index of bentonite hydrated in Cu-PS and then tested in DIW or Cu-PS was consistently between 5.5 and 6.0 mL/2-g. This range of swell index was comparable to the swell index of non-hydrated bentonite tested in Cu-PS. This observation indicates that any exposure to Cu-PS during hydration or during the swell index test considerably influenced the clay structure and swell behavior of the bentonite. Considering that the primary purpose of GCLs is to provide hydraulic resistance, results of swell index tests with Cu-PS raise a concern regarding applicability of GCLs containing natural sodium bentonite in copper mining applications if exposure to copper mine solutions is anticipated.

5.5 Summary

The purpose of this study was to evaluate the effect of non-standard solutions on the internal and interface shear behavior of GCLs. For this aim a series of internal and interface direct shear tests were performed on specimens hydrated with DIW as well as two synthesized mining solutions, namely Cu-PS and B-PS, representative of Copper and Bauxite mining process liquids. The observations in internal and interface direct shear tests were further investigated via a series of peel strength tests and swell index tests. The following conclusions were obtained from the results of this study:

- The τ - δ_h relationships in all internal shear tests in this study included a localized peak, a well-defined peak shear strength, and displacement softening behavior. The general shape of τ - δ_h relationships in internal shear tests with B-PS and DIW were comparable. However, the τ - δ_h relationships of specimens hydrated with Cu-PS was different as specimens experienced a higher localized peak and lower δ_{h-p} .
- the range of τ_p in internal shear tests with B-PS and Cu-PS were comparable to the range of τ_p in benchmark internal shear tests with DIW, and no correlation was found between the τ_p and either the hydration solutions or hydration period (t_H). The wide τ_p range in internal shear tests is attributed the reinforcement fiber variabilities among different GCL specimens.
- The range of large-displacement shear strength was comparable between specimens tested with DIW, B-PS, and Cu-PS, and no correlation have been found between the ϕ_{s-ld} in internal shear tests and either hydration solution or t_H .
- Different τ - δ_h relationships were observed in GCL-GMX interface shear tests with different hydration solutions that indicate the different failure mode of GCL/GMX composite systems in interface shear tests. In interface shear tests with DIW and B-PS, increase in σ_{n-s} resulted in a systematic transition of failure mode from complete

interface failure to complete internal failure regardless of the t_H . However, the failure mode in interface shear tests with Cu-PS was generally complete interface failure.

- Relatively comparable τ_p was observed in GCL-GMX interface shear tests at $\sigma_{n-s} \leq 500$ kPa regardless of the hydration solution or t_H . However, variation in τ_p values was observed at $\sigma_{n-s} = 1000$ and 2000 kPa. The τ_p variation is attributed to partial interface/internal failure or complete internal failure modes in experiments on B-PS and DIW in which variation of GCL internal shear strength causes variation in the τ_p in interface shear tests.
- The value of τ_{id} in GCL-GMX interface shear tests depended on the failure mode of the GCL-GMX composite. In interface shear tests with complete interface failure or partial interface/internal failure mode (with low internal deformation in GCL), the τ_{id} and ϕ_{s-id} of specimens were comparable regardless of the hydration solution or t_H . However, the ϕ_{s-id} in interface shear tests with complete internal failure was significantly lower and was comparable to the ϕ_{s-id} in internal shear tests.
- High variabilities were observed within the peel strength of both non-hydrated specimens and specimens hydrated with a specific solution for a specific t_H . Regardless of the variability, no significant difference was observed in the peel strength range of non-hydrated GCLs and pre-hydrated GCLs.
- Exposure to Cu-PS resulted in a significant reduction in the swell behavior of sodium bentonite. No conclusion could be made regarding the effect of B-PS on the bentonite swell behavior.

Table 5.1. Summary of material characteristics and properties for geosynthetic clay liners (GCLs) used in this study.

Property	
Peel strength (N/m) ^a	2170
Heat Treatment Method	NHT
Carrier geotextile type	NW
Cover geotextile type	NW
Carrier geotextile mass/area (g/m ²) ^b	280
Cover geotextile mass/area (g/m ²) ^b	240
Bentonite Type	Granular
Bentonite mass per area (g/m ²) ^c	5610
Plasticity Index (%)	34

Notes: NHT = Non-heat treated; NW = non-woven

^a Average value based on 10 peel strength tests on non-pre-hydrated specimens (ASTM D6496/6496M)

^b Average value based on 10 measurements (ASTM D5261)

^c Average value based on 10 measurements (ASTM D5993)

Table 5.2. Properties of synthetic solutions prepared to represent a Copper mine process solution (Cu-PS) and bauxite mine process solution (B-PS).

Parameter	Symbol	unit	Cu-PS	B-PS
Aluminum	Al ³⁺	mg/L	2036	-
Calcium	Ca ²⁺	mg/L	588	94
Copper	Cu ²⁺	mg/L	1300	-
Potassium	K ⁺	mg/L	789	-
Magnesium	Mg ²⁺	mg/L	5100	12
Manganese	Mn ²⁺	mg/L	1948	-
Sodium	Na ⁺	mg/L	230	1010
Chloride	Cl ⁻	mg/L	20587	-
Hydroxide	OH ⁻	mg/L	-	340
Phosphate	PO ₄ ³⁻	mg/L	2298	-
Sulfate	SO ₄ ²⁻	mg/L	27028	1430
pH	pH	-	1	12.3
Ratio of monovalent to divalent cations	RMD	M ^{1/2}	0.33	1.2
Ionic strength	<i>I</i>	(M)	0.848	0.06

Table 5.3. Properties of synthetic solutions prepared to a represent a Copper mine process solution (Cu-PS) and bauxite mine process solution (B-PS).

Hydration Solution	t_H (m)	σ_{n-s} (kPa)	τ_p (kPa)	ϕ'_{s-p} (°)	δ_{h-p} (mm)	AC σ_{ld} (kPa)	AC τ_{ld} (kPa)	ϕ'_{s-ld} (°)	W (%)
DIW	6	500	307.0	31.5	21.3	924.8	84.0	5.2	71.0
		500	355.2	35.4	22.3	924.8	84.2	5.2	61.0
		2000	476.6	13.4	18.1	3699.0	239.3	3.7	47.1
		2000	868.9	23.5	21.4	3699.0	310.7	4.8	51.8
B-PS	1	500	402.4	38.8	24.6	924.8	86.9	5.4	63.6
		500	390.1	38.0	23.3	924.8	90.4	5.6	66.2
		2000	684.2	18.9	19.5	3699.0	216.4	3.3	55.7
		2000	700.2	19.3	20.2	3699.0	289.1	4.5	54.9
B-PS	6	500	430.7	40.7	23.3	924.8	89.7	5.5	71.3
		500	363.5	36.0	22.7	924.8	114.5	7.1	71.4
		2000	867.4	23.4	22.7	3699.0	247.1	3.8	53.5
		2000	724.0	19.9	20.8	3699.0	230.8	3.6	46.7
B-PS	10	500	338.6	34.1	24.5	924.8	105.6	6.5	70.4
		500	387.7	37.8	23.9	924.8	120.4	7.4	63.6
		2000	579.4	16.2	19.5	3699.0	204.2	3.2	52.8
		2000	750.6	20.6	20.1	3699.0	311.1	4.8	59.0
Cu-PS	1	500	363.8	36.0	20.1	924.8	130.2	8.0	59.8
		500	316.9	32.4	20.6	924.8	144.8	8.9	68.3
		2000	650.5	18.0	15.1	3699.0	339.0	5.2	50.7
		2000	689.0	19.0	15.7	3699.0	350.7	5.4	53.7
Cu-PS	6	500	384.6	37.6	19.5	924.8	137.0	8.4	69.8
		500	515.9	45.9	21.4	924.8	138.5	8.5	66.9
		2000	622.3	17.3	13.2	3699.0	288.0	4.5	61.3
		2000	716.7	19.7	14.4	3699.0	329.8	5.1	60.2
Cu-PS	10	500	438.2	41.2	19.5	924.8	128.5	7.9	59.0
		500	443.7	41.6	20.1	924.8	152.6	9.4	65.1
		2000	683.6	18.9	16.1	3699.0	350.7	5.4	54.3
		2000	619.7	17.2	13.2	3699.0	288.0	4.5	54.6

Notes: t_H = hydration period; σ_{n-s} = shearing normal stress; τ_p = peak internal shear strength; ϕ'_{s-p} = secant friction angle for peak shear strength; δ_{h-p} = horizontal displacement at peak shear strength; AC σ_{ld} = area-corrected shearing normal stress; AC τ_{ld} = area-corrected shear strength at horizontal displacement (δ_h) = 70 mm; ϕ'_{s-ld} = secant friction angle at large-displacement shear strength; W = average specimen bentonite water content (%)

Table 5.4. Summary of displacement-controlled interface direct shear tests.

Hydration Solution	t_H (m)	σ_{n-s} (kPa)	τ_p (kPa)	ϕ'_{s-p} (°)	δ_{h-p} (mm)	τ_{ld} (kPa)	ϕ'_{s-ld} (°)	Failure mode
DIW	6	100	56.1	29.3	13.0	47.5	25.4	IF
		300	153.6	27.1	16.2	106.2	19.5	IF
		500	249.9	26.6	14.5	161.4	17.9	IF
		1000	443.6	23.9	16.3	276.6	15.5	IF/IN
		2000	700.5	19.3	19.4	209.2	6.0	IN
B-PS	1	100	56.34	29.4	8.8	39.9	21.8	IF
		300	145.3	25.8	12.6	108.8	19.9	IF
		500	181.5	20.0	10.1	133.6	15.0	IF
		1000	372.9	20.5	15.1	267.8	15.0	IF/IN
		2000	619.0	17.2	17.0	221.8	6.3	IN
B-PS	6	100	64.2	32.7	13.9	45.8	24.6	IF
		300	126.1	22.8	8.8	104.2	19.2	IF
		500	197.2	21.5	11.3	137.4	15.4	IF
		1000	321.0	17.8	13.9	214.9	12.1	IF/IN
		2000	677.9	18.7	17.0	461.7	13.0	IF/IN
B-PS	10	100	47.63	25.5	9.4	38.2	20.9	IF
		300	111.1	20.3	8.8	79.3	14.8	IF
		500	234.5	25.1	13.2	153.5	17.1	IF
		1000	376.0	20.6	18.9	277.1	15.5	IF/IN
		2000	706.0	19.4	18.2	212.4	6.1	IN
Cu-PS	1	100	54.0	28.4	5.1	33.2	18.4	IF
		300	129.9	23.4	5.7	89.2	16.6	IF
		500	213.9	23.2	9.5	164.7	18.2	IF
		1000	347.9	19.2	6.3	259.5	14.5	IF
		2000	601.4	16.7	13.2	244.9	7.0	IN
Cu-PS	6	100	49.2	26.2	5.0	34.6	19.1	IF
		300	128.4	23.2	5.7	81.1	15.1	IF
		500	215.7	23.3	7.6	144.8	16.2	IF
		1000	401.7	21.9	8.2	279.9	15.6	IF
		2000	607.4	16.9	6.3	444.2	12.5	IF
Cu-PS	10	100	58.9	30.5	6.1	37.1	20.4	IF
		300	140.1	25.0	6.1	95.4	17.6	IF
		500	208.8	22.7	5.8	154.8	17.2	IF
		1000	426.4	23.1	13.2	221.7	12.5	IF/IN
		2000	706.6	19.5	7.6	522.5	14.6	IF

Note: t_H = Hydration period; σ_{n-s} = shearing normal stress; τ_p = peak internal shear strength; ϕ'_{s-p} = secant friction angle at peak shear strength; δ_{h-p} = horizontal displacement at peak shear strength; τ_{ld} = large-displacement shear strength at horizontal displacement (δ_h) = 70 mm; ϕ'_{s-ld} = secant friction angle at large-displacement shear strength IF = complete interface failure; IF/IN = partial interface/internal failure; IN = complete internal failure.

Table 5.5. Peel strength test results for non-hydrated geosynthetic clay liner (GCL) specimens and GCL specimens hydrated with B-PS and Cu-PS for hydration durations of 1, 6, and 10 months.

Hydration Solution	Non-hydrated	B-PS	B-PS	B-PS	Cu-PS	Cu-PS	Cu-PS
Hydration duration (months)		1	6	10	1	6	10
Minimum peel strength (N/m) ^a	2376	2338	2231	2488	2298	2214	1952
Maximum peel strength (N/m) ^a	3517	2926	3097	3153	3202	3128	3240
Average peel strength (N/m) ^a	2822	2593	2668	2720	2789	2670	2713
Standard deviation (N/m) ^a	300	167	260	209	264	269	352

^a Averages based on the results of 10 peel strength tests.

Table 5.6. Summary of swell index tests performed on non-pre-hydrated bentonite and bentonite hydrated with non-standard solutions

Bentonite Description	SI test Solution	SI test-1 (mL/2g)	SI test-2 (mL/2g)	SI test-3 (mL/2g)	Average SI (mL/2g)
Non-hydrated	DIW	34	35	34	34.5
	B-PS	24	25	25	24.5
	Cu-PS	7	8	7	7.5
Hydrated with B-PS, $t_H = 1$ m	DIW	24	25	24.5	24.5
	B-PS	35	34	34	34.5
Hydrated with B-PS, $t_H = 6$ m	DIW	24	23	24	23.5
	B-PS	31	31	31.5	31
Hydrated with B-PS, $t_H = 10$ m	DIW	23.5	24	24	24
	B-PS	34	33	33	33.5
Hydrated with Cu-PS, $t_H = 1$ m	DIW	6	6	6	6
	Cu-PS	6	5.5	6	6
Hydrated with Cu-PS, $t_H = 6$ m	DIW	5.5	6	5.5	5.5
	Cu-PS	6	5.5	6	6
Hydrated with Cu-PS, $t_H = 10$ m	DIW	5.5	6	6	6
	Cu-PS	6	6	5.5	6

Notes: SI = swell index; t_H = hydration period of the GCL bentonite in non-standard solutions. Average swell index = arithmetic average of the results of three swell index tests rounded to the nearest 0.5 mL/2g

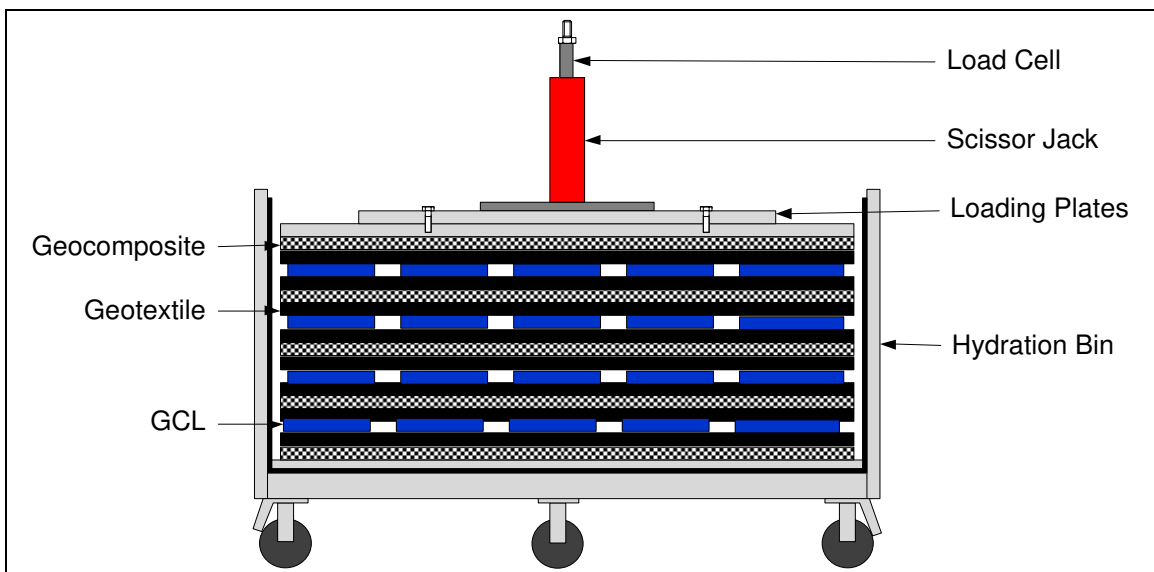


Fig. 5.1. Schematic of a hydration bin used for the prolonged hydration of geosynthetic clay liner specimens.

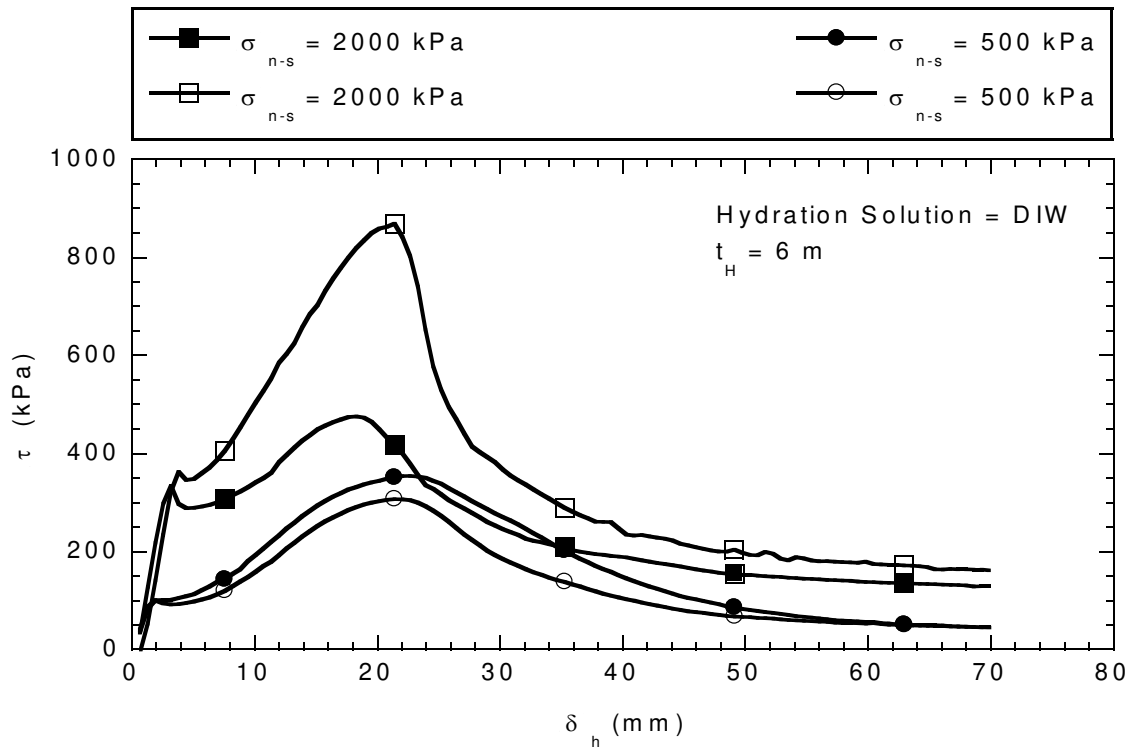


Fig. 5.2. Relationships of shear stress (τ) versus horizontal displacement (δ_h) in internal shear tests on geosynthetic clay liner (GCL) specimens hydrated with de-ionized water (DIW) for a hydration time (t_H) of 6 months.

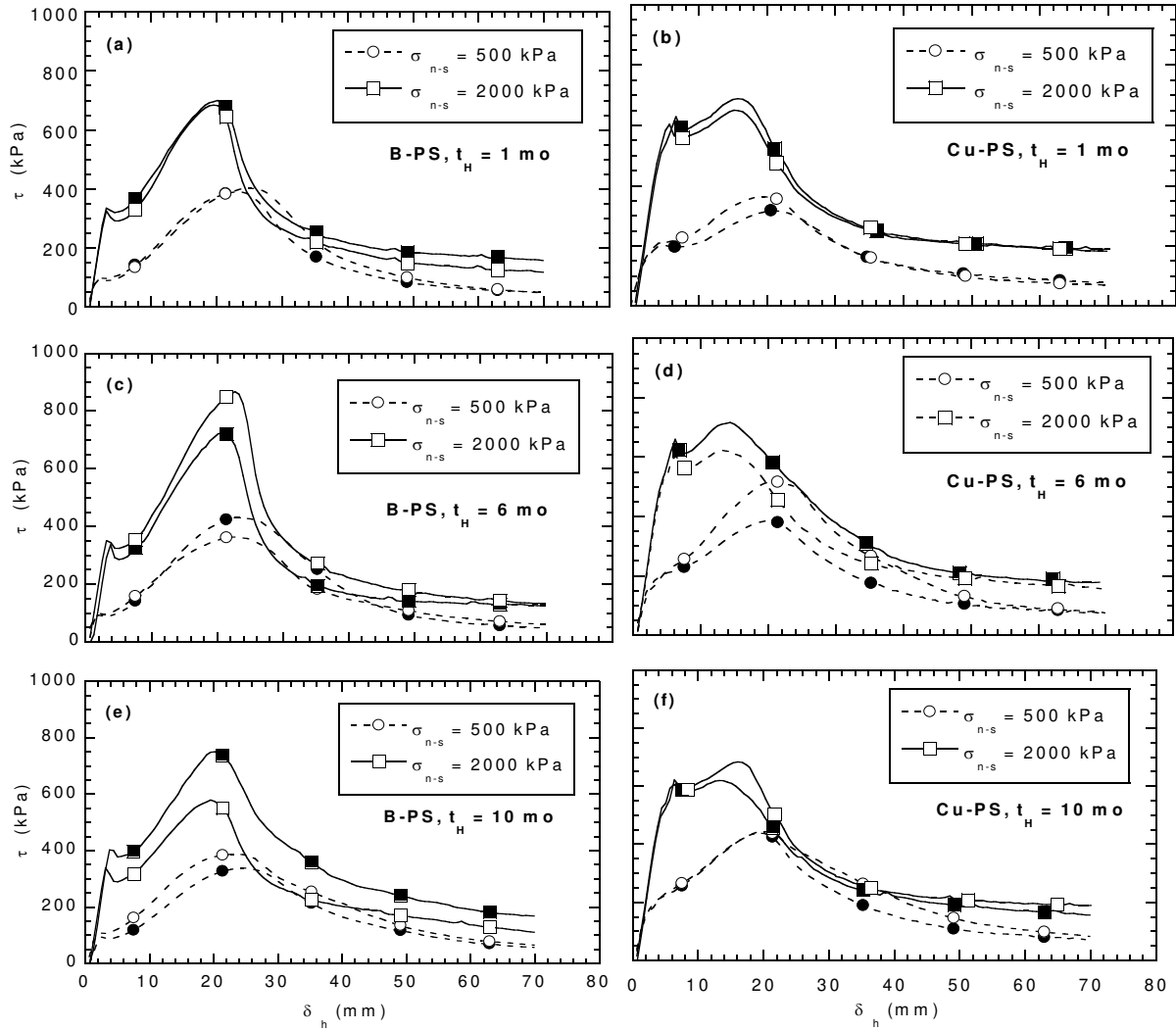


Fig. 5.3. Relationships of shear stress (τ) versus horizontal displacement (δ_h) in internal shear tests on GCL specimens hydrated with (a) B-PS for $t_H = 1$ m, (b) Cu-PS for $t_H = 1$ m, (c) B-PS for $t_H = 6$ m, (d) Cu-PS for $t_H = 6$ m, (e) B-PS for $t_H = 10$ m, and (f) Cu-PS for $t_H = 10$ m. Open and closed symbols represent the duplicate tests conducted on for each hydration and normal stress condition.

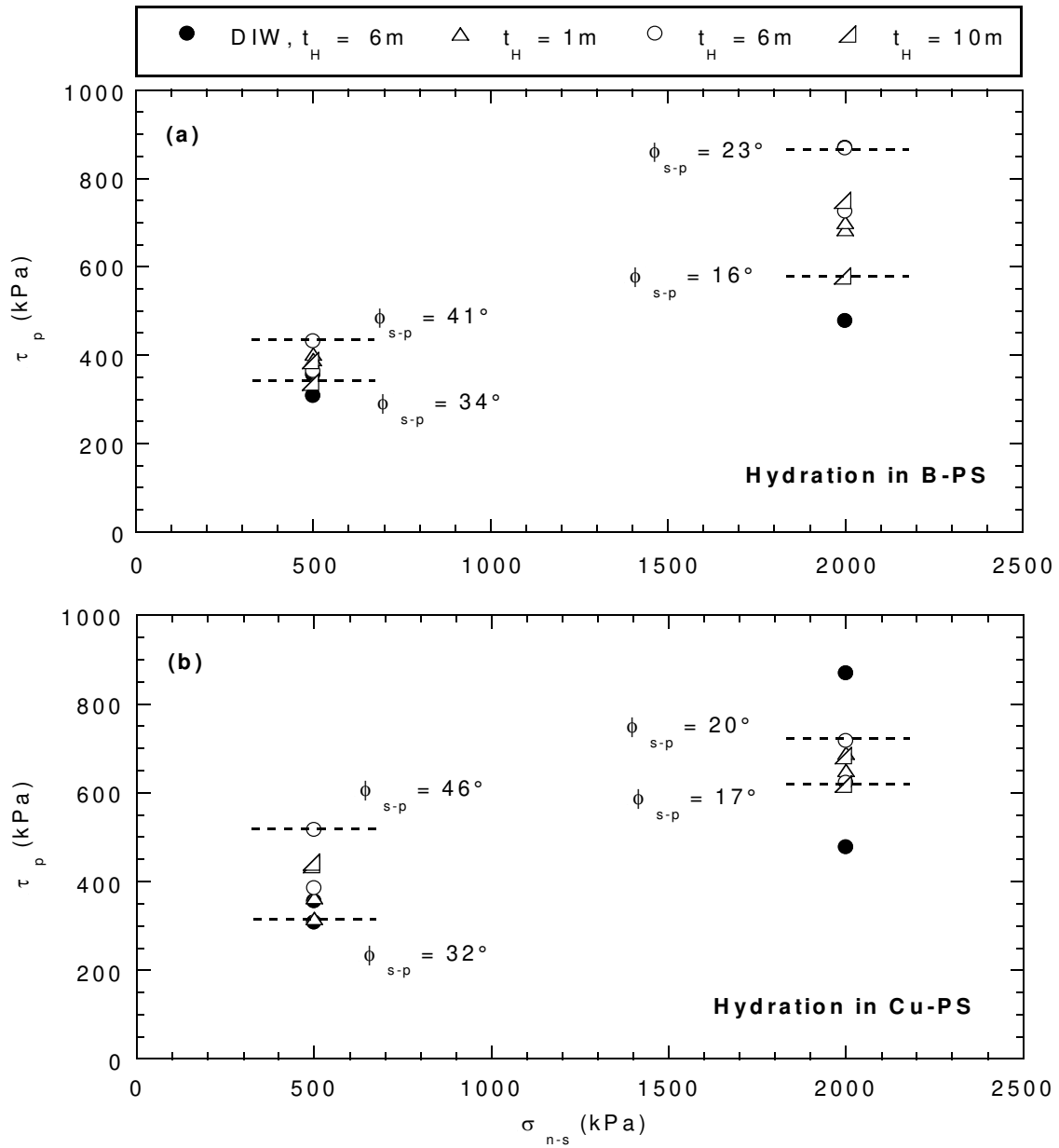


Fig. 5.4. Peak shear strength (τ_p) versus shearing normal stress (σ_{n-s}) from internal direct shear tests on GCL specimens hydrated with B-PS (a) and Cu-PS (b). Results of the experiments with DIW included for comparison.

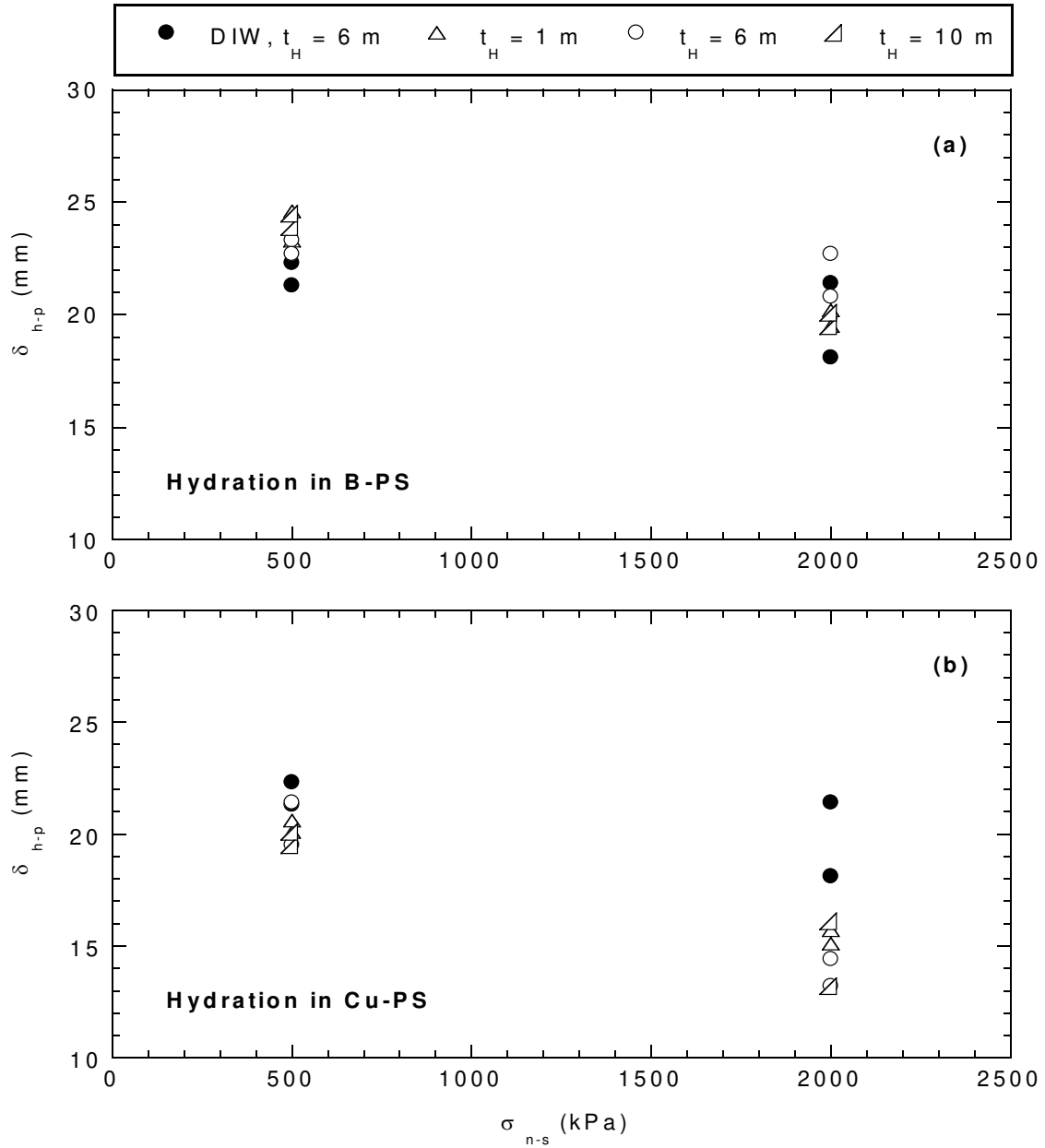


Fig. 5.5. Horizontal displacement at peak shear stress (δ_{h-p}) versus shearing normal stress (σ_{n-s}) from internal direct shear tests on GCL specimens hydrated with B-PS (a) and Cu-PS (b). Results of the experiments with DIW included for comparison.

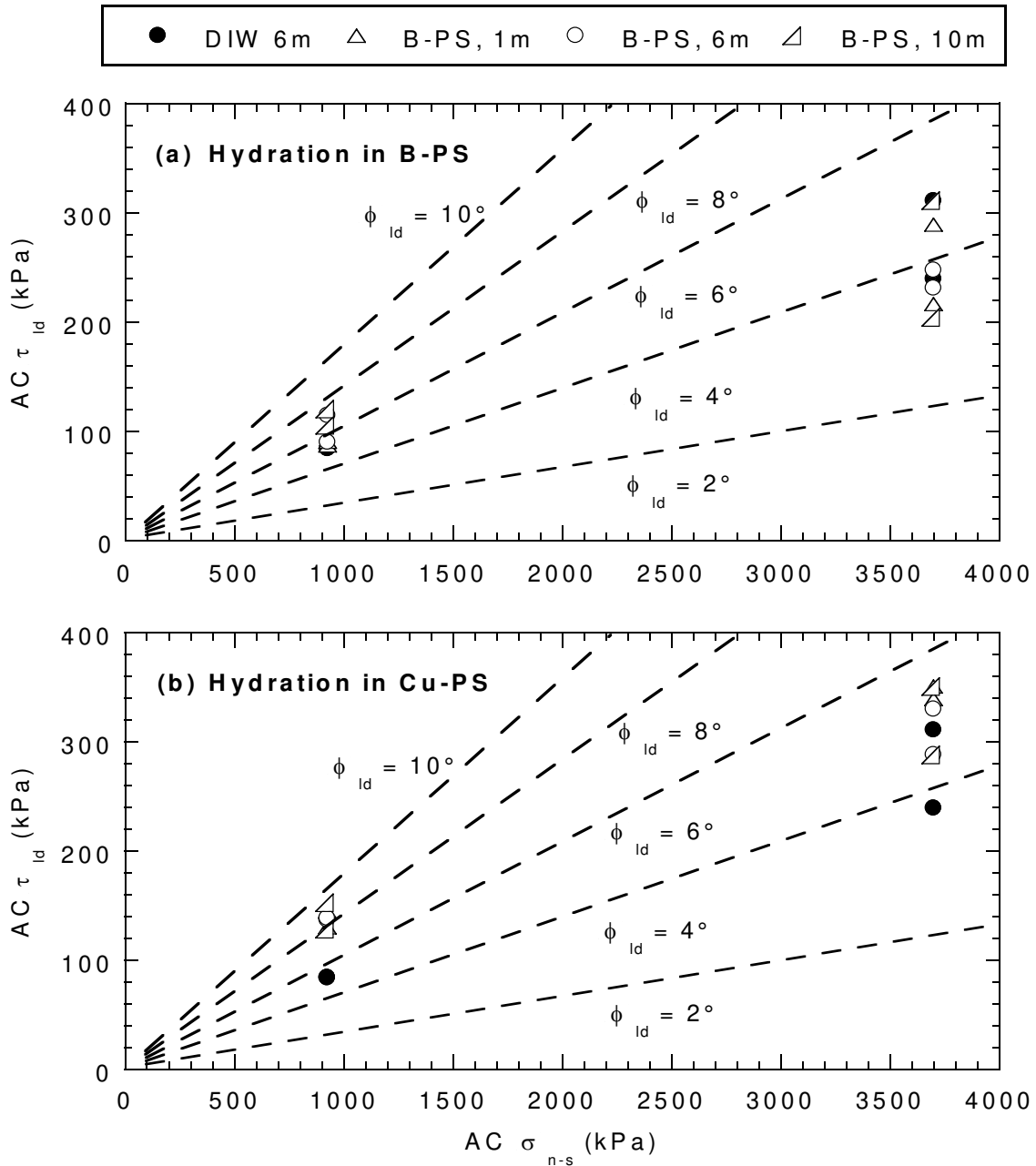


Fig. 5.6. Area-corrected large-displacement shear strength ($AC \tau_{ld}$) versus area-corrected shearing normal stress ($AC \sigma_{n-s}$) from internal direct shear tests on GCL specimens hydrated with B-PS (a) and Cu-PS (b). Results of the experiments with DIW included for comparison. Dash lines are contours of large-displacement friction angle (ϕ_{ld}).

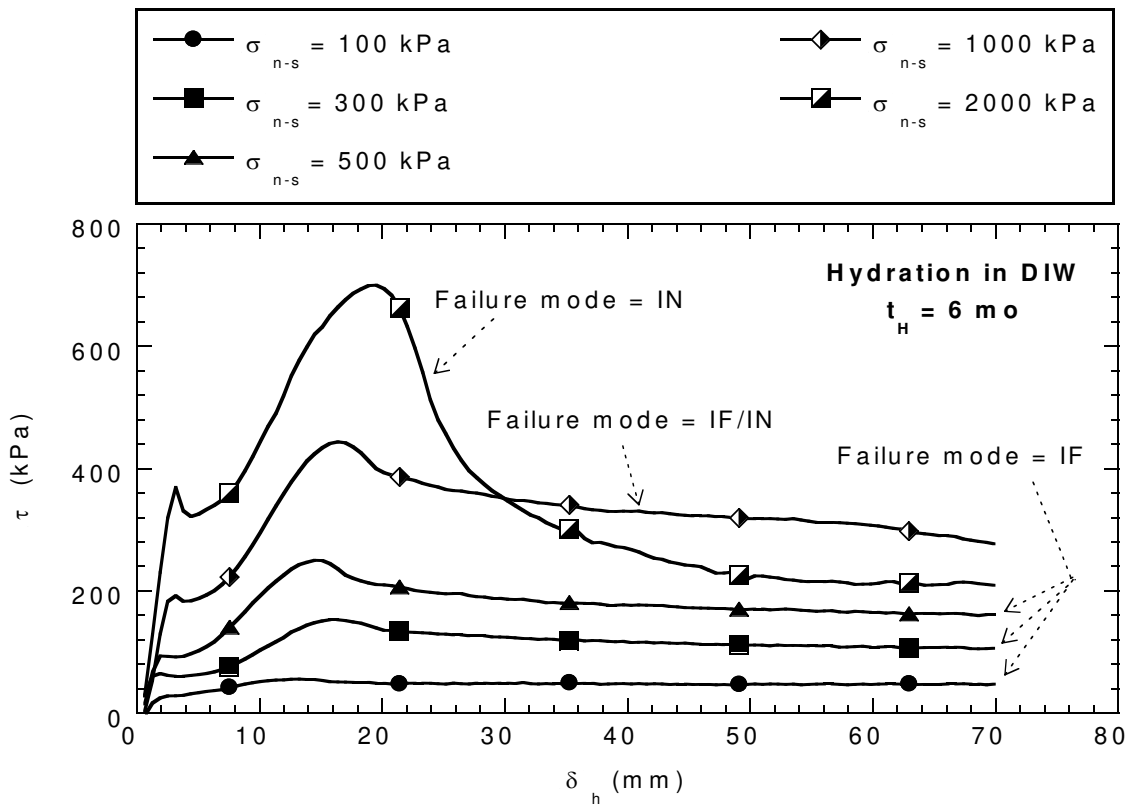


Fig. 5.7. Relationship between shear stress (τ) versus horizontal displacement (δ_h) for interface shear tests between GCL and GMX specimens hydrated with de-ionized water (DIW) for hydration time (t_H) = 6 mo.

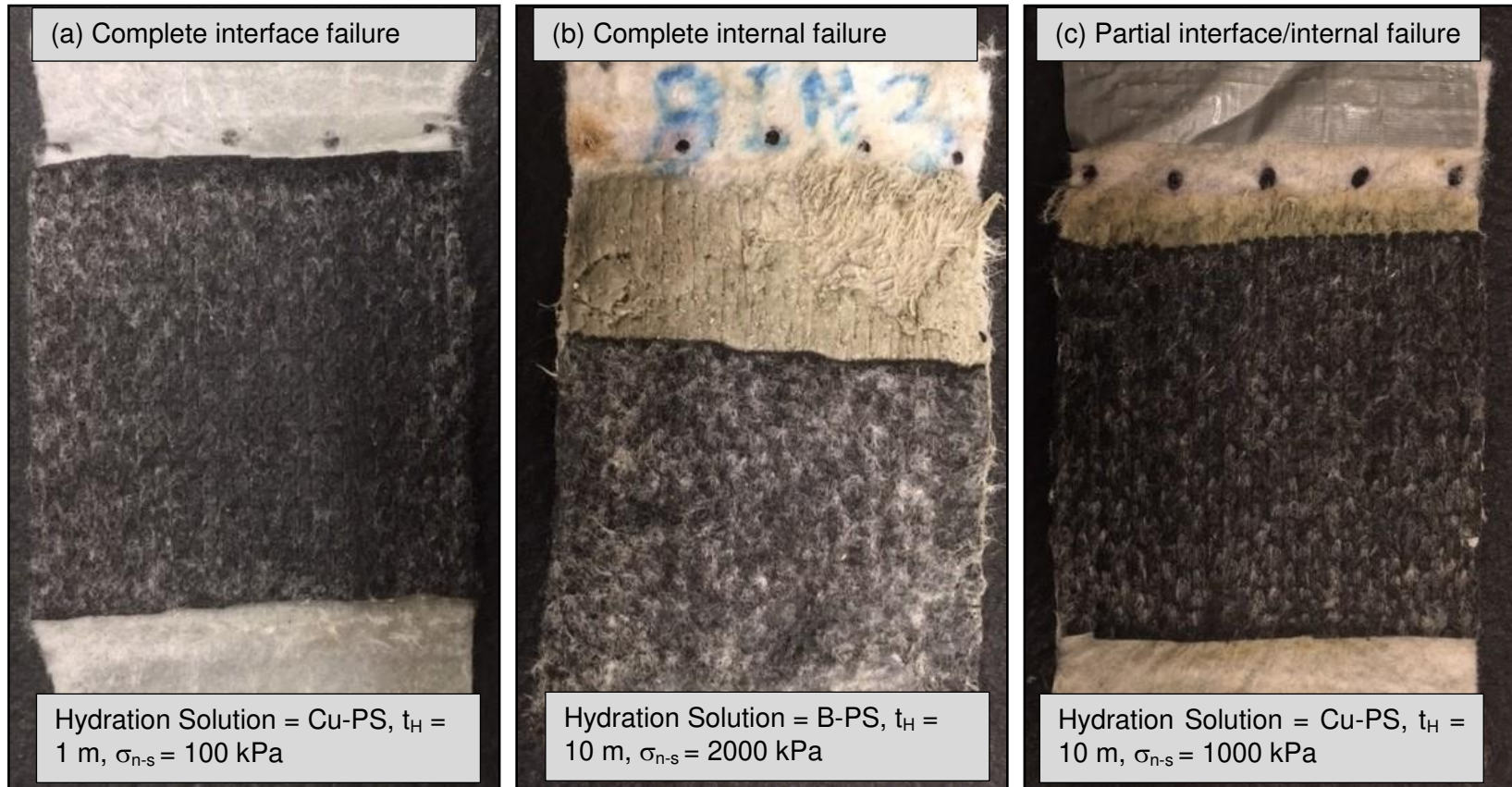


Fig. 5.8. Post-shear photographs of GCL specimens from interface direct shear tests showing examples of (a) complete interface failure mode, (b) complete internal failure mode, and (c) partial interface/internal failure mode.

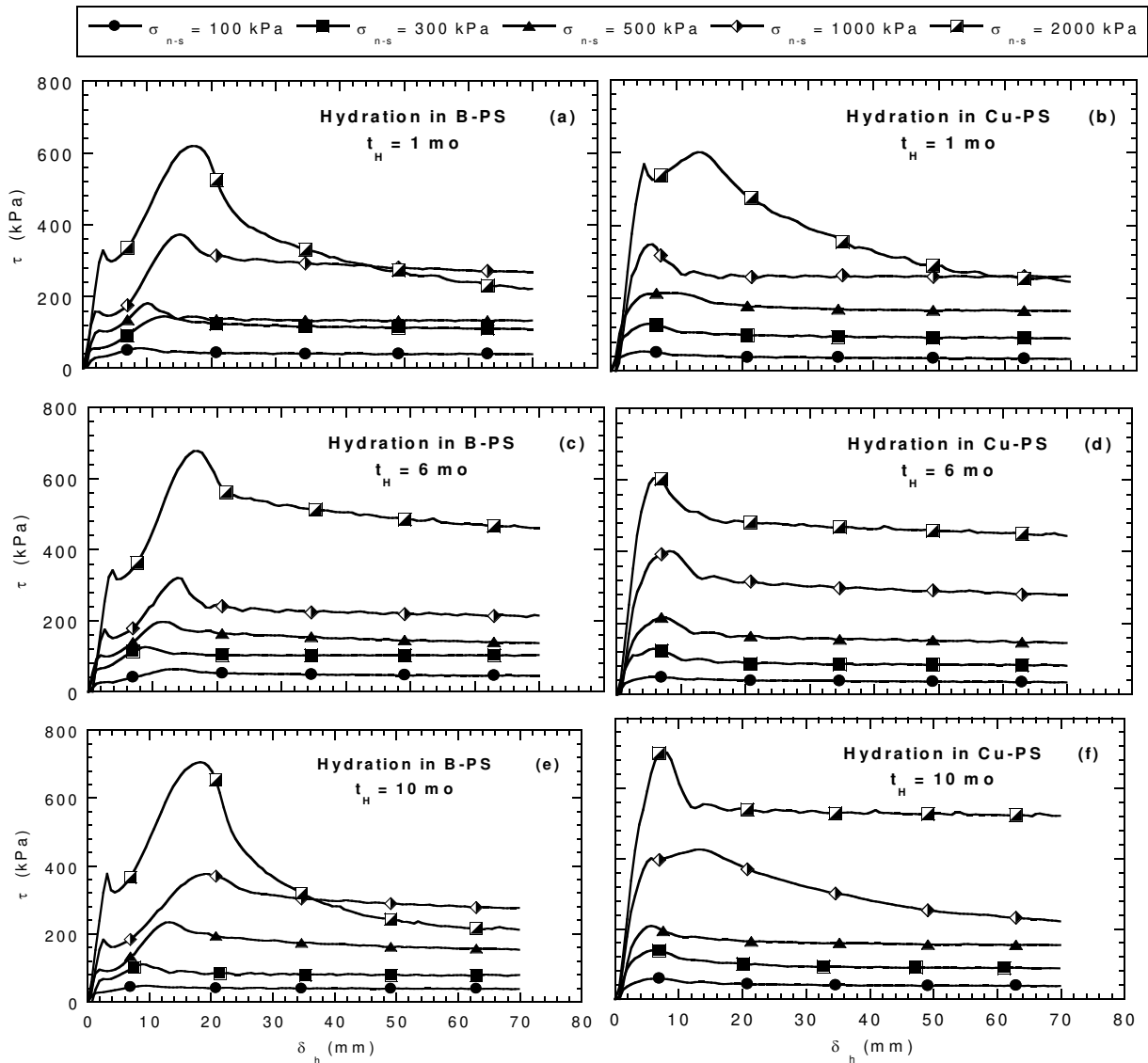


Fig. 5.9. Relationships of shear stress (τ) versus horizontal displacement (δ_h) from interface direct shear tests on GCL and GMX specimens hydrated with (a) B-PS for a hydration time (t_H) = 1 m, (b) Cu-PS for t_H = 1 m, (c) B-PS for t_H = 6 m, (d) Cu -PS for t_H = 6 m, (e) B-PS for t_H = 10 m, and (f) for t_H = 10.

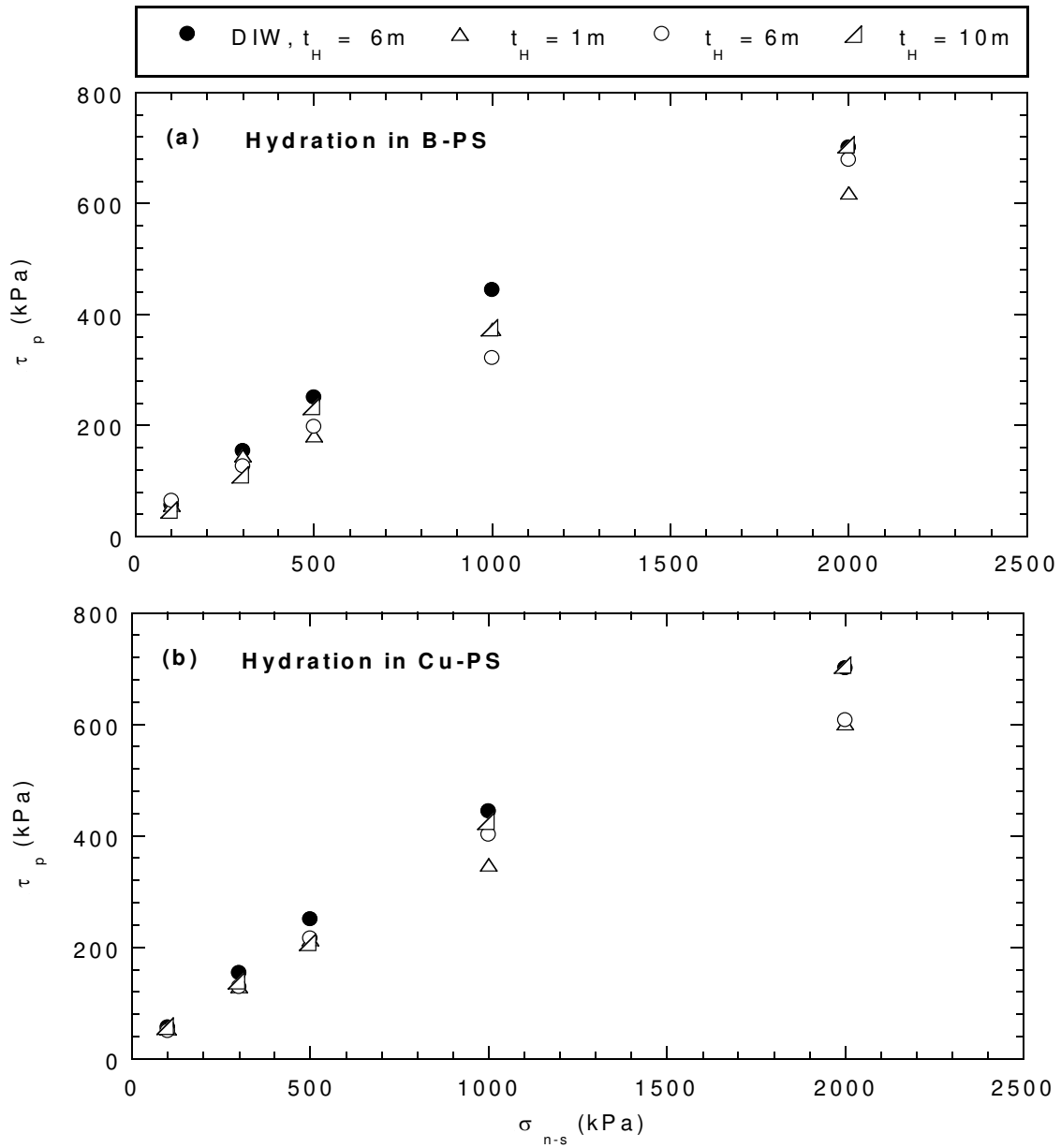


Fig. 5.10. Relationships between peak shear strength (τ_p) versus shearing normal stress (σ_{n-s}) from interface direct shear tests on GCL specimens hydrated with (a) B-PS and (b) Cu-PS. Results of the experiments with DIW included for comparison.

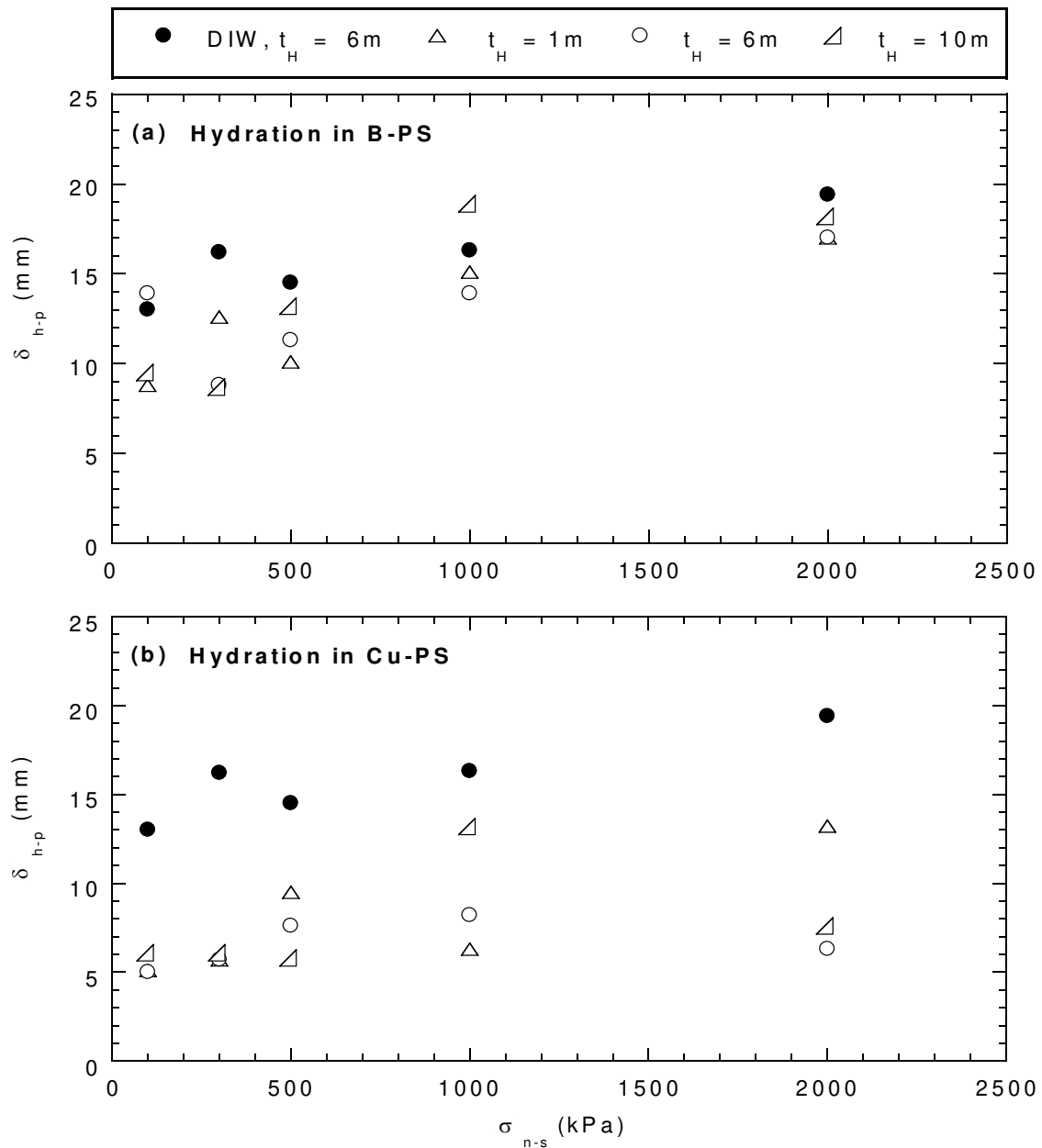


Fig. 5.11. Relationships between horizontal displacement at peak shear stress (δ_{h-p}) versus shearing normal stress (σ_{n-s}) from interface direct shear tests on GCL and GMX specimens hydrated with (a) B-PS and (b) Cu-PS. Results of the experiments with DIW included for comparison.

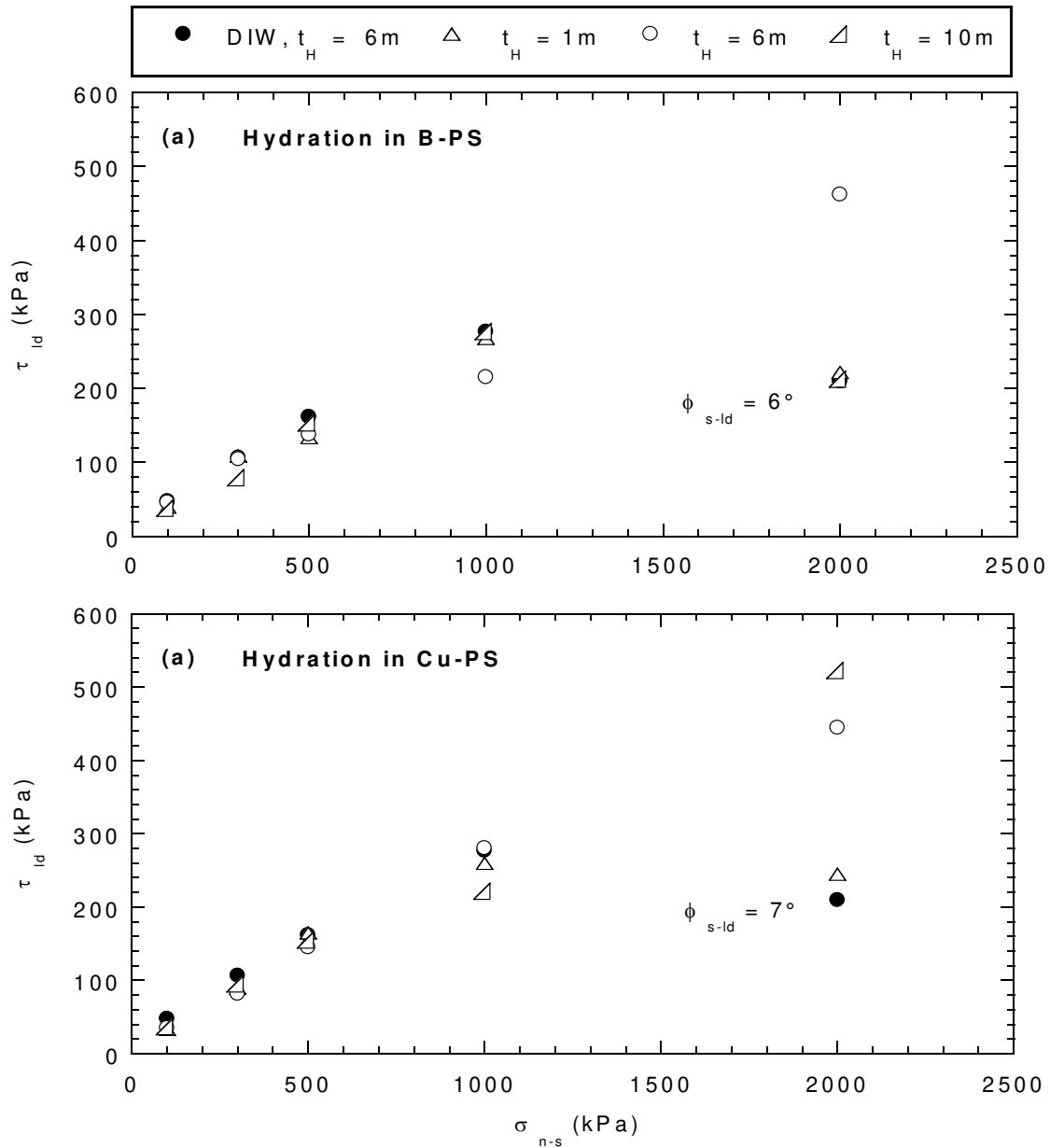


Fig. 5.12. Relationship between large-displacement shear strength (τ_{ld}) versus shearing normal stress (σ_{n-s}) from interface direct shear tests on GCL and GMX specimens hydrated with (a) B-PS and (b) Cu-PS. Results of the experiments with DIW included for comparison.

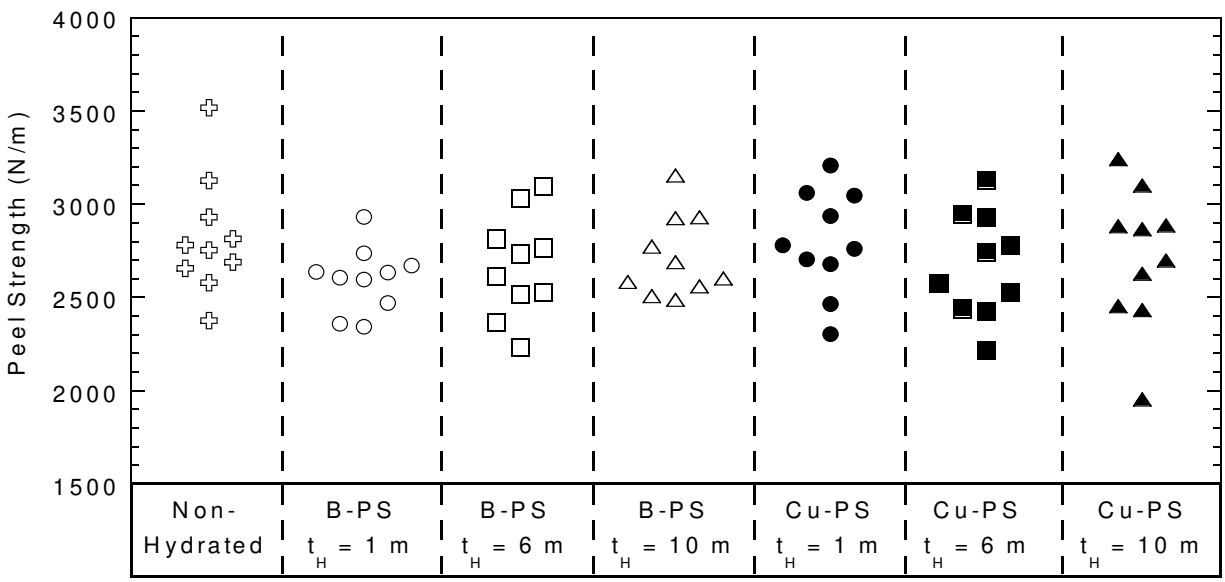


Fig. 5.13. Dot plots of peel strength for geosynthetic clay liner specimens that were tested prior to any hydration (i.e., non-hydrated) as well as specimens hydrated with B-PS or Cu-PS for hydration times (t_H) = 1, 6, or 10 m.



Fig. 5.14. Photograph of swell index tests conducted with non-hydrated bentonite (i.e., exhumed dry from as-received GCL) in de-ionized water (DIW), B-PS, and Cu-PS.

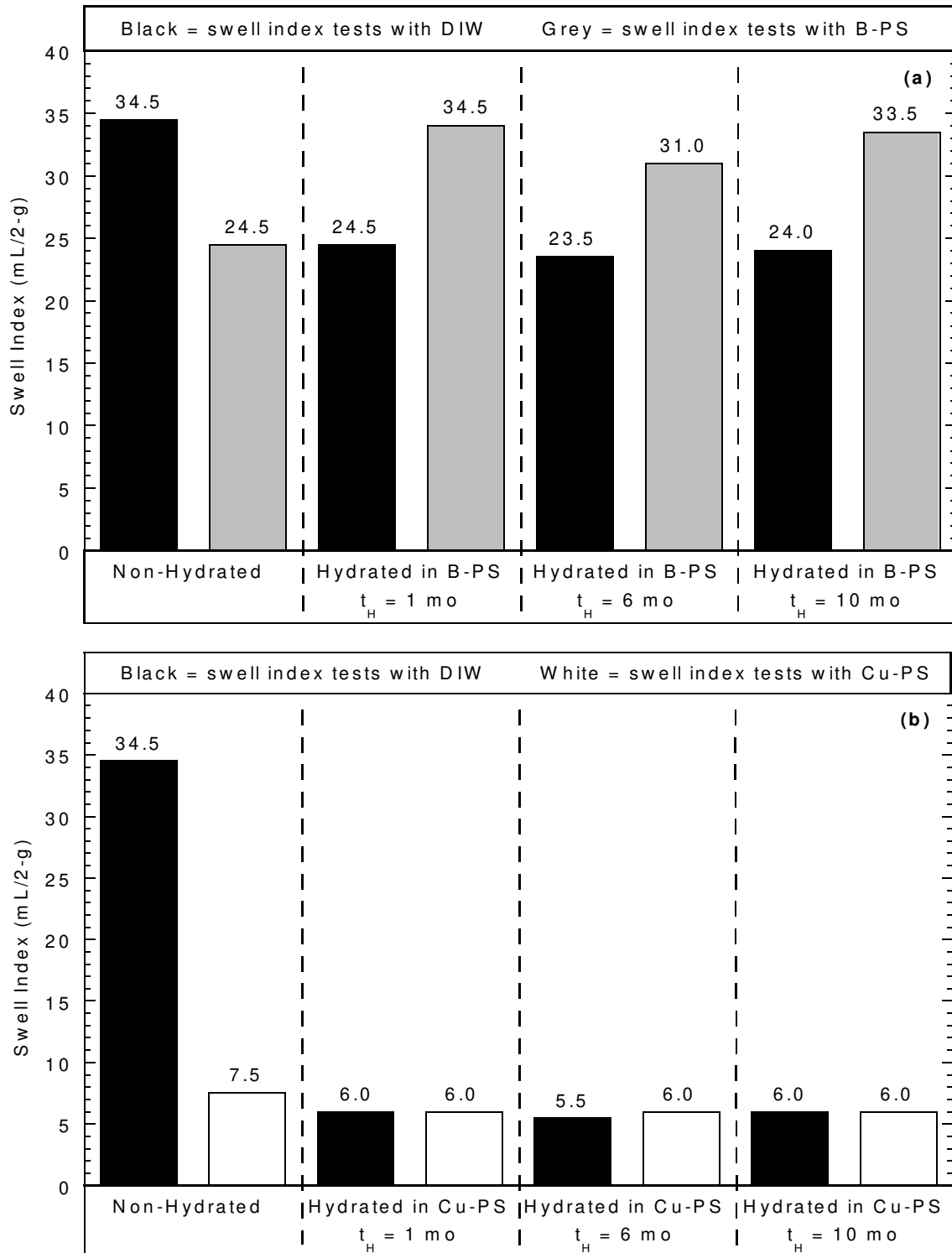


Fig. 5.15. Bar charts of average swell index measured on bentonite that was non-hydrated and bentonite exhumed from GCLs hydrated in (a) B-PS and (b) Cu-PS.

CHAPTER 6: FUTURE RESEARCH

The focus of this study was to evaluate the shear behavior of GMX/GCL composite systems for mining applications. This research project has been completed in two main parts. The first part of this research, which is presented electronically as Appendix (i) to Appendix (v), was preliminary research that was completed to develop the experimental methods and support the objectives of this dissertation. The second part of the research was the main body of the dissertation and was discussed in Chapter 2 to Chapter 5.

Although the outcome of this research contributed to the current understanding of the GCL internal and interface shear behavior, a thorough understanding of the shear behavior of GCL/GMX composite system requires significant amount of additional research considering the complexity of the shear behavior of the composite systems and the broad range of applications that involve numerous environmental factors. In what follows, four research projects are proposed as examples of potential future research.

6.1 Variability in texturing properties of textured geomembranes

The objective of Chapter 2 was to quantify spatial variability of reinforcement fiber properties and internal shear strength in GCL rolls. Considering that the behavior of GMX/GCL composite systems are also dependent on the interface shear behavior between the GMX and GCL, variabilities in texturing characteristics of a GMX (e.g., asperity height, asperity spacing, etc.) can result in different mobilized interface shear resistance between a GMX and GCL. In this situation, laboratory interface shear tests on a limited number of specimens can lead to unconservative or overly conservative designs.

Two different factors are expected to cause variability in GMX rolls: (i) variability in surface roughness due to the manufacturing procedure, and (ii) damage to surface roughness

during shipment and delivery. The significance of each factor is different between spike structured and co-extruded GMXs due to different manufacturing processes. Co-extruded GMXs are manufactured via injecting a blowing agent into a molten resin. As the mixture exits the extrusion system, the mixture cools and the blowing agent bursts at the surface creates textured patterns. In manufacturing of a structured GMX, spike patterns with a specific high and spacing are formed on the surface of a high temperature geomembrane using rollers with an embossed inverse spike pattern.

The variability in GMX surface roughness due to manufacturing is expected to be higher in co-extruded GMX where the surface is textured via random bursts of a blowing agent. The variability in surface roughness due to surface damage during transportation and shipment is expected to be higher for a structured GMX due to geometry of the structured GMX spikes.

To address the aforementioned concerns, displacement-controlled interface shear tests and surface profilometry analyses are proposed on specimens from two 4 m x 1 m samples of a structured and co-extruded GMX. Displacement-controlled interface shear tests should be performed at low normal stress on the two GMXs with a high peel strength GCL to ensure that failure of the composite system is complete interface failure. The GMX specimens for profilometry analysis should be chosen in spaces between shear specimens in a similar pattern as peel strength specimens in Chapter 2. The surface roughness can be quantified based on profilometry analysis and spatial variability in surface roughness can be compared to spatial variability in interface shear strength.

6.2 Effect of geomembrane texturing on shear behavior of GMX/GCL composite systems

The main objective of Chapter 3 was to optimize the design of liner and cover systems via choosing the appropriate GMX and GCLs for a liner or cover system subjected to a specific shear and normal stresses. As a part of Chapter 3 objectives, the effect of GMX spike density on shear behavior of GMX/GCL composite systems was evaluated. Based on the results, an

increase in spike density of a structured GMX increased the critical strength of GMX/GCL composite system.

Research conducted in this study only focused on a spike-structured GMX. However, co-extrusion is also a popular technique in manufacturing of textured geomembranes, and co-extruded GMXs are used in liner and cover systems. Considering that the interface shear resistance between a GCL and GMX is mobilized via a combination of (i) interface friction between the GMX and geotextile of the GCL, and (ii) interlocking between GMX spikes and the geotextile of the GCL, different shear behavior and interface shear strength mechanisms are expected between co-extruded GMXs and structured GMXs. In a spike structured GMX, the GMX-geotextile interlocking was observed at medium and high normal stresses, whereas friction was the dominant interface shear resistance mechanism at low normal stress. In composite systems with a co-extruded GMX, surface friction is expected to be the dominant mechanism at a wider range of normal stresses and the contribution of interlocking to interface shear strength is expected to be minimal. The following questions are proposed: (i) Can higher interface shear strength be achieved at low normal stress using a co-extruded GMX? (ii) How does shear behavior of co-extruded GMXs differ from spike-structured GMXs at high normal stress? and (iii) Considering negligible interlocking strength at all normal stresses in composite systems with woven geotextiles in contact with a GMX, can a co-extruded GMX lead to higher mobilized friction and higher interface shear strength?

To answer the aforementioned questions, displacement-controlled interface shear tests are proposed on three needle-punched GCLs (e.g., GCL-C, GCL-D, GCL-E) and three GMXs: (i) high spike density structured GMX, (ii) low spike density structured GMX, and (iii) co-extruded GMX. The experimental program could be a relevant project for a Masters student.

6.3 Evaluation of internal and interface shear behavior of enhanced bentonite GCLs

Hydraulic conductivity of sodium bentonite is susceptible to the chemistry of the permeant solution, and high ionic strength solutions, particularly those with multi-valent ions, can lead to high hydraulic conductivity. Due to concerns regarding chemical compatibility of sodium bentonite, recent advances in amending sodium bentonite with polymers had led to the production of enhanced bentonite GCLs.

Although enhanced bentonite GCLs have received attention in recent research, the majority of past studies have focused on hydraulic behavior. However, there are concerns regarding internal and interface shear behavior of polymer-modified GCLs due to formation of polymer hydrogels after GCL hydration. The potential for migration of the polymer hydrogels from the hydrated bentonite to the carrier and cover geotextile of GCLs can lead to surface lubrication and reduction in interface shear strength between the GCL and GMX. This mechanism is of greater concern for GCLs with woven geotextiles used as the carrier geotextile. The formation of polymer hydrogels is also expected to influence the internal shear strength of GCLs via reducing fiber bundles geotextile entanglement strength due to lubrication of the fiber bundle-geotextile connections.

To address the aforementioned concerns, displacement-controlled internal and interface shear tests are proposed with a low spike density GMX and up to four needle-punched GCLs to isolate effects of (i) polymer-amendment and (ii) woven versus non-woven carrier geotextile for polymer-amended GCLs. Use of a low spike density GMX would permit failure in the GCL/GMX composite systems to vary from complete interface to complete internal over a range of normal stress. The level of effort anticipated for this project would be sufficient for a Masters student.

6.4 Shear behavior of GCLs in MSW leachates with high surfactant concentrations.

The GMX/GCL composite systems commonly are used in liner system for municipal solid waste (MSW). As the result, the composite system can be subjected to leachates

containing high percentage of surfactants. A high surfactant concentration may lubricate the surfaces of the GCL and GMX to reduce interface shear strength. The reduction in interface shear strength would be expected to be a greater concern in composite systems consisting of co-extruded GMX and in composite systems with a woven geotextile (of the GCL) in contact with the GMX.

To address the aforementioned concerns, displacement-controlled interface shear tests are proposed on GMX/GCL composite systems consisting a GCL with a woven carrier and non-woven cover geotextile and two GMXs: (i) low spike density GMX, and (ii) co-extruded GMX with the same nominal thickness and average spike height as the low spike density GMX. The GCLs and GMXs would be hydrated in de-ionized water and a synthetic MSW leachate with surfactant concentration. The experimental program would include interface shear tests on composite systems consisting of both GMXs in contact with the woven carrier and non-woven cover geotextiles.

REFERENCES

- Akpinar, M. V., and Benson, C. H. (2005). Effect of temperature on shear strength of two geomembrane–geotextile interfaces, *Geotextiles and geomembranes*, 23(5), 443-453.
- Allen, J. M. and Fox, P. J. (2007). Pyramid-tooth gripping surface for GCL shear testing, *Geosynthetics '07*, North American Geosynthetics Society, Washington, DC, (CD-ROM).
- Andrawes, K. Z., McGown, A., and Kabir, M. H. (1984). Uniaxial strength testing of woven and nonwoven geotextiles, *Geotextiles and Geomembranes*, 1(1), 41-56.
- Apiwantragoon, P., Benson, C. H., and Albright, W. H. (2014). Field hydrology of water balance covers for waste containment. *Journal of Geotechnical and Geoenvironmental Engineering*, 141(2), 04014101.
- Ariyama, T., Mori, Y., and Kaneko, K. (1997). Tensile properties and stress relaxation of polypropylene at elevated temperatures, *Polymer Engineering and Science*, 37(1), 81-90.
- ASTM (2010). Standard Test Method for Measuring Mass per Unit Area Of Geotextiles. D5261, *ASTM International*, West Conshohocken, PA, USA.
- ASTM (2011). Standard Specification for Reagent Water. D1193-06, *ASTM International*, West Conshohocken, PA, USA.
- ASTM (2014). Standard Test Method for Measuring Mass per Unit Area Of Geosynthetic Clay Liners. D5993, *ASTM International*, West Conshohocken, PA, USA.
- ASTM D6072 (2015). Standard Practice for Obtaining Samples of Geosynthetic Clay Liners. D6072, *ASTM International*, West Conshohocken, PA, USA.
- ASTM (2015). Standard Terminology for Geosynthetics, Annual Book of ASTM Standards, ASTM D4439-15a, *ASTM International*, West Conshohocken, PA, USA.
- ASTM (2015). Standard Test Method for Determining Average Bonding Peel Strength Between Top and Bottom Layers of Needle-Punched Geosynthetic Clay Liners. D6496/6496M, *ASTM International*, West Conshohocken, PA, USA.
- ASTM (2016). Standard Test Method for Determining the Internal and Interface Shear Resistance of Geosynthetic Clay Liner by the Direct Shear Method, D6243, *ASTM International*, West Conshohocken, Pennsylvania, USA.
- Athanassopoulos, C. and Yuan, Z. (2011). Correlation between needle punch-reinforced geosynthetic clay liner peel strength and internal shear strength. *Geo-Frontiers 2011: Advances in Geotechnical Engineering*, Han, J. and Alzamora, D. E., (eds.), ASCE, Reston, VA, USA, GSP No. 211, 1922-1930.
- Bacas, B. M., Blanco-Fernandez, E. and Cañizal, J. (2013). Comparison of the adhesion and shear tensile strength of needle-punched GCLs. *Geotextiles and Geomembranes*, 41, No. 1, 17–25.
- Bacas, B. M., Cañizal, J., and Konietzky, H. (2015). Shear strength behavior of geotextile/geomembrane interfaces. *Journal of Rock Mechanics and Geotechnical Engineering*, 7(6), 638-645.

- Bacas, B. M., Konietzky, H., Berini, J. C., and Sagaseta, C. (2011). A new constitutive model for textured geomembrane/geotextile interfaces. *Geotextiles and Geomembranes*, 29(2), 137-148.
- Bareither, C. A., Soleimanian, M., and Ghazizadeh, S. (2018). Direct shear testing of GCLs at elevated temperature and in a non-standard solution. *Geosynthetics International*, 25(3), 350-368.
- Benson, C.H., Wang, X., Gassner, F.W., and Foo, D.C.F. (2008). Hydraulic Conductivity of two geosynthetic clay liners permeated with an alumina residue leachate. *Proceedings Geoamericas*, Cancun, 2-5.
- Benson, C.H., Ören, A.H., and Gates, W. P. (2010). Hydraulic conductivity of two geosynthetic clay liners permeated with a hyperalkaline solution. *Geotextiles and Geomembranes*, 28(2), 206-218.
- Bergaya, F., and Lagaly, G. (2013). *Handbook of clay science* (Vol. 5). Newnes.
- Bouazza, A. and Bowders, J.J. (2010). *Geosynthetic Clay Liners for Waste Containment Facilities*, CRC Press, Boca Raton, FL, 239.
- Bouazza, A., Nahlawi, H., and Aylward, M. (2011). In situ temperature monitoring in an organic-waste landfill cell, *Journal of Geotechnical and Geoenvironmental Engineering*, 137(12), 1286-1289.
- Bouazza, A., and Gates, W. P. (2014). Overview of performance compatibility issues of GCLs with respect to leachates of extreme chemistry. *Geosynthetics International*, 21(2), 151-167.
- Budiman, J., (1994). Effects of temperature of physical behavior of geomembrane, *Proceedings of the Fifth International Conference on Geotextiles, Geomembranes, and Related Products*. International Geosynthetics Society, Easley, SC, USA, pp. 1093–1096.
- Chen, Y. M., Lin, W. A., and Zhan, T. L. (2010). Investigation of mechanisms of bentonite extrusion from GCL and related effects on the shear strength of GCL/GM interfaces. *Geotextiles and Geomembranes*, 28(1), 63-71.
- Chiu, P., and Fox, P.J. (2004). Internal and interface shear strengths of unreinforced and needle-punched geosynthetic clay liners. *Geosynthetics International*, 11(3), 176-199.
- Daniels, C. A. (1989). *Polymers: structure and properties*. CRC Press.
- Dixon, N., Jones, D. R. V., and Fowmes, G. J. (2006). Interface shear strength variability and its use in reliability-based landfill stability analysis. *Geosynthetics International*, 13 (1), pp. 1 - 14.
- Dove, J. E., and Frost, J. D. (1996). A method for measuring geomembrane surface roughness. *Geosynthetics International*, 3(3), 369-392.
- Dove, J. E., and Frost, J. D. (1999). Peak friction behavior of smooth geomembrane-particle interfaces. *Journal of Geotechnical and Geoenvironmental Engineering*, 125(7), 544-555.
- Eid, H. T. (2011). Shear strength of geosynthetic composite systems for design of landfill liner and cover slopes. *Geotextiles and Geomembranes*, 29(3), 335-344.
- Eid, H. T., Stark, T. D., and Doerfler, C. K. (1999). Effect of shear displacement rate on internal shear strength of a reinforced geosynthetic clay liner. *Geosynthetics International*, 6(3), 219-239.

- Evans, D. F., and Ninham, B. W. (1986). Molecular forces in the self-organization of amphiphiles. *The Journal of Physical Chemistry*, 90(2), 226-234.
- Fox, P. J. (2010). Internal and interface shear strengths of geosynthetic clay liners. In *3rd International Symposium on Geosynthetic Clay Liners* (pp. 1-17).
- Fox, P. J. and Kim, R. H. (2008). Effect of progressive failure on measured shear strength of geomembrane/GCL interface. *Journal of Geotechnical and Geoenvironmental Engineering*, 134(4), 459-469
- Fox, P. J. and Ross, J. D. (2011). Relationship between GCL internal and GMX/GCL interface shear strength. *Journal of Geotechnical and Geoenvironmental Engineering*, 137(8), 743-753.
- Fox, P. J., and Stark, T. D. (2015). State-of-the-art report: GCL shear strength and its measurement—ten-year update. *Geosynthetics International*, 22(1), 3-47.
- Fox, P. J., Nye, C. J., Morrison, T. C., Hunter, J. G., and Olsta, J. T. (2006). Large dynamic direct shear machine for geosynthetic clay liners. *Geotechnical Testing Journal*, 29(5), 392-400.
- Fox, P. J., Rowland, M. G., and Scheithe, J. R. (1998). Internal shear strength of three geosynthetic clay liners. *Journal of Geotechnical and Geoenvironmental Engineering*, 124(10), 933–944.
- Frost, J. D. (Ed.). (2010). Characterization and Behavior of Interfaces: *Proceedings of Research Symposium on Characterization and Behavior of Interfaces*, 21 September 2008, Atlanta, Georgia, USA. IOS Press.
- Frost, J. D., and Karademir, T. (2015). Shear-induced changes in smooth geomembrane surface topography at different ambient temperatures. *Geosynthetics International*, 23(2), 113-128.
- Frost, J. D., and Lee, S. W. (2001). Microscale study of geomembrane-geotextile interactions. *Geosynthetics International*, 8(6), 577-597.
- Ghazizadeh, S., and Bareither, C. A. (2018^a). Critical strength of high peel strength geosynthetic clay liners at low normal stresses, *Tailing and Mine waste 2018*, pp xx-yy.
- Ghazizadeh, S., and Bareither, C. A. (2018^b). Stress-controlled direct shear testing of geosynthetic clay liners I: Apparatus development. *Geotextiles and Geomembranes*, 46(5), 656-666.
- Ghazizadeh, S., and Bareither, C. A. (2018^c). Stress-controlled direct shear testing of geosynthetic clay liners II: Assessment of shear behavior. *Geotextiles and Geomembranes*, 46(5), 667-677.
- Ghazizadeh, S., and Bareither, C. A. (2019a). Temperature effects on the mechanisms of internal shear behavior in needle-punched reinforced GCLs, *Journal of Geotechnical and Geoenvironmental Engineering*, In review.
- Ghazizadeh, S., and Bareither, C. A. (2019b). Evaluation of GCL and Geomembrane Characteristics on Failure Modes and Critical Shear Strength of GCL/Geomembrane Composite Systems. In *Geo-Congress 2019: Earth Retaining Structures and Geosynthetics* (pp. 344-353). Reston, VA: American Society of Civil Engineers.

- Ghazizadeh, S., Bareither, C. A., Scalia, J., and Shackelford, C. D. (2018). Synthetic Mining Solutions for Laboratory Testing of Geosynthetic Clay Liners. *Journal of Geotechnical and Geoenvironmental Engineering*, 144(10), 06018011.
- Gilbert, R. B., Fernandez, F. and Horsfield, D. W. (1996). Shear strength of reinforced geosynthetic clay liner. *Journal of Geotechnical Engineering*, 122, No. 4, 259–266.
- Gilbert, R. B., Scranton, H. B., and Daniel, D. E. (1997). Shear strength testing for geosynthetic clay liners. In *Testing and acceptance criteria for geosynthetic clay liners*. ASTM International.
- Gouy, M. (1910). Sur la constitution de la charge électrique à la surface d'un électrolyte. *J. Phys. Theor. Appl.*, 9(1), 457-468.
- Gulec, S.B., Edil, T.B., and Benson, C.H (2004). Effect of acid mine drainage on the polymer properties of a HDPE geomembrane, *Geosynthetics International*, 11(2), 60–72.
- Gulec, S.B., Benson, C.H., and Edil, T.B. (2005). Effect of acidic mine drainage on the mechanical and hydraulic properties of three geosynthetics, *Journal of Geotechnical and Geoenvironmental Engineering*, 131(8), 937-950.
- Guyonnet, D., Touze-Foltz, N., Norotte, V., Pothier, C., Didier, G., Gailhanou, H., ... and Warmont, F. (2009). Performance-based indicators for controlling geosynthetic clay liners in landfill applications. *Geotextiles and Geomembranes*, 27(5), 321-331.
- Halse, Y., Koerner, R. M., and Lord Jr, A. E. (1987). Effect of high levels of alkalinity on geotextiles. Part 1: Ca (OH) 2 solutions. *Geotextiles and Geomembranes*, 5(4), 261-282.
- Hanson, J. L., Chrysovergis, T. S., Yesiller, N., and Manheim, D. (2015). Temperature and moisture effects on GCL and textured geomembrane interface shear strength. *Geosynthetics International*, 22(1), 110-124
- Heerten, G., Saathoff, F., Scheu, C., von Maubeuge, K.P., 1995. Testing, interpreting and designing the long-term shear strength of geosynthetic clay liners. Proceedings of Geosynthetics '95, Nashville, Tennessee, USA, pp. 867–877.
- Hebeler, G. L., Frost, J. D., and Myers, A. T. (2005). Quantifying hook and loop interaction in textured geomembrane–geotextile systems. *Geotextiles and Geomembranes*, 23(1), 77-105.
- Hewitt, R. D., Soydemir, C., Stulgis, R. P., and Coombs, M. T. (1997). Effect of normal stress during hydration and shear on the shear strength of GCL/textured geomembrane interfaces. In *Testing and acceptance criteria for geosynthetic clay liners*. ASTM International.
- Hillman, R. P., and Stark, T. D. (2001). Shear strength characteristics of PVC geomembrane-geosynthetic interfaces. *Geosynthetics International*, 8(2), 135-162.
- Hornsey, W.P., Scheirs, J., Gates, W.P., and Bouazza, A. (2010). The impact of mining solutions/liquors on geosynthetics. *Geotextiles and Geomembranes*, 28(2), 191-198.
- Hosney, M. S., and Rowe, R. K. (2013). Changes in geosynthetic clay liner (GCL) properties after 2 years in a cover over arsenic-rich tailings. *Canadian Geotechnical Journal*, 50(3), 326-342.
- Hsieh, C. W., and Tseng, Y. C. (2008). Tensile creep behavior of a PVC coated polyester geogrid at different temperatures, *Journal of GeoEngineering*, 3(3), 113-119.

- Hsuan, Y. G., and Koerner, R. M. (2002). Durability and lifetime of polymer fibers with respect to reinforced geosynthetic clay barriers, *ie reinforced GCLs*. pp. 73-86.
- Hsuan, Y. G., Koerner, R. M., and Lord, A. E. (1993). A review of the degradation of geosynthetic reinforcing materials and various polymer stabilization methods. In *Geosynthetic Soil Reinforcement Testing Procedures*. ASTM International.
- Hsuan, Y. G., and Koerner, R. M. (1998). Antioxidant depletion lifetime in high density polyethylene geomembranes. *Journal of Geotechnical and Geoenvironmental Engineering*, 124(6), 532-541.
- Hunter, R. J. (2013). Zeta potential in colloid science: principles and applications (Vol. 2). Academic press.
- Jafari, N. H., Stark, T. D., and Rowe, R. K. (2013). Service life of HDPE geomembranes subjected to elevated temperatures, *Journal of Hazardous, Toxic, and Radioactive Waste*, 18(1), 16-26.
- Jafari, N. H., Stark, T. D., and Thalhamer, T. (2017). Spatial and temporal characteristics of elevated temperatures in municipal solid waste landfills, *Waste management*, 59, 286-301.
- Jeon, H.Y. (2006). Chemical resistance and transmissivity of nonwoven geotextiles in waste leachate solutions, *Polymer Testing*, 25(2), 176-180.
- Jo, H.Y., Katsumi, T., Benson, C.H., and Edil, T.B. (2001). Hydraulic conductivity and swelling of nonprehydrated GCLs permeated with single-species salt solutions. *Journal of Geotechnical and Geoenvironmental Engineering*, 127(7), 557-567.
- Jo, H.Y., Benson, C.H., Shackelford, C.D., Lee, J.M., and Edil, T.B. (2005). Long-term hydraulic conductivity of a geosynthetic clay liner permeated with inorganic salt solutions. *Journal of Geotechnical and Geoenvironmental Engineering*, 131(4), 405-417.
- Jones, D. R. V., and Dixon, N. (1998). Shear strength properties of geomembrane/geotextile interfaces, *Geotextiles and Geomembranes*, 16(1), 45-71.
- Karademir, T. (2011). Elevated temperature effects on interface shear behavior (*Doctoral dissertation*, Georgia Institute of Technology).
- Karademir, T., and Frost, J. D. (2011). Elevated temperature effects on geotextile-geomembrane interface strength, *In Geo-Frontiers 2011: Advances in Geotechnical Engineering* (pp. 1023-1033).
- Karademir, T. and Frost, J. D. (2014). Micro-scale tensile properties of single geotextile polypropylene filaments at elevated temperatures, *Geotextiles and Geomembranes*, 42(3), 201-213.
- Kashir, M., and Yanful, E. K. (2001). Hydraulic conductivity of bentonite permeated with acid mine drainage. *Canadian Geotechnical Journal*, 38(5), 1034-1048.
- Katsumi, T., Ishimori, H., Ogawa, A., Yoshikawa, K., Hanamoto, K., and Fukagawa, R. (2007). Hydraulic conductivity of nonprehydrated geosynthetic clay liners permeated with inorganic solutions and waste leachates. *Soils and Foundations*, 47(1), 79-96.
- Katsumi, T., Ishimori, H., Onikata, M., and Fukagawa, R. (2008). Long-term barrier performance of modified bentonite materials against sodium and calcium permeant solutions. *Geotextiles and Geomembranes*, 26(1), 14-30.

- Khilnani, K., Stark, T. D., and Bahadori, T. M. (2017). Comparison of Single and Multi-Layer Interface Strengths for Geosynthetic/Geosynthetic and Soil/Geosynthetic Interfaces, *Geotechnical Frontiers 2017* pp. 42-51.
- King, R. F. and Tabor, D. (1953). The effect of temperature on the mechanical properties and the friction of plastics, *Proceedings of the Physical Society*. Section B, 66(9), 728.
- Koerner, G. R., Hsuan, Y. G., and Koerner, R. M. (2007). The durability of geosynthetics. *Geosynthetics in civil engineering*, 36-65.
- Koerner, R. M. (2012). Designing with geosynthetics (Vol. 1). Xlibris Corporation.
- Koerner, R. M., Lord Jr, A. E., and Halse, Y. H. (1988). Long-term durability and aging of geotextiles. *Geotextiles and Geomembranes*, 7(1-2), 147-158.
- Koerner, R. M., Soong, T. Y., Gontar, A. (1998). Selected aspects of GCL shear strength testing. Proc. *Geo-Bento '98*, Paris, 97-110.
- Koerner, R.M., Soong, T.-Y., Koerner, G.R., and Gontar, A. (2001). Creep testing and data extrapolation of reinforced GCLs, *Geotextiles and Geomembranes*, 19(7), 413-425.
- Kolstad, D.C., Benson, C.H., Edil, T.B., and Jo, H.Y. (2004). Hydraulic conductivity of a dense prehydrated GCL permeated with aggressive inorganic solutions. *Geosynthetics International*, 11(3), 233-241.
- Kongkitkul, W., Tabsombut, W., Jaturapitakkul, C., and Tatsuoka, F. (2012). Effects of temperature on the rupture strength and elastic stiffness of geogrids, *Geosynthetics International*, 19(2), 106-123.
- Lakes, R., and Lakes, R. S. (2009). Viscoelastic materials. Cambridge University Press
- Lange, K., Rowe, R.K., and Jamieson, H. (2007). Metal retention in geosynthetic clay liners following permeation by different mining solutions, *Geosynthetics International*, 14(3), 178-187.
- Lange, K., Rowe, R.K., and Jamieson, H. (2010). The potential role of geosynthetic clay liners in mine water treatment systems, *Geotextiles and Geomembranes*, 28(2), 199-205.
- Li, M. H., and Gilbert, R. B. (2006). Mechanism of post-peak strength reduction for textured geomembrane–nonwoven geotextile interfaces. *Geosynthetics International*, 13(5), 206-209.
- Lord, A., Soong, T., Koerner, R., (1995). Relaxation behavior of thermally induced stress in HDPE geomembranes, *Geosynthetics International*, 2 (3), 626–634.
- Ludema, K. C. and Tabor, D. (1966). The friction and visco-elastic properties of polymeric solids, *Wear*, 9(5), 329-348.
- Lupo, J. F. (2010). Liner system design for heap leach pads, *Geotextiles and Geomembranes*, 28(2), 163-173.
- Lyklema, J. (2005). Fundamentals of interface and colloid science: soft colloids (Vol. 5). Elsevier.
- Mathur, A., Netravali, A. N., and O'Rourke, T. D. (1994). Chemical aging effects on the physio-mechanical properties of polyester and polypropylene geotextiles. *Geotextiles and Geomembranes*, 13(9), 591-626.

- McBride, M. B. (1997). A critique of diffuse double layer models applied to colloid and surface chemistry. *Clays and Clay minerals*, 45(4), 598-608.
- McCartney, J. S., Zornberg, J. G., Swan, R. H. Jr. and Gilbert, R. B. (2004). Reliability-based stability analysis considering GCL shear strength variability. *Geosynthetics International*, 11, No. 3, 212–232.
- McCartney, J. S., Zornberg, J. G., and Swan Jr, R. H. (2009). Analysis of a large database of GCL-geomembrane interface shear strength results. *Journal of Geotechnical and Geoenvironmental Engineering*, 135(2), 209-223.
- McKeen, L. W. (2014). The effect of temperature and other factors on plastics and elastomers. William Andrew.
- Mesri, G. and Olson, R. E. (1970). Shear strength of montmorillonite, *Geotechnique*, 20(3), 261-270.
- Mitchell, J. K., and Soga, K. (2005). Fundamentals of soil behavior (Vol. 3). New York: John Wiley and Sons.
- Müller, W., Jakob, I., Seeger, S., and Tatzky-Gerth, R. (2008). Long-term shear strength of geosynthetic clay liners, *Geotextiles and Geomembranes*, 26(2), 130-144.
- Myshkin, N. K., Petrokovets, M. I., and Kovalev, A. V. (2005). Tribology of polymers: adhesion, friction, wear, and mass-transfer, *Tribology International*, 38(11-12), 910-921.
- Norrish, K. (1954). The swelling of montmorillonite. *Discussions of the Faraday society*, 18, 120-134.
- Norrish, K., and Quirk, J. P. (1954). Crystalline swelling of montmorillonite: Use of electrolytes to control swelling. *Nature*, 173(4397), 255.
- Nye, C. J., and Fox, P. J. (2007). Dynamic shear behavior of a needle-punched geosynthetic clay liner, *Journal of Geotechnical and Geoenvironmental Engineering*, 133(8), 973-983.
- Olst, J. T. and Swan, R. H. (2001). Internal shear strength of a geosynthetic clay liner at high normal loads, *Tailings and Mine Waste*, Colorado State University, Fort Collins, CO, USA, 197-200.
- Pasqualini, E., Sand, D., Roccatto, M., 1993. Factors influence geomembrane interface friction. In: Sarsby, R. (Ed.), *Waste Disposal by Landfill Green '93*. Bolton Institute of Higher Education, United Kingdom, pp. 349–356.
- Petrov, R.J., and Rowe, R.K. (1997). Geosynthetic clay liner (GCL)-chemical compatibility by hydraulic conductivity testing and factors impacting its performance. *Canadian Geotechnical Journal*, 34(6), 863-885.
- Richardson, G.N., 1997. GCL internal shear strength requirements. Geotechnical Fabrics Report, vol. 15(2), *Industrial Fabrics Association*, pp. 20–25.
- Ross, J. D., and Fox, P. J. (2015). Dynamic shear strength of GMX/GCL composite liner for monotonic loading. *Journal of Geotechnical and Geoenvironmental Engineering*, 141(7), 04015026.
- Rowe, R. K. (2005). Long-term performance of contaminant barrier systems, *Geotechnique*, 55(9), 631-678.

- Rowe, R. K., and Sangam, H. P. (2002). Durability of HDPE geomembranes. *Geotextiles and Geomembranes*, 20(2), 77-95.
- Rowe, R. K., Brachman, R. W., Hosney, M. S., Take, W. A., and Arnepalli, D. N. (2017). Insight into hydraulic conductivity testing of geosynthetic clay liners (GCLs) exhumed after 5 and 7 years in a cover. *Canadian Geotechnical Journal*, 54(8), 1118-1138.
- Rowe, R.K., Rimal, S., and Sangam, H. (2009). Ageing of HDPE geomembrane exposed to air, water and leachate at different temperatures, *Geotextiles and Geomembranes*, 27(2), 137-151.
- Ruhl, J.L. and Daniel, D.E. (1997). Geosynthetic clay liners permeated with chemical solutions and leachates, *Journal of Geotechnical and Geoenvironmental Engineering*, 123(4), 369-381.
- Sabatini, P. J., Griffin, L. M., Bonaparte, R., Espinoza, R. D., and Giroud, J. P. (2002). Reliability of state of practice for selection of shear strength parameters for waste containment system stability analyses. *Geotextiles and Geomembranes*, 20(4), 241-262.
- Scalia, J. and Benson, C.H. (2010). Hydraulic conductivity of geosynthetic clay liners exhumed from landfill final covers with composite barriers, *Journal of Geotechnical and Geoenvironmental Engineering*, 137(1), 1-13.
- Scalia IV, J., Bohnhoff, G. L., Shackelford, C. D., Benson, C. H., Sample-Lord, K. M., Malusis, M. A., and Likos, W. J. (2018). Enhanced bentonites for containment of inorganic waste leachates by GCLs. *Geosynthetics International*, 25(4), 392-411.
- Seed, H. B., Wookward, R. J., and Lundgren, R. (1964). Clay mineralogical aspects of the Atterberg limits. *Journal of Soil Mechanics & Foundations Div*, 90(Proc. Paper 3983).
- Shackelford, C.D. (1994). Waste-soil interactions that alter hydraulic conductivity. *Hydraulic Conductivity and Waste Contaminant Transport in Soil*, D.E. Daniel and S.J. Trautwein, Eds., STP 1142, ASTM, West Conshohocken, PA, 111-168.
- Shackelford, C.D., Benson, C.H., Katsumi, T., Edil, T.B., and Lin, L. (2000). Evaluating the hydraulic conductivity of GCLs permeated with nonstandard liquids, *Geotextiles and Geomembranes*, 18, 133-161.
- Shackelford, C.D., Sevick, G.W., and Eykholt, G.R. (2010). Hydraulic conductivity of geosynthetic clay liners to tailings impoundment solutions, *Geotextiles and Geomembranes*, 28(2), 149-162.
- Siebken, J.R., Swan, R. H. Jr., and Yuan, Z. (1997). Short-term and creep shear characteristics of a needle punched thermally locked geosynthetic clay liner, STP 1308 Testing and Acceptance Criteria for Geosynthetic Clay Liners, Well, L.W. (ed.), ASTM International, West Conshohocken, PA, USA, 89-102.
- Stark, T. D., and Choi, H. (2004). Peak versus residual interface strengths for landfill liner and cover design. *Geosynthetics International*, 11(6), 491-498.
- Stark, T. D., Martin, J. W., Gerbasi, G. T., Thalhamer, T., and Gortner, R. E. (2011). Aluminum waste reaction indicators in a municipal solid waste landfill, *Journal of Geotechnical and Geoenvironmental Engineering*, 138(3), 252-261.
- Stark, T. D., Niazi, F. S., and Keuscher, T. C. (2015). Strength envelopes from single and multi geosynthetic interface tests. *Geotechnical and Geological Engineering*, 33(5), 1351-1367.

- Stark, T. D., Williamson, T. A., and Eid, H. T. (1996). HDPE geomembrane/geotextile interface shear strength. *Journal of Geotechnical Engineering*, 122(3), 197-203.
- Stemson, M. L. and Smith, M. E. (2009). The development of nickel laterite heap leach projects, In *ALTA 2009 Nickel/Cobalt Conference*, 25-30.
- Stępień, S., and Szymański, A. (2015). Influence of strain rate on tensile strength of woven geotextile in the selected range of temperature, *Studia Geotechnica et Mechanica*, 37(2), 57-60.
- Thiel, R. and Smith, M. E. (2004). State of the practice review of heap leach pad design issues, *Geotextiles and Geomembranes*, 22(6), 555-568.
- Thielmann, S. S., Fox, P. J., and Athanassopoulos, C. (2016). Shear strength of GMX/GCL composite liner under high normal stress. *Journal of Geotechnical and Geoenvironmental Engineering*, 142(5), 1-11.
- Touze-Foltz, N., Lupo, J., and Barroso, M. (2008). Geoenvironmental applications of geosynthetics, Keynote Lecture, *Proceedings EuroGeo4*, 98.
- Trauger, R.J., Swan, R.H., and Yuan, Z. (1997). Long-term shear strength behavior of a needle punched geosynthetic clay liner, STP 1308 Testing and Acceptance Criteria for Geosynthetic Clay Liners, Well, L. W. (ed.). *ASTM International*, West Conshohocken, PA, USA, 103-120.
- Triplett, E. J. and Fox, P. J. (2001). Shear strength of HDPE geomembrane/geosynthetic clay liner interfaces, *Journal of Geotechnical and Geoenvironmental Engineering*, 127(6), 543-552.
- Vaid, Y. P., and Rinne, N. (1995). Geomembrane coefficients of interface friction. *Geosynthetics International*, 2(1), 309-325.
- von Maubeuge, K. P., and Ehrenberg, H. (2000). Comparison of peel bond and shear tensile test methods for needlepunched geosynthetic clay liners. *Geotextiles and Geomembranes*, 18(2-4), 203-214.
- von Maubeuge, K., and Ehrenberg, H. (2013). Peel and shear test comparison and geosynthetic clay liner shear strength correlation. In *Current and Future Practices for the Testing of Multi-Component Geosynthetic Clay Liners*. *ASTM International*.
- Vukelić, A., Szavits-Nossan, A., and Kvasnička, P. (2008). The influence of bentonite extrusion on shear strength of GCL/geomembrane interface. *Geotextiles and Geomembranes*, 26(1), 82-90.
- Wang, B., Dong, X., Chen, B., and Dou, T. (2019). Hydraulic Conductivity of Geosynthetic Clay Liners Permeated with Acid Mine Drainage. *Mine Water and the Environment*, 1-9.
- Yeşiller, N., Hanson, J. L., and Liu, W. L. (2005). Heat generation in municipal solid waste landfills, *Journal of Geotechnical and Geoenvironmental Engineering*, 131(11), 1330-1344.
- Yeşiller, N., Hanson, J. L., and Yee, E. H. (2015). Waste heat generation: A comprehensive review. *Waste management*, 42, 166-179.
- Zanzinger, H. (2016). Contribution to the long-term shear strength of a needle punched GCL. *International Journal of Geosynthetics and Ground Engineering*, 2(1), 8.

- Zanzinger, H., and Saathoff, F. (2012). Long-term internal shear strength of a reinforced GCL based on shear creep rupture tests, *Geotextiles and Geomembranes*, 33, 43-50.
- Zornberg, J. G., McCartney, J. S., and Swan, R. H. Jr. (2005). Analysis of a large database of GCL internal shear strength results, *Journal of Geotechnical and Geoenvironmental Engineering*, 131, (3), 367–380.
- Zornberg, J. G., McCartney, J. S., and Swan, R. H. Jr. (2006). Closure to ‘Analysis of a large database of GCL internal shear strength results’ by Zornberg, J. G., McCartney, J. S. and Swan, R. H. Jr. *Journal of Geotechnical and Geoenvironmental Engineering*, 132, No. 10, 1376–1379.
- Zornberg, J. G., and McCartney, J. S. (2009). Internal and interface shear strength of geosynthetic clay liners. In *Geosynthetic Clay Liners for Waste Containment Facilities* (pp. 149-174). CRC Press.